In-Band Full-Duplex Cross-Layer Design for Next-Generation Vehicular Networks

Zang, Junwei

Awarding institution:
King's College London

KING'S COLLEGE LONDON

In-Band Full-Duplex Cross-Layer Design for Next-Generation Vehicular Networks

This thesis is submitted for the degree of
Dodoctor of Philosophy
in
Telecommunications
at
Centre for Telecommunications Research
Department of Engineering
King's College London

Author:
MR. JUNWEI ZANG
Supervisor:
PROF. MOHAMMAD SHIKH-BAHAEI

Sep 2021

To
My parents

Abstract

The rapid and enormous proliferation of expectation on future vehicular system has led to numerous challenges in deploying vehicular networks, which is also known as vehicle-to-everything (V2X) communication networks. V2X communication is a vehicular communication system that allows future connected and autonomous vehicles to share safety-related and infotainment information wirelessly to any entity. The main objective is to propose novel designs, so that they can be considered for next-generation V2X networks to improve road safety as well as transportation experience. For both industrial and academic areas, one of the most significant challenges is ensuring safety whilst providing required services. One promising technology for enhancing the performance of next-generation vehicular networks is the in-band full-duplex (FD) communication technology. It allows the transceivers to send and receive/sense signals simultaneously over the same frequency band.

In this thesis, I have investigated applying FD technology to future vehicular networks from physical (PHY) layer to transport (TRANS) layer aspects. Since two different families of technologies have been standardised as the benchmark designs, which are known as the dedicated short range communications (DSRC) standard and the cellular V2X (C-V2X) communication standard, respectively, I started from investigating how FD technology can be applied to future vehicular networks based on the DSRC standard. Then, I continued to investigate its novel designs on the application to the networks based on the C-V2X standard.

Specifically, based on the DSRC standard, I firstly proposed a FD signal collision avoidance scheme. Next, I considered the medium access challenges, and proposed a PHY- and medium access control- (MAC) layers cross-layer design to address these challenges. After that, based on the C-V2X standard, I also applied the FD technology to a beyond 5G (B5G) vehicular ad hoc network (VANET) scenario, and proposed a novel FD MAC layer protocol. Then, I expanded our research further by jointly taken machine learning techniques into consideration, an adaptive FD deep reinforcement learning design has been proposed. Finally, I surveyed the related works, and proposed our understanding and novel ideas on how to apply FD technology in 6G-V2X networks.

A few tools and methods were used in this thesis. I introduced a FD energy detection scheme for collision detection and avoidance; Poisson distribution, Central Limit Theorem, etc. were used for evaluating the network performance; and Markov Chain was used to study the protocols. Besides, OMNeT++ was used for wireless communication simulation, SUMO was used for traffic simulation, and MATLAB was used for mathematical and simulation results analysis.

Consequently, I found that the proposed FD energy detection method outperforms the standardised half duplex (HD) energy detection method, and it is also feasible with the state-of-the-art FD hardware design achievements. Moreover, since reliability and latency are the two most significant evaluation parameters for next-generation vehicular networks, I proved that the reliability can be enhanced and latency can be shortened by deploying our proposed FD-based protocols, in both DSRC-based and C-V2X-based standards.

Acknowledgement

First and foremost, let me start by thanking my supervisor Prof. Mohammad Shikh-Bahaei for his unconditional support and continuous guidance. His discerning vision inspired me to discover my area of interests and propose novel ideas, his outstanding reputation and professionalism encouraged me to discipline myself with high standards. Besides, I should also thank Dr. Vasilis Friderikos for his co-supervision, his achievements also set an example for me to produce novel research papers.

In the past four years, I also worked as a Teaching Assistant at King's College London, and I am grateful to the teachers who provided me the opportunities of working as their Teaching Assistant. They include my supervisor Prof. Mohammad Shikh-Bahaei, who gave me the opportunity to work in the circuit theory module, the communication system module and the digital communications module; Dr. Josh Murphy and Dr. Matthew Howard, who gave me the opportunity to work in the computer system module and the physical computing module; Dr. Mohammad Reza Nakhai, who was the other module leader of the communication system module; Prof. Samjid Mannan, who gave me the opportunity to work in the mathematical methods in physics module; Dr. Jamie Barras, who gave me the opportunity to work in the electronic applications project and engineering lab I & II modules. I also appreciate Dr. Christopher Hampson for providing multiple opportunities of working as an exam invigilator and marker. Working with different professional module leaders in different modules enriched my teaching experience and various skills, it has also broadened my visions of working in academics. Special thanks to my supervisor Prof. Mohammad Shikh-Bahaei, who also provided opportunities to co-supervise bachelor and master individual research projects.

In the patent application, I am grateful to my supervisor and co-inventor Prof. Mohammad Shikh-Bahaei for his efforts and continuous support. I am also grateful to Prof. Hamid Aghvami, who provided valuable comments. Thanks to the King's intellectual property managers Miss Mugdha Joshi and Dr. Pushkar Wadke, for their management and guidance. Thanks also to the patent attorneys Mr. Nick Wallin, Mr. Matthew Holden and Miss. Judith Coghlan, for their efforts and outstanding work on law-related suggestions and documentation.

I should appreciate my colleagues at Centre for Telecommunications Research,

King's College London: thanks to Dr. Sandeep Narayanan, Dr. Xi Lu, Dr. Xun Liu, Dr. Vahid Towhidlou, Dr. Zhaohui Yang and Dr. Tong Peng, Dr. Mahdi Shahabi, for being senior researchers and sharing their valuable research experience unconditionally; thanks to numerous teaching assistants such as Enric, Maliheh, Waleed and professional administrators in the Engineering and the Informatics Departments such as Benedict, Nikki, for their continuous support in teaching, the modules would not be successful without their generous help; thanks to all my research group members such as Yirun, Mohammed and Weihang, for being good teammates and having profound discussions; thanks also to all my dear friends such as Wen, Renhao and Wenli, for being amazing friends and provided strongest motivation to my PhD and life.

Last but not least, I have to express my greatest gratefulness and respect to my parents, for their love, selfless dedication and unconditional support. You are my family, shields, and friends.

Table of Contents

List of Figures

List of Tables

Author's Contributions

0.1 List of Presentations

[P1] **J. Zang**, "Collision Avoidance in V2X Communication Networks [oral presentation]," in *2019 IEEE Wireless Communications and Networking Conference Workshop (2019 IEEE WCNCW)*, 2019.

[P2] **J. Zang**, "A Priority-Based Cross-Layer Design for Future VANETs through Full-Duplex Technology [poster presentation]," in *the 3rd year Poster Competition of Natural & Mathematical Sciences, King's College London*, 2019.

[P3] **J. Zang**, "Full-Duplex Multiple Access Mechanism for Connected Vehicles Operating at Different Autonomous Levels in NR eV2X Networks [oral presentation]," in *King's Intellectual Property Committee*, 2020.

[P4] **J. Zang**, "Full Duplex-Based Scheduling Protocol for Latency Enhancement in 5G eV2X VANETs [oral presentation]," in *2021 IEEE Wireless Communications and Networking Conference (2021 IEEE WCNC)*, 2021.

[P5] **J. Zang**, "An Adaptive Full-Duplex Deep Reinforcement Learning-Based Design for 5G Mode 4 VANETs [oral presentation]," in *2021 IEEE Wireless Communications and Networking Conference (2021 IEEE WCNC)*, 2021.

0.2 List of Conference Papers

[C1] **J. Zang**, V. Towhidlou and M. Shikh-Bahaei, "Collision Avoidance in V2X Communication Networks," *2019 IEEE Wireless Communications and Networking Conference Workshop (2019 IEEE WCNCW)*, pp. 1–6, 2019.

[C2] **J. Zang** and M. Shikh-Bahaei, "Full Duplex-Based Scheduling Protocol for Latency Enhancement in 5G eV2X VANETs," *2021 IEEE Wireless Communications and Networking Conference (2021 IEEE WCNC)*, pp. 1-6, 2021.

[C3] **J. Zang** and M. Shikh-Bahaei, "An Adaptive Full-Duplex Deep Reinforcement Learning-Based Design for 5G Mode 4 VANETs," *2021 IEEE Wireless Communications and Networking Conference (2021 IEEE WCNC)*, pp. 1-6, 2021.

[C4] W. Ding, **J. Zang** and M. Shikh-Bahaei, "An Efficient Relay Selection Scheme for Relay-assisted HARQ," *to be submitted*, pp. 1-6, 2021.

0.3 List of Journal Papers

[J1] **J. Zang**, V. Towhidlou and M. Shikh-Bahaei, "A Priority-Based Cross-Layer Design for Future VANETs Through Full-Duplex Technology," in *IEEE Transactions on Vehicular Technology*, vol. 69, no. 7, pp. 7531-7544, 2020.

[J2] **J. Zang** and M. Shikh-Bahaei, "Full-Duplex Multiple Access Mechanism for Connected Vehicles Operating at Different Automation Levels in NR eV2X Networks," in *IEEE Transactions on Intelligent Transportation Systems, Accepted/In press*, 2021.

[J3] **J. Zang**, M. Aljubayri, W. Ding and M. Shikh-Bahaei, "Feasibility Analysis of Full Duplex Technology in Enhancing MPTCP for URLLC Applications in B5G-IoV Networks," in *IEEE Transactions on Vehicular Technology, under* 2^{nd} *round review*, 2021.

[J4] **J. Zang**, Y. Zhang, Z. Yang and M. Shikh-Bahaei, "Full Duplex Technology in Next-Generation Wireless Communication Systems: Applications, Challenges and Opportunities," *to be submitted*, 2021.

[J5] **J. Zang**, W. Ding and M. Shikh-Bahaei, "Next-Generation Vehicular Communication and Networking: Vision, Challenges and Opportunities," *to be submitted*, 2021.

0.4 List of Patent

[Patent] **J. Zang** and M. Shikh-Bahaei, "Ad-Hoc Communication System for Intelligent Transportation with Simultaneous Transmission and Sensing," PCT Patent, PCT/GB2021/052454, 2021.

Nomenclature and Acronyms

IEEE	the **I**nstitute of **E**lectrical and **E**lectronics **E**ngineering
3GPP	**3**rd **G**eneration **P**artnership **P**roject
V2X	**V**ehicle-to-**E**verything
V2V	**V**ehicle-to-**V**ehicle
V2I	**V**ehicle-to- **I**frastructure
V2P	**V**ehicle-to- **P**edestrian
DSRC	**D**edicated **S**hort **R**ange **C**ommunication
WLAN	**W**ireless **L**ocal **A**rea **N**etwork
VANET	**V**ehicular **Ad H**oc **N**etwork
WAVE	**W**ireless **A**ccess in **V**ehicular **E**nvironment
ETSI	**E**uropean **T**elecommunications **S**tandards **I**nstitute
ITS	**I**ntelligent **T**ransportation **S**ystem
CSMA/CA	**C**arrier-**s**ense **M**ultiple **A**ccess with **C**ollision **A**voidance
CSMA/CA	**C**arrier-**s**ense **M**ultiple **A**ccess with **C**ollision **D**etection
C-V2X	**C**ellular **V2X**
LTE	**L**ong **T**erm **E**volution
FCC	**F**ederal **C**ommunications **C**ommission
NR	**N**ew **R**adio
KPI	**K**ey **P**erformance **I**ndicator
IBFD/FD	**I**n-**B**and **F**ull-**D**uplex
HD	**H**alf-**D**uplex
CW	**C**ontinuous **W**ave
SI	**S**elf-**I**nterference
SIS/SIC	**SI S**uppresion/**SI C**ancellation
ML	**M**achine **L**earning
PHY	**P**ysical Layer
MAC	**M**edium **A**ccess **C**ontrol Layer
NET	**N**etwork Layer
TRANS	**T**ransportation Layer
URLLC	**U**ltra-**R**eliable **L**ow-**L**atency **Communications**
eV2X	**e**nhanced-**V2X**
B5G	**B**eyond **5G**
IoV	**I**nternet-**o**f-**V**ehicles
BER	**B**it **E**rror **R**ate
SER	**S**ymbol **E**rror **R**ate
PSK	**P**hase **S**hift **K**eying

QAM	**Q**uadrature **A**mplitude **M**odulation
TDMA	**T**ime **D**ivision **M**ultiple **A**ccess
FDMA	**F**requency **D**ivision **M**ultiple **A**ccess
OFDMA	**O**rthogonal **F**requency **D**ivision **M**ultiple **A**ccess
AWGN	**A**dditive **W**hite **G**aussian **N**oise
DSB-SC	**D**ouble-**S**ide**B**and **S**uppressed **C**arrier
BPSK	**B**inary **PSK**
QPSK	**Q**uadrature **PSK**
ADC	**A**nalogue-to-**D**igital **C**onverter
CRC	**C**arrier **R**ecovery **C**ircuit
STRC	**S**ymbol **T**iming **R**ecovery **C**ircuit
PSD	**P**ower **S**pectrum **D**ensity
PAM	**P**ulse-**A**mplitude **M**odulation
DC	**D**irect **C**urrent
UL	**U**p**l**ink
DL	**D**own**l**ink
SL	**S**ide**l**ink
PDF	**P**ower **D**ensity **F**unction
NLoS	**N**-one-**L**ine-**o**f-**S**ight
AF	**A**mount of **F**ading
SNR	**S**ignal-to-**N**oise **R**atio
SINR	**S**ignal-to-**N**oise-plus-**I**nterference **R**atio
BS	**B**ase **S**tation
MS	**M**obile **S**tation
RSU	**R**oad**S**ide **U**nit
CSI	**C**hannel **S**tate **I**nformation
ACK	**A**cknowledgement
NACK	**N**egative **ACK**
AP	**A**ccess **P**oint
OBU	**O**n **B**oard **U**nit
i.i.d.	**i**ndependent and **i**dentically **d**istributed
DRL	**D**eep **R**einforcement **L**earning
DQN	**D**eep **Q** **N**etwork
FL	**F**ederated **L**earning
EDCA	**E**hanced **D**istributed **C**hannel **A**ccess
CAM	**C**ooperative **A**wareness **M**essage
BSM	**B**asic **S**afety **M**essage
AC	**A**ccess **C**ategory
AIFS	**A**rbitrary **I**nter-**F**rame **S**pace
PPP	**P**oisson **P**oint **P**rocess
RV	**R**andom **V**ariable
SB-SPS	**S**ensing-**B**ased **S**emi-**P**ersistent Protocol
FCFS	**F**irst **C**ome **F**irst **S**erve
RC	**R**eselection **C**ounter
RAC	**R**e-**A**ttempt **C**ounter

MPTCP	**M**ulti-**P**ath **T**ransmission **C**ontrol **P**rotocol
RB	**R**esource **B**lock
RPC	**R**e-**A**ttempt **P**ath **C**ounter
RTC	**R**e-**A**ttempt **T**ime **C**ounter
D2D	**D**evice-to-**D**evice
VUE	**V**ehicular **U**ser **E**quipment
UAV	**U**nmmaned **A**erial **V**ehicle
MDP	**M**arkov **D**ecision **P**rocess
CRN	**C**ognitive **R**adio **N**etwork
TS	**T**ransmission and **S**ensing
TR	**T**ransmission and **R**eception
PU	**P**rimary **U**ser
SU	**S**econdary **U**ser
LBT	**L**isten-**B**efore-**T**alk
LAT	**L**isten-**A**nd-**T**alk

1 Introduction

1.1 Background and Objectives

With the continuous and increasing expectations of future more intelligent transportation environment, next-generation vehicular systems have to be supported by advanced technologies, so that future transportation can be safer, greener and more efficient. To achieve this goal, vehicles has to be capable of sharing both safety- and non-safety-related (a.k.a. infotainment) information wirelessly with surrounding vehicles, infrastructures and even pedestrians. The general concept of sharing information between a vehicle and any entity was named as Vehicle-to-Everything (V2X) communication, which comprises of more specific types as Vehicle-to-Vehicle (V2V), Vehicle-to-Infrastructure (V2I), Vehicle-to-Pedestrian (V2P) communications and so on.

In 1999, the first family of standards that support V2X communication released, which was named as the Dedicated Short Range Communication (DSRC) [1], or IEEE 802.11p standard. As the standard name shows, DSRC was built upon the IEEE 802.11 series of wireless local area network (WLAN) technologies. It enabled vehicles (i.e. V2V) and infrastructures (i.e. V2I) to form a vehicular ad hoc network (VANET) as transceivers to communicate, which is the key to improve the quality of future transportation system. The radio technology was a part of the IEEE 802.11 family of standards and known as Wireless Access in Vehicular Environments (WAVE) in the U.S., and European Telecommunications Standards Institute Intelligent Transportation System G5 (ETSI ITS-G5) in Europe.

Besides the DSRC standard, the other and more recent family of standards that can also support V2X communications is namely the 3^{rd} Generation Partnership Project (3GPP) cellular V2X (C-V2X) standard. It operates based on the cellular technologies including the 4G Long Term Evolution (LTE) V2X communications, namely 4G-V2X or LTE-V2X, in Release 14 [2], and the 5G or New Radio (NR)

V2X communications, namely 5G-V2X or NR-V2X, in Release 15 [3] and currently ongoing Releases 16 [4] and 17 [5], respectively. Since both LTE-V2X and NR-V2X communications operate based on the cellular technologies (i.e. 4G and 5G), they utilise the 4G and 5G infrastructures and technologies to provide the communication capability, which is different from the paradigm of the DSRC standard.

Although the DSRC and the C-V2X standards have been compared with each other thoroughly in terms of various Key Performance Indicators (KPIs), the goal of having a global unified family of V2X standards have not been achieved yet, because both standards are undergoing extensive enhancements to satisfy future abundant and dynamic V2X applications, and each standard has its own pros and cons. Therefore, it is meaningful to explore and propose novel technologies to improve the performance of both DSRC and C-V2X standards, which is also one of the objectives of this PhD project. Furthermore, another important reason to propose novel designs based on both DSRC and C-V2X standards is because neither of them can achieve the target performance. For example, in [6] and [7], the authors have shown that the access delay of the EDCA mechanism in the DSRC standard can go up to 900 ms, which is 9 times of the target performance, which is 100 ms [1]. A real-world field test has been conducted to evaluate its performance, which has also been shown in [8] that the latency goes beyond the 100 ms target when the speed of the vehicle is higher than 35 mph. Similarly, despite the more detailed classification of different use cases in the C-V2X standard, the general target of an LTE-based V2X system is expected to also provide at most 100 ms delay performance, and 5G NR-based V2X system has even much more stringent QoS requirements. However, according to the analysis papers such as [9] and [10], neither the reliability nor the latency has achieved the target QoS requirements. Therefore, novel designs are needed to be proposed.

The In-Band Full-Duplex (IBFD) communication technology, hereafter FD technology, is one of the most promising wireless communication technologies for beyond 5G (B5G) and 6G networks, because it enables a transceiver to transmit and receive simultaneously over the same frequency band, which in turn can theoretically double the link capacity and spectrum efficiency as well as significantly reduce latency compared to the conventional Half-Duplex (HD) technology [11]. FD technology has a long history, it was firstly considered and developed in the

continuous wave (CW) radar systems in the 1940s [12]. But until 2000s, FD technology has not been widely considered for wireless communication systems [11], let alone applying it to the recently raised V2X communications. The most challenging obstacle of applying FD technology is its severe inherent loop-back signals, or Self-Interference (SI) signals, caused by the reception of signals from its own transmission antenna. In addition, the high mobility characteristic of V2X communications makes the SI Suppression (SIS), or SI Cancellation (SIC) processes even more difficult compared to normal cellular communications. However, due to the fact that vehicles have a much bigger size which is beneficial for passive SIS, applying the FD technology to V2X communications is easier than applying it to conventional small mobile devices such as a mobile phone [13]. Unlike most FD applications which are designed based on the simultaneous bi-directional information transmission and reception feature [11], this thesis focuses on investigating how to take advantage of the simultaneous information transmission and sensing feature, which is an area that has paid less attention to, especially in applying it to the V2X communications [11]. For example, in both DSRC and C-V2X systems, the PHY layer technologies for supporting a VANET are sensing-based approaches, and the safety-related information is shared in a broadcasting manner [1], [2]-[5]. Therefore, an ACK mechanism is not needed, and the FD simultaneous information transmission and sensing feature can be used to provide instantaneous feedback [11].

Furthermore, at the end of the 20^{th} century, machine learning (ML) technologies, which are a set of effective methods that can solve problems where conventional methods struggle to provide outstanding performance, started to flourish in a number of fields such as education and finance. Besides these fields, applying ML to the field of wireless communication has also become a hot and promising research direction. ML technologies have been shown to be an effective tool in solving many wireless communication problems such as coverage and mobility prediction, energy efficiency optimisation, resource allocation and so on [14]. However, investigating the feasibility of each and every ML technology and proposing novel and suitable ML solutions for future V2X networks is a relatively new topic, it requires more research effort.

In this PhD project and thesis, the objectives include the study of various Physical (PHY) layer modulation and multiple access technologies, interference and

wireless channel models, spectrum sensing technologies, Multiple Access Control (MAC) layer protocols, Network (NET) and Transport (TRANS) layer protocols, FD technologies, ML technologies, DSRC standard as well as C-V2X standard. Specifically, I have started from the theoretical study and regeneration of various modulation and multiple access technologies. Then, I have investigated multiple popular spectrum sensing and FD technologies. Next, I have proposed an adaptive FD energy sensing method based on the DSRC standard, which can be applied to the C-V2X-based sensing process due to the fact that the core sensing technology of both standards is the energy detection method. On the basis of the proposed FD sensing strategy, I have considered the MAC layer challenges of DSRC, and proposed a priority-based cross-layer design across the PHY and MAC layers for future VANETs through FD technology. It has been shown that both latency and reliability performances have been improved compared to the standardised DSRC technologies. Besides the contribution based on the DSRC family of standards, based on the 5G-V2X standard, I have also proposed a FD-based scheduling protocol that has been shown to be capable of reducing latency. After that, I have extended this research to the reliability analysis, as future V2X applications belong to the ultra-reliable low-latency communications (URLLC) area. It has been shown that the proposed FD multiple access mechanism has not only enhanced the latency performance, but also the reliability performance compared to the 5G-V2X standardised technologies. Afterwards, I have explored the feasibility of combining ML and FD technologies for future enhanced-V2X (eV2X) networks. I have proposed an adaptive FD deep reinforcement learning-based design, which has been shown to outperform the 5G-V2X standardised technologies, and can be considered for supporting the next-generation eV2X networks. Furthermore, motivated by the lack of study in the TRANS layer for B5G/6G-Internet of Vehicles (IoV) networks, I have proposed a FD-based multi-path transmission control protocol, namely FDMP, to address the concern about the feasibility of FD technology in enhancing TRANS layer protocols for URLLC applications in future vehicular networks. It has been shown that the proposed FDMP can significantly reduce the latency. I have also found that the FDMP design is more suitable for dense network scenarios in terms of reliability, as it has been shown that FDMP has a much better reliability performance in the dense network scenario compared to the sparse network scenario. Finally, in order to help other researchers understand the next-generation FD technology

and V2X technology, I have surveyed literature and proposed my vision, applications, challenges and opportunities of both technologies.

1.2 Thesis Structure

In Chapter 2, I provide an overview of various modulation and multiple access technologies along with common interference, channel models and corresponding Bit Error Rate (BER)/Symbol Error Rate (SER) regeneration results, spectrum sensing technologies, FD technologies, DSRC standard and C-V2X standard. Respective literature review sections in Chapter 3 to Chapter 6 accompany this Chapter with focuses on frontier research works.

In Chapter 3, I introduce the proposed adaptive FD energy sensing method for collision detection and avoidance in V2X communication networks.

In Chapter 4, I deliver the proposed FD cross-layer design which was developed on the basis of the DSRC standardised technologies and their challenges.

In Chapter 5, I demonstrate the proposed 5G-based FD scheduling and multiple access mechanism, in which different operating autonomous levels have been taken into consideration for the first time.

In Chapter 6, I present the proposed adaptive FD deep reinforcement learning-based design, which was developed for 5G-V2X Mode 4 VANETs.

In Chapter 7, I first give the applications, challenges and opportunities of FD technology in multiple next-generation wireless communication systems, including FD 6G-V2X networks, FD unmanned aerial vehicle (UAV) networks with energy harvesting systems and ML aided FD communication systems. Next, I give my vision, challenges and opportunities of next-generation vehicular communications and networking, including the evolved communication architectures, the DSRC-based technologies and C-V2X-based technologies.

Finally, I conclude this PhD project and thesis, and present my future works in Chapter 8, before the Bibliography and Appendix.

2 Background

Synopsis of Chapter

This chapter reviews the fundamentals of the following technologies, as they are the most important integral parts of my proposed designs in Chapters 3 to 7.

Section 2.1 presents the regeneration results, which refer to the BER and/or SER performance of transmitting a message by using various combinations of the M-PSK and/or M-QAM technologies with/without the OFDMA technology when AWGN and/or fading exist.

Section 2.2 reviews major spectrum sensing technologies, which include energy detection, matched filter, cyclostationary feature detection and eigenvalue detection. Since the energy detection technology is the most widely applied method, which is also the technology being deployed in both DSRC and C-V2X standards, I focus on the theory, mathematical interpretation and performance analysis of the energy detection technology.

Section 2.3 reviews history, developments and state-of-the-art achievements of FD technology.

Finally, Section 2.4 focuses on introducing the standardised supporting technologies for V2X communications and networking in the DSRC standard and the C-V2X standard.

2.1 Regeneration Results - BER/SER Performance

BER/SER performance of various combinations of different modulation, multiple access technologies in the presence of different channel conditions are shown in this section. *MATLAB* is the simulation platform used for the regeneration.

2.1.1 BPSK Systems

2.1.1.1 AWGN

Fig. 2.1 shows the BER performance of BPSK systems in the presence of AWGN. Neither Rayleigh fading nor Rician fading is considered.

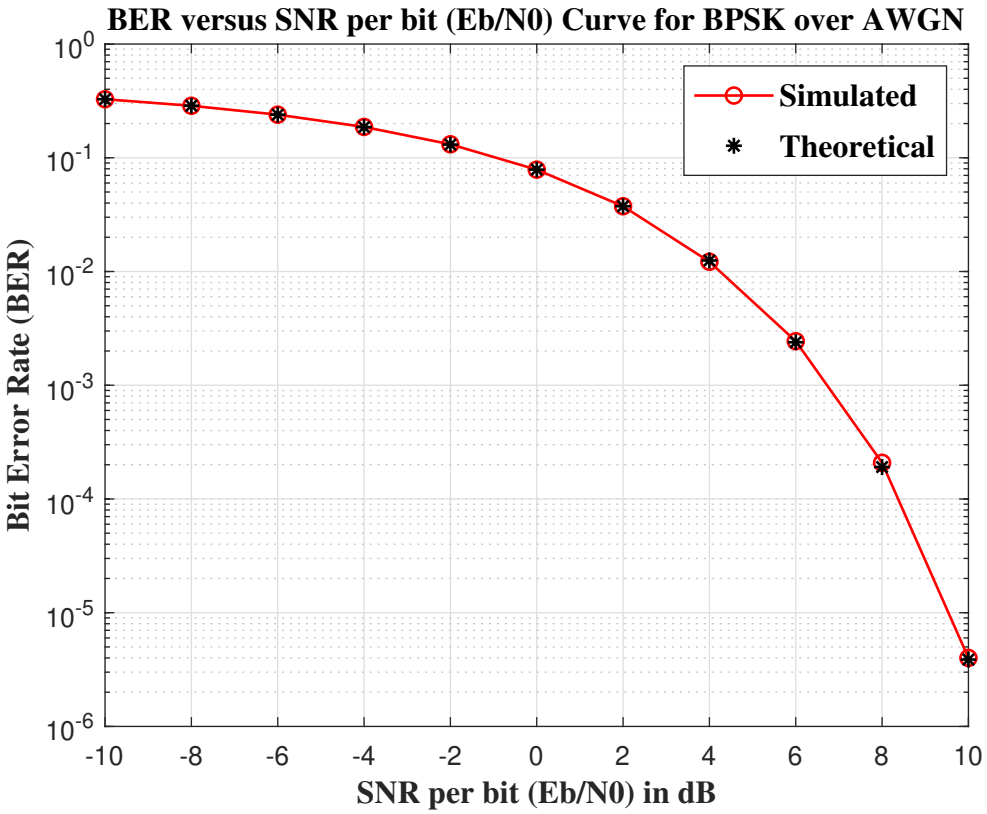

FIGURE 2.1: BER versus SNR per bit E_b/N_0 curve for BPSK systems over AWGN

Theoretical BER, P_e, in this case is given by

$$P_e = \frac{1}{2} \cdot erfc(\sqrt{\frac{E_b}{N_0}}), \tag{2.1}$$

where $erfc(.)$ refers to the complementary error function.

2.1.1.2 AWGN and Rayleigh fading

Fig. 2.2 shows the BER performance of BPSK systems in the presence of AWGN over a Rayleigh fading channel.

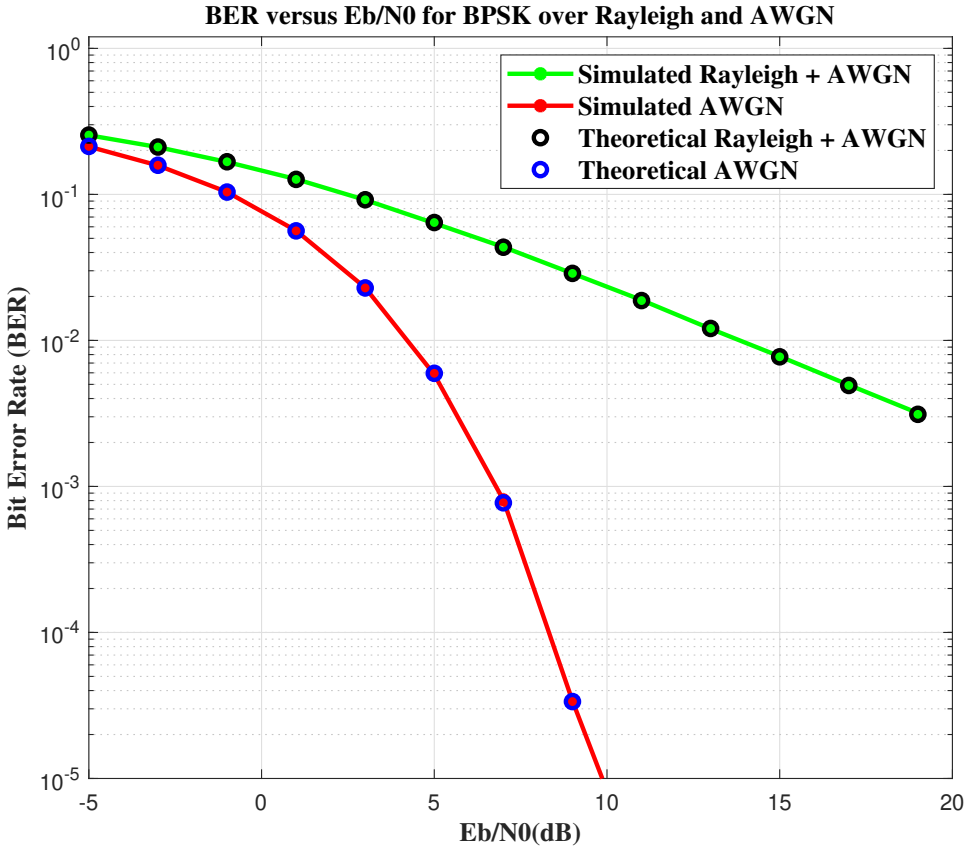

FIGURE 2.2: BER versus SNR per bit E_b/N_0 curve for BPSK systems over AWGN and Rayleigh

Theoretical BER, P_e, in this case is given by

$$P_e = \frac{1}{2} \cdot (1 - \sqrt{\frac{\frac{E_b}{N_0}}{1 + \frac{E_b}{N_0}}}). \tag{2.2}$$

2.1.1.3 AWGN and Rician fading

Fig. 2.3 shows the simulated BER performance of BPSK systems in the presence of AWGN over a Rician fading channel.

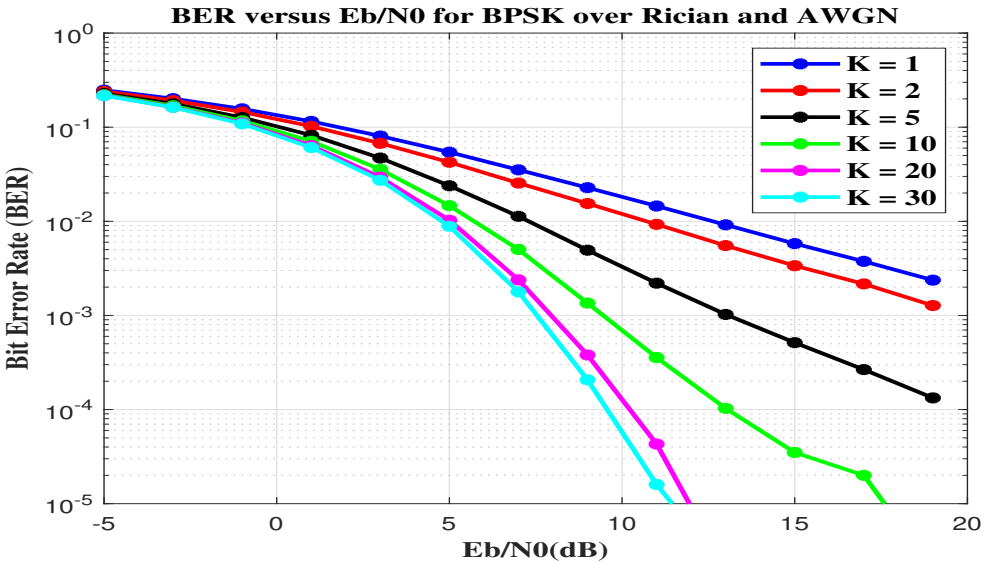

FIGURE 2.3: Simulated BER versus SNR per bit E_b/N_0 curve for BPSK systems over AWGN and Rician

Theoretical BER performance in this case is cross-checked with the *BERTOOL*, which is a built-in tool in *MATLAB* that generates theoretical values according to the provided conditions such as the values for K and channel model.

The *BERTOOL* is shown in Fig. 2.4.

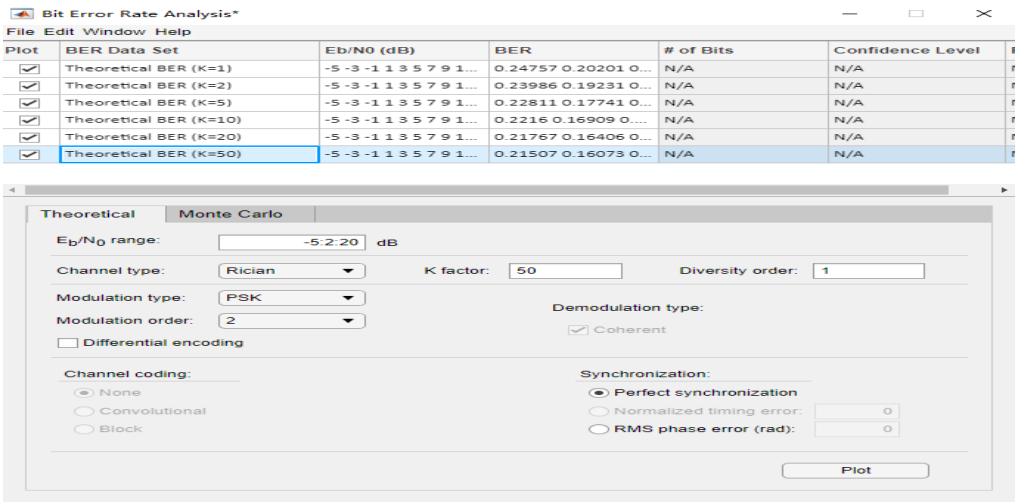

FIGURE 2.4: BERTOOL

Theoretical BER performance is shown in Fig. 2.5.

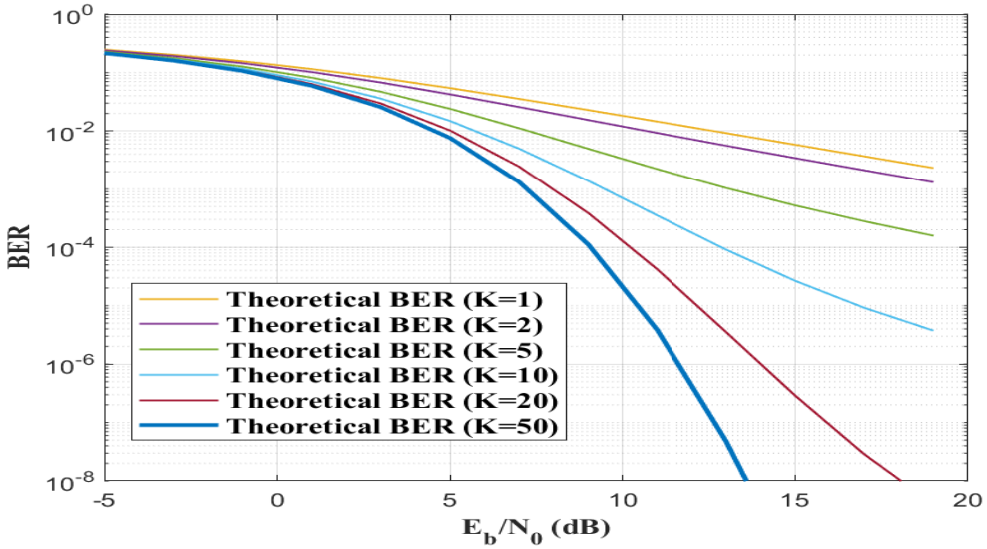

FIGURE 2.5: Theoretical BER versus SNR per bit E_b/N_0 curve for BPSK systems over AWGN and Rician

2.1.2 QPSK Systems

2.1.2.1 AWGN

Fig. 2.6 shows the BER performance of QPSK systems in the presence of AWGN. Neither Rayleigh fading nor Rician fading is considered.

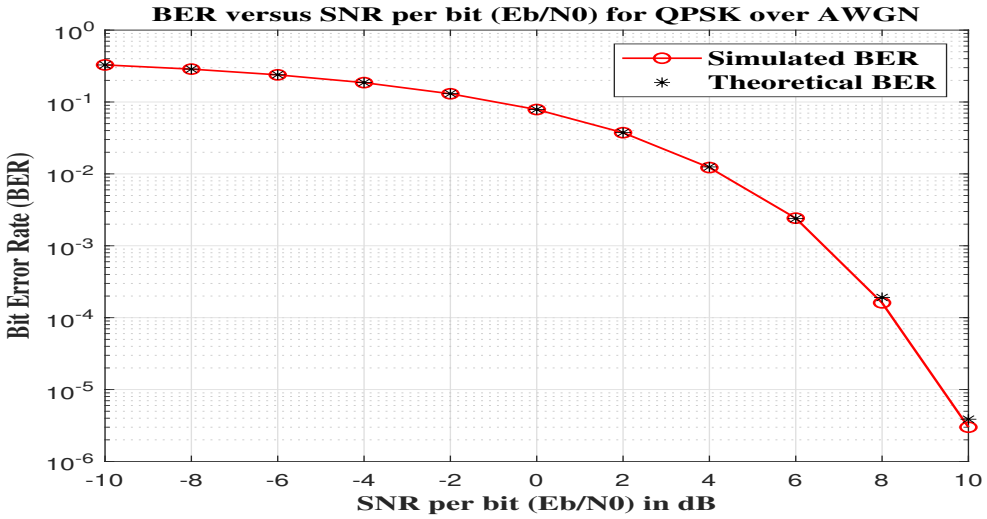

FIGURE 2.6: BER versus SNR per bit E_b/N_0 curve for QPSK systems over AWGN

Since a QPSK system consists of two orthogonal BPSK systems, they do not interfere with each other, and the BER curve for QPSK systems in the presence of

AWGN is identical to that of BPSK systems, which is given by Eq. (2.1).

2.1.2.2 AWGN and Rayleigh fading

Fig. 2.7 shows the BER performance of QPSK systems in the presence of AWGN over a Rayleigh fading channel.

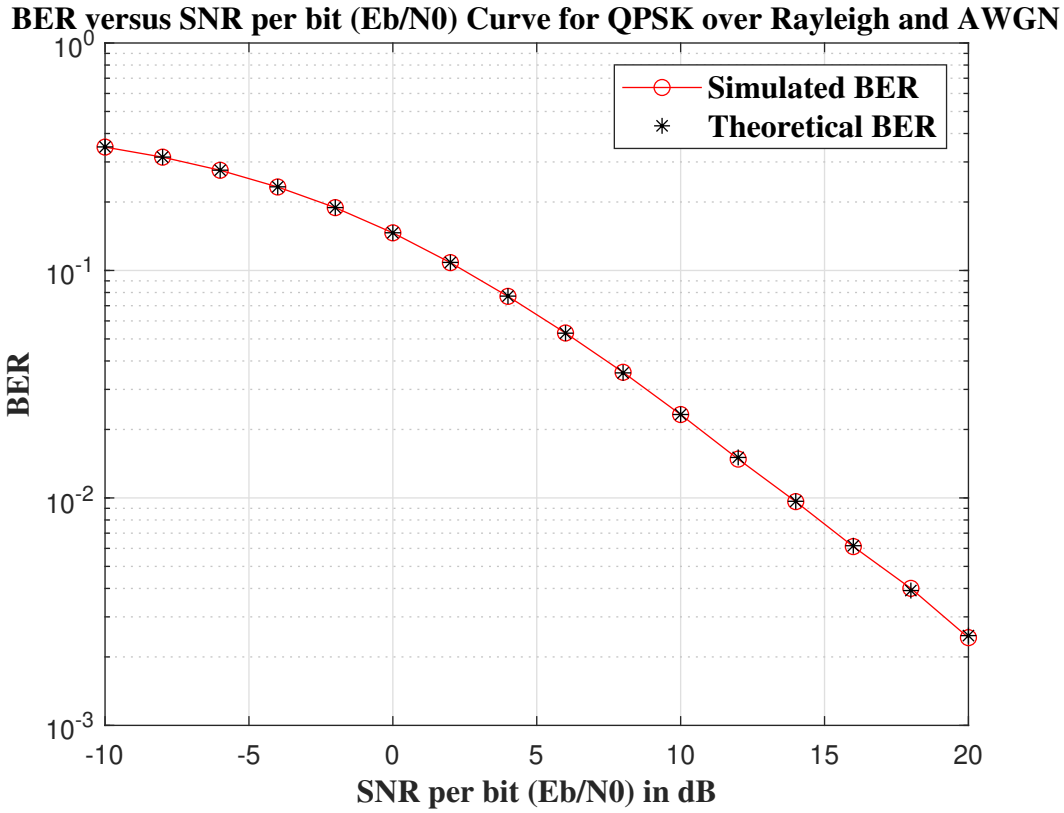

FIGURE 2.7: BER versus SNR per bit E_b / N_0 curve for QPSK systems over AWGN and Rayleigh

2.1.3 Higher-Order M-PSK Systems

2.1.3.1 AWGN

Fig. 2.8 shows the SER performance of various M-PSK systems in the presence of AWGN. Neither Rayleigh fading nor Rician fading is considered.

Theoretical SER, P_s, for M-PSK systems in the presence of AWGN is given by [15]

$$P_s = erfc[\sqrt{(\frac{E_b}{N_0} \cdot k)} \cdot \sin(\frac{\pi}{M})], \tag{2.3}$$

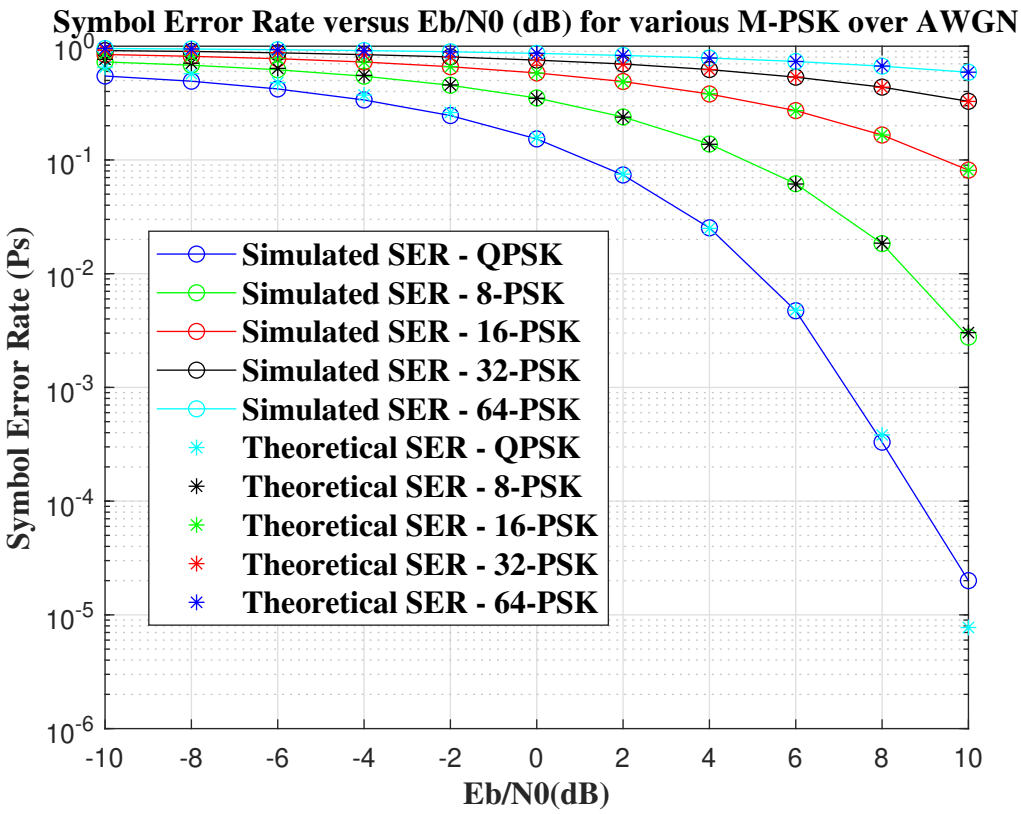

FIGURE 2.8: SER versus SNR per bit E_b/N_0 for various M-PSK systems over AWGN

where $k = log_2(M)$, and M refers to the order of the M-PSK systems.

2.1.3.2 AWGN and Rayleigh fading

Fig. 2.9 shows the SER performance of various M-PSK systems in the presence of AWGN over a Rayleigh fading channel.

Theoretical SER, P_s, for M-PSK systems in the presence of AWGN over Rayleigh fading channel is given by [15]

$$P_s = \frac{1}{\pi}\int_0^{(M-1)\frac{\pi}{M}} \prod_{l=1}^{L} M_{\gamma l}\left(-\frac{\sin^2(\frac{\pi}{M})}{\sin^2\theta}\right)d\theta, \tag{2.4}$$

where L refers to the number of diversity branches.

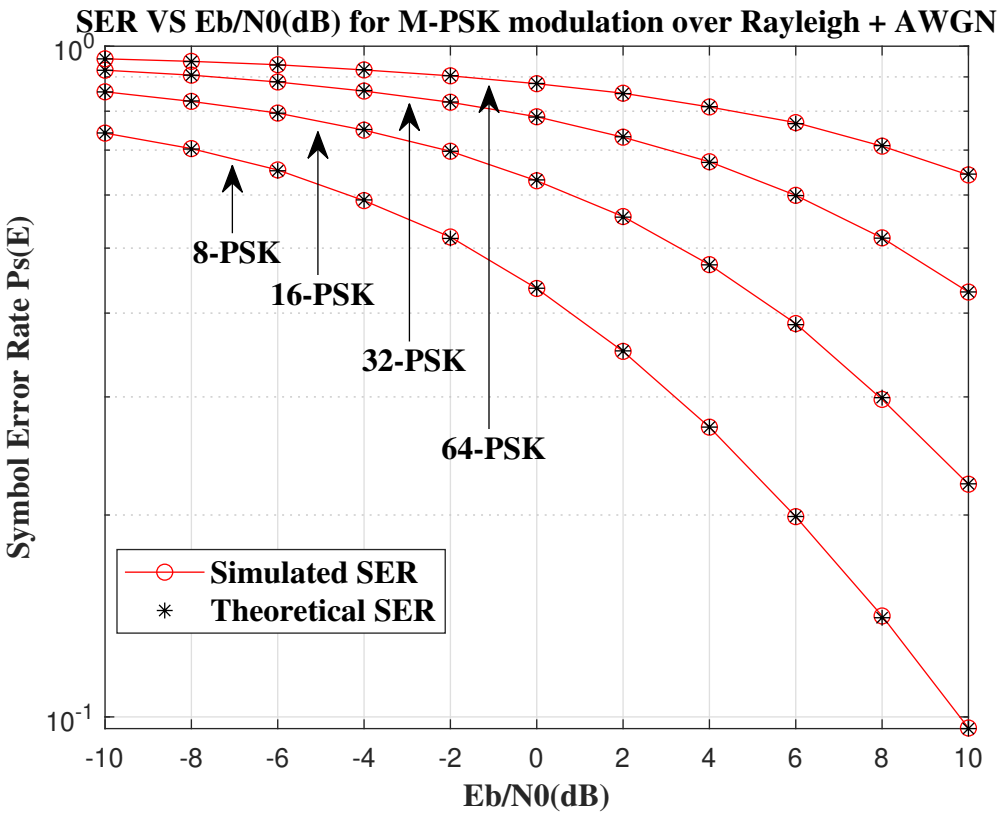

FIGURE 2.9: SER versus SNR per bit E_b/N_0 for various M-PSK systems over AWGN and Rayleigh

2.1.4 16-QAM Systems

2.1.4.1 AWGN

Fig. 2.10 and Fig. 2.11 illustratively show the constellation diagrams of the transmitted and received 16-QAM symbols in the presence of AWGN. Neither Rayleigh fading nor Rician fading is considered.

Compared the received 16-QAM symbols to the transmitted symbols in the constellation diagrams, we can see that both the quadrature component and the in-phase component are drifted from the designed points due to the impact of AWGN, which degrades the demodulation accuracy, and leads to transmission errors. However, if the SNR per bit, E_b/N_0, is increased, as shown in Fig. 2.11, it is more likely for the demodulator to demodulate correctly, because with a larger E_b/N_0, the received symbols have smaller Hamming distances to the expected and ideal constellation points. In other words, the higher the order of the modulation technology (i.e. M) is used, the weaker the anti-interference capability is,

due to the closer distance between two arbitrary constellation points.

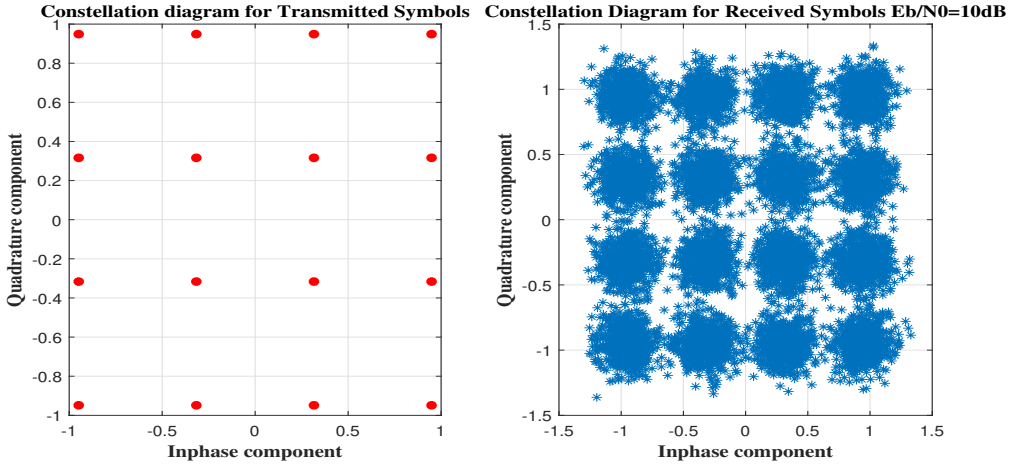

FIGURE 2.10: An illustrative constellation diagram of the transmitted and received 16-QAM symbols in the presence of AWGN with 10 dB E_b/N_0

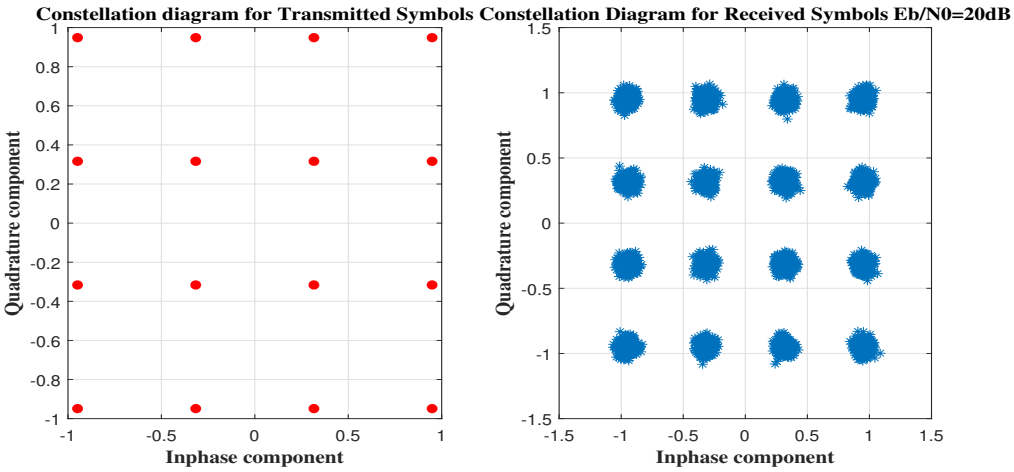

FIGURE 2.11: An illustrative constellation diagram of the transmitted and received 16-QAM symbols in the presence of AWGN with 20 dB E_b/N_0

Fig. 2.12 shows the SER performance of 16-QAM systems in the presence of AWGN. No fading is considered.

Theoretical SER, P_s, and $k = log_2 M$ is even, for square M-QAM systems in the presence of AWGN is given by [15], [16]

$$P_s = \frac{4\sqrt{M}-1}{\sqrt{M}} Q\left(\sqrt{\frac{3}{M-1}\cdot\frac{kE_b}{N_0}}\right) - 4\left(\frac{\sqrt{M}-1}{\sqrt{M}}\right)^2 Q^2\left(\sqrt{\frac{3}{M-1}\cdot\frac{kE_b}{N_0}}\right). \quad (2.5)$$

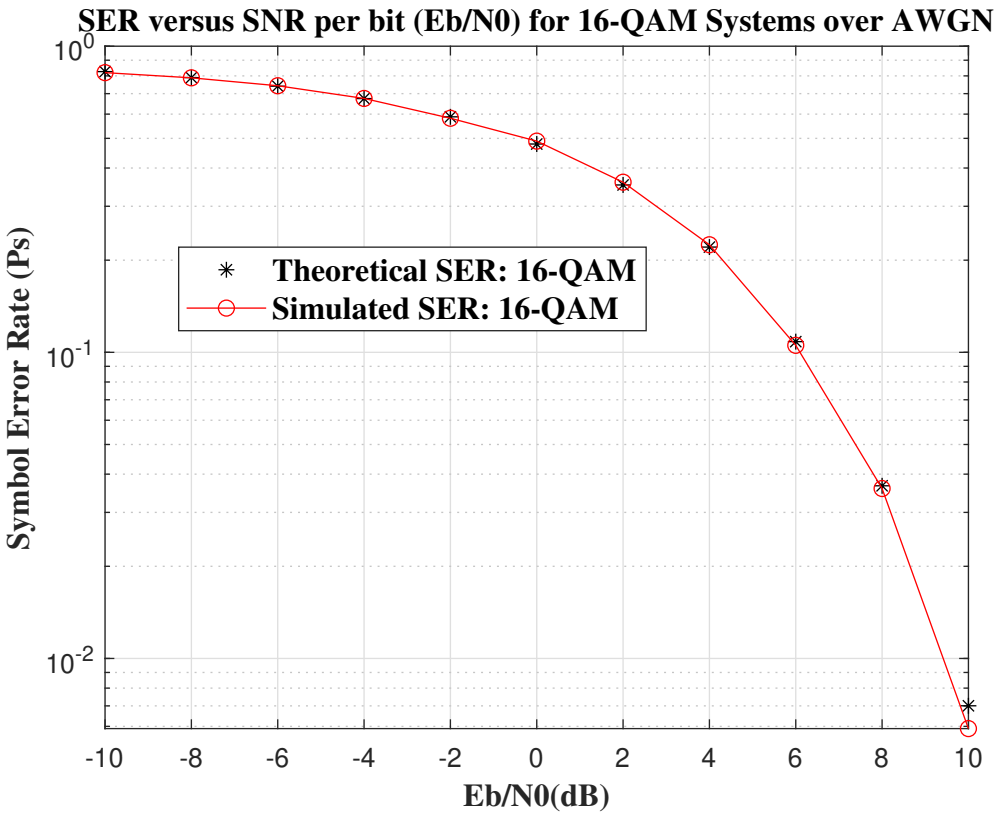

FIGURE 2.12: SER versus SNR per bit E_b/N_0 for 16-QAM systems over AWGN

2.1.4.2 AWGN and Rayleigh fading

Fig. 2.13 shows the SER performance of 16-QAM systems in the presence of AWGN over a Rayleigh fading channel.

Theoretical SER, P_s, and $k = log_2 M$ is even, for square M-QAM systems in the presence of AWGN over Rayleigh fading channel is given by [15]

$$\begin{aligned} P_s =& \frac{4}{\pi}(1-\frac{1}{\sqrt{M}})\int_0^{\frac{\pi}{2}}\prod_{l=1}^{L} M_{\gamma l}(-\frac{\frac{3}{2(M-1)}}{\sin^2\theta})d\theta \\ &- \frac{4}{\pi}(1-\frac{1}{\sqrt{M}})^2\int_0^{\frac{\pi}{4}}\prod_{l=1}^{L} M_{\gamma l}(-\frac{\frac{3}{2(M-1)}}{\sin^2\theta})d\theta. \end{aligned} \tag{2.6}$$

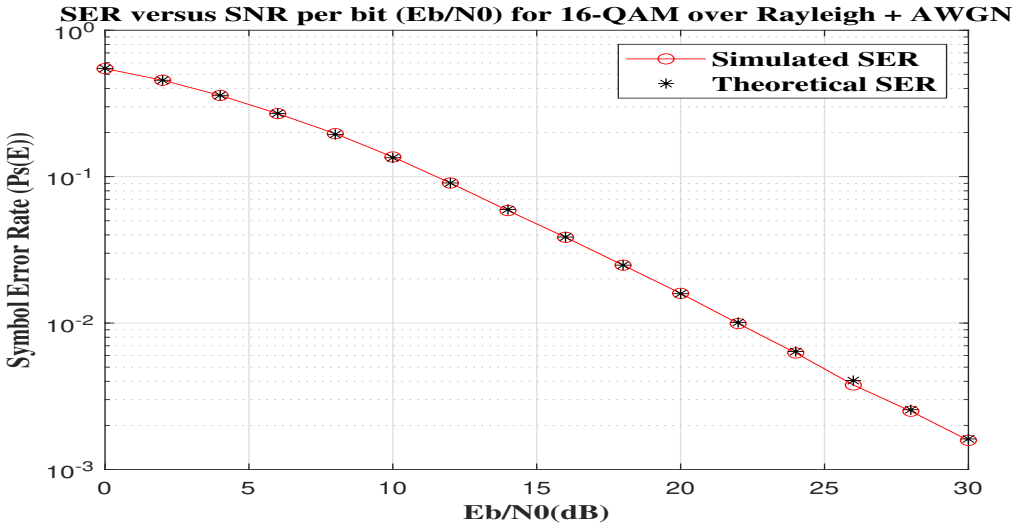

FIGURE 2.13: SER versus SNR per bit E_b/N_0 for 16-QAM systems over AWGN and Rayleigh

2.1.5 64-QAM Systems

2.1.5.1 AWGN

Fig. 2.14 shows an illustrative constellation diagram of the transmitted and received 64-QAM symbols in the presence of AWGN. Neither Rayleigh fading nor Rician fading is considered.

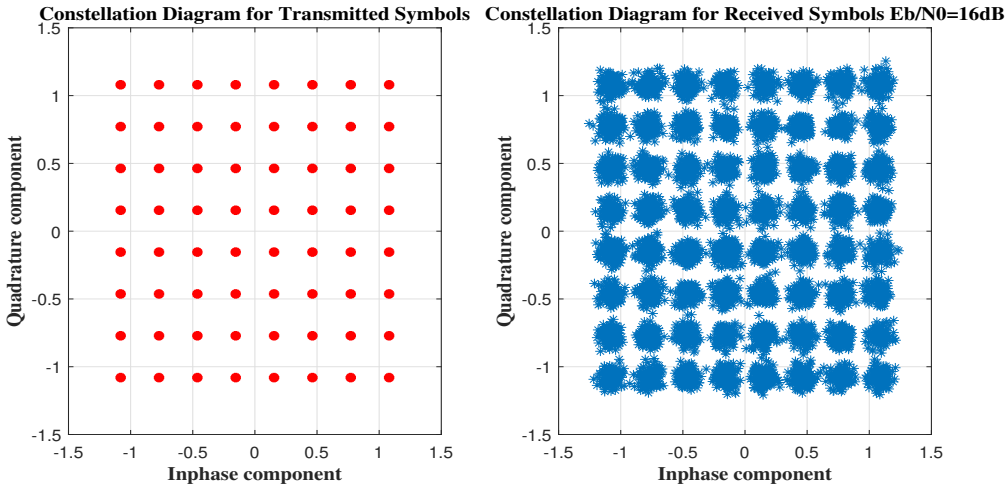

FIGURE 2.14: An illustrative constellation diagram of the transmitted and received 64-QAM symbols over AWGN

Fig. 2.15 shows the SER performance.

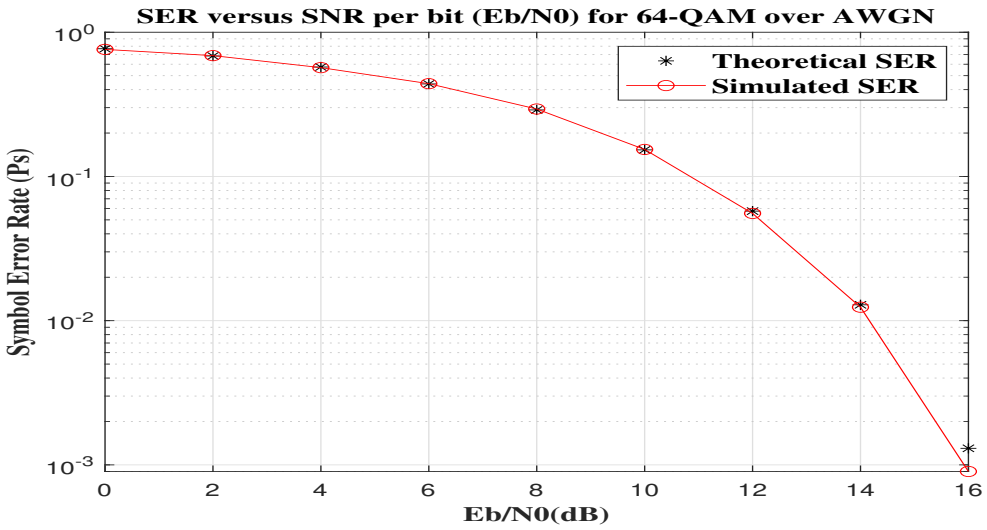

FIGURE 2.15: SER versus SNR per bit E_b/N_0 for 64-QAM systems over AWGN

2.1.5.2 AWGN and Rayleigh fading

Fig. 2.16 shows the SER performance of 64-QAM systems in the presence of AWGN over a Rayleigh fading channel. Neither Rayleigh fading nor Rician fading is considered.

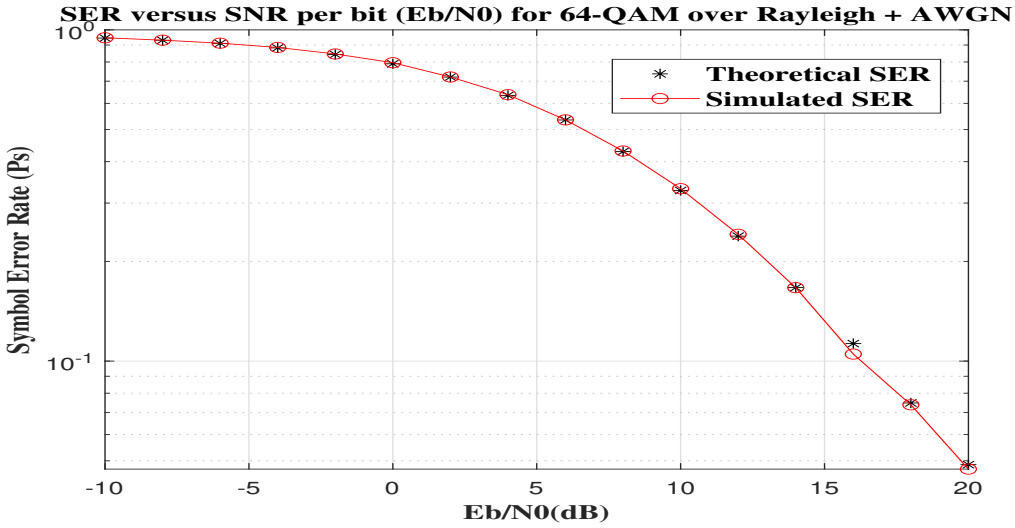

FIGURE 2.16: SER versus SNR per bit E_b/N_0 for 64-QAM systems over AWGN and Rayleigh

2.1.6 OFDMA + M-PSK Systems

2.1.6.1 AWGN

Fig. 2.17 shows the SER performance of an OFDMA system with various M-PSK modulation technologies in the presence of AWGN. Neither Rayleigh fading nor Rician fading is considered.

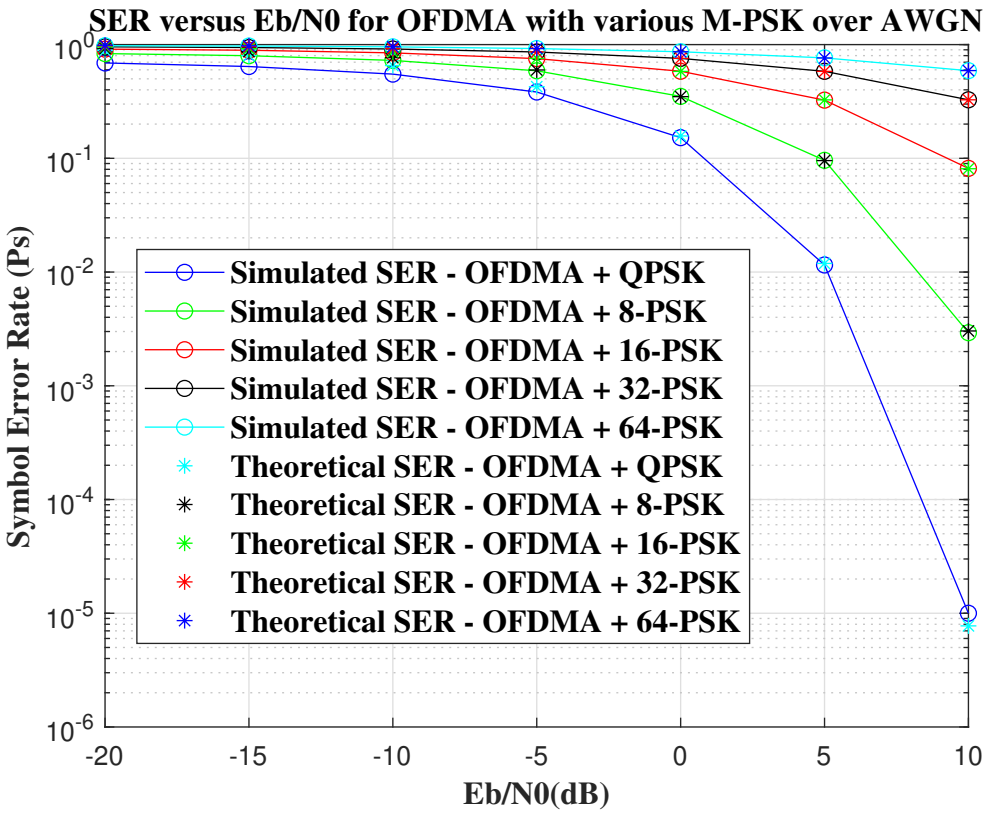

FIGURE 2.17: SER versus SNR per bit E_b / N_0 for OFDMA with various M-PSK in the presence of AWGN

2.1.6.2 AWGN and Rayleigh fading

Fig. 2.18 shows the SER performance of various M-PSK systems in the presence of AWGN over a Rayleigh fading channel.

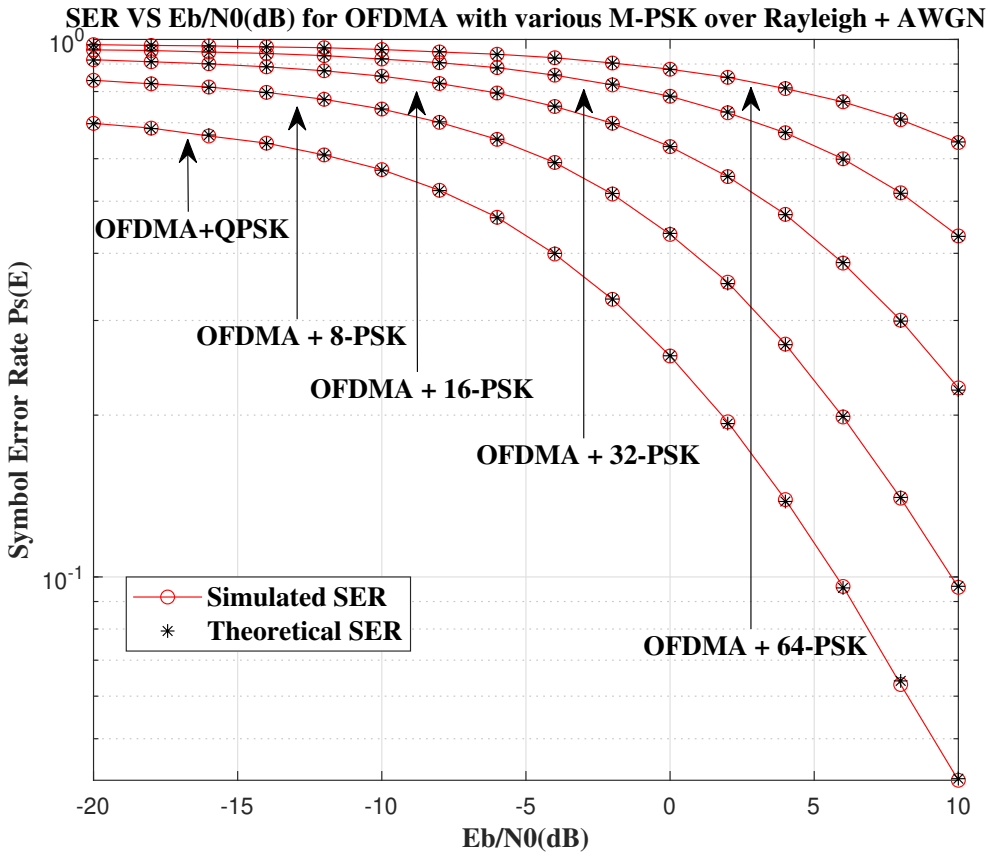

FIGURE 2.18: SER versus SNR per bit E_b / N_0 for OFDMA with various M-PSK over AWGN and Rayleigh

2.1.7 OFDMA + 16-QAM Systems

2.1.7.1 AWGN

Fig. 2.19 shows the SER performance of an OFDMA system with 16-QAM modulation technology in the presence of AWGN. Neither Rayleigh fading nor Rician fading is considered.

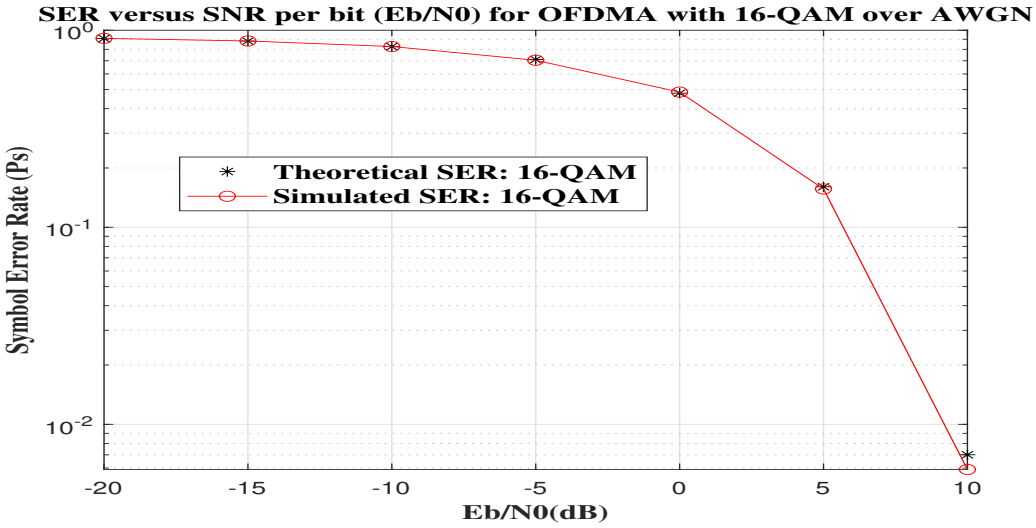

FIGURE 2.19: SER versus SNR per bit E_b/N_0 for OFDMA with 16-QAM in the presence of AWGN

2.1.7.2 AWGN and Rayleigh fading

Fig. 2.20 shows the SER performance of an OFDMA system with 16-QAM in the presence of AWGN over a Rayleigh fading channel.

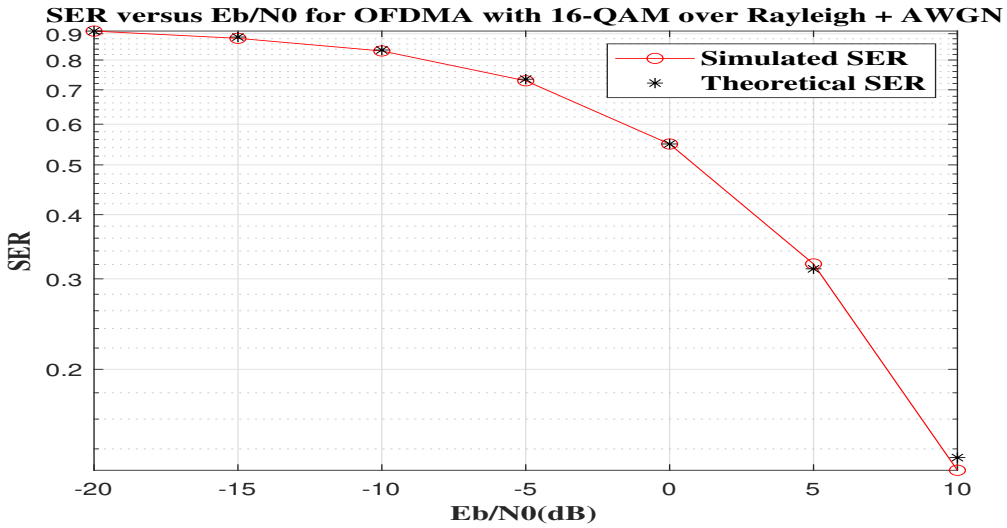

FIGURE 2.20: SER versus SNR per bit E_b/N_0 for OFDMA with 16-QAM in the presence of AWGN over a Rayleigh fading channel

2.1.8 OFDMA + 64-QAM Systems

2.1.8.1 AWGN

Fig. 2.21 shows the SER performance of an OFDMA system with 64-QAM in the presence of AWGN. Neither Rayleigh fading nor Rician fading is considered.

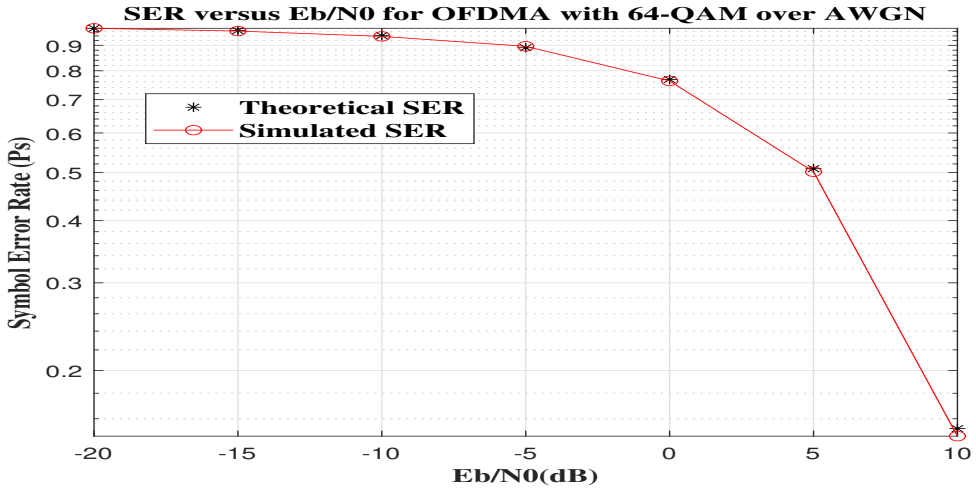

FIGURE 2.21: SER versus SNR per bit E_b/N_0 for OFDMA with 64-QAM in the presence of AWGN

2.1.8.2 AWGN and Rayleigh fading

Fig. 2.22 shows the SER performance of an OFDMA system with 64-QAM in the presence of AWGN over a Rayleigh fading channel.

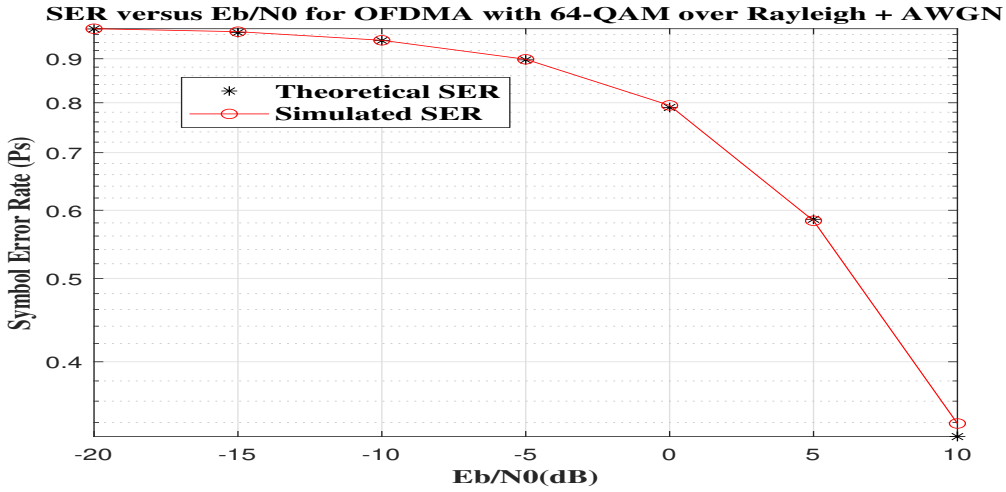

FIGURE 2.22: SER versus SNR per bit E_b/N_0 for OFDMA with 64-QAM in the presence of AWGN over a Rayleigh fading channel

2.2 Spectrum Sensing Technologies

Spectrum sensing is one of the core integral parts of multiple wireless networks, since spectrum sensing technologies provide awareness of the spectrum status to different nodes, which in turn is used as the foundation of further actions such as resource allocation and scheduling. In this section, I present some of the most widely-applied spectrum sensing technologies.

2.2.1 Energy Detection

Among all spectrum sensing technologies, energy detection is the most common and widely-applied method due to its low implementation cost, low computational complexity and its advantage of not requiring neither channel gains nor other parameter estimates [17], [18].

An energy detector first measures the received signal energy within the target bandwidth and time period. Then the measured energy is compared to a threshold which depends on the noise floor to determine the status of the spectrum. The main challenges of designing and deploying an energy detector include setting up the right threshold, differentiate interference and enhance performance in low SNR regions [18]. Besides energy detectors have also been shown that they cannot provide accurate and efficient sensing results in detecting spread spectrum signals [19], [20].

The received signal, r, at an energy detector, is sampled, the n^{th} sample, $r(n)$, is given by

$$r[n] = \begin{cases} w[n]; & H_0 \\ x[n] + w[n]; & H_1, \end{cases} \tag{2.7}$$

where $x[n]$ refers to the signal to be detected, $w[n]$ refers to the AWGN signal. Moreover, in this binary hypothesis testing problem, H_0 refers to the hypothesis that the signal to be detected, $x[n]$, is absent, and H_1 refers the hypothesis that the signal to be detected, $x[n]$, is present.

The test statistic of this energy detector, E, is given by

$$E = \frac{1}{N} \sum_{n=0}^{N} |r[n]|^2, \tag{2.8}$$

where N refers to the number of samples, which is given by

$$N = f_s \cdot T_s, \tag{2.9}$$

where f_s refers to the sampling frequency, and T_s refers to the sampling duration.

Next, in order to determine whether the target bandwidth has been occupied or not, the energy test statistic, E, is compared against a pre-defined fixed threshold, ϵ. The bandwidth is regarded as an occupied resource if the measured energy is greater than the threshold. Otherwise, the medium is regarded as a free resource that can be allocated to a user. Thus sensing errors may occur, and we have to evaluate the performance of this method.

The performance of the energy detection technology is normally evaluated by three types of probabilities, which are detection probability, false alarm probability and mis-detection probability. The detection probability is defined as the probability that the measured energy is greater than the threshold when the signal $x[n]$ is actually present. The false alarm probability is defined as the probability that the measured energy is greater than the threshold when the signal $x[n]$ is actually absent. The mis-detection probability is defined as the probability that the measured energy is smaller than the threshold when the signal $x[n]$ is actually present.

The detection probability, P_d, is formulated as [18]

$$P_d = Pr\{E > \epsilon | H_1\} = \int_0^{+\infty} p_1(x)dx, \tag{2.10}$$

where $p_1(x)$ refers to the PDF of the energy test statistic, E, under hypothesis H_1. The false alarm probability, P_f, is formulated as [18]

$$P_f = Pr\{E > \epsilon | H_0\} = \int_0^{+\infty} p_0(x)dx, \tag{2.11}$$

where $p_0(x)$ refers to the PDF of the energy test statistic, E, under hypothesis H_0, and the mis-detection probability, P_m, is formulated as [18]

$$P_m = Pr\{E < \epsilon | H_1\} = 1 - P_d. \tag{2.12}$$

According to the CLT, the AWGN can be modeled as a zero-mean Gaussian random variable with variance σ_w^2, which can be represented as

$$w[n] = N(0, \sigma_w^2). \tag{2.13}$$

For a simplified evaluation, the signal $x[n]$ can also be modeled as a zero-mean Gaussian random variable, which is given by

$$x[n] = N(0, \sigma_s^2). \tag{2.14}$$

Note that the model for $x[n]$ will become much more complicated when fading is taken into consideration.

According to the above assumptions, the energy test statistic, E, follows Chi-square distribution with $2N$ degrees of freedom, χ_{2N}^2, which is given by

$$E = \begin{cases} \frac{\sigma_w^2}{2}\chi_{2N}^2; & H_0 \\ \frac{\sigma_w^2 + \sigma_s^2}{2}\chi_{2N}^2; & H_1, \end{cases} \tag{2.15}$$

Hence, the detection probability, P_d, is given by

$$P_d = Q((\frac{\epsilon}{\sigma_w^2} - \mathrm{Y} - 1) \cdot \sqrt{\frac{N}{2\mathrm{Y}+1}}), \tag{2.16}$$

where Y refers to the SNR of the signal to be detected, $x[n]$, $Q(.)$ refers to the tail distribution function of standard normal distribution, or the complementary error function, which is given by

$$\begin{aligned} Q(x) &= \frac{1}{\sqrt{2\pi}} \int_x^{+\infty} exp(-\frac{-u^2}{2}) du \\ &= \frac{1}{2} - \frac{1}{2} erf(\frac{x}{\sqrt{2}}) = \frac{1}{2} erfc(\frac{x}{\sqrt{2}}). \end{aligned} \tag{2.17}$$

The false alarm probability,P_f, is given by

$$P_f = Q((\frac{\epsilon}{\sigma_w^2} - 1) \cdot \sqrt{N}). \tag{2.18}$$

2.2.2 Matched Filter Detection

The matched filter detection method performs coherent operations, and hence requires perfect knowledge of the signal to be detected and the knowledge of the channel response [18]. Therefore, it is also known as the optimum method for sensing when the signal to be detected and the channel response are known [21]. The main advantage of the matched filter detection is its fast speed of achieving a target false alarm probability and a mis-detection probability [22], so that not too many transmission opportunities are missed, as well as more potential signal collisions are avoided. On the other hand, since a matched filter detector requires perfect synchronisation in both PHY and MAC layers, it also has a high complexity. Additionally, the performance decreases significantly when the channel response varies rapidly [18]. Moreover, since the wireless environment becomes more and more complicated with the rise of the user density, and a detector normally has to receive all types of signals, which are compound at the receivers, the implementation of such a matched filter detector has high complexity, and therefore is not practical.

2.2.3 Cyclostationary Feature Detection

Cyclostationary feature detection is a method of spectrum sensing that uses the cyclostationary features of the signal to be detected, which refer to the periodicity or the statistical features such as the mean or autocorrelation [18]. Or such features can also be intentionally introduced to the signal to be detected for assisting the spectrum sensing [23]. One way of distinguishing the cyclostationary features is to use the input-output spectrum correlation density. It is based on the fact that noise does not have any periodicity, so noise also has no correlation, whilst the modulated signals do have periodicity features. The disadvantage of this method is its high computational complexity, which is caused by the high sampling rate, because this detection method requires sufficient samples of the signals to distinguish among different components of the compound signal. Besides, cyclostationary feature detection also suffers from frequency offset and sampling timing errors, because they affect the spectrum correlation density significantly, and in turn affect the detection accuracy [18]. Therefore, this spectrum sensing method is not a suitable candidate for high-speed communication scenarios, such as the V2X communications.

2.2.4 Eigenvalue Detection

Eigenvalue detection uses the ratio of the maximum or the average eigenvalue to the minimum eigenvalue of the covariance matrix of the sensed signal vector to compare against a pre-defined fixed threshold to determine the channel status, above which the channel is regarded as occupied. Otherwise, the channel is free to be allocated [18]. However, the method is not applicable if the correlation of the signal to be detected is zero. In other words, in the case where the signal to be detected appears closely to the characteristics of the white noise. Compared to other spectrum sensing technologies, the eigenvalue detection method requires neither the knowledge of the signal to be detected nor the knowledge of the channel condition, which is one of the main advantages same as the energy detection method. However, the eigenvalue detection technology has high computational complexity due to the covariance matrix computation and the eigenvalue decomposition. In addition, similar to the energy detection technology, selecting a suitable threshold is a challenge in the eigenvalue detection method, because it will also affect the detection accuracy performance significantly.

2.2.5 Alternative Spectrum Sensing Technologies

Apart from the four most common and widely-used spectrum sensing technologies, which are introduced in Sections 2.2.1 - 2.2.4, there are also some alternative sensing technologies. They can be selected according to their characteristics and the suitable applications.

One method that can differentiate non-Gaussian distributed signals from Gaussian distributed signals uses the cumulants property which can be expressed as moments. The cumulants of Gaussian distributed signals higher than second order are zero [24]. In [25], the authors have proposed a single and multiple cumulants-based sensing technology, which uses the property that modulated signals induces non-Gaussian property.

In addition, the Anderson-Darling method is another example, which senses the channel by introducing a non-parametric hypothesis test problem [26], [27]. This method tests the sensed samples. If the test satisfy the properties of the noise distribution, the output is that the channel is free. Otherwise, if the test does not satisfy the properties, the output is that the channel is occupied.

Moreover, there are many other spectrum sensing technologies such as the diffusion detection method [28], and the Kolmogorov-Smirnov method [29]. The proposed Kolomogorov-Smirnov method in [29] is also a non-parametric method that determines the presence or absence of a signal based on the empirical cumulative distribution function. The proposed recursive least square and least-mean square algorithms in [28] are two diffusion detection methods, which track changes of the parameters associated with transmitters, receivers and channels to determine the presence or absence of the signal to be detected.

2.3 FD Technologies

Traditionally, information in a wireless communication system is transmitted in a HD or out-of-band FD manner, which means that the information is transmitted and received either in different time frames or different frequency bands.

Different from the HD and the out-of-band FD communication systems, the IBFD technology, hereafter FD technology, is capable of transmitting and receiving in the same time frames over the same frequency bands. For a long period of time, most researchers do not believe that FD would be a possible and practical technology for mobile communication networks, such as base stations, mobile terminals and so on, because transmitting and receiving simultaneously in the same frequency band with very limited space for physical isolation between the transmission and receiving antennas will lead to extremely strong self-interference (SI) from the transmission antenna to the receiving antenna, which will overwhelm the desired signal, and in turn makes the communication impossible to be completed. However, FD technology has been deployed in other types of applications in history. For example, FD technology can be found in the design of continuous wave (CW) radar systems since 1940s. But each application has limitations, since the FD technology was used in special cases. It was not applied to general wireless communication systems and scenarios.

With recent development and achievement in FD technology, especially in the SI suppression/cancellation (SIS/SIC) technology, FD technology is feasible to be applied to more general wireless systems and scenarios, such as cellular and V2X communications [11]. Therefore, this thesis focuses on proposing novel FD cross-layer approaches for V2X networks. Herein, the cross-layer approach is defined as the approach that incorporates designs in both the PHY and MAC layers jointly for the purpose of performance improvement. Specifically, in this thesis, the FD simultaneous transmission and sensing is deployed in the PHY layer, whilst the sensing results are also used in the MAC layer to follow the proposed novel transmission rules.

2.3.1 SIS/SIC Technology

To apply the FD technology to modern wireless communication systems, the biggest drawback (i.e. the SI signal) must be addressed. As shown in Fig. 2.23, the SI signal refers to the interference signal that is from the FD station's own

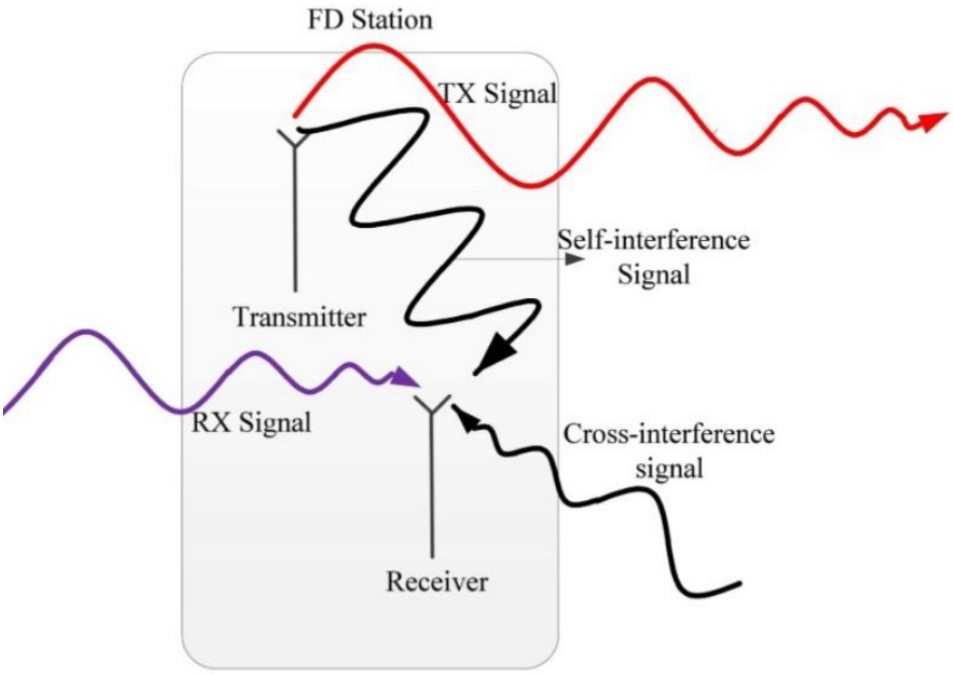

FIGURE 2.23: Illustration of the SI at a FD Station

transmission antenna to its receiving antenna. Since this distance is much shorter than the distance between the receiving antenna and the transmitting antenna of the desired signal, the power of the SI signal is much higher than the desired signal strength, which makes the reception impossible, if the SI signal cannot be suppressed.

Existing SIS/SIC methods can be divided into the following two types: passive SIS/SIC methods, which refer to physical isolation of the transmitting and receiving antenna of the FD station, and active SIS/SIC methods, which refer to the use of the FD station's known transmitting information to suppress the SI.

Passive SIS methods suppress the SI signal before it enters into the receiver's RF chain circuit [30]. Therefore, the amplitude of the received signal can be suppressed before the analogue-to-digital converter (ADC) process. The most widely-applied method approach is the use of propagation path loss, which depends on the placement design of the transmission and receiving antenna. Moreover, the placement design also normally incorporate other technologies to further enhance the overall performance, such as antenna directionality, and beamforming. Comparing to conventional mobile stations (MS), such as mobile

phones, vehicles has a much bigger size for physical isolation, which in turn leads to larger path loss, and better passive SIS/SIC performance.

Active SIS methods normally starts from analogue suppression, which subtracts an estimated SI signal after the passive SIS/SIC method, and followed by a digital SIS/SIC method. There are two different types of analogue SIS/SIC. The first type is to use the transmitting signal to generate a replica signal with a transformer or multiple parallel lines of varying delays and tunable attenuators [30], whilst the other type is to convert the delay and attenuation in the digital domain to the analogue domain to suppress/cancel the SI signal [31].

By deploying various combinations of the SIS/SIC methods, we can control the SI, and therefore, enjoy the following advantages of the FD technology.

2.3.2 Advantages of FD Technology

- Link Capacity: More efficient use of the time and frequency resources can theoretically double the link capability compared to the HD technology [11].
- Feedback Delay: Simultaneous reception of feedback signalling, such as control information, channel state information (CSI), and acknowledgement (ACK) and negative acknowledgement (NACK) information, which leads to the reduction in delay, whilst improving the throughput [32].
- End-to-End Delay: In a relay system, if the relay station is equipped with the FD technology, it is able to transmit data to the destination whilst receiving data from the source. Thus, the end-to-end delay is reduced [11].
- Security and Secrecy: FD technology allows two nodes to transmit at the same time in the same frequency. Thus an eavesdropper receives a mixed signal on a single channel. Comparing to HD transmission, this blended signal is more difficult to be separated without side information [33].
- Hidden Terminal Effect: In an ad-hoc network scenario, each MS can use the simultaneous transmission and sensing feature of the FD technology, which means that each MS can detect collisions during transmission. Thus, the effect of the hidden terminal problem is reduced [34].
- Resource Fairness: In a centralised network, if HD technology is used, the access point (AP) has much higher load, since one AP is designed to serve

multiple MSs. The resource fairness is different for each MS. By deploying FD technology, the AP and a MS can send information simultaneously in the same frequency. Thus, a better fairness between upstream and downstream can be achieved [35].

2.4 V2X Communications and Networking

Vehicle-to-Everything (V2X) communications refer to the technologies that can support information exchange between vehicles. V2X technologies allow vehicles to share both safety and infotainment messages to any other entity. Depending on different applications, V2X communications can be categorised into more specific types, including Vehicle-to-Vehicle (V2V) communications, Vehicle-to-Infrastructure (V2I) communications, Vehicle-to-Pedestrian (V2P) communications and so on. Generally, the motivations for V2X communications are transportation safety and efficiency.

There are two standards for supporting V2X communications, which are Dedicated Short Range Communications (DSRC) standard [36], and Cellular-V2X (C-V2X) standard [2]. Although the history of V2X communications can be traced back to 1970s, a unified set of technical standards has not been achieved, because each standard has pros and cons in different scenarios.

The background of the DSRC and C-V2X standards are introduced in Section 2.4.1 and Section 2.4.2, respectively. Related technologies such as MAC protocols are introduced in Chapters 3 - 7 where needed. They are used as the benchmarks for comparing to the proposed technologies.

2.4.1 DSRC Standard

DSRC is a set of short to medium-range communication standards specifically designed for V2X applications and Intelligent Transportation Systems (ITS). Its PHY and MAC layer technical specifications are also know as the IEEE 802.11p standard. DSRC is also the first international standard for V2X communications and ITS. Over the years, the performance of DSRC has been evaluated by developing analytical models [7], using extensive computer simulations [37], and field tests [8]. The results show that DSRC is satisfactory for most basic vehicular applications, where the end-to-end latency requirement is approximately 100 ms, and the network density is not too high. However, when the network density increases and exceeds a certain limit, its performance degrades rapidly. The first major reason is the packet collision, which is the result of simultaneous transmission from different vehicles. The second major reason is the hidden node problem, which is caused by the network topology, because DSRC is mainly designed for broadcast scenario, and there is no acknowledgement mechanism.

To enhance the performance of DSRC standard, and support future more diverse V2X applications, a new IEEE 802.11bd Task Group was formed in 2019. The objectives of IEEE 802.11bd focus on improving the reliability, decreasing the latency, and supporting more types of V2X applications and scenarios. Besides, the Task Group also requires that this new standard to be backward compatible with the IEEE 802.11p standard, which implies that devices using either standardised technology must be able to communicate with any other device on the same channel. Furthermore, as mobility is one of the most significant characteristics of V2X communications, increasing the maximum relative velocity up to 500 km/h is also one of the primary objectives for IEEE 802.11bd standard.

2.4.2 C-V2X Standard

Comparing to the DSRC standard, C-V2X standard is a more recent set of technologies, which are designed based on the existing cellular communication technologies, such as the 4G Long-Term Evolution (LTE) technologies and 5G New Radio (NR) technologies. Literature shows that C-V2X outperforms DSRC in terms of additional link budget, higher resilience to interference and better Non-Line-of-Sight (NLoS) capability [38]. C-V2X standard can also support basic basic safety V2X applications where the end-to-end latency requirement is about 100 ms. In addition, C-V2X standard has the same design objectives as IEEE 802.11bd in terms of reliability and latency. But it does not have any constraint on the backward capability. NR-V2X devices are designed to communicate with LTE-V2X devices through a dual-radio system, where one set of device for LTE-V2X communication, and another set of device for NR-V2X communication.

In terms of system model, two modes have been introduced in C-V2X standard, which are Mode 3 and Mode 4. Mode 3 is used when vehicles are in the coverage area of a base station (BS) or roadside unit (RSU), whilst Mode 4 is used when vehicles are out of the coverage area of a BS or RSU, or the connection to the infrastructure is not stable. In addition to the conventional Uplink (UL) and Downlink (DL) communication, the Sidelink (SL) communication is the characteristic of V2X communications, which refers to the direct communication between vehicles. SL communication cannot only be used in Mode 4, but also in Mode 3. In this case, control messages such as signalling is transmitted by using the UL and DL resources in the charge of a BS or RSU, whilst data messages are shared between vehicles by using the assigned resources.

To investigate thoroughly based on both standards, this PhD project started from the DSRC standard, since it is released earlier than the C-V2X standards. Corresponding contributions are presented in Chapters 3 to 4. Then, the works that are based on the C-V2X standards are presented in Chapters 5 to 7. Finally, this thesis is concluded in Chapter 8, in which future works are also incorporated.

3 Collision Avoidance in V2X Communication Networks

Synopsis of Chapter

In Chapter 3, I investigate collision detection and avoidance in a vehicular network of FD operating nodes, which refers to my paper [39]. Probabilities of detection and false alarm, detection threshold before and during transmission, and effect of SI on these metrics have been formulated. It is shown that the proposed scheme would experience a shorter collision duration. Meanwhile, it also requires a minimum SIC capability for acceptable operation, below which, system throughput would be poor due to high false alarm probability. Numerical simulations verify the accuracy of my analysis. They also illustrate that the proposed model perform better than the fixed threshold strategy. A trade-off between half duplex (HD) and FD has been found and the scheme would be applicable even if SIC capability of OBUs is relatively poor, with no need for complicated and expensive devices for future vehicular communication.

We introduce the background, motivation and contributions of this work in Section 3.1. Next, I present the considered system model and assumptions in Section 3.2. Furthermore, I formulate the probabilities of detection, false alarm and misdetection, and the dynamic thresholds in Section 3.3. In addition, I demonstrate the analytical and simulation results with discussions in Section 3.4. Finally, I conclude this work in Section 3.5.

3.1 Introduction

Over the past few years, intelligent transportation systems (ITSs) and autonomous driving have attracted the attention of auto makers and academia towards introduction of vehicular communication systems. In such networks, information such as safety messages are exchanged between vehicles (vehicle-to-vehicle V2V) or between vehicles and any other object (vehicle-to-everything V2X) to provide a better transportation system in terms of safety, latency, and energy efficiency. Two different V2X communication standards are widely considered as promising applicants for future vehicular networks. One of them is DSRC [1], which is also known as IEEE 802.11p (WAVE). While the other is cellular-V2X communication (C-V2X) such as release-15 published by 3GPP [3]. Many works have compared performance of these two technologies such as [9]. However, which technology would be the better solution is still an open question, since each of them has its own pros and cons. This work is built upon DSRC.

One of the main challenges based on IEEE 802.11 legacy standard (especially ad hoc networks) is the access protocol and prevention of data loss due to collision of concurrent transmission of two or many nodes. In this standard, carrier sense multiple access with collision avoidance (CSMA/CA) protocol has been deployed to minimise the probability of collision and data loss. However, this protocol will not eliminate such incidents and the condition becomes worse when there are too many nodes in the network (dense networks) [40]. This problem is more serious in vehicular networks in which safety messages known as cooperative awareness messages (CAMs) are broadcasted without acknowledgement and loss of them may result in a higher risk of accidents. Finding a way to eliminate the loss of data due to signal collision in V2X networks is an important problem to be solved.

Deploying FD technology in vehicular networks seems a promising solution to this problem. FD technology enables the nodes in a V2X network to sense the carrier while they are transmitting at the same time over the same channel. Thanks to recent advances in SIC techniques, SI suppression as high as 110 dB could be obtained under certain conditions [11]. Therefore, deploying FD technology in legacy CSMA/CA protocol enables collision detection (CD) so that vehicles would be able to detect probable collisions while broadcasting and go to backoff process in an earlier phase.

In this work I have considered collision detection and avoidance in V2X networks where the transmitting nodes would sense the channel, in a FD manner, to detect any probable concurrent transmissions. Sensing is carried out through measuring the energy level of the channel, which is a simple and widely-applied method. To the best of my knowledge, I am among the first ones exploring this method in vehicular networks. Other related works are either in the area of cognitive radio networks such as [18] and [41], or in vehicular communications but assumed ideal energy detection such as [42] and [43]. Unlike these works, I have assumed imperfect energy detection and investigated the effect of threshold, transmit power, SIC capability, sensing time, collision duration and throughput on the network performance.

3.2 System Model

We consider a vehicular ad hoc network (VANET) in which vehicles broadcast CAMs periodically. All vehicles are equipped with FD capability. Rayleigh fading channels are assumed to be the channel model between vehicles. The noise component is assumed to be Gaussian, independent and identically distributed (i.i.d.) with zero mean and unit variance. Regarding the hidden node problem, the proposed method is not focusing on eliminating it. However, the effect of the hidden node problem could be weakened by setting up a wider sensing range such as double of the transmission range. This could be done by adjusting the thresholds formulated in section III. Since this is not the focus of this work, the transmit power level of all vehicles would be set to the same and fixed value based on the required coverage area of the vehicular network, and the sensing range is considered to be equal to the transmission range.

In my model, energy detection is the core technology and the level of the received energy depends on the distance between the sensing vehicle and the potential concurrent transmitting vehicle(s). To be conservative, I have developed my model to be able to detect the signal collision from the farmost vehicle, as shown in Fig. 3.1. All vehicles are able to transmit and sense simultaneously. Here vehicle A is assumed to be a transmitting and sensing vehicle, vehicle B and C are probable concurrent transmitting vehicles. It is obvious that A can easily detect the transmission of B if B is also broadcasting since B is close to A, and the measured SNR of B at A is relatively high. However, C is far away from A. If C is competing with A for broadcasting, the difficulty of detecting its transmission would be much higher than detecting B. So, I set the thresholds to satisfy the detection of signals sent by C (farmost vehicle). Certain requirements for the received SNR, sensing time and SIC capability are found, which will be discussed in later sections. Furthermore, my method performs even better when multiple CAMs are competing for broadcasting at the same time, because the energy level of the received signal would be much higher and the colliding signal is much easier to be accurately detected, comparing to the case where there is only one concurrent broadcasting vehicle.

The system works as follows, whenever a vehicle would like to broadcast a CAM, it first probes the medium to measure the energy level of the channel. If the measured energy is less than the threshold ϵ_{th_0} which is derived from the theoretical

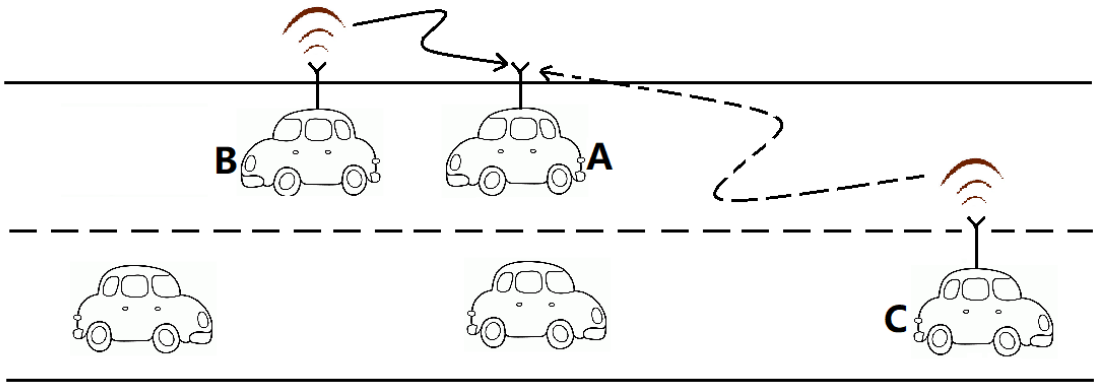

FIGURE 3.1: Demonstration of the signal detection between vehicles

formulation in Section III, the vehicle knows the channel is free for broadcasting; if the sensed energy is greater than the threshold ϵ_{th_0}, the vehicle knows there is another or even more vehicles occupying the channel and will not broadcast until the channel is free. Sensing process continues during the broadcasting period in a FD manner. The measured energy would be compared to an elevated threshold ϵ_{th_1} which is dependent on the amount of residual SI after cancellation. If the measured energy is higher than this elevated threshold ϵ_{th_1}, the vehicle knows its transmission is in collision with another vehicle(s) transmitting at the same time. Otherwise, the vehicle itself is regarded as the only one using the channel in the network.

However, the aforementioned detection is not perfect. All decisions are made with certain probabilities. Detection probability is defined as the probability that a vehicle successfully detect the presence of an event (an ongoing transmission or a collision) when the event actually exists, and false alarm probability is defined as the the probability that a vehicle falsely declare the presence of an event when the event does not exist. In order to have a high probability of detection, both thresholds (ϵ_{th_0}, ϵ_{th_1}) should be set to a low value. However, this will result in a high false alarm probability. In other words, vehicles are missing opportunities to transmit. In this work, I focus on keeping the detection probability to a high value while attempting to find the requirements for an acceptable probability of false alarm in terms of transmission power, sensing duration and SIC capability. In this work I just focus on detecting collisions of signals, and further actions to be followed when collision or false alarm occurs will be left to a MAC layer

scheduling protocol considered in my future work.

In order to make the mathematical formulations clear, I list the important notations in Table. 3.1. Specifically, η refers to SIC factor which is the percentage of residual SI after SIC and it varies between 0 and 1. If $\eta = 0$, it means that SIC is perfect and there is no residual SI.

TABLE 3.1: Important Notations

Parameters	**Notes**
N	number of samples (maximum integer that is smaller than or equal to $\tau \cdot f_s$)
r[n]	the received signal at a FD node, where n = 1, 2, ..., N
τ	sensing time
f_s	sampling frequency
$w[n]$	noise signal with mean zero and variance σ_w^2
$s_i[n]$	SI signal with mean zero and variance σ_i^2
$s[n]$	transmit signal from a FD node with mean zero and variance σ_s^2
η	SIC factor
$E\|.\|$	Expectation operator
σ_w^2	variance of $w[n]$ ($\sigma_w^2 = E\|w[n]\|^2$)
σ_i^2	variance of $s_i[n]$ ($\sigma_i^2 = E\|s_i[n]\|^2$)
σ_s^2	variance of $s[n]$ ($\sigma_s^2 = E\|s[n]\|^2$)
E	energy detection test statistic
Y_1	measured SNR of the node itself ($Y_1 = \frac{\sigma_i^2}{\sigma_w^2}$)
Y_2	measured SNR of other transmitting node ($Y_2 = \frac{\sigma_s^2}{\sigma_w^2}$)
ϵ_{th_0}	first threshold
ϵ_{th_1}	second threshold
H_i	hypothesis i where i = 0, 1, 2, 3
$P_{f,bt}$	probability of false alarm before transmission
$P_{f,dt}$	probability of false alarm during transmission
$P_{d,bt}$	probability of detection before transmission
$P_{d,dt}$	probability of detection during transmission
$Q(.)$	Q function operation
$p_i(x)$	PDF of E under hypothesis H_i
μ_i	mean value of $p_i(x)$
σ_i^2	variance of $p_i(x)$

3.3 Mathematical Analysis

From now on when I refer to transmitting vehicle I mean the vehicle which is or going to transmit and sense the channel, and colliding vehicle(s) means that the vehicle(s) that are causing collision due to concurrent transmission.

We have four different hypotheses for different transmission scenarios. Hypothesis H_0 is defined as when there is no vehicles broadcasting; H_1 is defined as when there is an ongoing transmission from colliding vehicle(s); H_2 is defined as when the transmitting vehicle is the only vehicle occupying the channel and H_3 is defined as when there are at least 2 vehicles competing for broadcasting.

So the received signal at a FD-enabled vehicle would be

$$r[n] = \begin{cases} w[n]; & H_0 \\ s[n] + w[n]; & H_1 \\ \sqrt{\eta} s_i[n] + w[n]; & H_2 \\ \sqrt{\eta} s_i[n] + s[n] + w[n]; & H_3 \end{cases} \tag{3.1}$$

The energy detection test statistic is given by

$$E = \frac{1}{N} \cdot \sum_{n=1}^{N} |r[n]|^2. \tag{3.2}$$

- Under H_0:

  E is a random variable (RV) whose probability density function (PDF) $p_0(x)$ follows a Chi-square distribution for the complex-valued case, therefore, probability of false alarm can be expressed as [41]

$$P_{f,bt}(FD) = Q((\frac{\epsilon_{th_0}}{\sigma_w^2} - 1) \cdot \sqrt{N}). \tag{3.3}$$

- Under H_1:

  Probability of detection under this hypothesis is given by [41]

$$P_{d,bt}(FD) = Q((\frac{\epsilon_{th_0}}{\sigma_w^2} - \Upsilon_2 - 1) \cdot \sqrt{\frac{N}{2\Upsilon_2 + 1}}). \tag{3.4}$$

- Under H_2:

Similar to H_1, probability of false alarm is derived from

$$P_{f,dt}(FD) = Pr\{E > \epsilon_{th_1} | H_2\} = \int_{\epsilon_{th_0}}^{\infty} p_2(x)dx. \tag{3.5}$$

According to Central Limit Theorem (CLT), for a large N, $p_2(x)$ can be approximated by a Gaussian distribution with mean $\mu_2 = \eta^2\sigma_i^2 + \sigma_w^2$ and variance $\sigma_2^2 = \frac{1}{N} \cdot [\eta^4\sigma_i^4 + 4\sigma_w^2 - (\eta^2\sigma_i^2 - \sigma_w^2)^2]$.

Then PDF of the measured energy would be

$$p_2(x) = \frac{1}{\sqrt{2\pi\sigma_2^2}} \cdot exp(-\frac{(x-\mu_2)^2}{2\sigma_2^2}). \tag{3.6}$$

Therefore, probability of false alarm is given by

$$P_{f,dt}(FD) = \int_{\epsilon_{th_1}}^{\infty} \frac{1}{\sqrt{2\pi}} \cdot \frac{1}{\sqrt{\frac{1}{N} \cdot (2\eta^2\sigma_i^2\sigma_w^2 + \sigma_w^4)}} \cdot exp(-\frac{[x-(\eta^2\sigma_i^2+\sigma_w^2)]^2}{2[\frac{1}{N} \cdot (2\eta^2\sigma_i^2\sigma_w^2+\sigma_w^2)]})dx. \tag{3.7}$$

After simplification, I can represent $P_{f,dt}(FD)$ in terms of the Q function as

$$P_{f,dt}(FD) = Q((\frac{\epsilon_{th_1}}{\sigma_w^2} - \eta^2\mathrm{Y}_1 - 1) \cdot \sqrt{\frac{N}{2\eta^2\mathrm{Y}_1+1}}). \tag{3.8}$$

- Under H3:

  Similar to the previous hypotheses, probability of detection during transmission is given by

  $$P_{d,dt}(FD) = Pr\{E > \epsilon_{th_1} | H3\} = \int_{\epsilon_{th_1}}^{\infty} p_3(x)dx. \tag{3.9}$$

  $p_3(x)$ can be approximated by a Gaussian distribution with mean $\mu_3 = \sigma_s^2 + \eta^2\sigma_i^2 + \sigma_w^2$ and variance $\sigma_3^2 = \frac{1}{N} \cdot (2\eta^2\sigma_i^2\sigma_w^2 + 2\eta^2\sigma_i^2\sigma_s^2 + 2\sigma_s^2\sigma_w^2 + \sigma_w^4)$.

  I use the same method to derive $P_{d,dt}(FD)$ as

  $$P_{d,dt}(FD) = Q((\frac{\epsilon_{th_1}}{\sigma_w^2} - \mathrm{Y}_2 - \eta^2\mathrm{Y}_1 - 1) \cdot \sqrt{\frac{N}{2\eta^2\mathrm{Y}_1+2\eta^2\mathrm{Y}_1\mathrm{Y}_2+2\mathrm{Y}_2+1}}). \tag{3.10}$$

- Thresholds ϵ_{th_0} & ϵ_{th_1}:

Threshold ϵ_{th_0} is found from Eq. (3.4) by calculating the inverse Q function, which is given by

$$\epsilon_{th_0} = \left(\frac{(Q^{-1}(\overline{P_{d,bt}(FD)})}{\sqrt{\frac{N}{2Y_2+1}}} + Y_2 + 1\right) \cdot \sigma_w^2. \tag{3.11}$$

Threshold ϵ_{th_1} is defined from Eq. (3.9) as

$$\epsilon_{th_1} = \left(\frac{(Q^{-1}(\overline{P_{d,dt}(FD)})}{\sqrt{\frac{N}{2\eta^2 Y_1 + 2\eta^2 Y_1 Y_2 + 2Y_2 + 1}}} + Y_2 + \eta^2 Y_1 + 1\right) \cdot \sigma_w^2. \tag{3.12}$$

Assume the target probabilities of detection before and during transmission are identical, then the relationship between the two thresholds can be derived as

$$\epsilon_{th_1} = \frac{\frac{\epsilon_{th_0}}{\sigma_w^2} - Y_2 - 1}{\sqrt{\frac{2Y_2+1}{2\eta^2 Y_1 + 2\eta^2 Y_1 Y_2 + 2Y_2 + 1}}} + \eta^2 Y_1 + Y_2 + 1. \tag{3.13}$$

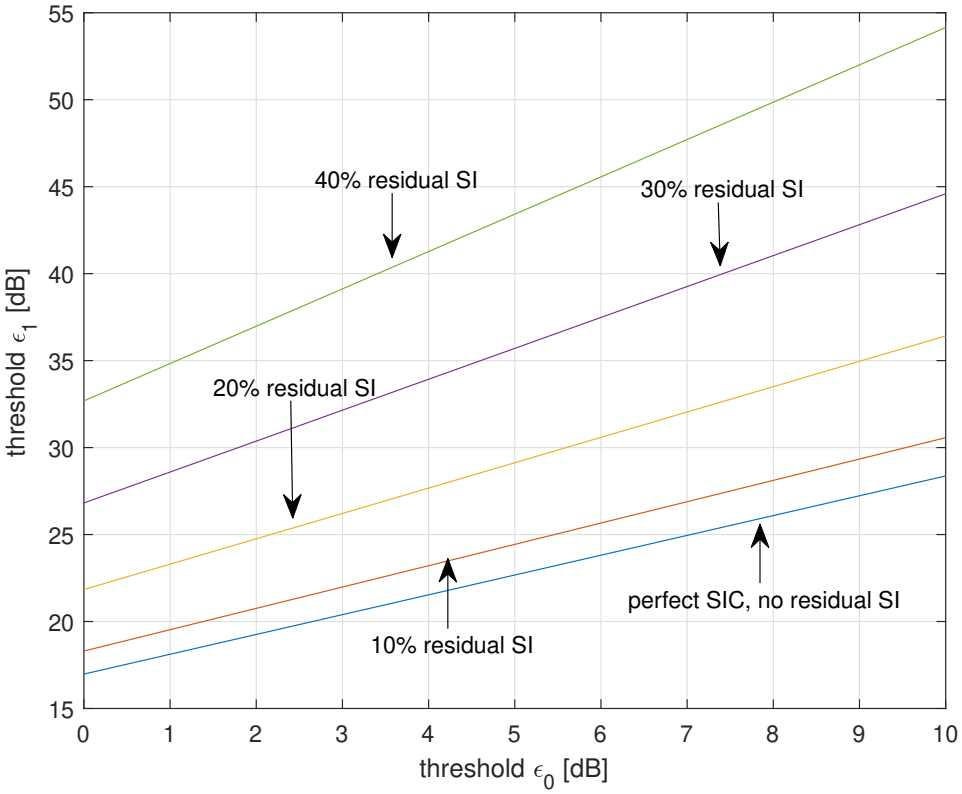

FIGURE 3.2: relationship between threshold ϵ_{th_0} and threshold ϵ_{th_1}

This relationship is depicted in Fig. 3.2 by using Eq. (3.13). It can be seen that the higher the residual SI is, the higher the thresholds would be, and the bigger the difference between the two thresholds would be.

- SIC factor η:

  SIC capability plays an important role in detecting collisions during transmission. With a huge amount of residual SI, both probabilities become worse. In order to see the impact of residual SI, I derive the SIC factor η in terms of the false alarm probability as

$$\begin{aligned}\eta =& \frac{2N(\frac{\epsilon_{th_1}}{\sigma_w^2}-0.5)+2[Q^{-1}(\overline{P_{f,dt}(FD)})]^2-N}{2N\mathrm{Y}_1} \\ &+\frac{\sqrt{8(\frac{\epsilon_{th_1}}{\sigma_w^2}-0.5)N[Q^{-1}(\overline{P_{f,dt}(FD)})]^2+4[Q^{-1}(\overline{P_{f,dt}(FD)})]^4}}{2N\mathrm{Y}_1}.\end{aligned} \tag{3.14}$$

  Eq. (3.14) has solutions only when

  $\Delta = \frac{8yN[Q^{-1}(\overline{P_{f,dt}(FD)})]^2+4[Q^{-1}(\overline{P_{f,dt}(FD)})]^4}{N^2} \geqslant 0$, where $y = \frac{\epsilon_{th_1}}{\sigma_w^2} - 0.5$.

- Average probability of false alarm:

  SIC factor is not always fixed, it may fluctuate due to the imperfection of the hardware or channel variations. For a given SIC factor η_0 with $\pm m\%$ fluctuation distributed uniformly, the average probability of false alarm can be calculated by

$$\begin{aligned}\overline{P_{f,dt}(FD)} = &\int_{\eta_0-m}^{\eta_0+m} Q((\frac{\epsilon_{th_1}}{\sigma_w^2}-\eta_0^2\mathrm{Y}_1-1)\cdot \\ &\sqrt{\frac{N}{2\eta_0^2\mathrm{Y}_1+1}})\cdot PDF(\eta)d\eta.\end{aligned} \tag{3.15}$$

  According to [44], the Q function could be approximated as $Q(x) \approx \frac{1}{2}e^{-\frac{x^2}{2}}$. Thus, the average probability of false alarm is derived as

$$\overline{P_{f,dt}(FD)} = \frac{1}{4m}\int e^{-\frac{(y-z)^2N}{4z}}\cdot\frac{1}{\mathrm{Y}_1}dz, \tag{3.16}$$

  where $y = \frac{\epsilon_{th_1}}{\sigma_w^2} - 0.5$ and $z = \eta_0^2\mathrm{Y}_1 + 0.5$. This integral cannot be solved and the closed-form expression cannot be found. However, I can approximate the average probability of false alarm according to the simulation result shown in Fig. 3.3 by using Eq. (3.15) and Eq. (3.16) as an example. I found

that regardless of target probability, initial SIC factor and SIC fluctuation, the average probability of false alarm is always the average of P_f for $\eta_0 + m$ and $\eta_0 - m$.

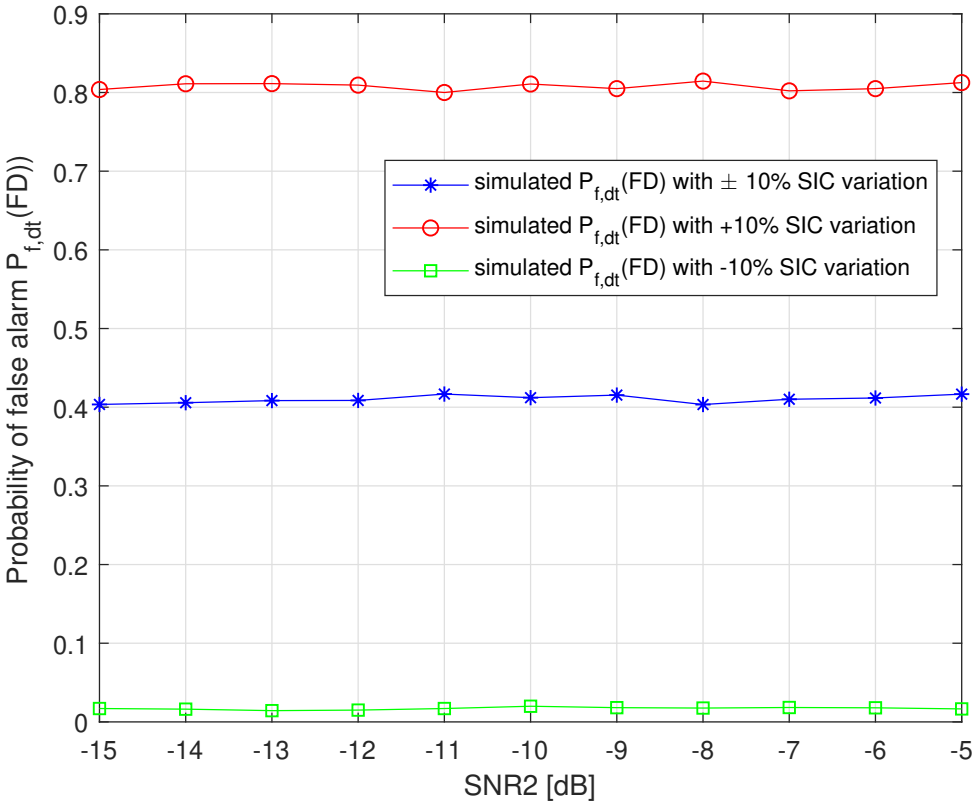

FIGURE 3.3: Probability of false alarm $P_{f,dt}(FD)$ VS SNR2 with SIC variation

Thus the average probability of false alarm is expressed as

$$\overline{lP_{f,dt}(FD)} \approx \frac{Q((\frac{\epsilon_{th_1}}{\sigma_w^2} - (\eta_0 + m)^2 \mathrm{Y}_1 - 1)\sqrt{\frac{N}{2(\eta_0+m)^2\mathrm{Y}_1+1}})}{2} + \frac{Q((\frac{\epsilon_{th_1}}{\sigma_w^2} - (\eta_0 - m)^2 \mathrm{Y}_1 - 1)\sqrt{\frac{N}{2(\eta_0+m)^2\mathrm{Y}_1+1}})}{2}. \tag{3.17}$$

3.4 Simulation Results

Following the mathematical analysis discussed in Section 3.3, simulations have been done in *MATLAB* to observe and verify the performance of the proposed scheme. Specifically, the computer simulation conducted in this work is numerical analysis. An urban area where vehicles are moving with an average speed of 20 miles per hour is assumed. Furthermore, vehicles are focusing on measuring the energy level of the received signal, which means that Doppler effect would not be important in this scenario. The simulation is performed by firstly setting up the thresholds according to Eq. (3.11) and Eq. (3.12). Then, the channel and AWGN are constructed by using the built-in function in MATLAB according to the Chi-square and Gaussian distribution, respectively. Afterwards, random information packets are generated and broadcasted. Finally, vehicles take samples and do integration over the given sensing time to find the measured energy level, which is in turn compared to the pre-defined threshold depending on before or during the transmission case. Monte-Carlo simulation is conducted to find the average performance. Relevant simulation parameters are shown in Table 3.2. The chosen values for the parameters are realistic, because they are the values and scheme suggested in the standard [1], which have also been used in the field test [8] and other research papers such as [7] and [37]. The reason why only the standard instead of prior art has been chosen as the benchmark is because to the best of my knowledge, applying the FD simultaneous transmission and sensing feature for V2X was firstly proposed in 2017 in [13], and no prior art working on the same topic was found.

TABLE 3.2: Parameters and Assumptions

Parameters	**Values**
target $P_{d,bt}(FD)$ & $P_{d,dt}(FD)$	90% & 50%
modulation scheme	BPSK, QPSK
measured SNR from SI signal before SIC (SNR1)	+10 dB
measured SNR from another vehicle (SNR2)	(-20)→0 dB
Residual SI	0%-40%
vehicle density	0-200 vehicles/km

Fig. 3.4 shows a good match between the simulated $P_{d,dt}(FD)$ and $P_{f,dt}(FD)$ and their theoretical values, which verifies my mathematical analysis to be correct and accurate, where the theoretical curves are plotted by using Eq. (3.8) and Eq.

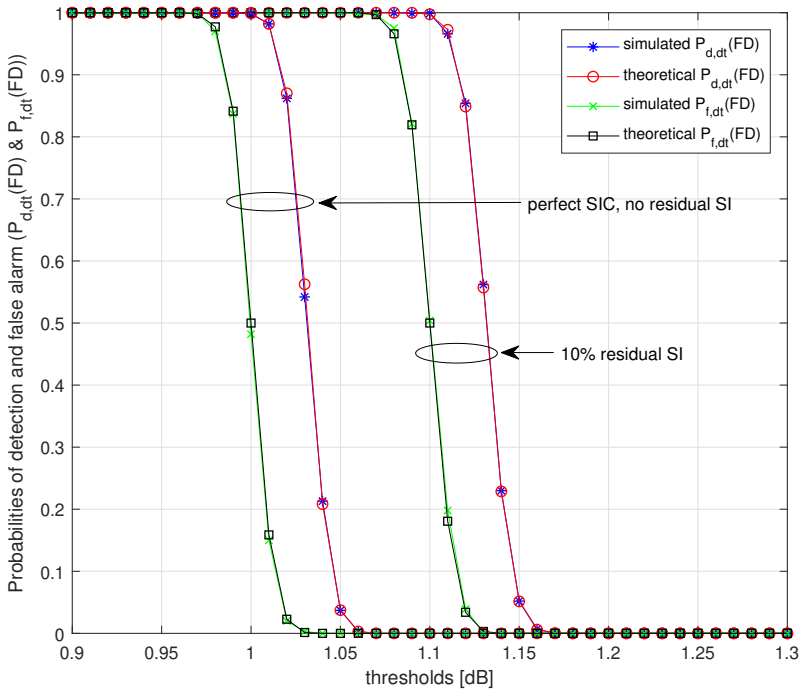

FIGURE 3.4: Probabilities of detection $P_{d,dt}(FD)$ and false alarm $P_{f,dt}(FD)$ VS threshold ϵ_{th_1} under different SIC assumptions

(3.10). When residual SI becomes stronger, in order to achieve the same detection probability, thresholds should be set to a higher value because more energy (from SI signal) is received. Moreover, a small variation of the threshold ϵ_{th_1} would result in a huge deviation in the probabilities even when SIC is perfect. For example, if the threshold changes from 1 dB to 1.025 dB, such a small change would lead to 45% drift of the probabilities of detection and false alarm. This result highlights the calculation of the threshold is of great importance and should be done as accurate as possible.

Fig. 3.5 and Fig. 3.6 illustrate the significant impact of transmit power and the difference between two threshold setting strategies, where Eq. (3.3) and Eq. (3.4) are used to plot the theoretical curves in Fig. 3.5, and Eq. (3.8) and Eq. (3.10) are used to plot the theoretical curves in Fig. 3.6. One is my proposed method where the threshold is dynamically changing, while the other is the fixed threshold method. For the fixed threshold strategy, along with the rise of the transmit power, probability of detection increases while having a high and unacceptable

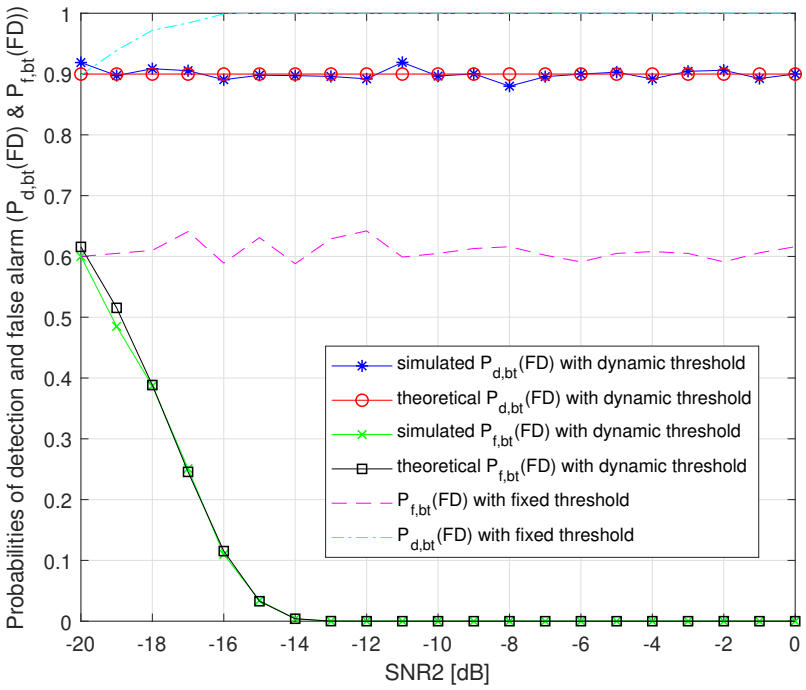

FIGURE 3.5: Probabilities of detection $P_{d,bt}(FD)$ and false alarm $P_{f,bt}(FD)$ VS measured SNR before transmission

probability of false alarm. my proposed method would have a lower detection probability which is still in the acceptable range. But because the threshold is increasing too with the rise of the measured SNR, false alarm probability would decrease at the same time. Compared to the fixed threshold method, although my proposed method will sacrifice some detection probability by dynamically changing the threshold, a much better false alarm probability would be rewarded, while keeping the probability of detection in an acceptable range.

Fig. 3.7 shows the effect of residual SI on the probabilities, where the theoretical curves are plotted by using Eq. (3.8) and Eq. (3.10). Firstly, target probability of detection is achievable regardless of SIC factor by using the dynamic threshold. However, when SIC factor η increases, false alarm probability increases too since more energy is received. In order to achieve detection probability to be at least 90% and false alarm probability to be at most 10%, my model would have acceptable performance when SIC factor is less than 15%. In other words, my system does not operate only when SIC is extremely well, it works quite acceptable when SIC is relatively poor.

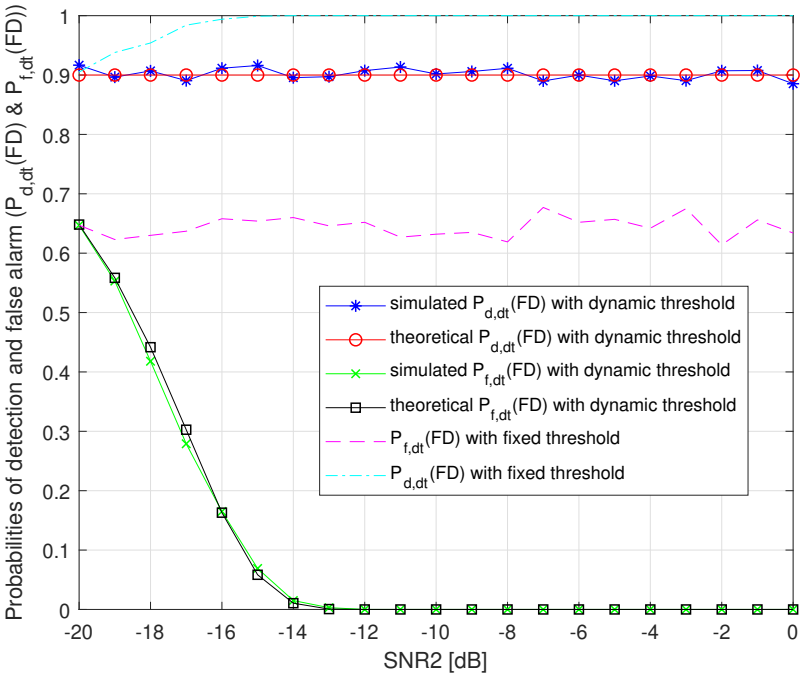

FIGURE 3.6: Probabilities of detection $P_{d,dt}(FD)$ and false alarm $P_{f,dt}(FD)$ VS measured SNR during transmission

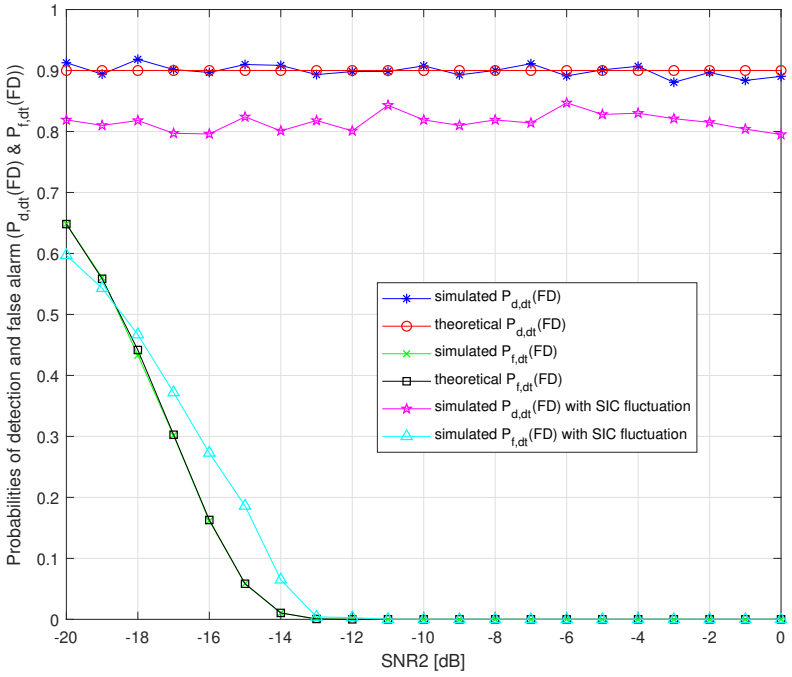

FIGURE 3.8: Probabilities of detection $P_{d,dt}(FD)$ and false alarm $P_{f,dt}(FD)$ VS measured SNR during transmission with 10% SIC fluctuation

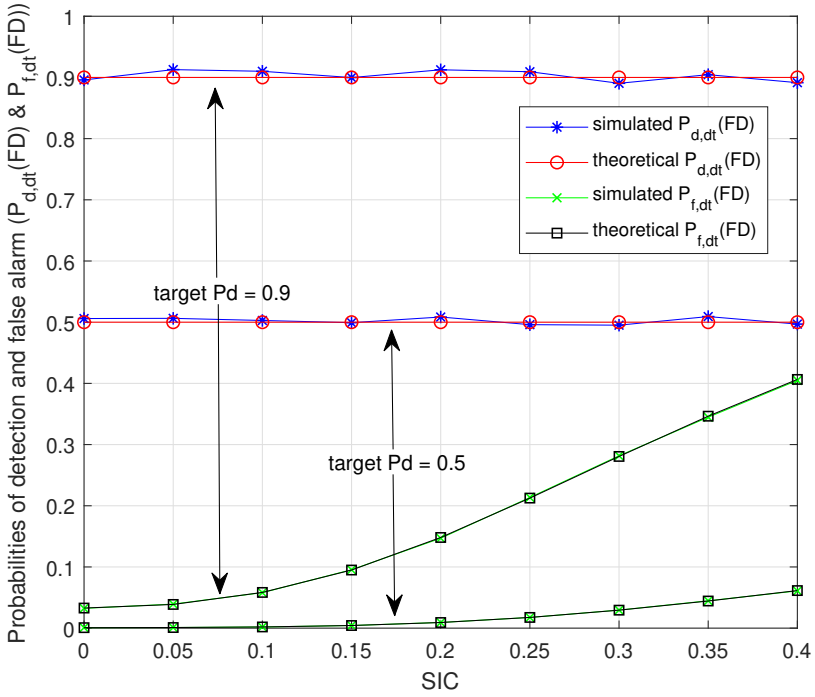

FIGURE 3.7: Probabilities of detection $P_{d,dt}(FD)$ and false alarm $P_{f,dt}(FD)$ VS SIC factor η

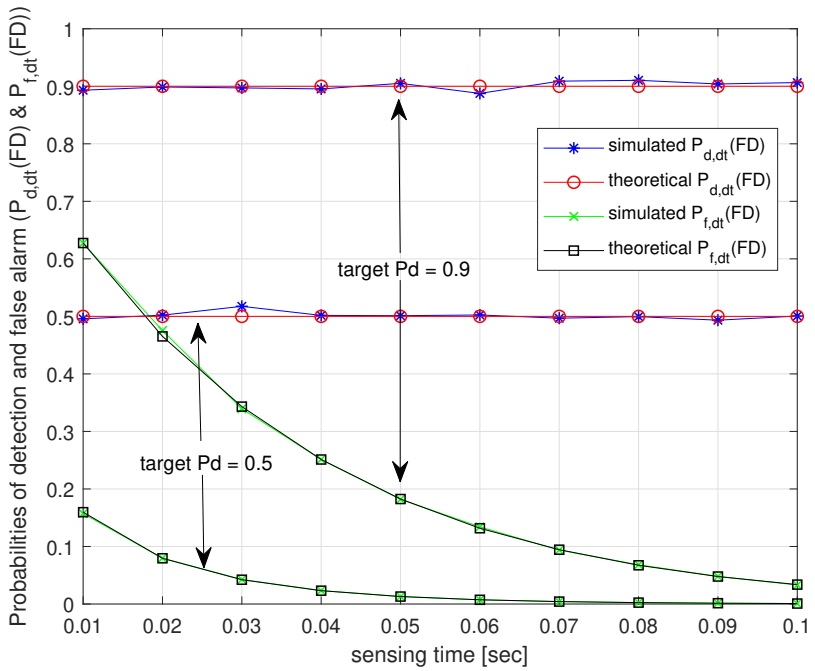

FIGURE 3.9: Probabilities of detection $P_{d,dt}(FD)$ and false alarm $P_{f,dt}(FD)$ VS sensing time during transmission

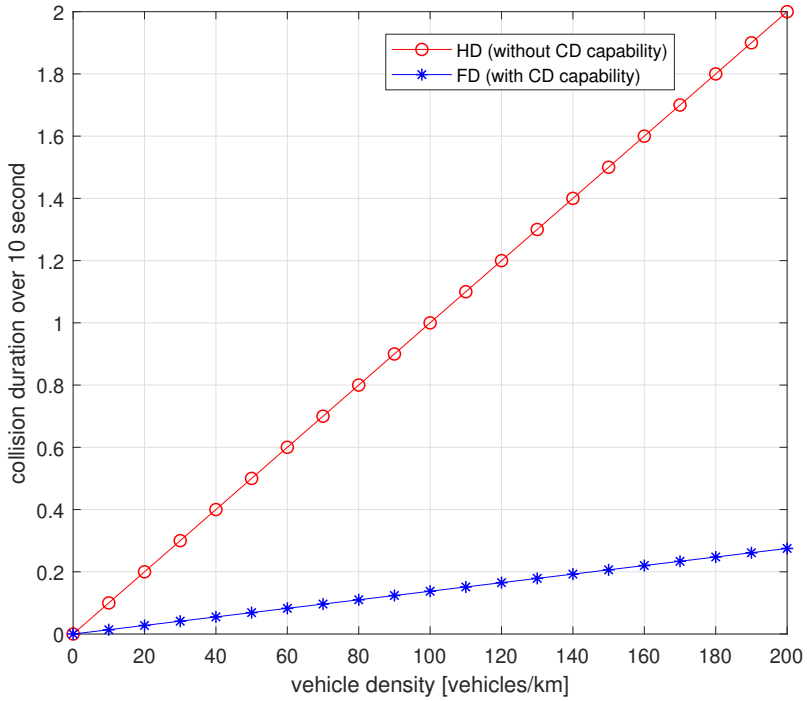

FIGURE 3.10: Collision duration over 10 seconds VS average vehicle density

Fig. 3.8 highlights the damage of SIC fluctuation, where Eq. (3.8), Eq. (3.10), and Eq. (3.17) are used to plot the theoretical curves. When a 10% random SIC fluctuation is considered, both probabilities of detection and false alarm become worse compared to the case where such a fluctuation does not considered. Thus, a space for SIC fluctuation should be left when deploying the scheme in future V2X systems.

Fig. 3.9 shows the impact of the sensing time on the precision of detection, where Eq. (3.8) and Eq. (3.10) are used to plot the theoretical curves. By setting the thresholds properly, the system can achieve the target detection performance. Meanwhile, the longer the sensing time is, the lower chance the system would wrongly alarm an impending collision. This is because I am measuring and averaging the received energy over a longer period of time, which gives a more accurate detection result. Another way to reduce the false alarm probability is to increase the sampling frequency, since $N = \tau \cdot f_s$. However, the accuracy of the detection performance cannot be improved by only increasing f_s. When the number of samples taken of a signal is large enough, more samples would not give a more accurate measured energy level.

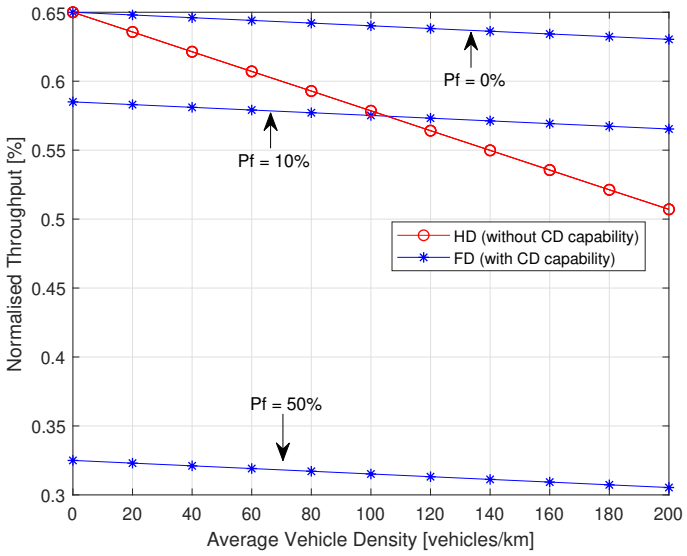

FIGURE 3.11: Normalised throughput VS average vehicle density under different probabilities of false alarm

Fig. 3.10 shows the collision duration over 10 seconds versus the average vehicle density. Vehicles are assumed to be placed on a line according to Poisson distribution, which is the same as the assumption in [42]. It is clear that vehicles with CD capability experience a shorter period of collision compared to the vehicles which operate in HD mode. The difference becomes larger when the number of vehicles increases. In other words, FD technology helps vehicles to avoid impending collisions by aborting transmissions at an earlier stage, while vehicles without CD capability would experience collision for an entire packet duration.

Fig. 3.11 demonstrates the drawback of enabling CD capability. While detecting probable collisions at an early stage, I am sacrificing throughput compared to HD mode, especially when probability of false alarm is high. However, since probability of false alarm can be reduced while keeping the probability of detection in an acceptable range as shown earlier, throughput could be improved. Thus, a trade-off between HD and FD modes is found. When the number of vehicles in a VANET is relatively low, HD mode is preferred. FD mode is more suitable for dense VANETs.

3.5 Summary

In this Chapter, I studied FD collision detection and avoidance through energy detection method in V2X communication networks. By deploying the proposed model, a vehicle would be able to detect and avoid collisions with certain probabilities without losing too many opportunities to transmit useful data. Two thresholds which are dynamically changing according to the transmit power levels, sensing time and instantaneous SIC factor have been formulated. Simulation results have shown that my model does not require near perfect SIC, it works well even when SIC is poor. On the basis of these results, detecting and avoiding collisions in V2X communication networks could be better, more suitable MAC layer protocol based on original CSMA/CA could be proposed to provide better communication environment, which will also be my future work.

4 A Priority-Based Cross-Layer Design for Future VANETs

Synopsis of Chapter

Among all requirements for vehicle-to-everything (V2X) communications, successful delivery of packets with small delay is of the highest significance. Especially, the delivery of a message before a potential accident (i.e. emergency message) should be guaranteed. In this Chapter, I propose a novel cross-layer design to enhance the delivery of emergency messages so that accidents can be further avoided. This design refers to my paper [45]. Particularly, in the PHY layer, imperfect FD simultaneous transmitting and sensing is analysed and dynamic thresholds are mathematically formulated. Then a novel FD MAC protocol, named priority-based multiple access (PBMA) is proposed. Comparisons have been made among three different mechanisms. Benchmark is the DSRC standard. I also compare my proposed protocol with FD EDCA. Simulations have verified the accuracy of my analysis. They have also illustrated the delivery of emergency messages has been enhanced by deploying my proposed design.

We introduce the background, motivation and contributions of this work in Section 4.1. Next, the proposed PBMA design is introduced in Section 4.2. Afterwards, I present the considered system model and assumptions in Section 4.3. Furthermore, Corresponding mathematical analysis of both PHY and MAC layers are given in Section 4.4. In addition, numerical simulations are conducted and discussed based on the mathematical analysis in Section 4.5. Finally, this work is concluded in Section 4.6.

4.1 Introduction

V2X communication has been proposed to reduce accidents in future intelligent transportation system (ITS). Two promising standards are considered as potential candidates. One of them is IEEE 802.11p which is also known as the PHY/MAC specifications of dedicated short-range communication (DSRC) [1]; while the other solution is cellular-V2X (C-V2X) [4], which is built upon 4G or 5G platforms. Comparison between these two standards has been extensively studied in many works such as [9]. However, the goal of having an unified method for future V2X networks is not accomplished yet due to the fact that each of them has its own advantages. This work is built upon DSRC.

In current DSRC standard, safety messages known as cooperative awareness messages (CAMs) are exchanged periodically between vehicles in a broadcasting manner. In this case, acknowledgement (ACK) messages cannot be used to detect a failed transmission, and ACK messaging is not incorporated in the DSRC standard. In other words, nodes cannot detect collisions, and loss of these CAMs due to concurrent broadcasting would lead to a higher risk of accident. Current enhanced distributed channel access (EDCA) method adopted by DSRC needs further improvement, since the performance is shown to degrade significantly when the number of nodes in the network increases (dense network) [40], [6].

Another weak aspect of DSRC is related to the priority of CAMs. The levels of priority are named as access categories (ACs). Four ACs are defined (AC0-AC3), where AC0 has the highest priority and AC3 has the lowest priority. In addition, a backoff mechanism is used to avoid collisions. Smaller maximum contention window (CW) size and arbitrary inter-frame space (AIFS) are used to differentiate a high-priority AC from a low-priority AC. Therefore, high-priority ACs will access channel with a higher probability, and are expected to experience less backoff time and total waiting time. This collision avoidance and prioritised messaging mechanism adopted by EDCA is also known as internal collision handling mechanism [46], [47], as shown in Fig. 4.1 [46]. However, if CAMs with different priority levels are not generated at the same time, EDCA even cannot provide a higher access probability to the vehicle which has a high-priority CAM. The vehicle which has a low-priority CAM may complete the backoff process and take the channel before the high-priority CAM. In addition, when a collision has already happened between CAMs from different vehicles with different priority

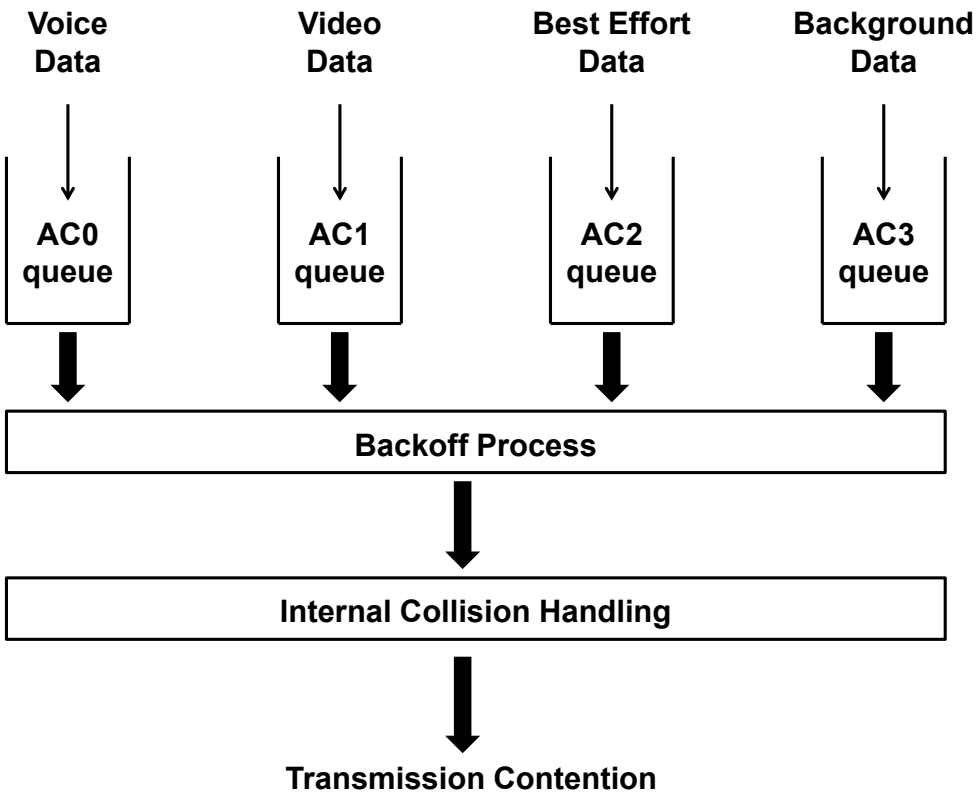

FIGURE 4.1: EDCA prioritised channel access

levels (a.k.a. external collision [46], [47]), all colliding CAMs are lost, because vehicles neither can recognise the collision, nor identify the priority of the colliding CAM. In other words, when multiple vehicles have selected the same slot to broadcast, EDCA neither can guarantee the transmission of high-priority CAMs, nor provide high-priority CAMs a greater probability to broadcast. The reason is that a vehicle is not able to detect concurrent transmissions, and it is also not able to identify the priority of a CAM from another vehicle. So emergency messages could be delayed or even lost, which would in turn result in a higher risk of accident.

There has been extensive work on CAM broadcast in DSRC. H. Luong et al. focused on optimising the CAM broadcast repetition interval [48]. F. Lyu et al. proposed a time slot-sharing MAC protocol for CAM broadcast [49]. They defined a danger coefficient for investigating the rear-end collisions, and then proposed a distributed congestion control scheme in [50]. Afterwards, they have collected DSRC communication traces, and proposed a beaconing scheme in [51]

to enhance broadcast reliability. In addition, Z. Tong et al. worked on the modeling of DSRC by using stochastic geometry [52]. Besides, many other works are showing potential congestion control mechanisms for future vehicular networks [53], [54]-[55]. However, none of these works applied in-band full-duplex (FD) technology [11] to V2X networks. Thus vehicles cannot detect collisions whilst transmitting. An overview of FD technology in vehicular communications is provided in [13]. In addition, an example of FD simultaneous sensing and transmitting is provided in [56]. Furthermore, M. Yang et al. used FD technology in vehicular networks and focused on managing the interference. Their results have shown the feasibility of deploying FD technology in future V2X networks [57]. To the best of my knowledge, the most recent and relevant work is [42], in which A. Bazzi et al. introduced FD technology and an enhanced CSMA/CA protocol into vehicular communications. Their results have shown the effectiveness on the reliability of deploying FD technology in terms of collision probability of packets and packet delivery ratio. However, the operation of simultaneous transmission and sensing was considered to be perfect, which is not realistic. In addition, their proposed MAC layer protocol did not differentiate the priority of CAMs between vehicles, hence low-priority messages could still transmit before high-priority messages. In other words, emergency messages, which are supposed to be transmitted before normal update messages to prevent accidents, may be delayed.

In order to conquer the aforementioned challenges, I propose to equip on-board units (OBUs) with my design. By deploying FD technology, vehicles are able to broadcast CAMs and sense the channel status at the same time over the same frequency band. Sensing is carried out through measuring the energy level of the channel, which is the simplest and the most widely-applied sensing method. Then vehicles can react to message collisions as soon as collisions are detected. Due to the fact that the existing prioritisation (i.e. ACs) in DSRC is designed for internal collisions, I introduce a new prioritisation scheme for detecting external collisions, and for enhancing the transmission of high-priority CAMs, when external collisions have happened. After detecting another ongoing transmission prior to a vehicle's own transmission, or collisions during a vehicle's transmission, proper actions should be followed immediately. I also propose a novel FD MAC protocol named priority-based multiple access (PBMA) to further schedule transmissions according to the priority of colliding CAMs. A vehicle which is in

an emergency situation has an opportunity to re-attempt to broadcast immediately before going through a backoff process whilst periodic update CAMs defer their transmission normally according to the same backoff rules in DSRC.

The contributions of this work are summarised as follows.

- I extend the PHY layer sensing method in my recent work in [39] by analysing the Doppler effect. Furthermore, herein I introduce a novel cross-layer design across PHY and MAC layers for efficient vehicular communications. In particular, here I propose a novel prioritisation scheme which is dedicated to CAMs and a MAC layer protocol named PBMA.
- Unlike other works such as [42] and [43], FD sensing results are not assumed to be perfect. Dynamic thresholds and increased sensing window size for deciding the channel status before and during broadcasting are mathematically derived. Closed-form expressions of detection and false alarm probabilities are also found based on transmit power, target probabilities of detection and false alarm, sensing time and SIC capability.
- Based on my design, a vehicle can enjoy prioritised CAM messaging when competing with other vehicles' broadcast messages. When a collision is detected, emergency messages can re-attempt to broadcast immediately before going to the backoff process. Average collision probability, collision duration, waiting time as well as successful delivery rate of the system are formulated. The delivery of emergency messages are also analysed through mathematics and simulations, and its performance is shown to be enhanced.

4.2 The Proposed PBMA Protocol

In order to cope with the priority issue between messages from different vehicles, I propose a novel MAC protocol named priority-based multiple access (PBMA) mechanism, in which FD technology is used for simultaneous transmission and sensing. First of all, a new prioritisation of CAMs is proposed for external collision detection and external transmission contention. I categorise CAMs into three types: critical CAMs (M_c), emergency CAMs (M_e) and normal vehicle status update CAMs (M_n). M_c CAMs have the highest priority and M_n CAMs have the lowest priority. The relationship between them and example generation scenarios of each type of CAMs are detailed in Table. 4.1. All types of CAMs contain information about the status of the vehicle such as speed and location. However, any sudden change of the status of the vehicle, such as a harsh breaking, is a critical and dangerous activity which should be sent out as soon as possible (generation scenario of M_c). Emergency messages (M_e) are generated when other gentle manoeuvres happen such as lane merging, because this type of message also shows the change of the vehicle status from normal cruising activity, which should also be recognised by other vehicles as soon as possible. The third category of CAMs (M_n) is generated when there is no potential danger and the vehicle is moving smoothly. In summary, I prioritise CAMs according to the status of the vehicle. Critical CAMs and emergency CAMs are event-triggered, vehicles would generate normal update CAMs for most of the time. my proposed categorisation only shows one approach to differentiate priorities between vehicles, any other number of priority levels could be considered.

TABLE 4.1: PRIORITISATION OF SAFETY MESSAGES

Priority	**CAM type**	**Example Generation Scenario**
High	M_c	Harsh breaking, skidding etc.
Middle	M_e	lane merging, gentle breaking etc.
Low	M_n	normal cruising etc.

The proposed PBMA protocol operates as follows. When a CAM is generated at a generic vehicle, same as in legacy HD EDCA mechanism, it first probes the medium for t_{sens} to determine whether the channel is busy or idle. If the channel is idle, the CAM is broadcast immediately in a FD manner, i.e. transmit and sense at the same time (TS mode). Otherwise, if the channel is occupied, normal update messages would defer its transmission by a random time interval (the backoff

process) same as in the accessing rule in DSRC; critical and emergency messages would keep sensing the channel instead of initiating the backoff process, and start broadcasting as soon as the channel is sensed idle for t_{sens} seconds.

During the transmission, unlike HD EDCA mechanism, collision detection (CD) capability is enabled in PBMA protocol. So vehicles which have M_c or M_e CAMs would not initiate backoff process immediately when a collision is detected. Instead they will re-attempt to broadcast in the following time slot. If another collision is detected, vehicles with M_e CAMs will go through a backoff process and vehicles with M_c CAMs will re-attempt one more time in the following slot before going to the backoff process. Such a mechanism is another difference compared to DSRC. The accessing mechanism of my proposed PBMA protocol has been depicted in Fig. 4.2.

The backoff process operates same as DSRC. First, a backoff counter is initialised with an integer random number of time slot which is randomly selected from uniformly distributed CW interval [0, CW_{max}]. Vehicles in the backoff process will sense the channel status continuously. If the channel is sensed idle for a slot duration, t_{slot}, counter is decremented by 1. Otherwise, counter will be frozen until the channel is sensed idle again for t_{slot} seconds. CAM is not transmitted until the counter reaches 0.

In summary, the proposed FD PBMA protocol has the following differences and advantages compared to DSRC:

- CD capability: FD technology has matured significantly in recent years, and given the less-constrained physical dimensions in OBUs, vehicles in future are expected to be able to detect collisions during transmission by incorporating full-duplex communication.
- Reliability: Vehicles are capable of detecting impending collision of a transmission without ACK messages. They can abort a transmission as soon as a collision is detected, so collision duration would be shortened. In addition, results show my design would work even when SIC is relatively poor.
- Compatibility: my design does not require ACK messages and further signalling, so it has great compatibility with current DSRC standard.
- Enhanced priority: my design has conquered the priority challenge between CAMs from different vehicles. In DSRC, priority only exists between

messages queued in a vehicle's buffer, when collisions happen between vehicles, all the colliding CAMs are lost, which may lead to severe delay or loss of emergency messages.

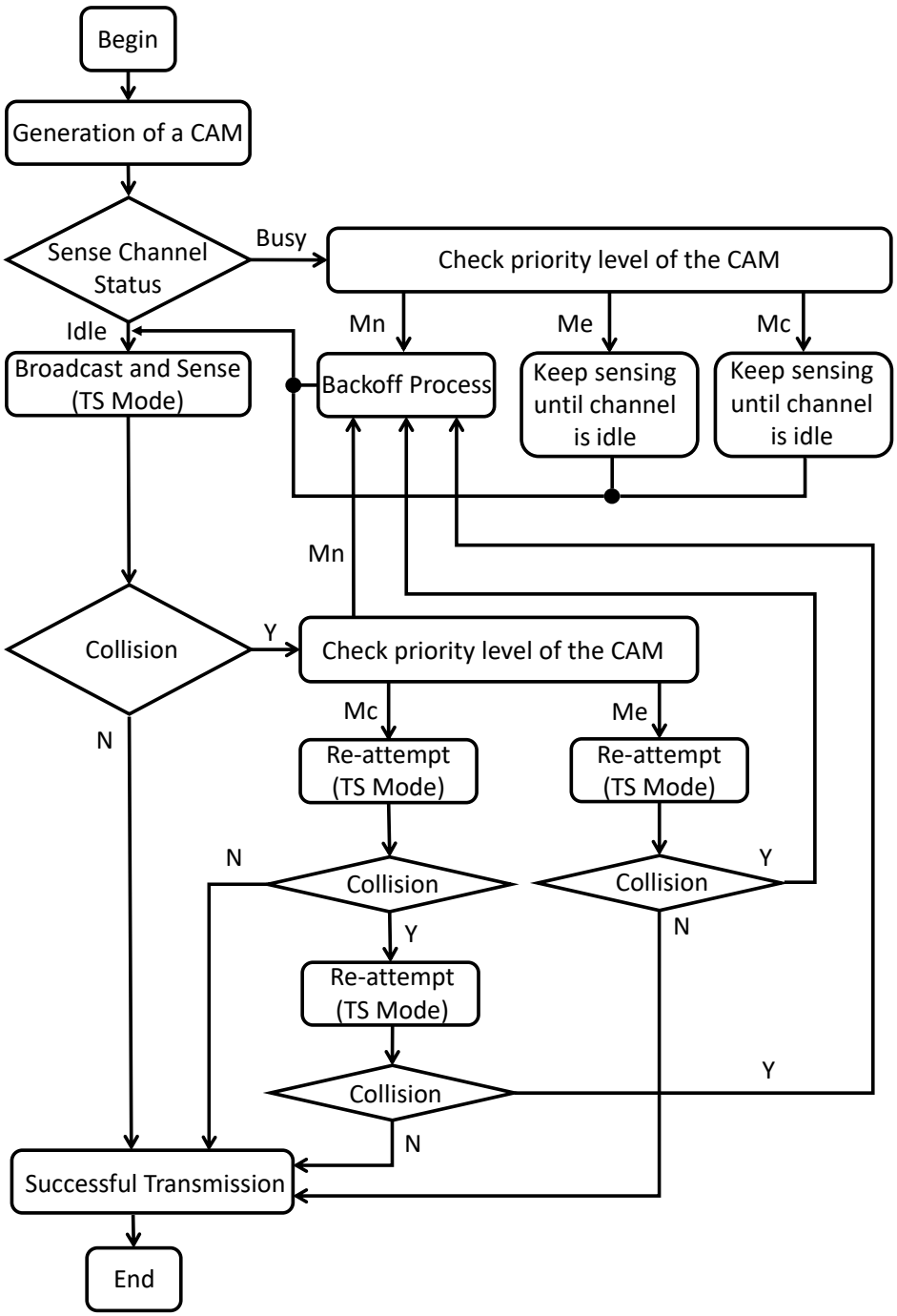

FIGURE 4.2: PBMA prioritised channel access, external collision handling mechanism

4.3 System Model

We consider a VANET in which vehicles broadcast CAMs periodically with a fixed CAM repetition interval t_{CAM}. All vehicles are equipped with FD capability. Rayleigh flat fading is assumed to be the channel model between vehicles. The noise component is assumed to be Gaussian, independent and identically distributed (i.i.d.) with zero mean and unit variance. Vehicles are distributed according to a Poisson Point Process (PPP) with density β as shown in Fig. 4.3. Such an assumption holds when the transmission range of vehicles is larger than the width of the road [52], [58]-[59]. In addition, vehicles have different transmission (R_{tx}) and sensing ranges (R_{sens}), and sensing range is larger than transmission range. Although the effect of hidden node problem is not eliminated, it can be weakened by increasing the sensing range R_{sens} and setting up thresholds according to the analysis in section IV.

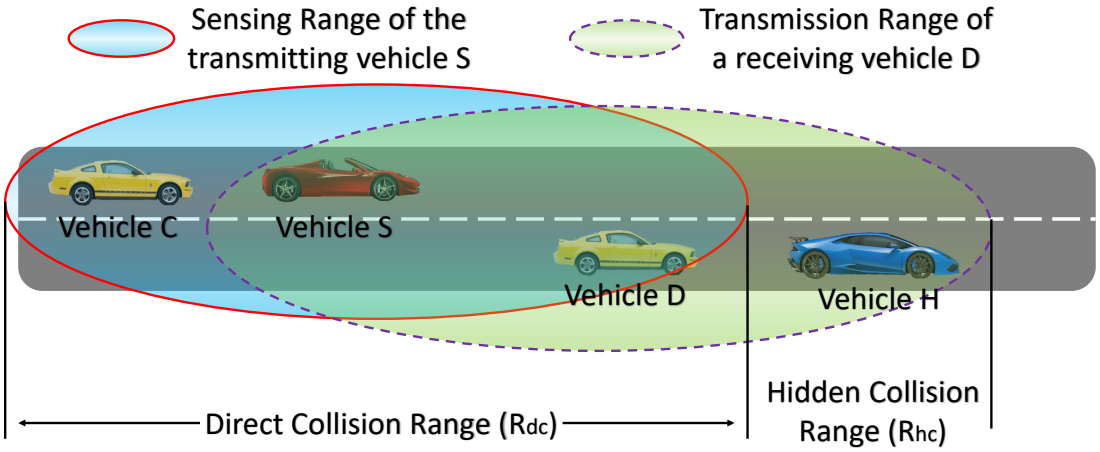

FIGURE 4.3: Demonstration of the VANET model and analysis of sections according to the position of vehicles

From now on when I refer to transmitting vehicle I mean the vehicle which is or going to transmit and sense the channel. Colliding vehicle(s) refer to the vehicle(s) that incur collision due to concurrent transmission. Hidden vehicle(s) are those vehicle(s) that are hidden to the transmitting vehicle (beyond the sensing range of the transmitting vehicle), but their transmissions would cause interference to a generic receiving vehicle.

Fig. 4.3 demonstrates two different ranges in which transmission of vehicles could possibly collide with the transmission of a generic transmitting vehicle S. Direct collision is defined as the collision of transmission by S with any vehicle (e.g. vehicle C) which is within the sensing range of S. The range of distance in which vehicles may lead to direct collision is called direct collision range and its range is represented by R_{dc}. Hidden collision is defined as the collision of transmission by S with any vehicle (e.g. vehicle H) which is beyond the sensing range of S and within the transmission range of a generic receiving vehicle such as D. The range of distance in which vehicles may lead to hidden collision is called hidden collision range and its range is represented by R_{hc}. Therefore, the average number of vehicles in the direct collision range is $N_{tx} = 2 \cdot R_{sens} \cdot \beta$ and the average number of vehicles in the hidden collision range is $N_{hc} = max(0, d + R_{sens} - R_{tx}) \cdot \beta$.

In my model, sensing is carried out through measuring the energy level of the channel. Since the received energy depends on the distance between the sensing vehicle and the potential concurrent transmitting vehicle(s), to be conservative, I have developed my model to be able to detect the signal collision from the farmost vehicle. Here vehicle S is assumed to be a transmitting and sensing vehicle, whilst vehicles C and D are potentially concurrent transmitting vehicles. It is obvious that S can easily detect the transmission of C if C is also broadcasting as C is close to S. However, D is relatively far away from S. If D is also broadcasting, the detecting of its transmission would be more difficult than detecting that of C. So, I set the thresholds to satisfy the detection of signals sent by D (farmost vehicle). Certain requirements for the received signal-to-interference-plus-noise ratio (SINR), sensing time and SIC capability are found, which will be discussed in section IV. Furthermore, my method performs even better when multiple CAMs are competing for broadcasting at the same time because the energy level of the received signal would be much higher and the colliding signal is much easier to be accurately detected. If the measured energy is less than the threshold ϵ_{th_0} which is derived in Section IV, the vehicle knows the channel is free for broadcasting; if the sensed energy is greater than the threshold ϵ_{th_0}, the vehicle knows there is another vehicle occupying the channel, and will not broadcast until the channel is free. Sensing process continues during the broadcasting period in a FD manner. The measured energy would be compared to an elevated threshold ϵ_{th_1} which is dependent on the amount of residual SI after cancellation. If the measured energy is higher than this elevated threshold ϵ_{th_1}, the vehicle knows

its transmission is in collision with another vehicle. Otherwise, the vehicle itself is regarded as the only one using the channel in the network.

TABLE 4.2: IMPORTANT NOTATIONS

Parameters	**Notes**
N	number of samples
r[n]	received signal at a FD node, where n = 1, 2, ..., N
τ	sensing time
f_s	sampling frequency
$w[n]$	noise signal with mean zero and variance σ_w^2
$s_i[n]$	SI signal with mean zero and variance σ_i^2
$s[n]$	transmit signal with mean zero and variance σ_s^2
η	SIC factor
$E\|.\|$	Expectation operator
σ_w^2	variance of $w[n]$ ($\sigma_w^2 = E\|w[n]\|^2$)
σ_i^2	variance of $s_i[n]$ ($\sigma_i^2 = E\|s_i[n]\|^2$)
σ_s^2	variance of $s[n]$ ($\sigma_s^2 = E\|s[n]\|^2$)
E	energy detection test statistic
Y_1	measured SNR of the node itself ($Y_1 = \frac{\sigma_i^2}{\sigma_w^2}$)
Y_2	measured SNR from other node ($Y_2 = \frac{\sigma_s^2}{\sigma_w^2}$)
ϵ_{th_0}	threshold used before transmission
ϵ_{th_1}	threshold used during transmission
H_i	hypothesis i where i = 0, 1, 2, 3
$P_{f,bt}$	probability of false alarm before transmission
$P_{f,dt}$	probability of false alarm during transmission
$P_{d,bt}$	probability of detection before transmission
$P_{d,dt}$	probability of detection during transmission
$Q(.)$	Q function operation
$p_i(x)$	PDF of E under hypothesis H_i
μ_i	mean value of $p_i(x)$
σ_i^2	variance of $p_i(x)$

However, the aforementioned detection is not perfect. All decisions are made with certain probabilities. Detection probability is defined as the probability that a vehicle successfully detects the presence of an event (an ongoing transmission or a collision) when the event actually takes place, and false alarm probability is defined as the probability that a vehicle falsely declare the presence of an event when the event does not occur. In order to have a high probability of detection, both thresholds (i.e. ϵ_{th_0}, ϵ_{th_1}) should be set to a low value. However, this setting

will also lead to a high false alarm probability. In other words, vehicles are missing opportunities to transmit. When a collision or false alarm occurs, it is left to the PBMA protocol to decide what course of actions should be followed.

In order to make the mathematical formulations clear, I list the important notations in Table. 4.2. Specifically, η refers to SIC factor which is the percentage of residual SI power after SIC and it varies between 0 and 1. If $\eta = 0$, it means that SIC is perfect and there is no residual SI.

In Section 4.4, I formulate the analytical performance of the proposed design, since it provides the theoretical performance from the mathematical point of view, which can be used not only to verify the simulation results, but also to provide values and rationale for developing the proposed design in a field test or in future applications.

4.4 Mathematical Analysis

First of all, I analyse the PHY layer FD simultaneous transmitting and sensing as follows. In the sensing phase, Doppler effect would affect detection accuracy. Doppler frequency shift formula is given by

$$\Delta f = \frac{\Delta v}{c} \cdot f_0, \tag{4.1}$$

where Δf denotes the frequency shift, Δv is the relative speed between vehicles, c represents the speed of light and f_0 refers to the emitted centre frequency.

In addition, required bandwidth for a CAM broadcast can be calculated by Shannon-Hartley theorem, which is given by:

$$C = B \times log_2(1 + SNR). \tag{4.2}$$

Taking the standardised parameters in DSRC [36] as an example, I assume that the SNR is 1 dB, transmit rate is 6 $Mbps$, maximum relative speed between vehicles is 500 km/h. Thus, the required bandwidth for a CAM broadcast is 6 MHz, and the maximum Doppler frequency shift is approximately 2.731 kHz. The results show that only a portion of the allocated 10 MHz bandwidth is used for a CAM broadcast, and there is enough guard frequency gap between channels.

Therefore, in order to mitigate Doppler effect in the sensing phase, instead of sensing the bandwidth used for broadcast, I increase the sensing bandwidth. The increased sensing bandwidth B', by taking Doppler frequency shift into consideration, is designed to be twice of the maximum Doppler frequency shift, which is given by

$$B' = B + 2 \cdot \Delta f. \tag{4.3}$$

As shown in Fig. 4.4, by increasing the sensing window size (i.e. sensing window 2), no information will be lost, as the whole signal falls into the sensing range. On the contrary, if sensing window size remains unchanged (i.e. sensing window 1), due to the effect of Doppler frequency shift, the shifted part of the signal (i.e. shadowed part) goes beyond the sensing range, resulting in losing some information of the signal. In addition, the higher the SNR is, the worse the sensing accuracy will be, as a higher percentage of the signal will go beyond the sensing window, resulting in more energy of the signal cannot be measured.

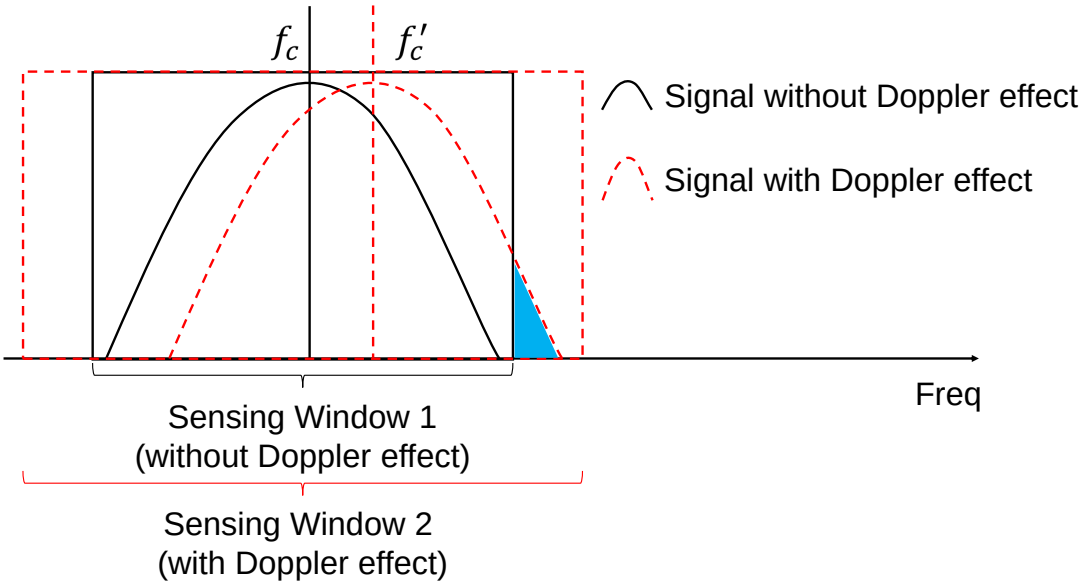

FIGURE 4.4: Demonstration of the increased sensing bandwidth strategy for mitigating Doppler effect on sensing accuracy

Hence, the measured energy will be lower than the actual energy of the signal. Accordingly, probability of detection will decrease, and probability of false alarm will increase.

Furthermore, this strategy will not be affected by inter-channel interference, because the sensing window size is much smaller than the allocated 10 MHz channel bandwidth.

A comparison of sensing accuracy between two sensing window sizes has been made later in the simulation section.

Then, I analyse probabilities of detection and false alarm before and during transmission with increased sensing window size. Under hypothesis H_0, E is a random variable (RV) whose probability density function (PDF) $p_0(x)$ follows a Chi-squared distribution, probability of false alarm can be expressed as [18]

$$P_{f,bt} = Q((\frac{\epsilon_{th_0}}{\sigma_w^2} - 1) \cdot \sqrt{N}). \tag{4.4}$$

Under hypothesis H_1, probability of detection under this hypothesis is given by

$$P_{d,bt} = Q((\frac{\epsilon_{th_0}}{\sigma_w^2} - \Upsilon_2 - 1) \cdot \sqrt{\frac{N}{2\Upsilon_2+1}}). \tag{4.5}$$

Under hypothesis H_2, similar to H_1, probability of false alarm is derived as

$$P_{f,dt} = Q((\frac{\epsilon_{th_1}}{\sigma_w^2} - \eta^2 \Upsilon_1 - 1) \cdot \sqrt{\frac{N}{2\eta^2 \Upsilon_1 + 1}}). \tag{4.6}$$

Under hypothesis H_3, similar to the previous hypotheses, probability of detection during transmission is given by

$$P_{d,dt} = Q((\frac{\epsilon_{th_1}}{\sigma_w^2} - \Upsilon_2 - \eta^2 \Upsilon_1 - 1) \times \sqrt{\frac{N}{2\eta^2 \Upsilon_1 + 2\eta^2 \Upsilon_1 \Upsilon_2 + 2\Upsilon_2 + 1}}). \tag{4.7}$$

Next, I analyse the relationship between thresholds ϵ_{th_0} and ϵ_{th_1}, when increased sensing window size strategy is deployed. Threshold ϵ_{th_0} is found from Eq. (4.5) by calculating the inverse Q function, which is given by

$$\epsilon_{th_0} = (\frac{(Q^{-1}(\overline{P_{d,bt}})}{\sqrt{\frac{N}{2\Upsilon_2 + 1}}} + \Upsilon_2 + 1) \cdot \sigma_w^2, \tag{4.8}$$

and threshold ϵ_{th_1} is given by Eq. (4.7) as

$$\epsilon_{th_1} = (\frac{(Q^{-1}(\overline{P_{d,dt}})}{\sqrt{\frac{N}{2\eta^2 \Upsilon_1 + 2\eta^2 \Upsilon_1 \Upsilon_2 + 2\Upsilon_2 + 1}}} + \Upsilon_2 + \eta^2 \Upsilon_1 + 1) \cdot \sigma_w^2. \tag{4.9}$$

Assume the target probabilities of detection before and during transmission are identical, then the relationship between the two thresholds can be derived as

$$\epsilon_{th_1} = \frac{\frac{\epsilon_{th_0}}{\sigma_w^2} - \Upsilon_2 - 1}{\sqrt{\frac{2\Upsilon_2 + 1}{2\eta^2 \Upsilon_1 + 2\eta^2 \Upsilon_1 \Upsilon_2 + 2\Upsilon_2 + 1}}} + \eta^2 \Upsilon_1 + \Upsilon_2 + 1. \tag{4.10}$$

This relationship is depicted in Fig. 4.5 by using Eq. (4.10). It shows that the higher the residual SI, the higher the thresholds, and the bigger the difference between the two thresholds would be.

In addition, SIC factor is not always fixed, it may fluctuate due to the imperfection of the hardware or channel variations. For a given SIC factor η_0 with $\pm m\%$ fluctuation distributed uniformly, with the help of the approximation of the Q

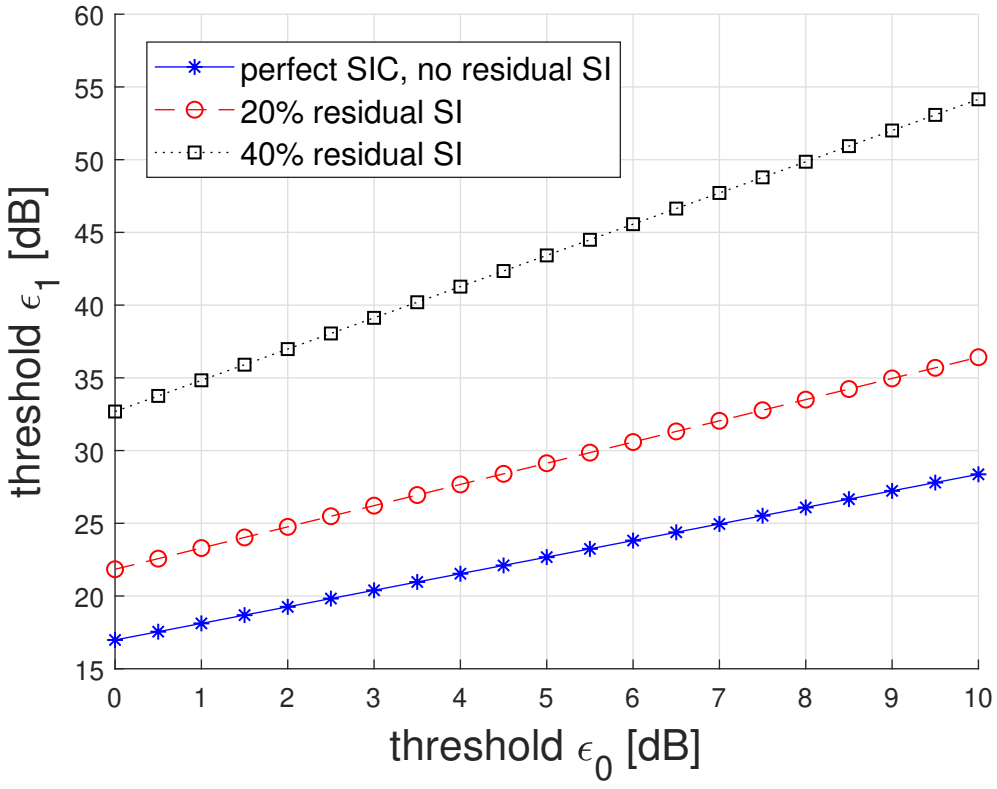

FIGURE 4.5: relationship between threshold ϵ_{th_0} and threshold ϵ_{th_1}

function [44], the average probability of false alarm can be calculated by

$$\begin{aligned}\overline{P_{f,dt}} \approx & \frac{1}{2}Q\left(\left(\frac{\epsilon_{th_1}}{\sigma_w^2} - (\eta_0+m)^2\Upsilon_1 - 1\right)\sqrt{\frac{N}{2(\eta_0+m)^2\Upsilon_1+1}}\right)+ \\ & \frac{1}{2}Q\left(\left(\frac{\epsilon_{th_1}}{\sigma_w^2} - (\eta_0-m)^2\Upsilon_1 - 1\right)\sqrt{\frac{N}{2(\eta_0+m)^2\Upsilon_1+1}}\right).\end{aligned} \tag{4.11}$$

According to the above analysis and thresholds settings, a vehicle can detect concurrent transmissions with certain probabilities of detection and false alarm. Then the vehicle will schedule its broadcast according to the deployed MAC layer protocol. I formulate collision probability, collision duration, waiting time as well as throughput by deploying three different mechanisms. The first mechanism is the current DSRC standard which uses HD EDCA method. The second method is FD EDCA scheme and the last strategy is my proposed FD PBMA design.

4.4.1 Collision Probability

Collisions happen due to direct collisions and hidden collisions. Direct collisions happen in two cases. The first case is when the channel is idle, there are at least two vehicles which have CAMs to broadcast and all of them do not wrongly detect (i.e. no false alarm) the channel status. The other case is when the channel is busy, there is at least one vehicle which has a CAM to transmit, but the vehicle(s) mis-detect(s) the presence of the ongoing transmission. So the overall direct collision probability is given by the sum of the probabilities in these two cases:

$$P_{dc}(HD) = P_{dc1}(HD) + P_{dc2}(HD). \tag{4.12}$$

Direct collision probability in the first case (i.e. channel idle) is given by

$$P_{dc1}(HD) = \sum_{i=2}^{i=N_{tx}} P_{idle}(HD)(1 - P_f)^i P_s(i), \tag{4.13}$$

where $P_{idle}(HD)$ represents the probability that the channel is idle. P_f is the false alarm probability, $P_s(i)$ represents the probability that i vehicles broadcast CAMs at the same time.

To find $P_{idle}(HD)$, I first build up a Markov model to evaluate the backoff process, because channel is idle when no vehicle is transmitting, and an arbitrary vehicle is not transmitting in two cases. The first case is where a vehicle has already finished transmission and has nothing to transmit within the current CAM repetition interval. The second case is where a vehicle has something to transmit but it is in the backoff process.

If I treat each backoff process independently, once the counter is decremented to 0, it never goes out of the state. Besides, it is possible to go from any state to state 0. Therefore the conditions for using an absorbing Markov chain model are satisfied and the model is shown in Fig. 4.6.

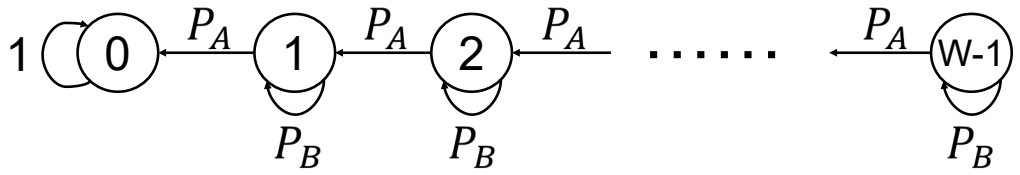

FIGURE 4.6: Markov model for analysing the backoff process

P_A represents the probability to find the channel idle for one slot duration, which is given by

$$P_A = P_{idle}(HD)(1 - P_f) + (1 - P_{idle}(HD))(1 - P_d), \tag{4.14}$$

where P_d refers to the detection probability.

P_B refers to the probability to find the channel busy for one slot duration, which is given by

$$P_B = P_{idle}(HD)P_f + (1 - P_{idle}(HD))P_d. \tag{4.15}$$

So the transition matrix P is

$$\begin{bmatrix} P_A & 0 & 0 & \dots & 0 & P_B \\ P_B & P_A & 0 & \dots & 0 & 0 \\ 0 & P_B & P_A & \dots & 0 & 0 \\ \vdots & \vdots & \vdots & \ddots & \vdots & \vdots \\ 0 & 0 & 0 & \dots & P_A & 0 \\ 0 & 0 & 0 & \dots & 0 & 1 \end{bmatrix}.$$

The fundamental matrix $N = (I - Q)^{-1}$ is

$$\begin{bmatrix} 1 - P_A & 0 & 0 & \dots & 0 \\ -P_B & 1 - P_A & 0 & \dots & 0 \\ 0 & -P_B & 1 - P_A & \dots & 0 \\ \vdots & \vdots & \vdots & \ddots & \vdots \\ 0 & 0 & 0 & \dots & 1 - P_A \end{bmatrix}^{-1}.$$

Thus average waiting time for each backoff process is

$$t_{BO} = \frac{1}{W} \cdot \left(\sum_{i=0}^{W-1} \sum_{j=0}^{W-1} (N_{ij}) \right) \cdot t_{slot}, \tag{4.16}$$

where i and j refer to the row and column index of the fundamental matrix, W refers to the contention window size and $i, j \in [0, W-1]$.

Therefore I get $P_{idle}(HD)$ as

$$P_{idle}(HD) = \sum_{i=0}^{i=N_{tx}} \left(\frac{t_{CAM} - t_{BO} - t_{pkt}}{t_{CAM}} \right)^i \cdot \left(\frac{t_{BO}}{t_{CAM}} \right)^{N_{tx} - i}, \tag{4.17}$$

where t_{CAM} is the CAM repetition interval and t_{pkt} is transmission duration of a CAM.

Now the only unknown variable is $P_s(i)$. To find $P_s(i)$, I introduce P_r which refers to the probability that there is a CAM waiting to be broadcast at a vehicle, and P_σ denoting the probability that the CAM is ready to be broadcast immediately (i.e. backoff counter is zero). Thus $P_s(i)$ is given by

$$P_s(i) = \sum_{i=2}^{i=N_{tx}} 1 - (1 - P_r P_\sigma)^{i-1}. \tag{4.18}$$

According to the absorbing Markov chain model shown in Fig. 4.6, P_σ is given by

$$P_\sigma = \frac{1}{W^2}\left(\sum_{i=0}^{W-1}\sum_{i=0}^{W-1}(N_{ij})\right) + \frac{1}{W}, \tag{4.19}$$

and the last unknown variable P_r can be found from

$$\begin{aligned} P_r = &\frac{1}{t_{CAM}}\{\frac{W \cdot (1 - P_{idle}(HD))}{2}[(1 - P_s(i))t_{slot} + P_s(i)(t_{slot} \\ &+ t_{AIFS} + t_{pkt})] + t_{pkt}\}. \end{aligned} \tag{4.20}$$

Similarly I can find the direct collision probability in the second case (i.e. channel busy) as

$$P_{dc2}(HD) = \sum_{i=1}^{i=N_{tx}} (1 - P_{idle}(HD))(1 - P_d)^i P_s(i). \tag{4.21}$$

Hidden collision probability is approximated in a same way as shown in [42] as double of the transmission time from the vehicles at R_{dc}:

$$P_{hc}(HD) = \frac{2(N_{hc}-1)}{t_{CAM}}(t_{AIFS} + t_{pkt})(1 - \frac{P_{dc}(HD)}{2}). \tag{4.22}$$

Thus the overall collision probability in DSRC is given by

$$P_c(HD) = P_{dc}(HD) + P_{hc}(HD) - P_{dc}(HD)P_{hc}(HD). \tag{4.23}$$

Then I analyse collision probability ($P_c(FD)$) when FD EDCA is deployed. Compared to HD EDCA mechanism, the only difference is that vehicles can sense

the channel whilst broadcasting. So vehicles can abort transmissions and initiate the backoff process as soon as collisions are detected. Direct collision is also composed of the aforementioned two cases (channel idle case and channel busy case), which is given by

$$P_{dc}(FD) = P_{dc1}(FD) + P_{dc2}(FD), \tag{4.24}$$

where $P_{dc1}(FD)$ represents the collision probability when channel is idle and $P_{dc2}(FD)$ represents the collision probability when channel is busy.

Direct collision probability in the first case (i.e. channel idle) is given by

$$P_{dc1}(FD) = \sum_{i=2}^{i=N_{tx}} P_{idle}(FD)(1-P_f)^i P_s(i), \tag{4.25}$$

and direct collision probability in the second case (i.e. channel busy) is given by

$$P_{dc2}(FD) = \sum_{i=1}^{i=N_{tx}} (1-P_{idle}(FD))(1-P_d)^i P_s(i), \tag{4.26}$$

Hidden collision probability is found by the same method as in the analysis of the DSRC standard as

$$P_{hc}(FD) = \frac{2}{t_{CAM}}(N_{hc}-1)(t_{AIFS}+t_{pkt})(1-\frac{P_{dc}(FD)}{2}). \tag{4.27}$$

Finally I get the overall collision probability when FD EDCA mechanism is deployed as

$$P_c(FD) = P_{dc}(FD) + P_{hc}(FD) - P_{dc}(FD)P_{hc}(FD). \tag{4.28}$$

Now I extend my analysis to my proposed PBMA design. Assume normal update, emergency and critical CAMs are generated with probabilities P_{gn}, P_{ge} and P_{gc}, respectively. Four cases could lead to direct collisions. The first case is when the channel is busy, there is at least one vehicle which has a CAM to transmit, but the vehicle(s) mis-detect(s) the presence of the ongoing transmission. Direct collision probability in this case is given by

$$P_{dc1}(PBMA) = \sum_{i=1}^{i=N_{tx}} (1-P_{idle}(PBMA))(1-P_d)^i P_s(i). \tag{4.29}$$

The second case is when the channel is idle, there are at least two M_c or M_e CAMs generated and at least two of these vehicles do not announce false alarm. Direct collision probability in this case is given by

$$P_{dc2}(PBMA) = \sum_{i=2}^{i=N_{tx}} P_{idle}(PBMA)(P_{gc} + P_{ge})^i(1 - P_f)^i P_s(i). \tag{4.30}$$

The third case is when the channel is idle, there is one critical or emergency CAM and at least one normal update CAM which is going to transmit at the same time. Direct collision probability in this case is given by

$$P_{dc3}(PBMA) = \sum_{i=1}^{i=N_{tx}} P_{idle}(PBMA)(P_{gc} + P_{ge})(1 - P_f)^i P_s(i). \tag{4.31}$$

The last case is when the channel is idle, there are only at least two normal messages ready to transmit at the same time(no M_c and M_e). Direct collision is given by

$$P_{dc4}(PBMA) = \sum_{i=1}^{i=N_{tx}} P_{idle}(PBMA)P_{gn}^i(1 - P_f)^i P_s(i). \tag{4.32}$$

Thus overall direct collision probability is given by

$$P_{dc}(PBMA) = P_{dc1}(PBMA) + P_{dc2}(PBMA) + P_{dc3}(PBMA) + P_{dc4}(PBMA). \tag{4.33}$$

Similar to the DSRC analysis, I obtain hidden collision probability as

$$P_{hc}(PBMA) = \frac{2}{t_{CAM}}(N_{hc} - 1)(t_{AIFS} + t_{pkt})(1 - \frac{P_{dc}(PBMA)}{2}). \tag{4.34}$$

Therefore the overall collision probability by deploying the PBMA design is given by

$$P_c(PBMA) = P_{dc}(PBMA) + P_{hc}(PBMA) - P_{dc}(PBMA) \cdot P_{hc}(PBMA). \tag{4.35}$$

4.4.2 Collision Duration

In DSRC whether a direct collision or hidden collision happens, collision lasts for a whole packet time because vehicles are not able to detect collisions. Average collision duration is

$$C_d^A(HD) = P_c(HD) \cdot t_{pkt}. \tag{4.36}$$

When FD EDCA mechanism is deployed and sensing is considered to be imperfect, since the probability that all vehicles in collision mis-detect for three consecutive time slots is very low, I only consider for up to three consecutive mis-detections. Average collision duration is given by

$$\begin{aligned} C_d^A(FD) =& P_{dc}(FD) \cdot t_h \cdot (2P_d - P_d^2) + P_{dc}(FD) \cdot 2t_h \cdot (1-P_d)^2 \times \\ & (2P_d - P_d^2) + P_{dc}(FD) \cdot 3t_h \cdot (1-P_d)^4 \cdot (2P_d - P_d^2) + P_{hc}(FD) \cdot t_{pkt}. \end{aligned} \tag{4.37}$$

The last strategy is based on my proposed PBMA design. Overall collision duration is given by the sum of collision durations in seven cases. The first case is direct collisions between normal CAMs, the second case is direct collisions between critical and normal CAMs, the third case is direct collisions between emergency and normal CAMs, the fourth case is direct collisions between critical CAMs, the fifth case is direct collisions between emergency CAMs, the sixth case is direct collisions between critical and emergency CAMs, and the last case is hidden collisions.

The first case happens with probability $P_1 = P_{gn}^2$:

$$\begin{aligned} C_{d,1}^A(PBMA) =& P_{dc}(PBMA) \cdot [(2P_d - P_d^2) \cdot t_h + (1-P_d)^2 \times \\ & (2P_d - P_d^2) \cdot 2t_h + (1-P_d)^4 (2P_d - P_d^2) \cdot 3t_h]. \end{aligned} \tag{4.38}$$

The second case happens with probability $P_2 = 2P_{gc}P_{gn}$:

$$\begin{aligned} C_{d,2}^A(PBMA) =& P_{dc}(PBMA) \cdot [P_d \cdot t_h + (P_d^3 - P_d^2 + P_d) \cdot 2t_h \\ & + (-2P_d^6 + 9P_d^5 - 15P_d^4 + 13P_d^3 - 7P_d^2 + 2P_d) \cdot 3t_h]. \end{aligned} \tag{4.39}$$

The third case happens with probability $P_3 = 2P_{ge}P_{gn}$:

$$\begin{aligned} C^A_{d,3}(PBMA) =& P_{dc}(PBMA) \cdot [P_d \cdot t_h + (P_d^3 - P_d^2 + 2P_d) \cdot 2t_h \\ &+ (P_d^5 - 5P_d^4 + 9P_d^3 - 7P_d^2 + 2P_d) \cdot 3t_h]. \end{aligned} \tag{4.40}$$

The fourth case happens with probability $P_4 = P_{gc}^2$:

$$\begin{aligned} C^A_{d,4}(PBMA) =& P_{dc}(PBMA) \cdot [(2P_d - P_d^2) \cdot 3t_h + (2P_d - P_d^4 + 4P_d^3 - 5P_d^2) \\ &\cdot 4t_h + (-P_d^6 + 6P_d^5 - 14P_d^4 + 16P_d^3 - 9P_d^2 + 2P_d) \cdot 5t_h]. \end{aligned} \tag{4.41}$$

The fifth case happens with probability $P_5 = P_{ge}^2$:

$$\begin{aligned} C^A_{d,5}(PBMA) =& P_{dc}(PBMA) \cdot [(2P_d - P_d^2) \cdot 2t_h + (2P_d - P_d^4 + 4P_d^3 - 5P_d^2) \cdot 3t_h \\ &+ (-P_d^6 + 6P_d^5 - 14P_d^4 + 16P_d^3 - 9P_d^2 + 2P_d) \cdot 4t_h]. \end{aligned} \tag{4.42}$$

The sixth case happens with probability $P_6 = 2P_{gc}P_{ge}$:

$$\begin{aligned} C^A_{d,6}(PBMA) =& P_{dc}(PBMA) \cdot [P_d \cdot 2t_h + (-P_d^2 + P_d) \cdot 3t_h + \\ &(-P_d^4 + 4P_d^3 - 5P_d^2 + 2P_d) \cdot 4t_h]. \end{aligned} \tag{4.43}$$

The last case happens with probability $P_{hc}(PBMA)$:

$$C^A_{d,7}(PBMA) = t_{pkt}. \tag{4.44}$$

Finally I find the average collision duration as:

$$C^A_d(PBMA) = \sum_{i=1}^{7} P_{idle} \cdot C^A_{d,i}(PBMA). \tag{4.45}$$

4.4.3 Waiting Time

We define average waiting time as the time duration a packet stays in the buffer, which includes the sensing delay and backoff time. In other words, it is equivalent to the access delay by assuming the queuing delay is zero, because the old

packet has been assumed to be dropped when a new packet is generated according to the standard [1]. Same definition has also been used in other papers such as [60].

Given the average waiting time for each backoff process in Eq. (4.16), the overall average waiting time in DSRC can be calculated as

$$T_w(HD) = P_{idle}(HD)t_h + (1 - P_{idle}(HD))(t_h + t_{BO}). \tag{4.46}$$

In the FD EDCA strategy, average waiting time is attributed to four different cases. The first case is when the channel is idle and no false alarm happens. So the waiting time would be one sensing duration:

$$T_{w,1}(FD) = P_{idle}(FD) \cdot (1 - P_f) \cdot t_h. \tag{4.47}$$

The second case is when the channel is sensed as busy whilst it is actually busy:

$$\begin{aligned} T_{w,2}(FD) =& (1 - P_{idle}(FD))P_d(t_h + t_{BO}) + \\ & (1 - P_{idle}(FD))^2 P_d^2(2t_h + t_{BO} + t'_{BO}) + \dots \quad , \end{aligned} \tag{4.48}$$

where t'_{BO} refers to the second continuous backoff duration.

The third case is when false alarm happens:

$$\begin{aligned} T_{w,3}(FD) =& P_{idle}(FD)P_f(t_h + t_{BO}) + \\ & P_{idle}(FD)P_f(1 - P_{idle}(FD))P_d(2t_h + t_{BO} + t'_{BO}) + \dots \quad . \end{aligned} \tag{4.49}$$

The last case is when mis-detection happens, so the vehicle starts transmission but it detects the collision during its transmission:

$$\begin{aligned} T_{w,4}(FD) =& (1 - P_{idle}(FD))^2 P_m P_d(FD)(2t_h + t_{BO}) + \\ & (1 - P_{idle}(FD))^3 P_m P_d^2(3t_h + t_{BO} + t'_{BO}) + \dots \quad . \end{aligned} \tag{4.50}$$

Finally I find the overall average waiting time as the sum of all above four cases:

$$T_w(FD) = \sum_{i=1}^{4} T_{w,i}(FD). \tag{4.51}$$

Now I analyse the average waiting time of the PBMA mechanism. When a normal update message is generated, the waiting time is equal to the waiting time by using the FD EDCA method:

$$T_{w,1}(PBMA) = P_{gn} \cdot T_w(FD). \tag{4.52}$$

When a critical message is generated and the channel is sensed as busy, the transmitting vehicle would keep sensing and broadcast as soon as the current transmission is finished. So the average waiting time in this case would be half the packet transmission duration. Otherwise when the channel is sensed as idle, the waiting time would be one sensing duration. In addition, because sensing is not perfect, false alarm and mis-detection could happen. In the false alarm case, vehicles which have critical CAMs will not go to the backoff process. The average waiting time would be half the packet transmission duration. In the mis-detection case, since the probability that continuous mis-detection occurs is small, I assume a correct detection with probability P_d in the first transmission and sensing slot. Then the vehicle would go to the backoff process, and the average waiting time in this case would be two sensing durations plus the backoff time. Therefore, the overall waiting time is given by

$$\begin{aligned} T_{w,2}(PBMA) =& P_{gc}(1 - P_{idle}(PBMA))P_d\frac{t_{pkt}}{2} + \\ & P_{gc}P_{idle}(PBMA)P_d t_h + \\ & P_{gc}P_{idle}(PBMA)P_f\frac{t_{pkt}}{2} + \\ & P_{gc}P_{idle}(PBMA)^4 P_m P_d^3(4t_h + t_{BO}) + \\ & P_{gc}P_{idle}(PBMA)^5 P_m P_d^4(5t_h + t_{BO} + t'_{BO}) + \ldots \quad . \end{aligned} \tag{4.53}$$

When the generated CAM is M_e, average waiting time would be

$$\begin{aligned} T_{w,3}(PBMA) =& P_{ge}(1 - P_{idle}(PBMA))P_d\frac{t_{pkt}}{2} + \\ & P_{ge}P_{idle}(PBMA)P_d t_h + \\ & P_{ge}P_{idle}(PBMA)P_f\frac{t_{pkt}}{2} + \\ & P_{ge}(1 - P_{idle}(PBMA))^3 P_m P_d^2(3t_h + t_{BO}) + \\ & P_{ge}(1 - P_{idle}(PBMA))^4 P_m P_d^3(4t_h + t_{BO} + t'_{BO}) + \ldots \quad . \end{aligned} \tag{4.54}$$

Therefore the overall average waiting time is given by the sum of the above three time durations:

$$T_w(PBMA) = \sum_{i=1}^{3} T_{w,i}(PBMA). \tag{4.55}$$

4.4.4 Throughput

We define the system throughput as the total number of successful broadcast packets within a CAM repetition interval, which can be calculated as

$$SR = N_{tx} \cdot (\frac{t_{CAM} - T_w}{t_{CAM}}) \cdot (1 - P_c). \tag{4.56}$$

4.4.5 Evaluation of Critical Messages Transmission

In addition to average system performance, it is also important to compare the performance of transmitting critical messages in different mechanisms. Since the successful delivery of M_c within a short amount of time is the key to avoid accidents.

The formulations of transmitting M_c in the legacy HD EDCA and FD EDCA mechanisms are the same as shown in the previous section, because there is no priority between CAMs from different vehicles. However, my proposed PBMA mechanism operates differently, for which the analysis is shown as follows.

1) Collision Probability: When M_c is generated, collision happens in three cases. The first case is mis-detection. The second case is simultaneous start of transmission when channel is idle. The last case is due to hidden collision. Therefore the collision probability of critical messages is given by

$$\begin{aligned} P_c(M_c) =& P_{gc}(1 - P_{idle}(PBMA))(1 - P_d) + \\ & P_{gc}P_{idle}(PBMA)P_dP_s(i) + P_{hc}(PBMA). \end{aligned} \tag{4.57}$$

2) Collision Duration: Critical CAMs could collide with normal, critical and emergency CAMs, and collision duration for each case is different. The corresponding collision durations are given by Eq. (4.39), Eq. (4.41) and Eq. (4.43), respectively. Besides, collision duration due to hidden collision is shown in Eq. (4.44). Therefore the average collision duration of critical messages is given by

$$C_d^A(M_c) = \sum_{i=2,4,6,7} P_i \cdot C_{d,i}^A(PBMA). \tag{4.58}$$

3) Waiting Time: Average waiting time of M_c has already been analysed and its formulation is shown in Eq. (4.53).

In addition to the mathematical analysis, computer simulation is another significant tool to observe and evaluate the performance of the proposed novel design before a real-world field test. The results can also be used to mutually verify or debug the mathematical analysis results. In particular, if the differences between the analytical and simulation results go beyond a reasonable error region, it is highly likely that there is a mistake. Furthermore, the trend and value of the figures can be helpful in positioning and debugging the mistake. Therefore, in Section 4.5, we present both the mathematical analysis and simulation results.

4.5 Simulation Results

Following the mathematical analysis, I now evaluate my proposed method through simulations. Specifically, the computer simulation conducted is realistic link-level simulation instead of numerical analysis. Vehicles are generated and movements are simulated in SUMO, data is then imported into MATLAB. The PHY and MAC layers of DSRC and my proposed PBMA protocol are simulated in MATLAB. CAMs are generated and broadcast according to the EDCA or the proposed PBMA protocols. Energy levels are measured by taking samples and integrating over the given sensing duration, which are then compared to the predefined thresholds depending on which transmission phase the vehicle is in (i.e., before or during transmission cases). Doppler effect has been added by using the built-in function in MATLAB. Finally, the results such as collision probability is calculated by firstly tabulating the total number of collisions and then divided by the total number of CAM transmissions. Simulation parameters are shown in Table 4.3, which are realistic, because they are the values and scheme suggested in the standard [1], which have also been used in the field test [8] and other research papers such as [42]. The reason why only the standard instead of prior art has been chosen as the benchmark is because to the best of my knowledge, the paper [42] was the only prior art working on the same topic. However, in [42], the metrics used for evaluation were for a tagged vehicle only, whilst in my work, all evaluation metrics are formulated from a system average performance perspective. Therefore, I chose the standard as the only benchmark, same as what other researchers did, such as the authors in [42].

Fig. 4.7 shows the impact of mobility on the detection probability, where the analytical curve is plotted by using Eq. (4.7). First of all, if vehicles are equipped with dynamic threshold and increased sensing window size, target detection probability (i.e. 90%) can be met. However, if the size of the sensing window remains unchanged, detection probability drops as the relative speed of vehicles increases, since a higher percentage of energy of the signal goes beyond the sensing window, and hence cannot be measured due to the Doppler frequency shift effect.

Fig. 4.8 and Fig. 4.9 illustrate the significant impact of transmit power and the difference between two threshold setting strategies, where the analytical curves are plotted by using Eq. (4.5) and Eq. (4.6), respectively. One strategy is based

TABLE 4.3: SIMULATION PARAMETERS

Parameters	**Values**
target $P_{d,bt}$ & $P_{d,dt}$	90%
modulation scheme	BPSK, QPSK
SNR1	+10 dB
SNR2	(-20)→0 dB
residual SI	0%-40%
vehicle density	0-200 vehicles/km
relative speed	0-500 km/h
transmission rate	6 Mbps
CAM length	350 bytes/pkt
arbitrary Inter-frame Space	58 μsec
slot duration (t_{slot})	13 μsec
CAM repetition interval (t_{CAM})	100 ms

on my proposed method where thresholds are dynamically changing, whilst the other strategy corresponds to the fixed threshold method. For the fixed threshold strategy, along with the rise of the transmit power, detection probability increases at the cost of having a high and unacceptable false alarm probability. my proposed method has a lower detection probability which is still in the acceptable range. But because the threshold is also increasing with the rise of the measured SNR, false alarm probability would decrease at the same time. To summarise, although my proposed method will sacrifice some detection probability by dynamically changing the threshold, a much better false alarm probability would be rewarded, whilst keeping the probability of detection in an acceptable range.

Fig. 4.10 shows the effect of residual SI on probabilities of detection and false alarm, where the analytical curves are plotted by using Eq. (4.6) and Eq. (4.7). Firstly, target detection probability is achievable regardless of SIC by dynamically changing the threshold. However, when η increases, false alarm probability increases too since more energy is received. In order to achieve detection probability to be at least 90% and false alarm probability to be at most 10%, my model would have acceptable performance when SIC is less than 15%. In other words, my system does not operate only when SIC is extremely well, it also works when SIC is relatively poor.

Fig. 4.11 highlights the negative effect of SIC fluctuation, where the analytical curves are plotted by using Eq. (4.11). When 10% random SIC fluctuation is considered, both probabilities of detection and false alarm become worse. Thus

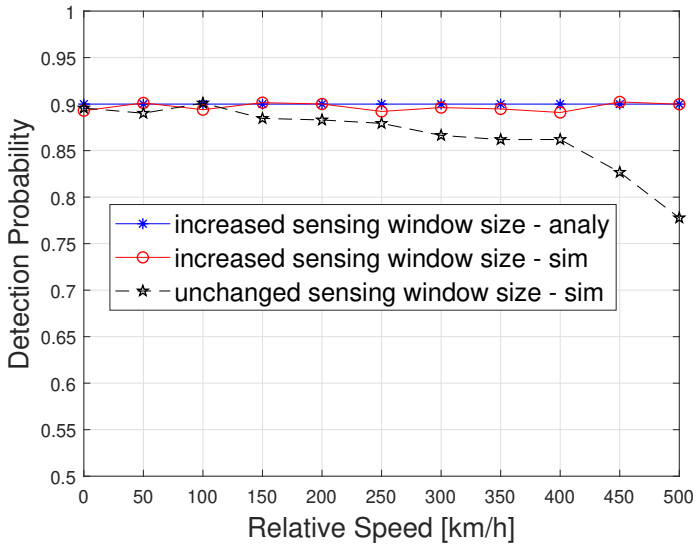

FIGURE 4.7: Impact of mobility on the detection probability

we should carefully consider SIC fluctuation when deploying the scheme.

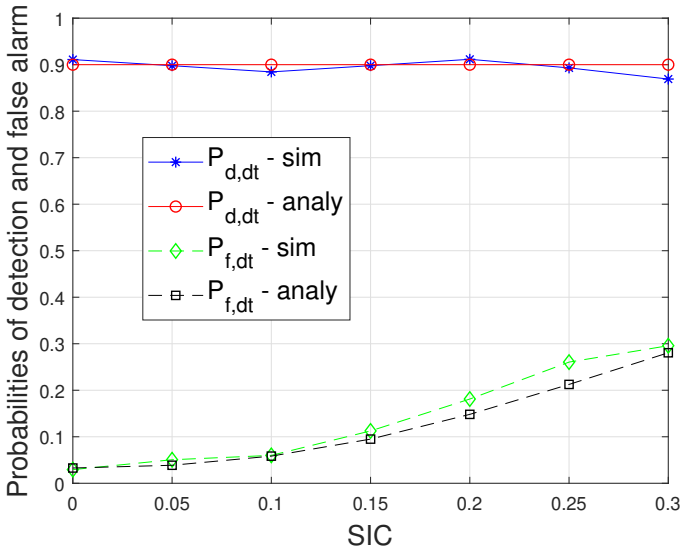

FIGURE 4.10: Probabilities of detection $P_{d,dt}$ and false alarm $P_{f,dt}$ vs. SIC factor η

Fig. 4.12 shows the impact of the sensing time on the precision of detection, where the analytical curves are plotted by using Eq. (4.6) and Eq. (4.7). By setting the thresholds properly, system can achieve the target detection performance. Meanwhile, the longer the sensing time is, the lower will be the chance for the system to wrongly alarm an impending collision. This is because we

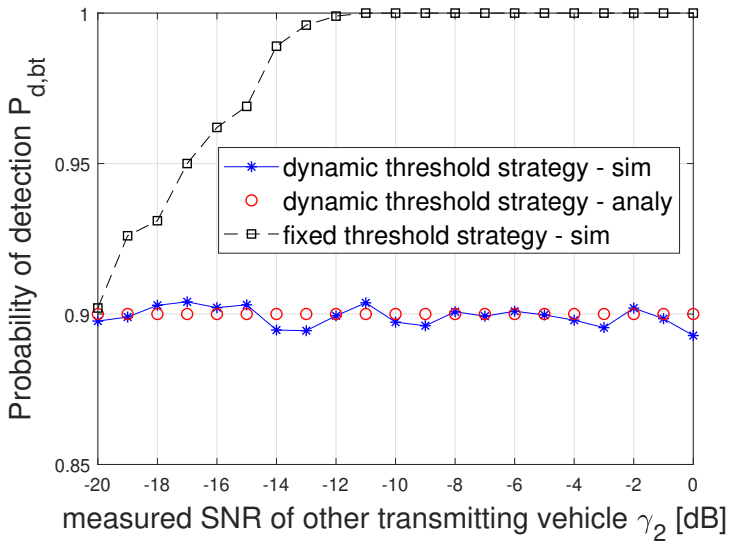

FIGURE 4.8: $P_{d,bt}$ vs. measured SNR before transmission

are measuring and averaging the received energy over a longer period of time, which gives a more accurate result. Another way to reduce the false alarm probability is to increase the sampling frequency, since the number of samples is equal to the production of sensing time and sampling frequency ($N = \tau \cdot f_s$). However, the accuracy cannot be improved by only increasing f_s. When the number of samples taken is large enough, more samples would not add to accuracy of the measured energy level.

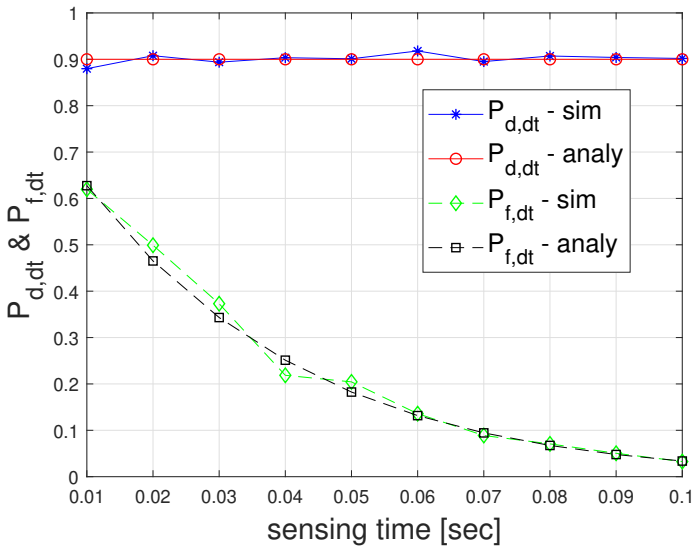

FIGURE 4.12: Probabilities of detection $P_{d,dt}$ and false alarm $P_{f,dt}$ vs. sensing time during transmission

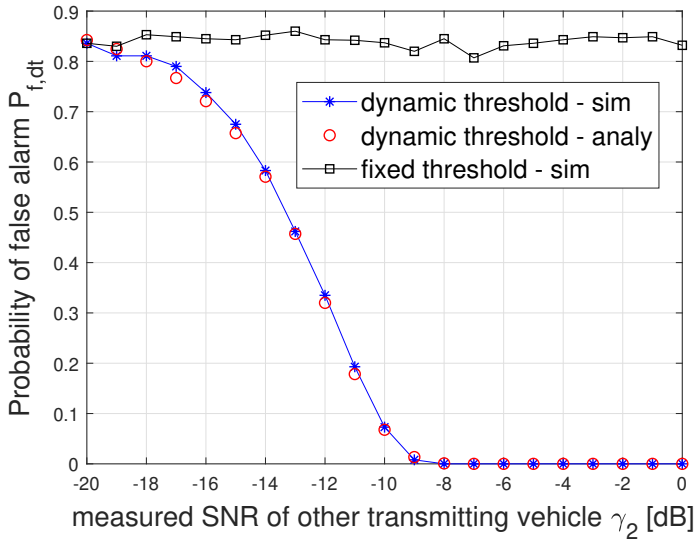

FIGURE 4.9: $P_{f,dt}$ vs. measured SNR during transmission

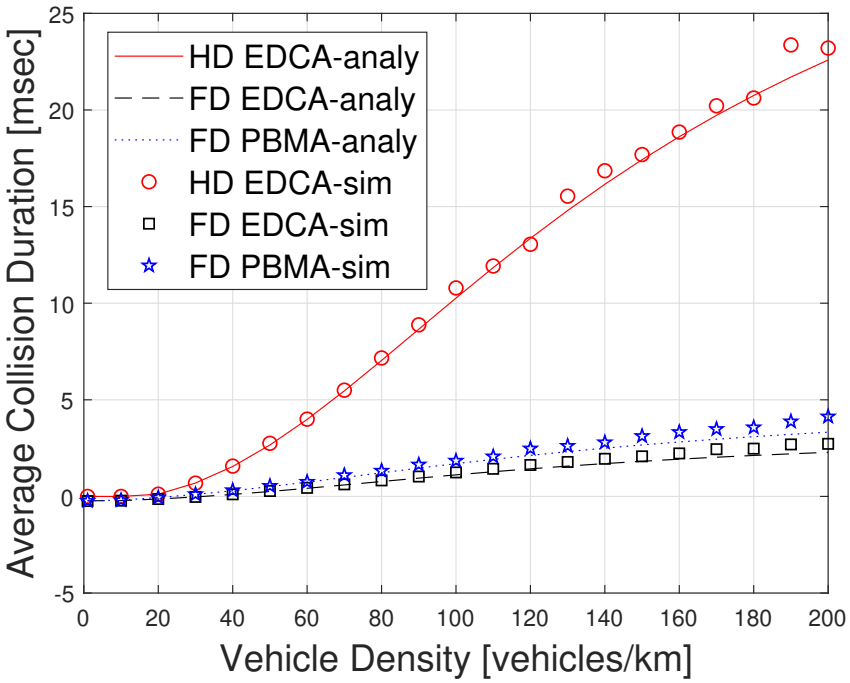

FIGURE 4.14: Average collision duration vs. vehicle density

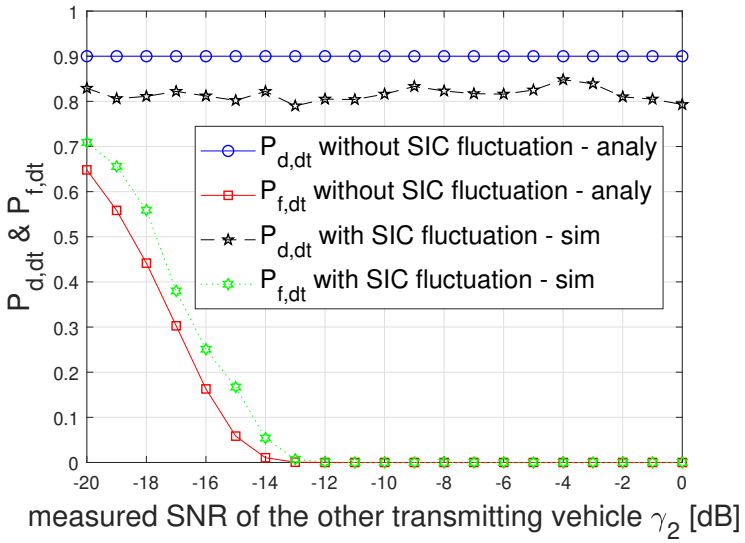

FIGURE 4.11: Probabilities of detection $P_{d,dt}$ and false alarm $P_{f,dt}$ vs. measured SNR during transmission with 10% SIC fluctuation

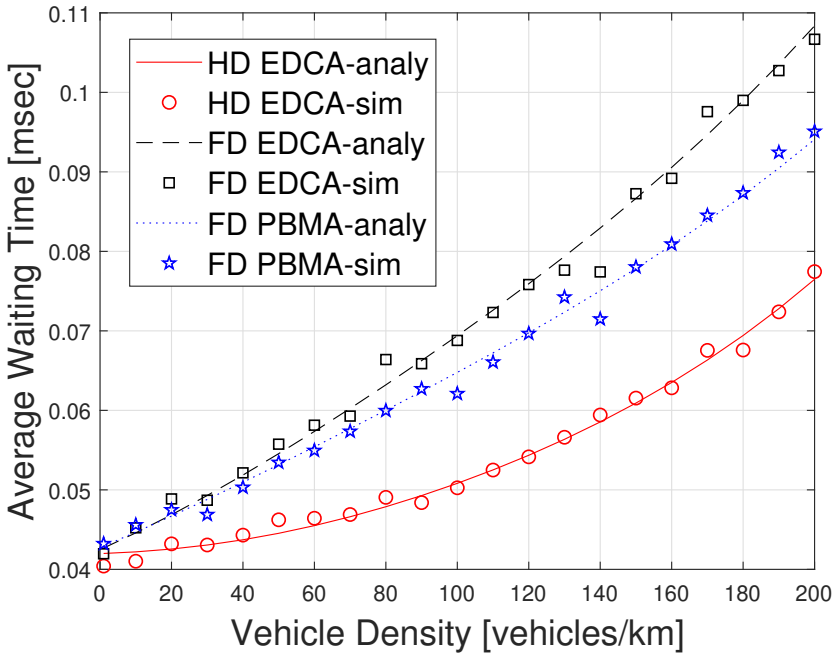

FIGURE 4.15: Average waiting time vs. vehicle density

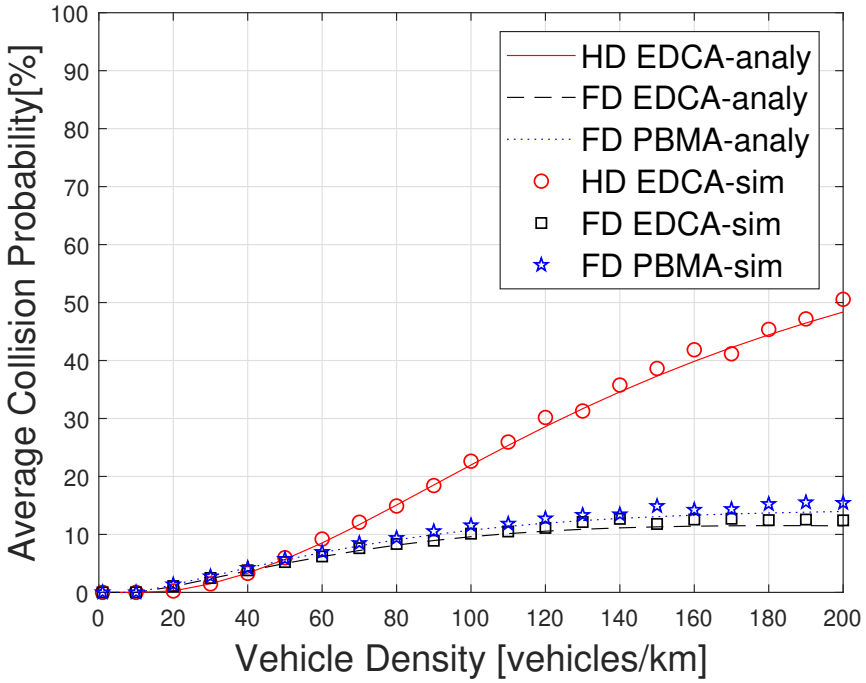

FIGURE 4.13: Average collision probability vs. vehicle density

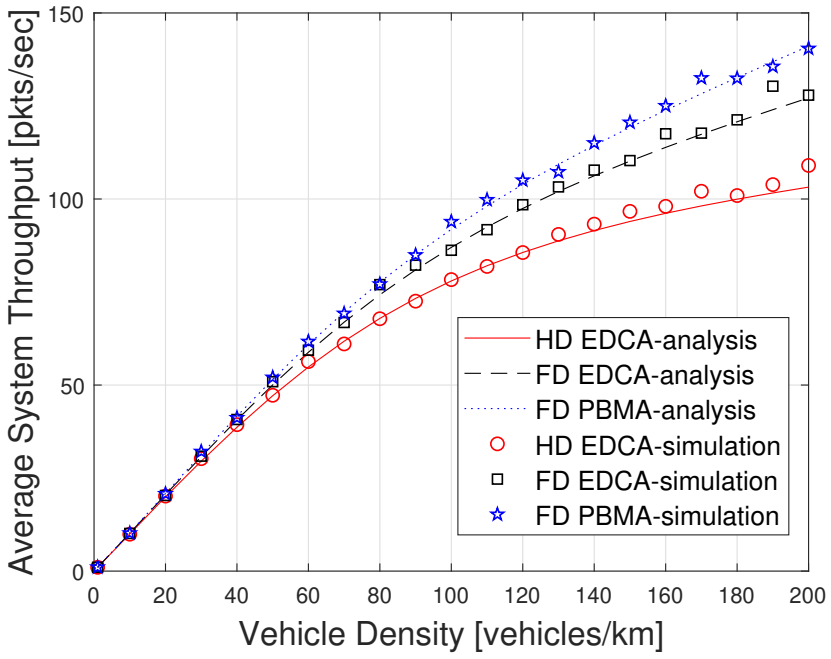

FIGURE 4.16: Average system throughput vs. vehicle density

Fig. 4.13 to Fig. 4.16 respectively show the average collision probability (Eq. (4.12) and Eq. (4.35)), collision duration (Eq. (4.36) and Eq. (4.45)), waiting time

(Eq. (4.46) and Eq. (4.55)) and system throughput (Eq. (4.56)) against the vehicle density by deploying different mechanisms. As shown in Fig. 4.13, when vehicle density increases, collision probability will go up accordingly due to the fact that more vehicles are competing for broadcasting at the same time. In addition, when a collision happens, it lasts longer (i.e. collision duration is longer) and the waiting time is also longer compared to the network where fewer vehicles exist, as shown in Fig. 4.14 and Fig. 4.15.

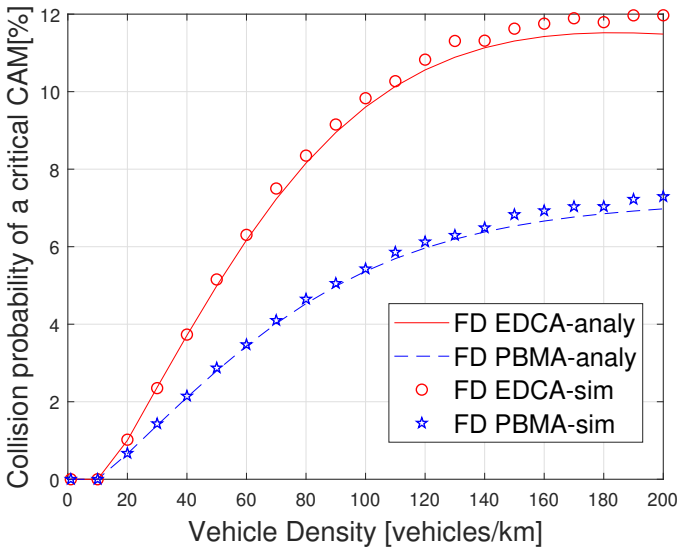

FIGURE 4.17: Collision probability of a M_c vs. vehicle density

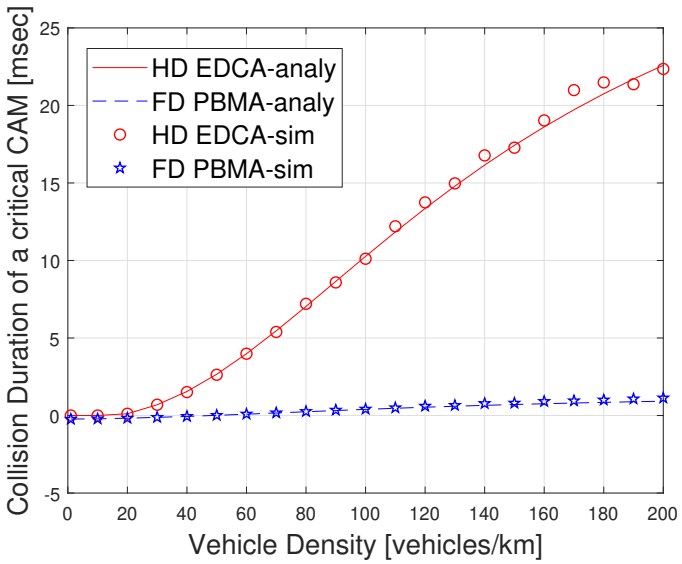

FIGURE 4.18: Collision duration of a M_c vs. vehicle density

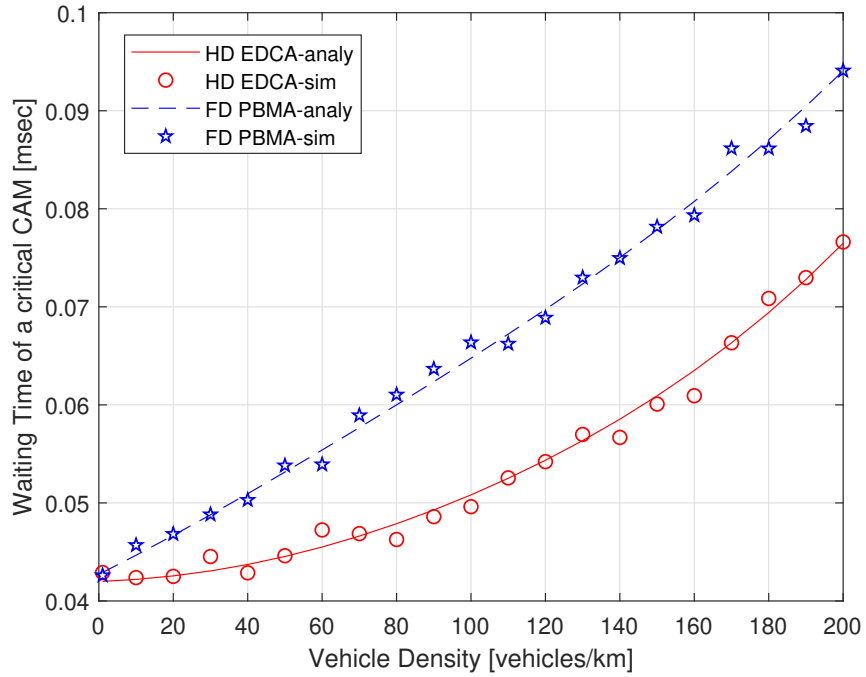

FIGURE 4.19: Waiting time of a M_c vs. vehicle density

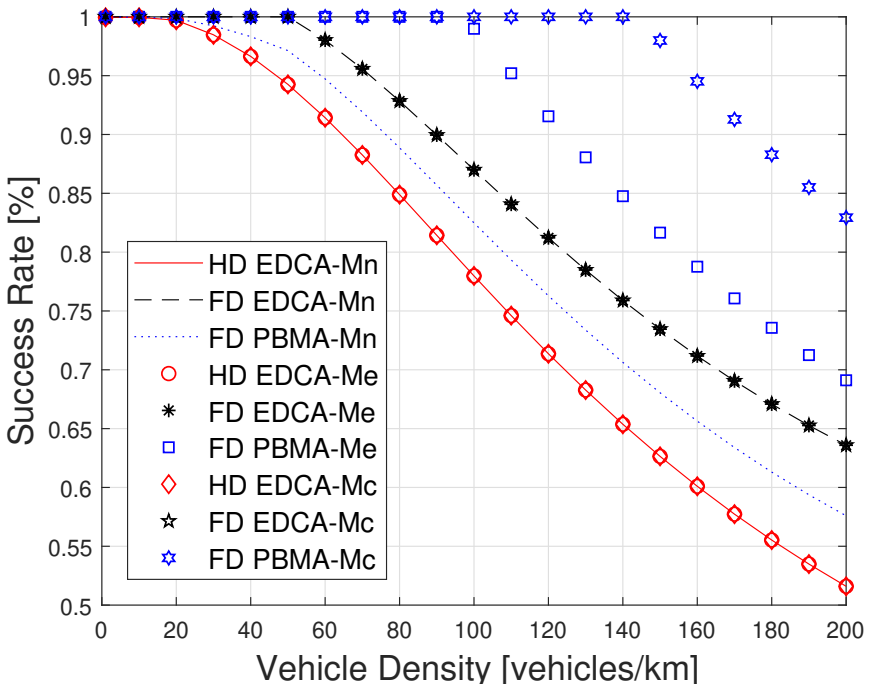

FIGURE 4.20: Success rates of transmitting different types of messages in different mechanisms

Furthermore, it can be seen that FD EDCA and my proposed PBMA mechanism outperform DSRC in terms of collision probability and collision duration. This is because CD capability is not enabled in DSRC and collisions cannot be detected through FD technology. DSRC provides the best performance in terms of waiting time as shown in Fig. 4.15, but a large portion of transmissions are in collisions, and CAMs are lost. This conclusion is drawn from Fig. 4.13 and Fig. 4.16, where DSRC gives the worst performance in terms of collision probability and successful packet delivery rate. In other words, compared to FD EDCA and FD PBMA methods, DSRC can broadcast messages quicker with more collisions. Comparing FD PBMA to FD EDCA method, FD PBMA has a slightly higher collision probability and collision duration, which is due to the fact that vehicles which have M_c or M_e would re-attempt to broadcast immediately in FD PBMA method. But FD PBMA has a shorter average waiting time as shown in Fig. 4.14. The system throughput in Fig. 4.16 shows the overall performance of different mechanisms, in which PBMA method provides the highest throughput. It is worth noting that same definition and unit have been used in other papers and the DSRC standard too, such as [1], [61], [62], and [63].

In addition to average system performance, it is even more important to observe the delivery performance of critical messages, because critical messages could be the last broadcast warning message before potential accidents. Successful delivery of critical messages within a short amount of time will lead to a totally different result. Collision probability, collision duration as well as the waiting time of broadcasting a critical CAM are demonstrated in Fig. 4.17 to Fig. 4.19. I did not plot the performance of broadcasting critical messages by deploying DSRC because FD EDCA method is already shown to outperform DSRC.

By analysing Fig. 4.17 to Fig. 4.19, where the analytical curves are plotted by using Eq. (4.57), Eq. (4.58) and Eq. (4.53), we can see that FD PBMA has significantly improved the delivery of critical CAMs compared to FD EDCA, because FD PBMA can broadcast critical messages with a much smaller collision probability, a much shorter collision duration and a much shorter waiting time too. In addition, it is shown in Fig. 4.20 that the success rates of transmitting critical messages as well as emergency messages by deploying my proposed FD PBMA design are both significantly enhanced and are higher than those in DSRC and FD EDCA methods. However, the successful delivery rate of broadcasting normal update messages by deploying FD PBMA is lower than that in FD EDCA

method and higher than that in the DSRC standard. In other words, when there is a vehicle status change, no matter the change is sudden (critical message) or gentle (emergency message), FD PBMA provides the best performance on letting other vehicles realise such a change from normal cruising activity.

4.6 Summary

In this Chapter I proposed a cross-layer design for future V2X networks. By deploying FD technology and setting thresholds as well as sensing bandwidth according to my design, a vehicle can detect and avoid collisions without losing too many opportunities to transmit useful data. Two thresholds which are dynamically changing and an increased sensing window size have been formulated for detection of channel status and collisions. Furthermore, a novel prioritisation scheme dedicated for CAMs and a novel MAC protocol named PBMA are proposed to schedule the access according to detection results and priorities of messages. Comparisons between DSRC, FD EDCA and my proposed PBMA design have been made through both mathematics and simulations in terms of average collision probability, collision duration, waiting time and throughput. Especially, the delivery of critical messages before a potential accident has also been analysed thoroughly. Results have shown that my design works well even when SIC is poor. Meanwhile, my PBMA design also has an overall better performance: The delivery of CAMs before a potential accident has been enhanced and accidents can be further avoided.

5 A 5G-Based FD Scheduling and Multiple Access Mechanism

Synopsis of Chapter

Future connected and autonomous vehicles (CAVs) will have different demands and capabilities for perceiving the surrounding safety-related information. Therefore, I propose a novel prioritisation scheme and a corresponding multiple access mechanism, to be named full-duplex prioritised scheduling (FDPS) protocol, to enhance the delivery of high-priority packets in future New Radio (NR) enhanced vehicle-to-everything (eV2X) communication vehicular ad hoc networks (VANETs). This design refers to my papers [64] and [65]. Compared to the standardised sensing-based semi-persistent scheduling (SB-SPS) protocol, this work presents how collision detection is enabled during broadcast, how collisions are resolved, how the priority of a packet from a colliding CAV is recognised and how the broadcast of high-priority packets is enhanced. Performance of the proposed FDPS protocol and the standardised SB-SPS protocol is evaluated through both mathematical formulations and simulations. Then, comparison has been made between the two aforementioned designs. Simulation results have firstly validated the accuracy of my analysis, they have also shown the enhancement of packets delivery in future NR eV2X VANETs.

The remainder of this Chapter is organised as follows. In Section 5.1, I introduce the background, challenges and contributions of this work. In Section 5.2, I introduce multiple access mechanisms, including the standardised Mode 4 communications and the proposed FDPS protocol. Next, I present the considered system model in Section 5.3. Afterwards, both the standardised SB-SPS protocol and the proposed FDPS protocol are analytically evaluated in Section 5.4. In addition, simulation results and discussion are given in Section 5.5, future works are given in Section 5.6. Finally, this work is concluded in Section 5.7.

5.1 Introduction

Intelligent transportation system (ITS) has become an explicit development prospect of future society according to many national strategic plans [66]-[67]. A key enabling technology is vehicle-to-everything (V2X) communications, which offers many benefits, such as innovative travelling services, improved safety and efficient traffic management [66]-[67]. Although countless researchers have worked on V2X communications for decades, the target of having an unified and agreed standard for future ITS is not accomplished yet. Among all technologies, two promising solutions are dedicated short range communications (DSRC) [47] and New Radio (NR) enhanced V2X (eV2X) communications [4].

Comparison between DSRC and cellular-eV2X standards has been extensively investigated, such as [68], in which comparison has been made in terms of a set of significant technical and non-technical aspects. The DSRC standard has been shown to successfully provide communication capability in both centralised and vehicular ad hoc networks (VANETs) [36]. However, existing literature also shows that NR eV2X standard outperforms DSRC in terms of many parameters [10]-[69], and further enhancements based on C-V2X have also been proposed [70]-[71]. The PHY and MAC layers technical specification of NR eV2X standard is provided in [72], in which connected and autonomous vehicles (CAVs) are designed to operate based on the 5G platform. Direct vehicle-to-vehicle (V2V) communications (a.k.a. sidelink communications) is supported in both Mode 3 and Mode 4. In Mode 3, radio resources are allocated by the cellular network (i.e. RSUs or gNBs) [73]; whilst in Mode 4, CAVs select resources autonomously according to the sensing-based semi-persistent scheduling (SB-SPS) protocol [73]. In other words, CAVs operate in Mode 3 when they are within the coverage area of gNBs, and operate in Mode 4 when they are out of the coverage area of gNBs.[1] Therefore, Mode 4 is also considered as the baseline mode in V2X communications [74].

[1]Note that resources can still be allocated to a vehicle by the cellular network (i.e. gNBs/RSUs) in Mode 4 communication, when the vehicle is under coverage. But I focus on the VANETs case in which resources are selected autonomously by vehicles according to the SB-SPS protocol [73]

5.1.1 Challenges

We focus on enhancing eV2X Mode 4 communications driven by the fact that CAV safety cannot fully rely on the coverage of gNBs. However, this is a challenging task due to the limitations of the network structure (i.e. VANETs). Firstly, since safety information is exchanged in a broadcasting manner [73], acknowledgement (ACK) mechanism cannot be deployed. In other words, there is no feedback for CAVs to determine whether a transmission is in collision or not. In order to enhance the broadcast reliability, an effective solution is that CAVs proactively detect collisions. Hence, when a packet is lost due to a signal collision, a course of actions can be designed in the MAC layer. However, CAVs are operating in half duplex (HD) mode, so they cannot detect a potential collision whilst broadcasting. A redundant transmission mechanism is provided as an optional solution in the extended version of the SB-SPS protocol [73]-[75], but this solution sacrifices spectral efficiency, as a redundant packet is re-broadcasted by using a different time-frequency resource [73]-[75]. To summarise, VANETs can be enhanced by proposing a novel method that helps CAVs detect collisions. In recent years, full duplex (FD) technology is one of the research hot spots. For example, in [76], the feature of simultaneous transmission from both ends of a link has been used for improving physical layer security. In [77], FD technology is applied to a base station which serves an uplink and a downlink simultaneously. Different from [76]-[77], in this work, I propose to use a different feature of FD technology, namely simultaneous transmission and sensing, to detect collisions in the NR eV2X VANET scenario.

In addition to the lack of knowledge on collisions, MAC layer protocol design in current NR eV2X standard (i.e. Rel-16 technical specification) [72], specifically the SB-SPS protocol [73], also needs a novel contention resolution mechanism, which has not been incorporated yet. If multiple CAVs have already selected the same time-frequency resource, signal collisions happen, and such collisions cannot be recognised by CAVs due to HD operation mode. Therefore, there is also no re-selection process designed before the start of data broadcast. The result is that collisions cannot be avoided and transmissions cannot be aborted. Meanwhile, these packets are even assumed to be successfully transmitted. Furthermore, when signal collisions happen, the collision episode persists across multiple messaging intervals without the colliding CAV realising it. The average duration of this collision episode is one second, if safety packets repetition

interval is set to 10 Hz [75], which is unacceptable. Besides, when the density of a VANET increases, the collision episodes will happen with a higher probability, because more CAVs will compete for the same limited resources. To summarise, when such a scenario happens, it is not only a waste of the precious and scarce spectrum-time resource, CAVs are also put into a dangerous situation.

Furthermore, prioritisation scheme and prioritised messaging mechanism also need to be enhanced. For example, context awareness approach is currently a research hot spot to achieve prioritisation [78], which can be considered when CAVs are operating in Mode 3 or partially distributed scenario in Mode 4. However, I consider the fully distributed VANET scenario in Mode 4, where there is no assistance from gNBs. According to the technical report [79], priority levels are defined on the basis of quality of service (QoS) constraints (e.g. latency and reliability) from different V2X applications. If a safety message is competing with a non-safety message within a CAV itself, the CAV will firstly transmit the safety message. However, the standard does not prioritise safety messages, they are processed according to the first come first serve (FCFS) algorithm [79]. In addition, when multiple CAVs have selected the same resource for broadcast, the standard also does not specify which CAV keeps broadcast, and which CAV defers its broadcast or find another available resource. In other words, there is no prioritisation scheme between safety messages from different CAVs. The reason is that CAVs neither can detect signal collisions, nor identify the type of colliding messages, after collisions have already happened.

5.1.2 Novelty & Contributions

For aforementioned reasons, I am motivated to propose a novel prioritisation scheme and a corresponding MAC layer protocol, named full duplex prioritised scheduling (FDPS), to enhance the message delivery performance in future NR eV2X VANETs. FD technology is proposed to be equipped onto on-board units (OBUs), because it allows a device to transmit and receive simultaneously over the same frequency band, which means that CAVs can broadcast data and sense the channel status simultaneously. Hence, collision detection capability is enabled without introducing further signalling or ACK messaging scheme. After a collision has been detected, CAVs can abort their transmissions and choose another time-frequency resource to broadcast packets according to the proposed prioritisation scheme and the FDPS protocol, which will be explained in details

in Section III. Therefore, collision duration is shortened, and reliability performance, especially for high-priority safety messages, is enhanced. The contributions of this work can be summarised as follows:

- I show that packet delivery rate, collision duration and latency can be enhanced by taking prioritisation into consideration.
- I show a comprehensive and tractable design for applying FD technology to NR eV2X VANETs from both PHY and MAC layers perspectives. CAVs are enabled to proactively detect collisions whilst broadcasting without ACK messaging or further signalling mechanisms.
- I propose a novel prioritisation scheme for NR eV2X VANETs, so that CAVs can enjoy prioritised messaging based on their communication demands.
- I introduce a novel MAC layer protocol, to be named FDPS, to support simultaneous transmission and sensing in PHY layer, and provide congestion control, broadcast abortion as well as collision resolution mechanisms for CAVs with prioritised messaging feature in MAC layer.
- I provide mathematical analysis of detection accuracy during transmission in terms of detection probability, false alarm probability and mis-detection probability. In addition, I also formulate overall analytical packet delivery performance in terms of average successful packet delivery rate (PDR), collision duration and latency, which have also been validated through extensive simulations.
- I compare my proposed design to the Rel-16 technical specifications. Results have shown that my proposed design outperforms the standardised technical specifications, packet delivery performance is enhanced, when the self-interference suppression (SIS) factor is better than 16%, which is achievable by deploying the existing SIS technologies.

5.2 Multiple Access Mechanisms

In this section, I first introduce the communication framework of the 3GPP Mode 4 VANET scenario. Then, I demonstrate the workflow of SB-SPS, which is adopted as the MAC layer solution in technical specifications of 3GPP for Mode 4 communications in VANETs [73]. Afterwards, I introduce my proposed prioritisation scheme and FDPS protocol. Finally, I analyse the differences between the standardised SB-SPS method and the proposed FDPS method.

5.2.1 Mode 4 VANET Communications

Fig. 5.1 depicts a fully decentralised VANET, in which CAVs operate in Mode 4 to share information. There is no base station that can allocate time-frequency resources and schedule transmissions for CAVs. Instead, CAVs select resources autonomously based on local sensing results, and share safety-related (i.e. control and data) messages in a broadcasting manner according to the SB-SPS protocol, which is introduced in Section 5.2.2.

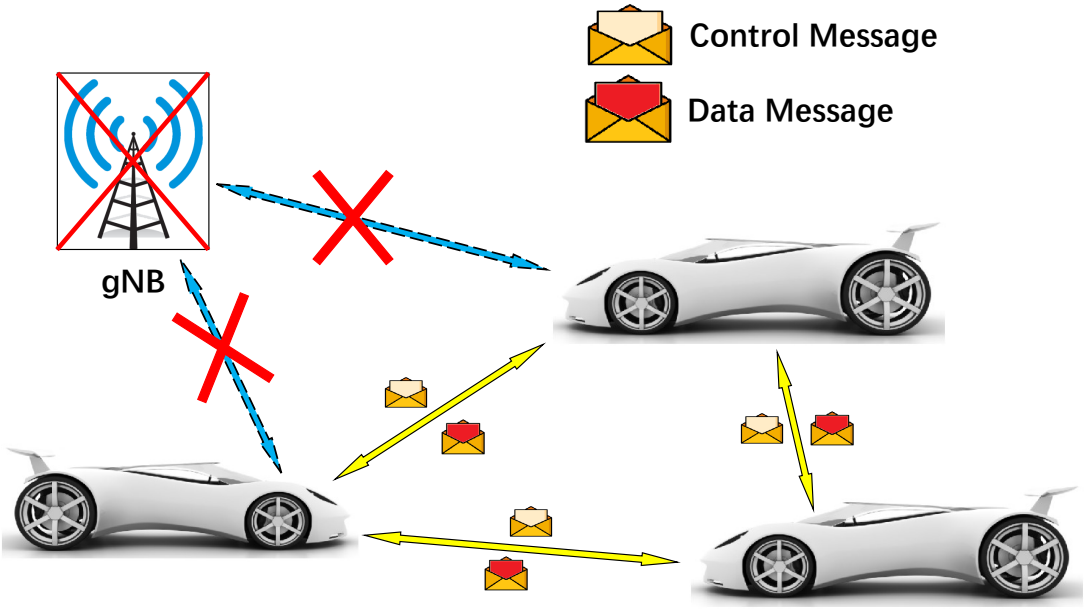

FIGURE 5.1: Mode 4 VANET Communication Framework

Therefore, Mode 4 VANET Communication has the following challenges waiting to be addressed. First, CAVs cannot detect signal collisions whilst broadcasting. Second, CAVs do not know whether a packet is broadcast successfully or not due

to the broadcast feature. Third, CAVs cannot resolve external collisions (i.e. collisions between different vehicles.) Last but not least, there is no communication priority between CAVs, although they have different communication demands and requirements.

5.2.2 SB-SPS Protocol

First of all, I introduce the PHY layer specifications of the current C-V2X standard [80]-[81]. In the PHY layer, single-carrier frequency-division multiple access is adopted, and channels of 10 MHz and 20 MHz bandwidth are both supported. In addition, channels are further divided into sub-channels, sub-frames and resource blocks (RBs). RB is defined as the smallest frequency resource unit that can be allocated to a CAV. The bandwidth of each RB is 180 kHz wide, which is consisted of twelve 15 kHz wide sub-carriers. Besides, each sub-frame is designed to be 1 ms long, which is equivalent to the transmission time interval. Furthermore, a sub-channel is defined as a group of RBs in the same sub-frame, and the number of RBs in a sub-frame can vary. Both data and the sidelink control information (SCI) are transmitted by using the sub-channels. Data is transmitted in transport blocks (TBs) over the physical sidelink share channels (PSSCH), and SCI is transmitted over the physical sidelink control channels (PSCCH). Each TB carries a full packet such as a basic safety message (BSM), which must be broadcast with its associated SCI message in the same sub-frame. In addition, two sub-channelisation schemes are supported. The first scheme is that a TB and its associated SCI message are transmitted in adjacent RBs. Whilst the other scheme is that a TB and its associated SCI message are transmitted in non-adjacent RBs. Both sub-channelisation schemes are shown in Fig. 5.2.

In the MAC layer, CAVs autonomously select sub-frames and sub-channels according to the SB-SPS protocol [73]. Before broadcast, a vehicle needs to reserve new resources for a random number of consecutive BSMs. This random number is also known as the re-selection counter (RC), whose value is randomly selected from the resource reservation range, which depends on the BSM repetition interval, or BSM transmission frequency λ. Relationship among them is shown in Table. 5.1.

After each BSM broadcast, RC decrements by one. When the value of RC goes to zero, a CAV has to re-select new resources with probability $(1 - P_{res})$, where

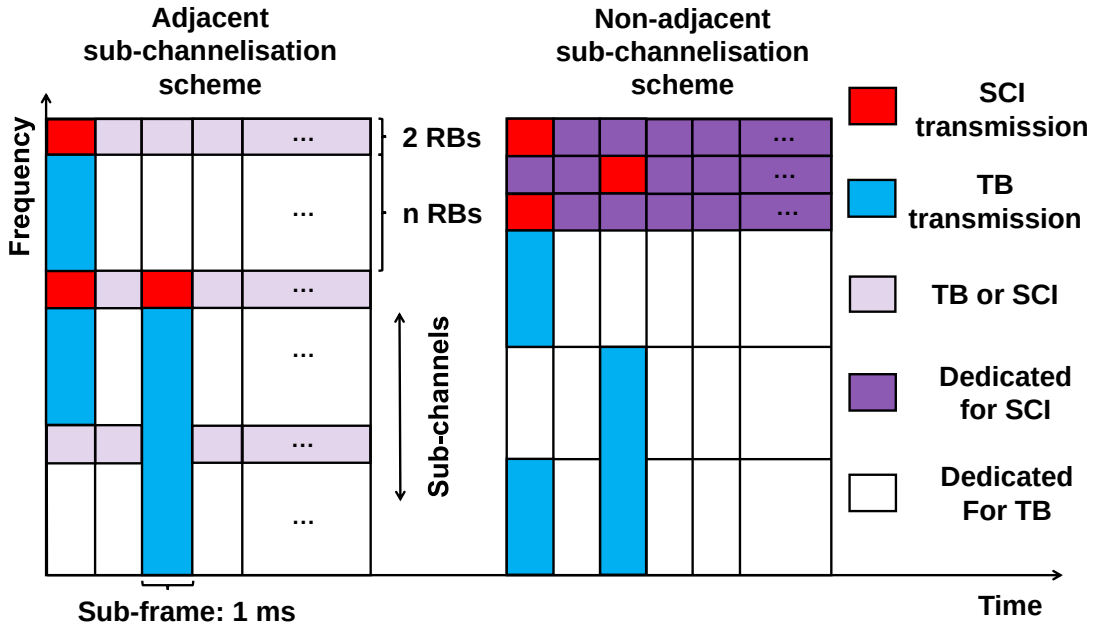

FIGURE 5.2: Sub-channelisation schemes

TABLE 5.1: RESOURCE RESERVATION RANGE

Resource reservation range	BSM repetition interval	Equivalent BSM transmission frequency *(packets per second)*
[5,15]	100 ms	10 pps (λ = 10 Hz)
[10,30]	50 ms	20 pps (λ = 20 Hz)
[25,75]	20 ms	50 pps (λ = 50 Hz)

$P_{res} \in [0, 0.8]$[2] according to [83], [72] in the standard. In other words, when the value of the RC decrements to zero, a CAV will definitely select and reserve a new resource for the next episode of consecutive BSM transmission, as shown in Fig. 5.3.

The resource reservation process is divided into the following three phases, which has also been depicted in Fig. 5.4.

Phase 1: Assume a generic CAV, V_{tx}, needs to reserve new resources at sub-frame N (i.e. RC is zero). Then the time period for V_{tx} to reserve new resources is named as *selection window*, which starts from the sub-frame N and finishes at the sub-frame $(N + \frac{1}{\lambda})$, where λ refers to the BSM transmission frequency. In addition, V_{tx} identifies and selects available resources according to the sensing

[2] P_{res} is normally set to 0 [82], which is also the value used in this work.

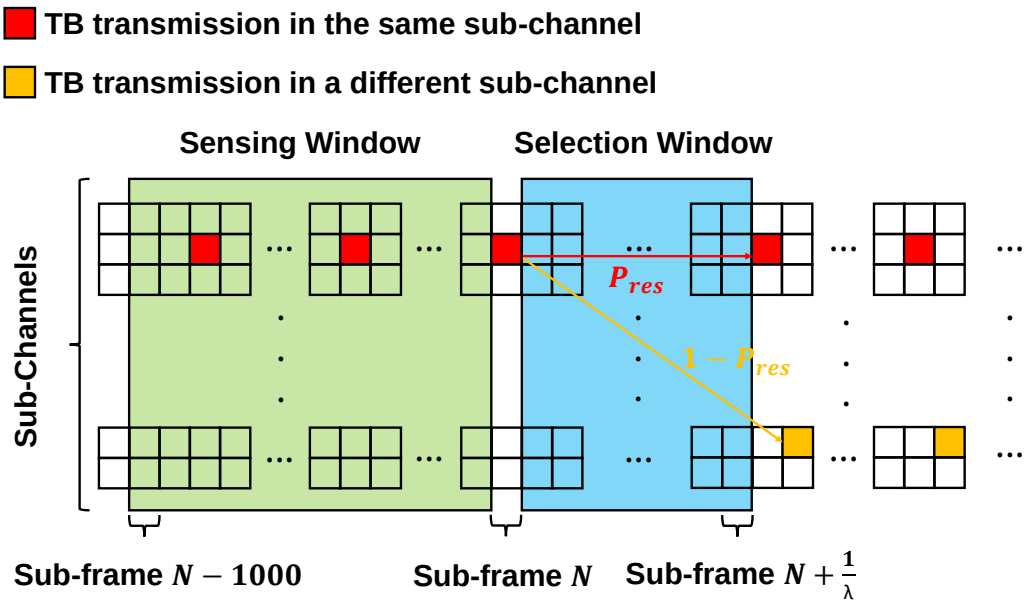

FIGURE 5.3: SB-SPS Workflow

results from the sensing window, where the sensing window starts from the sub-frame $(N - 1000)$ and finishes at the sub-frame N.

Phase 2: The CAV, V_{tx}, creates a list L_1 which contains all available resources. Then resources that meet either of the following three conditions are excluded from L_1:

1. resources which are indicated to be used by other CAVs within the selection window or next broadcast episode of V_{tx}.
2. sub-frames N_i in the selection window, if V_{tx} used sub-frames N_j in the previous broadcast episode, where $j = i - 100 \cdot k$. For $\lambda = 10\ Hz$, k is an integer number and its range is $k \in [1, 10]$.[3]
3. resources which have the average reference signal received power (RSRP) higher than a given threshold.

After the above exclusion process, if L_1 contains at least 20% of the resources which are identified in the selection window after *Phase 1*, the CAV can proceed to the third phase. Otherwise, *Phase 2* should be executed again with a 3 dB higher RSRP threshold.

[3]For $\lambda = 20\ Hz$, $j = i - 50 \cdot k$ and $k \in [1, 20]$. For $\lambda = 50\ Hz$, $j = i - 20 \cdot k$ and $k \in [1, 50]$.

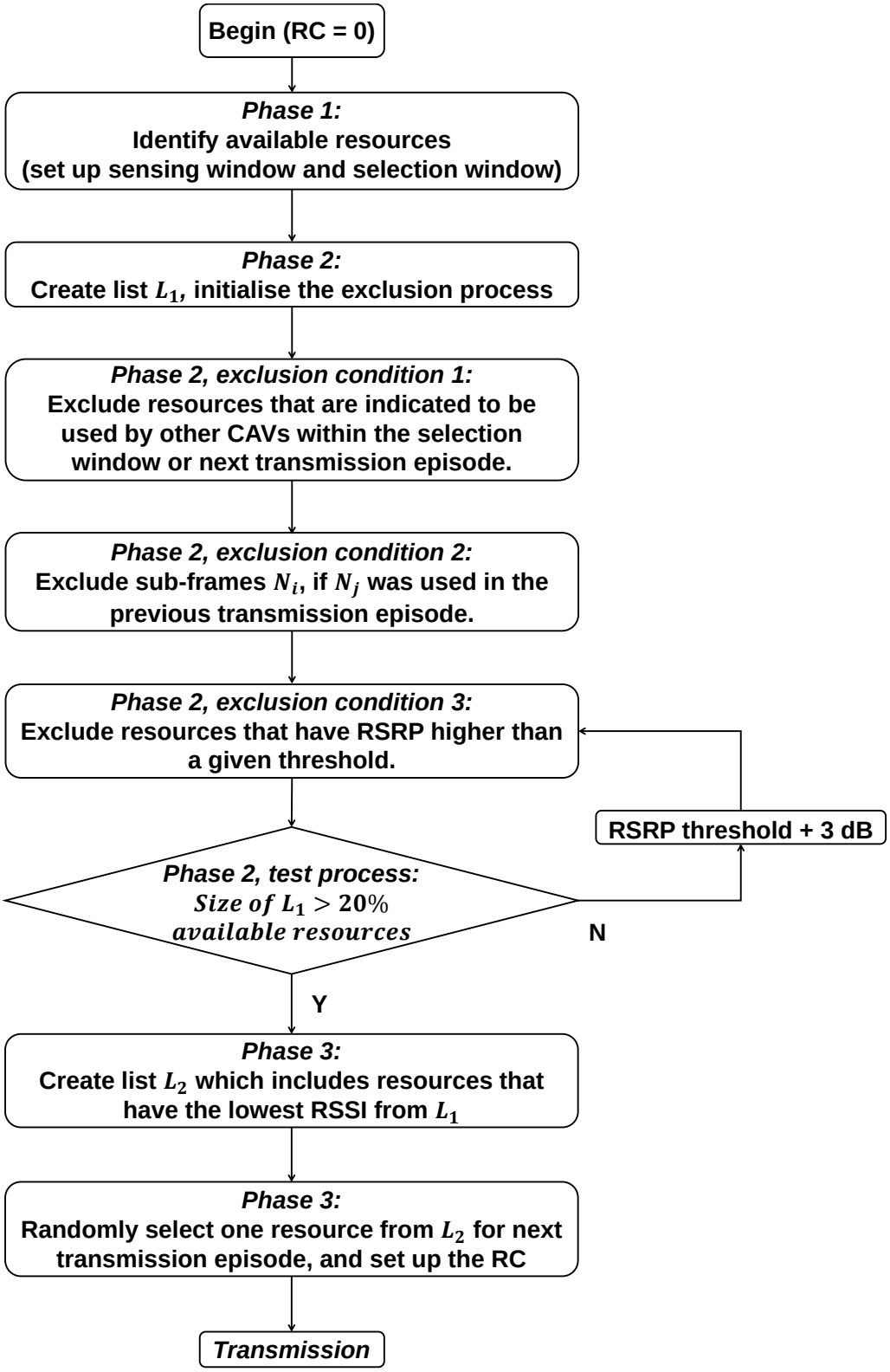

FIGURE 5.4: SB-SPS resource reservation process

Phase 3: The CAV, V_{tx}, creates another list L_2. The size of L_2 is equal to 20% of all

identified available resources in *Phase 1*. Then V_{tx} selects resources which have the lowest average received signal power indicator (RSSI) from L_1, and store these candidate resources into L_2. Finally, V_{tx} randomly selects one resource from L_2 for the next transmission episode, and set up the RC.

5.2.3 FDPS Protocol

The proposed prioritisation scheme incorporates three communication priority levels, which is shown in Table. 5.2.

TABLE 5.2: THE PROPOSED PRIORITISATION SCHEME

Communication Priority
Low
Middle
High

Next, I introduce the work flow of the proposed FDPS protocol, which is consisted of two processes: simultaneous broadcast and sensing process, and resource reservation process. As depicted in Fig. 5.5, CAVs sense channel status in both processes in a FD manner. Sustained sensing refers to the sensing process in each scheduled TB broadcast, which is the original sensing window in SB-SPS. Besides, I introduce a new sensing phase, named interim sensing, which refers to the sensing process in each re-attempt TB broadcast. During the sustained sensing process, every CAV monitors the resource usage and tabulates channel status for the immediate past one thousand sub-frames whilst broadcasting BSMs. Assume a generic CAV, named V_{tx}, needs to broadcast BSMs. It reserves new resources within the selection window according to the sustained sensing results, and sets up the RC according to Table. 5.1 prior to the broadcast. After every BSM broadcast, the RC value decrements by one. V_{tx} selects new resources with probability $(1 - P_{res})$ for next broadcast episode when the RC value is decreased to zero.

Afterwards, I present resource reservation process, transmission abortion and collision handling mechanisms of FDPS. As shown in Fig. 5.6, when a collision has been detected during a BSM broadcast, the CAV V_{tx} responses as follows. Firstly, I introduce a new re-attempt counter (RAC) which is used for counting how many times a BSM has been re-broadcast. V_{tx} sets up a RAC, whose value is set to zero. Secondly, V_{tx} selects the same sub-channel and the next available sub-frame to re-broadcast the collided BSM. The next available sub-frame

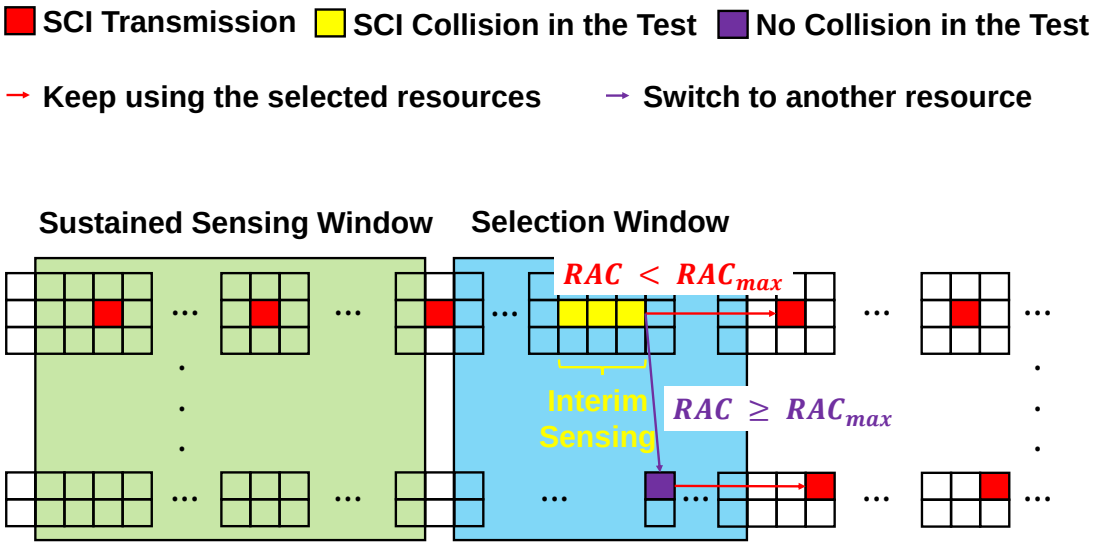

FIGURE 5.5: FDPS Workflow in RBs Diagram

is identified from the previous sustained sensing results, which is also prior to the generation of the new BSM. After every re-attempt, RAC value is increased by one. The maximum re-attempt limit (RAC_{max}) for high-, middle- and low-priority CAVs is set to 2, 1, 0, respectively, in order to differentiate the priority levels of the colliding BSMs. When the RAC value reaches the limit, V_{tx} aborts its current broadcast episode, and goes to the resource reservation process with $P_{res} = 0$.

The resource reservation process includes three phases:

Phase 1: When a BSM arrives at sub-frame N, and the RC value is equal to zero, V_{tx} initialises the resource reservation process to identify available resources by setting up the RC, sensing window and selection window. The range of the sensing window is between sub-frame $(N - 1000)$ and sub-frame N, and the range of the selection window is between sub-frame N and sub-frame $(N + \frac{1}{\lambda})$.

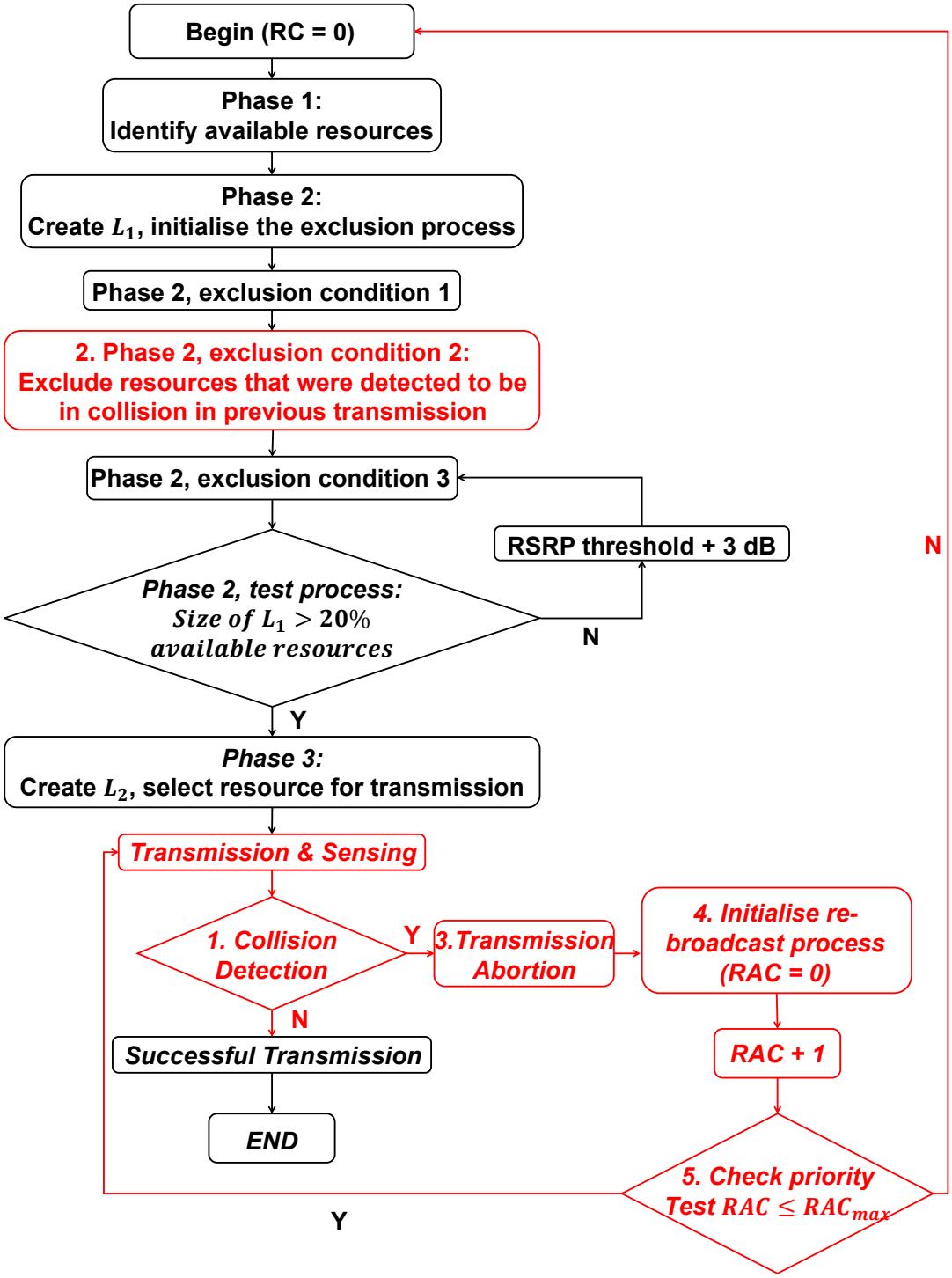

FIGURE 5.6: FDPS Flow Chart: resource reservation, transmission abortion and collision handling mechanisms (new features of FDPS are highlighted in red)

Phase 2: V_{tx} creates a list L_1 to tabulate all available resources. Then, resources which meet either of the following conditions are excluded from L_1:

1. resources which are indicated to be used by other CAVs within the selection window or next transmission episode of V_{tx}.
2. resources which were detected to be in collision with any previous transmission from V_{tx}.
3. resources which have the measured RSRP higher than a given threshold.

It should be noted that the second exclusion condition is one of the differences between SB-SPS and FDPS. RBs that were detected to be in collision are now excluded in order to avoid continuous collision, which is achieved based on the sustained sensing results, interim sensing results and the proposed RAC.

After the above exclusion process, if L_1 contains at least 20% of the resources which are identified in the selection window, V_{tx} proceeds to *Phase 3*. Otherwise, V_{tx} re-executes *Phase 2* with a 3 dB higher threshold.

Phase 3: V_{tx} creates another list L_2 to store candidate resources. The size of L_2 is equal to 20% of all identified available resources in *Phase 1*. Then it selects resources which have the lowest RSSI values from L_1. Finally, V_{tx} randomly selects one resource from L_2 for the next transmission episode, and sets up the RC.

5.2.4 Differences between FDPS and SB-SPS

TABLE 5.3: DIFFERENCES BETWEEN FDPS AND SB-SPS

Features	**FDPS**	**SB-SPS**
PHY Layer Energy Sensing Capability	✓	✓
1. Collision Detection Capability	✓	×
Occupied RBs Exclusion Feature	✓	✓
2. Collided RBs Exclusion Feature	✓	×
3. Transmission Abortion Feature	✓	×
Prioritisation Between CAVs	✓	×
Internal Collision Resolution	✓	✓
4. External Collision Resolution	✓	×
5. Prioritised Re-transmission Feature	✓	×

In this sub-section, I show the differences between SB-SPS and FDPS by highlighting the enhanced features in FDPS, which are also depicted in Table. 5.3.

Compared to SB-SPS, FDPS excludes resources which were detected to be in collision in the resource reservation process, which is labeled by 1. in Table. 5.3 and highlighted in Fig. 5.6. In addition, collision detection capability is embedded in the FDPS in the broadcasting process, CAVs can detect for potential collisions whilst broadcasting. This feature is labeled by 2. in Table. 5.3 and highlighted in Fig. 5.6. Besides, FDPS also has an ongoing transmission abortion feature, which can shorten the collision duration and let CAVs go to the next phase immediately. This feature is labeled by 3. in Table. 5.3 and highlighted in Fig. 5.6. Furthermore, a prioritised re-broadcast mechanism is introduced into FDPS, so CAVs can re-broadcast the collided BSMs to enhance their safety. This feature is labeled by 4. and 5. in Table. 5.3 and highlighted in Fig. 5.6. Meanwhile, FDPS has avoided the ACK mechanism and any further signalling, so it has great backward compatibility with the SB-SPS. Finally, SB-SPS suffers from broadcast storm problem, where FDPS does not have this problem, because there is no blind re-broadcast mechanism in FDPS.

5.3 System Model

We consider a NR eV2X VANET, in which CAVs broadcast BSMs according to the proposed prioritisation scheme or the FDPS protocol, as shown in Fig. 5.7.

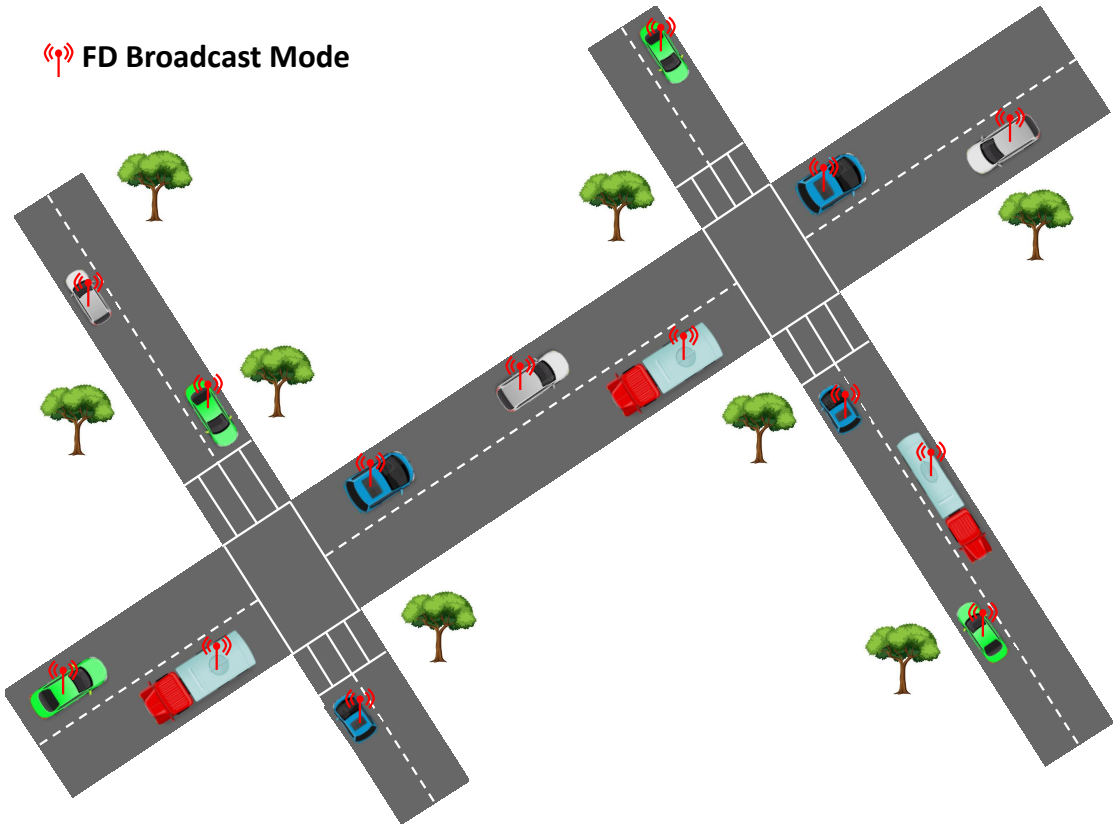

FIGURE 5.7: System Model: 5G NR eV2X VANET

I assume that CAVs have deployed FD technology to broadcast BSMs and sense channel status simultaneously. Same as [39], energy detection method is assumed to be deployed for sensing in this work, which is carried out by measuring the energy level of the sub-channels over each sub-frame. The accuracy of the sensing is considered to be imperfect, which will be affected by the environment, such as the received signal-to-noise ratio (SNR), sensing threshold setting strategy, Doppler effect and the self-interference suppression (SIS) capability. Rayleigh flat fading is assumed to be the channel model between vehicles. The noise component is assumed to be Gaussian, independent and identically distributed (i.i.d.) with zero mean and unit variance. Vehicles are distributed according to a Poisson Point Process (PPP) with density β. Such an assumption holds when the transmission range of CAVs is larger than the width of the

road [52], [58]-[59]. In addition, vehicles have different transmission and sensing ranges, and sensing range is larger than transmission range. Although the effect of hidden node problem is not eliminated, it can be weakened by increasing the sensing range and setting up thresholds according to the analysis in section 5.4. Since the received energy depends on the distance between the sensing vehicle and the potential concurrent transmitting vehicle(s), to be conservative, the model is designed to be able to detect the signal collision from the farmost vehicle. This assumption is the same as it is in [45]. I denote the sensing duration by T_s and sampling frequency by f_s, thus, detection probability is given by [39]

$$P_d^{FD} = Q((\frac{\epsilon_{th}}{\sigma_n^2} - \mathrm{Y}_{sig} - \eta^2 \mathrm{Y}_{SI} - 1) \times \sqrt{\frac{T_s \cdot f_s}{2\eta^2 \mathrm{Y}_{SI} + 2\eta^2 \mathrm{Y}_{SI} \mathrm{Y}_{sig} + 2\mathrm{Y}_{sig} + 1}}), \quad (5.1)$$

where ϵ_{th} represents the sensing threshold, above which the broadcast is deemed to be in collision, σ_n^2 represents the noise variance, η represents the SIS factor, Y_{SI} represents the measured SNR of the SI signal, Y_{sig} represents the measured SNR of the potential colliding signal, T_s represents the sensing time, f_s represents the sampling frequency and $Q(.)$ represents the Q function operator, which is the tail distribution of the standard normal distribution. The formal definition of the Q function operator is given by $Q(x) = \frac{1}{\sqrt{2\pi}} \int_x^\infty exp(-\frac{u^2}{2}) du$. Here, it gives the probability that a CAV finds its BSM broadcast is in collision when there is at least one other CAV broadcasting at the same time in the same frequency band.

False alarm probability is given by [39]

$$P_f^{FD} = Q((\frac{\epsilon_{th}}{\sigma_n^2} - \eta^2 \mathrm{Y}_{SI} - 1) \cdot \sqrt{\frac{T_s \cdot f_s}{2\eta^2 \mathrm{Y}_{SI} + 1}}). \quad (5.2)$$

Mis-detection probability is given by

$$\begin{aligned} P_m^{FD} =& 1 - Q((\frac{\epsilon_{th}}{\sigma_n^2} - \mathrm{Y}_{sig} - \eta^2 \mathrm{Y}_{SI} - 1) \times \\ & \sqrt{\frac{T_s \cdot f_s}{2\eta^2 \mathrm{Y}_{SI} + 2\eta^2 \mathrm{Y}_{SI} \mathrm{Y}_{sig} + 2\mathrm{Y}_{sig} + 1}}). \end{aligned} \quad (5.3)$$

In order to compensate the Doppler effect, the increased sensing window size and the dynamically changing sensing threshold strategy is deployed according to [45], so that CAVs can provide a stable detection probability whilst avoiding a

high false alarm probability. Specifically, a pre-defined target detection probability is achieved according to the received SNR, the SIS factor and the dynamically changing threshold setting.

In this work, based on the PHY layer sensing results, I have proposed a new MAC layer method, namely FDPS protocol. CAVs reserve resources, abort ongoing transmission and re-broadcast collided BSMs according to the proposed FDPS protocol, which is introduced in detail in Section 5.2.3.

5.4 Analytical Performance Evaluation

In this section, I analytically evaluate the performance of both SB-SPS and FDPS protocols. Notations are provided in Table. 5.4, Table. 5.5 and Table. 5.6.

TABLE 5.4: NOTATION TABLE

Symbols	Notes
P_d^{FD}	FD detection probability
P_f^{FD}	FD false alarm probability
P_m^{FD}	FD mis-detection probability
R_{SPS}	packet delivery rate of SB-SPS
P_e^{HD}	probability of losing a BSM due to HD error in SB-SPS
P_e^{SENS}	prob. of losing a BSM due to sensing error in SB-SPS
P_e^{PROP}	prob. of losing a BSM due to propagation error in SB-SPS
P_e^{COL}	prob. of losing a BSM due to signal collisions in SB-SPS
N_{EV}	total number of CAVs in a VANET (i.e. exposed CAVs)
N_{sc}	total number of sub-channels
N_{ar}	total number of available resource that can be selected
N_{sf}	total number of sub-frames within a selection window
ζ_{tx}	transmit power in SB-SPS
ζ_{PL}	path loss
ζ_{SH}	shadowing
ζ_N	noise
$f_{\zeta_{rx}}(x)$	the PDF of the received signal power
ϵ_{th}^{SENS}	sensing threshold
ϵ_{th}^{PROP}	propagation threshold
σ	the variance of $f_{\zeta_{rx}}(x)$
$D_{t,r}$	distance between a generic transmit and a receiving CAV
$P_{sf}(m)$	probability that $m(m \geqslant 1)$ CAVs initialise the resource reservation process in the same sub-frame
$P_{sr}(m)$	probability that at least one of these m CAVs selects the same resource as the generic CAV
N_{BSM}	number of BSMs that is transmitting in one resource reservation period

TABLE 5.5: NOTATION TABLE (CONT. I.)

$E[.]$	expectation operator
$E[N_c]$	expected number of candidate resources after the exclusion process
N_V	total number of CAVs including exposed and hidden CAVs
N_{HV}	average number of hidden CAVs
N_{or}	number of occupied resources that can be detected by each hidden CAV
P_{hid}^{COL}	probability that at least one hidden CAV collides with the generic transmitting CAV
D_{SPS}	average collision duration of SB-SPS
T_{BSM}	transmission time of a BSM
T_{RRI}	resource reservation interval
T_{PGI}	packet generation interval
S_{BSM}	BSM size
R_{trans}	transmission rate
L_{SPS}	latency of SB-SPS
L_{RRP}	latency caused by the resource reservation process
L_{COL}	latency caused by collisions
T_{SW}	width of the selection window
R_{FD}	packet delivery rate of FDPS
P_e^{FD}	probability of losing a BSM due to FD error in FDPS
P_e^S	prob. of losing a BSM due to sensing error in FDPS
P_e^P	prob. of losing a BSM due to propagation error in FDPS
P_e^C	prob. of losing a BSM due to collisions in FDPS
ζ_{SI}^{FD}	self-interference signal power
ζ_{tx}^{FD}	transmit power in FDPS
$f_{\zeta_{rx}^{FD}}(x)$	the PDF of the received signal power in FDPS
$D_{t,r}^{FD}$	distance between a generic FD transmit and receiving CAV
P_{lv}	percentage of low priority CAVs in the VANET
P_{mv}	percentage of middle priority CAVs in the VANET
P_{hv}	percentage of high priority CAVs in the VANET
$P_{e,i}^C$	collision probability in case i
D_{FD}	overall collision duration of FDPS
P_i	probability that case i happens

TABLE 5.6: NOTATION TABLE (CONT. II.)

$D_{FD,i}$	collision duration in case i
L_{FD}	latency of FDPS
L_{FD}^{RRP}	resource reservation delay in FDPS
L_{FD}^{RT}	re-transmission delay in FDPS
L_{RRI}	new resource reservation interval

5.4.1 Analytical Performance of SB-SPS

5.4.1.1 Packet Delivery Rate

By deploying the standardised SB-SPS protocol, BSMs can be lost due to four types of error [82]. The first type is named as half duplex (HD) error, which is produced when a CAV is transmitting BSMs, so that it cannot receive any BSM transmitted in the same sub-frame in a different sub-channel. The second type is sensing error, which is produced when mis-detection happens. The third type is propagation error, which is produced when the received signal power is not sufficient for a CAV to successfully decode the received BSMs. The last type of error is collision error, which is produced when multiple CAVs select the same time-frequency resource to broadcast BSMs. Thus the PDR is defined as the average probability of broadcasting a BSM without any error, which is given by [82]

$$R_{SPS} = (1 - P_e^{HD})(1 - P_e^{SENS})(1 - P_e^{PROP})(1 - P_e^{COL}). \tag{5.4}$$

For any CAV within the VANET, HD error is produced when there is at least one CAV other than the selected CAV broadcasts at the same time in a different sub-channel, so neither of the CAVs can receive BSMs from other CAVs in this sub-frame. In other words, the probability of this type of error is equal to the probability that at least one CAV selects a different sub-channel in the same sub-frame for transmission. Thus the probability of losing a packet due to HD error is given by

$$P_e^{HD} = 1 - (\tfrac{N_{ar} - N_{sc}}{N_{ar}})^{N_{EV}-1}, \tag{5.5}$$

where N_{EV} is given by

$$N_{EV} = 2 \cdot R_{SENS} \cdot \beta, \tag{5.6}$$

and N_{ar} is given by

$$N_{ar} = N_{sc} \cdot N_{sf}. \tag{5.7}$$

In addition to HD errors, BSMs can also be lost due to mis-detection, which depends on the path loss, shadowing as well as noise. This type of error happens when the received signal power/SNR is lower than a certain threshold, ϵ_{th}, and there is a BSM transmission from another CAV. The probability of losing a packet due to this type of error is given by

$$P_e^{SENS} = P_m^{FD} = 1 - P_d^{FD}. \tag{5.8}$$

Therefore, the probability of losing a packet due to sensing is given by

$$P_e^{SENS} = 1 - Q((\frac{\epsilon_{th}^{SENS}}{\sigma_w^2} - \gamma - 1) \cdot \sqrt{\frac{N_{sam}}{2\gamma+1}}). \tag{5.9}$$

Afterwards, I compute the error due to propagation, which happens when the received signal power/SNR is higher than the sensing threshold, ϵ_{th}^{SENS}, but it is still not sufficient for the receiving CAV to correctly decode the packet. The received signal power is given by the Friis transmission formula as

$$\zeta_{rx} = \zeta_{tx} - \zeta_{PL} - \zeta_{SH} - \zeta_N. \tag{5.10}$$

Therefore, the probability that the received signal power is not sufficient for correctly receiving the packet, even if the presence of the signal is detected, is given by

$$P_e^{PROP} = Pr\{\epsilon_{th}^{SENS} < \zeta_{rx} < \epsilon_{th}^{PROP}\} = \int_{\epsilon_{th}^{SENS}}^{\epsilon_{th}^{PROP}} f_{\zeta_{rx}}(x)dx. \tag{5.11}$$

Because the shadowing is assumed to follow a log-normal distribution [82], the PDF, $f_{\zeta_{rx}}(x)$, is given by

$$f_{\zeta_{rx}}(x) = \frac{1}{\sigma\sqrt{2\pi}} exp(-(\frac{\zeta_{tx} - \zeta_{PL} - \epsilon_{th}^{PROP}}{\sigma\sqrt{2}})^2). \tag{5.12}$$

Combining Eq. (5.10) - Eq. (5.12), I can find the probability of error due to propagation as

$$P_e^{PROP} = Q(\frac{\zeta_{tx} - (\frac{4\pi D_{t,r}}{\lambda})^2 - \epsilon_{th}^{PROP}}{\sigma\sqrt{2}}). \tag{5.13}$$

The last unknown variable is error due to collisions, P_e^{COL}. Collisions happen when multiple CAVs select the same sub-frame and sub-channel for transmission, thus the interference generated prevents correct reception of BSMs. Collisions can be further divided into two types. The first type of collisions is the collisions due to hidden node problem, I name it hidden collisions. On the contrary, I name the collisions that are happened within the sensing range of a generic transmitting CAV exposed collisions. Firstly, I derive the probability of exposed collisions, which is given by

$$P_{exp}^{COL} = \sum_{m=1}^{N_{EV}-1} P_{sf}(m) \cdot P_{sr}(m), \tag{5.14}$$

where $P_{sf}(m)$ is given by

$$P_{sf}(m) = (\frac{(N_{EV}-1)!}{m!(N_{EV}-1-m)!}) \cdot (\frac{P_{res}}{N_{BSM}})^m \cdot (1 - \frac{P_{res}}{N_{BSM}})^{N_{EV}-1-m}. \tag{5.15}$$

Besides, in order to calculate $P_{sr}(m)$, I have to find the expected number of candidate resources, $E[N_c]$, after the exclusion process, which can be expressed as

$$E[N_c] = \begin{cases} N_{ar} - N_{EV} + \frac{P_e^{COL} \cdot (N_{EV}-1)}{m}, & \text{if } N_{ar} \geqslant N_V \\ 0, & \text{if } N_{ar} < N_V \end{cases}. \tag{5.16}$$

Now I can find the probability that at least one of the m CAVs chooses the same resource as the transmitting CAV, $P_{sr}(m)$, as

$$P_{sr}(m) = 1 - (\frac{E[N_c]-1}{E[N_c]})^m. \tag{5.17}$$

Combining Eq. (5.14) - Eq. (5.17), I can compute the probability of losing a BSM due to exposed collisions.

Next, I formulate the probability of hidden collisions. According to the model described in Section IV, the average number of hidden CAVs is given by

$$N_{HV} = max(0, D_{t,r} + R_{SENS} - R_{tx}) \cdot \beta. \tag{5.18}$$

Since each hidden CAV deploys the same protocol (i.e. SB-SPS) and share the same time-frequency resources, the number of occupied resources that can be detected by each hidden CAV is given by

$$N_{or} = R_{SENS} \cdot \beta. \tag{5.19}$$

The probability that at least one hidden CAV collides with the generic transmitting CAV is given by

$$P_{hid}^{COL} = \begin{cases} 1 - \frac{N_{ar} - N_{or} - 1}{N_{ar} - N_{or}}, & \text{if } N_{ar} \geqslant N_V \\ 1, & \text{if } N_{ar} < N_V \end{cases}. \tag{5.20}$$

Therefore, the probability of losing a BSM due to signal collisions can be expressed as

$$P_e^{COL} = 1 - (1 - P_{exp}^{COL}) \cdot P_{hid}^{COL}. \tag{5.21}$$

Finally, the PDR is given by the combination of Eq. (5.4), Eq. (5.5), Eq. (5.9), Eq. (5.13) and Eq. (5.21).

5.4.1.2 Collision Duration

Collisions do not terminate instantly, they last for a period of time. The longer this duration is, the worse the protocol performs, because the resource is kept being occupied and cannot be released for other CAVs. In this sub-section, I evaluate the performance of SB-SPS in terms of collision duration.

We define collision duration of SB-SPS, D_{SPS}, as the average length of time that a generic CAV is in collision within one resource reservation interval. Hence, it depends on collision probability, packet generation interval, packet size, transmission rate and resource reservation interval. In SB-SPS scheme, when multiple CAVs have selected the same resource to broadcast, sustained message collisions

happen and they will not be realised by transmitting CAVs due to the HD transmission feature. Therefore when a collision happens, it lasts for the whole packet transmission process. Considering the average collision duration within a resource reservation interval, it is given by

$$D_{SPS} = P_e^{COL} \cdot N_{BSM} \cdot T_{BSM}. \tag{5.22}$$

The number of BSMs generated depends on the resource reservation interval and packet generation interval, which it is given by

$$N_{BSM} = \frac{T_{RRI}}{T_{PGI}}. \tag{5.23}$$

Transmission time of a packet depends on the transmission rate and packet size and it is given by

$$T_{BSM} = \frac{S_{BSM}}{R_{trans}}. \tag{5.24}$$

So the collision duration, D_{SPS}, can be expressed as

$$D_{SPS} = P_e^{COL} \cdot \frac{T_{RRI}}{T_{PGI}} \cdot \frac{S_{BSM}}{R_{trans}}. \tag{5.25}$$

5.4.1.3 Latency

In safety-related MAC layer protocol design, latency performance is more important than many other parameters, as the delay of a safety packet may put a CAV into a dangerous situation and in turn may lead to an accident. In this subsection, I evaluate the latency performance of SB-SPS, which is defined as the sum of the resource reservation delay, transmission delay, and the delay caused by collisions and in turn re-transmissions, where propagation delay and processing delay are assumed to be zero.

We define the latency of SB-SPS, L_{SPS}, as the average time interval between the following two time instants within one resource reservation interval, as shown in Fig. 5.8. The first time instant, t_1, is when the receiving CAV should have received a BSM broadcast from the transmitting CAV since the last received BSM. The second time instant, t_2, is when a generic receiving CAV actually receives a BSM broadcast from the transmitting CAV since the last received BSM. In other words, it incorporates the latency caused by the resource reservation process of

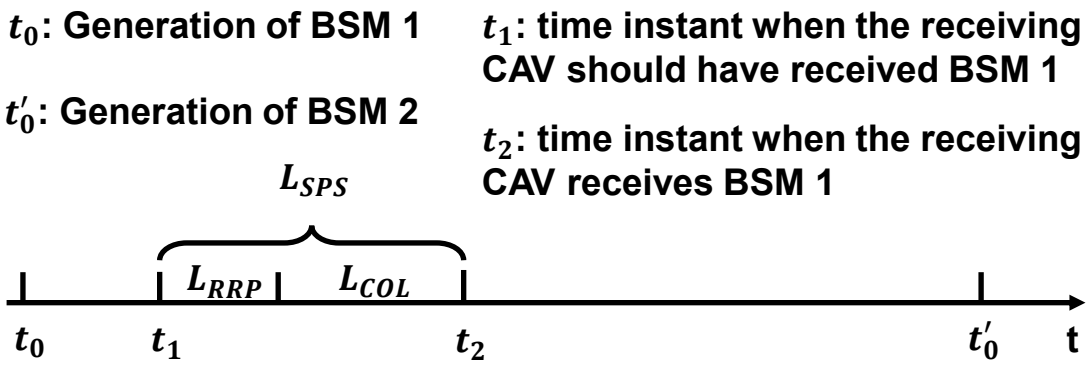

FIGURE 5.8: Two time instants for the latency analysis

the protocol, transmission time of BSMs, L_{RRP}, as well as the latency caused by collisions, L_{COL}. Propagation delay is assumed to be zero in this latency analysis, because the distance between CAVs in a VANET is small compared to the propagation speed of electromagnetic waves. Besides, processing delay is also ignored in my latency analysis, because it depends on the hardware processing capability, and this work focuses on the MAC layer protocol design. Hence, the latency of SB-SPS, L_{SPS}, is given by

$$L_{SPS} = L_{RRP} + L_{COL}. \tag{5.26}$$

The average latency due to the process of resource reservation depends on the width of the selection window and the transmission time, which is given by

$$L_{RRP} = \frac{T_{SW}+N_{BSM}\cdot T_{BSM}}{N_{BSM}}. \tag{5.27}$$

Whilst the average latency due to collisions depends on collision probability. In the SB-SPS protocol, if the first BSM within one transmission episode is in collision, the remaining BSMs are also in collisions. Thus the average latency due to collisions can be expressed as

$$L_{COL} = P_e^{COL} \cdot T_{RRI}. \tag{5.28}$$

So the latency of SB-SPS, L_{SPS}, is given by

$$L_{SPS} = \frac{T_{SW}+N_{BSM}\cdot T_{BSM}}{N_{BSM}} + P_e^{COL} \cdot T_{RRI}. \tag{5.29}$$

5.4.2 Analytical Performance of FDPS

5.4.2.1 Packet Delivery Rate

By deploying the proposed FDPS protocol, BSMs can be lost due to four types of error. The first type is FD error, which is produced when there are multiple CAVs other the transmitting CAV simultaneously sending BSMs, so that all BSMs are lost. The second type is sensing error, which is produced when mis-detection happens. The third type is propagation error, which is produced when the received signal power is not sufficient for a CAV to successfully decode the received BSMs. The last type of error is collision error, which is produced when multiple CAVs select the same time-frequency resource to broadcast BSMs. Thus the PDR is defined as the average probability of broadcasting a BSM without any error, which is given by

$$R_{FD} = (1 - P_e^{FD}) \cdot (1 - P_e^{S}) \cdot (1 - P_e^{P}) \cdot (1 - P_e^{C}). \tag{5.30}$$

FD error is produced when there are more than two CAVs other than the transmitting CAV simultaneously sending BSMs. In other words, the probability of this type of error is equal to the probability that multiple CAV other than a generic transmitting vehicle select different sub-channels in the same sub-frame for transmission. Thus the probability of losing a packet due to FD error is given by

$$P_e^{FD} = 1 - [(\tfrac{N_{ar} - N_{sc}}{N_{ar}})^{N_{EV}-1} \cdot (1 + \tfrac{N_{sc}}{N_{ar}})], \tag{5.31}$$

where N_{EV} is given by Eq. (5.6) and N_{ar} is given by Eq. (5.7).

In addition to FD errors, BSMs can also be lost due to mis-detection, which depends on the path loss, shadowing as well as noise. This type of error happens when the received signal power/signal-plus-interference-to-noise ratio (SINR) is lower than a certain threshold, ϵ_{th}^{S}, and there is a BSM transmission from another CAV. The probability of losing a packet due to this type of error is given by

$$\begin{aligned} P_e^{S} &= P_m^{FD} = 1 - P_d^{FD} \\ &= 1 - Q((\frac{\epsilon_{th}^{S}}{\sigma_n^2} - \Upsilon_{sig} - \eta^2 \Upsilon_{SI} - 1) \times \sqrt{\frac{T_s \cdot f_s}{2\eta^2 \Upsilon_{SI} + 2\eta^2 \Upsilon_{SI} \Upsilon_{sig} + 2\Upsilon_{sig} + 1}}). \end{aligned} \tag{5.32}$$

Afterwards, I compute the error due to propagation, which happens when the received signal power/SINR is higher than the sensing threshold, ϵ_{th}^{S}, but it is still not sufficient for the receiving CAV to correctly decode the packet. In other words, the received signal power/SINR is still smaller than the threshold ϵ_{th}^{P}. The received signal power is given by the Friis transmission formula as

$$\zeta_{rx}^{FD} = \sqrt{\eta}\zeta_{SI}^{FD} + \zeta_{tx}^{FD} - \zeta_{PL}^{FD} - \zeta_{SH}^{FD} - \zeta_{N}^{FD}. \tag{5.33}$$

Therefore, the probability that the received signal power is not sufficient for correctly receiving the packet, even if the presence of the signal is detected, is given by

$$P_e^P = Pr\{\epsilon_{th}^{S} < \zeta_{rx}^{FD} < \epsilon_{th}^{P}\} = \int_{\epsilon_{th}^{S}}^{\epsilon_{th}^{P}} f_{\zeta_{rx}^{FD}}(x)dx. \tag{5.34}$$

Because the shadowing is assumed to follow a log-normal distribution [82], the PDF is given by

$$f_{\zeta_{rx}^{FD}}(x) = \frac{1}{\sigma\sqrt{2\pi}} exp(-(\frac{\sqrt{\eta}\zeta_{SI}^{FD} + \zeta_{tx}^{FD} - \zeta_{PL}^{FD} - \epsilon_{th}^{P}}{\sigma\sqrt{2}})^2). \tag{5.35}$$

Combining Eq. (5.33) - Eq. (5.35), I can find the probability of error due to propagation as

$$P_e^P = Q(\frac{\sqrt{\eta}\zeta_{SI}^{FD} + \zeta_{tx} - (\frac{4\pi D_{t,r}^{FD}}{\lambda})^2 - \epsilon_{th}^{P}}{\sigma\sqrt{2}}). \tag{5.36}$$

The final step is to find the error probability due to signal collisions, P_e^C. The proposed FDPS protocol operates differently from the standardised SB-SPS protocol, because FDPS protocol has collision resolution mechanism, and partial collisions can be avoided. Assume the percentages of low, middle and high communication priority vehicles are denoted by P_{lv}, P_{mv} and P_{hv}, respectively. Collisions happen in the following three cases. The first case is when multiple CAVs have already selected the same resource for the next transmission episode in the selection window, and all CAVs mis-detect the presence of each other during the transmission. Thus, collision probability $P_{e,1}^{C}$ in this case is given by

$$P_{e,1}^{C} = \sum_{i=1}^{N_V} P_e^{COL} \cdot (1 - P_d^{FD})^{i-1}. \tag{5.37}$$

The second case is when multiple middle or high CAVs have selected the same

resource for the next transmission episode in the selection window, and at least two CAVs do not falsely detect the presence of the collision. Thus, collision probability $P_{e,2}^{C}$ in this case is given by

$$P_{e,2}^{C} = \sum_{i=2}^{N_V} P_e^{COL} \cdot (P_{mv} + P_{hv})^i \cdot (1 - P_f^{FD})^{i-1}. \tag{5.38}$$

The third case is when hidden collisions happen. Thus, the hidden collision probability is approximated according to [45] and is given by

$$P_{e,3}^{C} = \frac{2(N_{HV}-1)T_{RRI}(2-P_e^{C})}{2 \cdot T_{BSM}}. \tag{5.39}$$

Therefore, the overall error probability due to signal collisions is given by the combination of Eq. (5.37)-Eq. (5.39) as

$$P_e^{C} = P_{e,1}^{C} + P_{e,2}^{C} + P_{e,3}^{C}. \tag{5.40}$$

Finally, the PDR performance of the proposed FDPS protocol is given by the combination of Eq. (5.31), Eq. (5.32), Eq. (5.36) and Eq. (5.40), and can be computed according to Eq. (5.30).

5.4.2.2 Collision Duration

D_{FD} is defined as the average time duration that packets are in collision within a resource reservation interval. It depends on collision probability, packet generation interval, packet size, transmission rate and resource reservation interval. In addition, since the probability that all CAVs in collision mis-detect for consecutive sub-frames is very low, I ignore consecutive mis-detections. Overall average collision duration is given by the sum of seven cases. The first case is when collisions occur between BSMs from low-priority CAVs, which happens with probability $P_1 = P_{lv}^2$. Collision duration in this case is given by

$$D_{FD,1} = P_e^{C} \cdot (-2P_d^{FD4} + 8P_d^{FD3} - 11P_d^{F}D^2 + 6P_d^{FD}) \cdot T_{BSM}. \tag{5.41}$$

The second case is when collisions occur between BSMs from a high-priority

CAV and a low-priority CAV, which happens with probability $P_2 = 2P_{hv}P_{lv}$. Collision duration in this case is given by

$$D_{FD,2} = P_e^C \cdot (2P_d^{FD^3} - 2P_d^{FD^2} + 3P_d^{FD}) \cdot T_{BSM}. \tag{5.42}$$

The third case is when collisions occur between BSMs from a middle-priority CAV and a low-priority CAV, which happens with probability $P_3 = 2P_{mv}P_{lv}$. Collision duration in this case is given by

$$D_{FD,3} = P_e^C \cdot (2P_d^{FD^3} - 2P_d^{FD^2} + 5P_d^{FD}) \cdot T_{BSM}. \tag{5.43}$$

The fourth case is when collisions occur between BSMs from high-priority CAVs, which happens with probability $P_4 = P_{hv}^2$. Collision duration in this case is given by

$$D_{FD,4} = P_e^C \cdot (6P_d^{FD} - 3P_d^{FD^2}) \cdot T_{BSM}. \tag{5.44}$$

The fifth case is when collisions occur between BSMs from middle-priority CAVs, which happens with probability $P_5 = P_{mv}^2$. Collision duration in this case is given by

$$D_{FD,5} = P_e^C \cdot (4P_d^{FD} - 2P_d^{FD^2}) \cdot T_{BSM}. \tag{5.45}$$

The sixth case is when collisions occur between BSMs from a high-priority CAV and a middle-priority CAV, which happens with probability $P_6 = 2P_{mv}P_{hv}$. Collision duration in this case is given by

$$D_{FD,6} = P_e^C \cdot (5P_d^{FD} - 3P_d^{FD^2}) \cdot T_{BSM}. \tag{5.46}$$

The last case is when hidden collisions occur with probability $P_7 = P_{e,3}^C$, and the collision duration in this case is given by

$$D_{FD,7} = P_e^C \cdot T_{BSM}. \tag{5.47}$$

Therefore, I can compute the overall collision duration by the combination of the above seven cases as

$$D_{FD} = \sum_{i=1}^{i=7} P_i \cdot D_{FD,i}. \tag{5.48}$$

5.4.2.3 Latency

Same as the analysis of the standardised SB-SPS protocol, I define the latency of FDPS, L_{FD}, as the average time interval between the following two time instants within one resource reservation interval. The first time instant is when the receiving CAV should have received a BSM broadcast from the transmitting CAV since the last received BSM. The second time instant is when a generic receiving CAV actually receives a BSM broadcast from the transmitting CAV since the last received BSM. In other words, it incorporates the latency caused by the resource reservation process of the protocol, transmission time of BSMs, as well as the latency caused by collisions. Propagation delay and processing delay are also ignored. In other words, this latency is equivalent to the end-to-end delay in which propagation and processing delay are assumed to be zero. Hence, the latency of the proposed FDPS, L_{FD}, is equal to the sum of resource reservation delay, L_{FD}^{RRP}, and delay due to re-transmissions, L_{FD}^{RT}, which is given by

$$L_{FD} = L_{FD}^{RRP} + L_{FD}^{RT}. \tag{5.49}$$

Since the resource reservation process in FDPS protocol is the same as it is in the SB-SPS protocol, resource reservation delay is also the same as it is in the SB-SPS protocol, which is given by Eq. (5.27), L_{FD}^{RRP} is given by

$$L_{FD}^{RRP} = L_{RRP} = \frac{T_{SW}+N_{BSM}\cdot T_{BSM}}{N_{BSM}}. \tag{5.50}$$

However, because partial collided BSMs can be resolved and avoided through FD technology in the FDPS protocol, CAVs abort the current transmission and change to a new time-frequency resource only when the maximum re-attempt limit is reached. Therefore, the amount of time spent on the re-broadcast, L_{FD}^{RT}, is equal to the sum of the packet generation interval, T_{PGI}, and the new resource reservation interval, L_{RRI}, which is given by

$$L_{FD}^{RT} = P_e^C \cdot (T_{PGI} + L_{RRI}). \tag{5.51}$$

Finally, I can compute the overall average latency by combining Eq. (5.49)-Eq. (5.51), which is given by

$$L_{FD} = \frac{T_{SW}+N_{BSM}\cdot T_{BSM}}{N_{BSM}} + P_e^C \cdot (T_{PGI} + L_{RRI}). \tag{5.52}$$

Meanwhile, it would also be insightful to consider the worst case or maximum time interval for the latency. Since the collision detection capability is assumed to be imperfect, and continuous mis-detection will lead to continuous collisions in the re-broadcast phase, latency will be larger than the average latency performance when continuous mis-detection happens, which will in turn put CAVs into a dangerous situation. The worst case scenario corresponds to the case where a CAV can only wait for the generation of the new BSM, so the current BSM will be discarded. Therefore, the maximum time interval for the latency is 100 ms. Compared to the SB-SPS protocol, in which the maximum latency is 1 second when the packet generation interval is set to 10 Hz, FDPS has a much better performance in terms of maximum time interval for the latency.

5.4.3 Convergence and Complexity Analysis

5.4.3.1 Convergence Analysis

The proof of convergence of SB-SPS is established by showing that the total number of available resources that can be selected, N_{ar}, is non-increasing with the update of the total number of available sub-channels, N_{asc}, and the total number of available sub-frames, N_{asf}. As introduced in Section 5.2.2 and shown in Fig. 5.4, N_{ar} is given by Eq. (5.7) and can also be expressed as

$$N_{ar}^{N_{t-1}} = F(N_{sc}^{N_{t-1}}, N_{sf}^{N_{t-1}}) = N_{sc}^{N_{t-1}} \cdot N_{sf}^{N_{t-1}}, \tag{5.53}$$

where N_{t-1} denotes the sub-frame before the start of the resource reservation process. After that, N_{ar} will be updated according to the SB-SPS protocol, which is given by

$$\begin{aligned} N_{ar}^{N_{t-1}} = F(N_{sc}^{N_{t-1}}, N_{sf}^{N_{t-1}}) &\overset{(1)}{\geqslant} F_a(N_{asc}^{N_{t-1}}, N_{asf}^{N_{t-1}}) \overset{(2)}{\geqslant} F_b(N_{asc}^{N_{t-1}}, N_{asf}^{N_{t-1}}) \\ &\overset{(3)}{\geqslant} F_c(N_{asc}^{N_{t-1}}, N_{asf}^{N_{t-1}}) = N_{sr}^{N_t}, \end{aligned} \tag{5.54}$$

where (1), (2) and (3) denote the three exclusion conditions, respectively, which are introduced in Section 5.2.2. $F_i(.)$ denotes the remaining available resources after executed exclusion condition i, which is finite, and $N_{sr}^{N_t}$ denotes the selected resource for the next consecutive transmission period at sub-frame N_t which refers to the last sub-frame of the selection window. Therefore, the proof of convergence of SB-SPS is completed. SB-SPS is guaranteed to converge within each

resource reservation interval.

Same as the convergence analysis of SB-SPS, FDPS is also guaranteed to converge within each resource reservation interval. First, the total number of available resources, $N_{ar,FD}$ is non-increasing with the update of the total number of available sub-channels, N_{asc}, and the total number of available sub-frames, N_{asf}, which is given by

$$\begin{aligned} N_{ar,FD}^{N_{t-1}} &= F(N_{asc}^{N_{t-1}}, N_{asf}^{N_{t-1}}) \overset{(1)}{\geqslant} F_a(N_{asc}^{N_{t-1}}, N_{asf}^{N_{t-1}}) \\ &\overset{(2)}{\geqslant} F_b(N_{asc}^{N_{t-1}}, N_{asf}^{N_{t-1}}) \overset{(3)}{\geqslant} F_c(N_{asc}^{N_{t-1}}, N_{asf}^{N_{t-1}}) \\ &= N_{sr,FD}^{N_t}, \end{aligned} \tag{5.55}$$

where $N_{ar,FD}^{N_{t-1}}$ refers to the total number of available resources that can be selected in FDPS at sub-frame N_{t-1}, and $N_{sr,FD}^{N_t}$ refers to the selected resource for the next consecutive transmission episode at sub-frame N_t. (1), (2) and (3) refer to the three exclusion conditions, respectively, which are introduced in Section 5.2.3. Besides the decreasing resource reservation process, as introduced in Section 5.2.3 and shown in Fig. 5.6, the re-broadcast loop is finite. Therefore, the proof of convergence of FDPS is completed.

5.4.3.2 Complexity Analysis

The complexity of the proposed FDPS lies in the resource reservation and resource re-selection processes. In order to analyse the complexity of it, I need to calculate the complexity of the worst case, which corresponds to the continuous collisions problem. Besides, collision duration will also affect the total number of iterations for re-selecting new resources, which in turn will lead to the continuous collisions problem. The complexity will be maximum when collision duration is minimum, which corresponds to the case where collisions happen between BSMs from low-priority CAVs, because low-priority CAVs will go to resource re-selection process without any re-broadcast attempt. On the other hand, middle- and high-priority CAVs re-attempt to transmit when collisions have been detected. Therefore, the corresponding collision duration will be longer, and the respective complexity will be less. The collision duration of the worst case, $D_{FD,1}$, is given by Eq. (5.41). In addition, since latency is non-decreasing and finitely upper bounded by the packet generation interval, T_{PGI},

the complexity of the worst case is given when collisions cannot be resolved within the packet generation interval. Given the workflow of FDPS which is shown in Fig. 5.6, in the worst case, the complexity for each CAV to broadcast once is $\mathcal{O}(N_{ar} \cdot (3N_{ar} + N_{ar}^2 + 1))$. Therefore, the overall complexity of FDPS is $\mathcal{O}(N_{EV} \cdot (N_{ar} \cdot (3N_{ar} + N_{ar}^2 + 1) \cdot \delta)) = \mathcal{O}(N_{EV} \cdot N_{ar}^3 \cdot \delta)$, where $\delta = ceil(\frac{T_{PGI}}{D_{FD,1}})$, δ denotes the number of iterations for re-selecting new resources in the worst case, and $ceil(.)$ is the function which rounds the element to the nearest integer greater than or equal to the element.

5.4.4 Mathematical Difference Analysis

In this sub-section, I compare the mathematical results provided in sub-sections A and B for SB-SPS and FDPS. First, I compare the PDR of SB-SPS shown by Eq. (5.4) against the PDR of FDPS shown by Eq. (5.30). I can see that the differences are HD and FD errors (i.e. P_e^{HD} and P_e^{FD}) and collision errors (i.e. P_e^{COL} and P_e^{C}). The relationship between the HD and FD errors is given by

$$Eq.(5.5) = P_e^{HD} \geqslant P_e^{FD} = Eq.(5.31), \tag{5.56}$$

because

$$(\frac{N_{ar} - N_{sc}}{N_{ar}})^{N_{EV}-1} \cdot (1 + \frac{N_{sc}}{N_{ar}}) \geqslant (\frac{N_{ar} - N_{sc}}{N_{ar}})^{N_{EV}-1}. \tag{5.57}$$

Besides, the relationship between collision errors is given by

$$\begin{cases} Eq.(5.21) = P_e^{COL} \geqslant P_e^{FD} = Eq.(5.40), & \text{if } \eta \geqslant \eta_r \\ Eq.(5.21) = P_e^{COL} < P_e^{FD} = Eq.(5.40), & \text{if } \eta < \eta_r, \end{cases} \tag{5.58}$$

where η_r denotes requirement for SIS factor, because the collision probability of FDPS is reduced as shown by the second exclusion condition during the resource reservation interval in Fig. 5.6. Therefore, according to Eq. (5.4) and Eq. (5.30), I can obtain the relationship between the PDR of FDPS and the PDR of SB-SPS, which can be expressed as

$$\begin{cases} Eq.(5.30) = R_{FD} \leqslant R_{SPS} = Eq.(5.4), & \text{if } \eta \geqslant \eta_r \\ Eq.(5.30) = R_{FD} > R_{SPS} = Eq.(5.4), & \text{if } \eta < \eta_r. \end{cases} \tag{5.59}$$

Such a conclusion is also verified by Fig. 5.11 and Fig. 5.14 through simulation, which will be explained and analysed in detail in Section. 5.5.

Then, I analyse the difference between FDPS and SB-SPS in terms of the formulated collision duration. Same as in the PDR analysis method, I can obtain the relationship between the collision duration of FDPS and SB-SPS according to Eq. (5.25) and Eq. (5.48), which are given by

$$\begin{cases} Eq.(5.25) = D_{SPS} \leqslant D_{FD} = Eq.(5.48), & \text{if } \eta \geqslant \eta_r \\ Eq.(5.25) = D_{SPS} > D_{FD} = Eq.(5.48), & \text{if } \eta < \eta_r. \end{cases} \tag{5.60}$$

Such a conclusion is also verified by Fig. 5.12 and Fig. 5.15 through simulation, which will be explained and analysed in detail in Section. 5.5.

Finally, I can also compare the latency of FDPS and SB-SPS according to Eq. (5.29) and Eq. (5.52), respectively, which are given by

$$\begin{cases} Eq.(5.29) = L_{SPS} \leqslant L_{FD} = Eq.(5.52), & \text{if } \eta \geqslant \eta_r \\ Eq.(5.29) = L_{SPS} > L_{FD} = Eq.(5.52), & \text{if } \eta < \eta_r. \end{cases} \tag{5.61}$$

Such a conclusion is also verified by Fig. 5.13 and Fig. 5.16 through simulation, which will be explained and analysed in detail in Section. 5.5.

To summarise, FDPS is theoretically proved to be able to enhance the PDR, shorten the collision duration and reduce the latency, which are achieved by reducing the HD errors and collisions through the proposed FD simultaneous sensing strategy, transmission abortion policy and prioritised re-broadcast mechanism. However, the drawback of deploying FD technology is the need to consider the SIS factor, η_r, which is found and analysed in detail in Section 5.5.

5.4.5 Assumption & Approximation Analysis

The considered scenario in this work is consistent with the 3GPP standards [83], [72], [73], [79]-[81], and the assumptions and approximations are also consistent with the 3GPP standards [83], [72], [73], [79]-[81], and the related works such as [45] and [10]. They include the sensing technology, maximum relative speed between CAVs, modulation and coding scheme, transmit power, channel

bandwidth packet size, BSM generation interval, resource re-selection probability, propagation and processing delay. However, I also provide analysis in this sub-section to show how the performance of the proposed FDPS method would be affected when one of the assumptions is relaxed.

First, the deployed sensing strategy of FDPS is designed to endure and compensate a maximum Doppler frequency shift of 2.731 kHz, which can be translated into 500 km/h maximum relative speed when the transmission rate is 6 $Mbps$. If the Doppler frequency shift goes beyond the value, the measured SI signal strength, Υ_{SI}, and the measured colliding signal strength, Υ_{sig}, in Eq. (5.1) will both decrease. Therefore, the FD detection probability, P_d^{FD}, in Eq. (5.1) will decrease, the FD false alarm probability, P_f^{FD}, in Eq. (5.2) will increase, and the FD mis-detection probability, P_m^{FD}, will increase. In this case, the FD detection probability is given by

$$\begin{aligned} P_d^{FD\prime} =& Q((\frac{\epsilon_{th}}{\sigma_n^2} - \Delta\Upsilon_{sig} - \eta^2\Delta\Upsilon_{SI} - 1)\times \\ & \sqrt{\frac{T_s \cdot f_s}{2\eta^2\Delta\Upsilon_{SI} + 2\eta^2\Delta\Upsilon_{SI}\Delta\Upsilon_{sig} + 2\Delta\Upsilon_{sig} + 1}}), \end{aligned} \tag{5.62}$$

the FD false alarm probability is given by

$$P_f^{FD\prime} = Q((\frac{\epsilon_{th}}{\sigma_n^2} - \eta^2\Delta\Upsilon_{SI} - 1) \cdot \sqrt{\frac{T_s \cdot f_s}{2\eta^2\Delta\Upsilon_{SI} + 1}}), \tag{5.63}$$

and the FD mis-detection probability is given by

$$\begin{aligned} P_m^{FD\prime} =& 1 - Q((\frac{\epsilon_{th}}{\sigma_n^2} - \Delta\Upsilon_{sig} - \eta^2\Delta\Upsilon_{SI} - 1)\times \\ & \sqrt{\frac{T_s \cdot f_s}{2\eta^2\Delta\Upsilon_{SI} + 2\eta^2\Delta\Upsilon_{SI}\Delta\Upsilon_{sig} + 2\Delta\Upsilon_{sig} + 1}}), \end{aligned} \tag{5.64}$$

where $\Delta\Upsilon_{sig}$ and $\Delta\Upsilon_{SI}$ denote the measured colliding signal strength and the measured SI signal strength, respectively, when the Doppler frequency shift goes beyond the value. In turn, the sensing error probability, P_e^S, in Eq. (5.32) and the collision error probability, P_e^C, in Eq. (5.40) will both increase due to the decrease of detection accuracy, the PDR of FDPS, R_{FD}, in Eq. (5.30) will decrease due to the rise of sensing and collision errors. Besides of PDR, the average collision

duration, D_{FD}, in Eq. (5.48) will be longer due to the rise of collision error probability. Meanwhile, the average latency, L_{FD}, in Eq. (5.52) will also increase due to rise of collision error probability and number of re-broadcasts.

In addition, propagation delay is assumed to be negligible, because the distance between CAVs in a VANET is very small compared to the speed of the electromagnetic wave. However, when this assumption is relaxed, the overall average latency, L_{FD}, shown by Eq. (5.52) will be increased, because the propagation delay will be added to the overall latency. Similarly, processing delay depends on the hardware processing power. This delay is also approximated to be negligible in this work. When this approximation is not applicable, the overall latency has to include the processing delay, which will be greater than the formulated latency shown by Eq. (5.52). Meanwhile, the increased latency may also trigger BSM drop according to the design of FDPS, which leads to the decrease of PDR. In this case, the overall average latency, L_{FD}, is given by

$$L_{FD} = L_{FD}^{RRP} + L_{FD}^{RT} + L_{FD}^{PROP} + L_{FD}^{PROC}, \tag{5.65}$$

where L_{FD}^{PROP} and L_{FD}^{PROC} denote the latency of propagation delay and processing delay, respectively.

However, the changes in the above assumptions will not affect the convergence of FDPS, because the total number of available resources, $N_{ar,FD}$ is still non-increasing with the update of the total number of available sub-channels, N_{asc}, and the total number of available sub-frames, N_{asf}. In addition, the changes will also not affect the maximum latency in the worst case, because it is upper-bounded by the BSM generation interval. Therefore, the execution of FDPS will not be affected, because resource re-selection process will be triggered. Although the overall latency will be increased in this case, it will still be better than the overall average latency of SB-SPS, because the latencies will be the same only in the worst case, it is equal to the upper bound, which is the BSM generation interval. Otherwise, in other cases, the latency of FDPS is smaller, so the overall average latency of FDPS will still be smaller than the overall average latency of SB-SPS. Furthermore, PDR of FDPS will drop, but the overall PDR will be higher than the PDR of SB-SPS, because partially lost BSMs can still be recovered in FDPS, whilst SB-SPS does not have this capability.

5.5 Simulation Results & Discussions

5.5.1 Simulation Environment

We have developed a customised NR eV2X VANETs simulator over the *Veins* simulation framework [84], which integrates the wireless network simulator *OMNeT++* and the traffic simulator *SUMO*. Specifically, the FD simultaneous broadcasting and sensing feature has been developed in the PHY layer, and the standard SB-SPS and the proposed FDPS protocols have been developed in the MAC layer.

Besides, Strand, London, U.K. is chosen as the area for simulation, which is depicted in Fig. 5.9 and Fig. 5.10. An overview of Stand is provided in Fig. 5.9, and a closer view of a junction is given as an example in Fig. 5.10. As can be seen, traffic lights and multiple lanes are both considered and developed in the simulation. Objects such as roads and traffic lights are generated from *Open Street Map (OSM)* and converted into a *SUMO* network.

FIGURE 5.9: Overview of the simulation scenario

FIGURE 5.10: Close view of the simulation scenario

At the beginning of the simulation, CAVs are randomly generated according to the Poisson Point Process (PPP) model, because the distribution of CAVs has been shown to follow this model in the literature [85]-[86]. Next, destinations of CAVs are randomly chosen within the area, and CAVs move according to the received BSMs from *OMNeT++*. Meanwhile, the environment developed in *SUMO* is also synchronised into *OMNeT++*, which means that the quality of the channels depends on the location and surrounding environment of a CAV. Furthermore, analytical formulations are visualised in *MATLAB*. Simulation results (i.e. PDR, collision duration and latency) are tabulated in *OMNeT++*, which are then imported into *MATLAB*. Finally, figures are plotted by *MATLAB*.

5.5.2 Results & Discussions

In this section, I evaluate the proposed design through simulations, and compare it to the standardised SB-SPS protocol. Telecommunication-related values are selected from the Rel-16 of the 3GPP standard [83], and the percentages of CAVs operating at different levels are chosen from the national strategic plans [66]-[67], which are all shown in Table. 5.7. In other words, the chosen parameters and scheme are realistic. Furthermore, the reason why only the standard instead of prior art has been chosen as the benchmark is because to the best of my knowledge, at the time of this work, this was the first paper applying the FD

simultaneous transmission and sensing to C-V2X. Therefore, I believe the standardised SB-SPS protocol was the best benchmark.

TABLE 5.7: SIMULATION PARAMETERS

Parameters	**Values**
Target Detection Probability	90%
Modulation Scheme and coding scheme	MCS 9 (QPSK 0.7)
Antenna Height	1.5 m
Transmit Power	20 dBm
Residual Self-Interference	0%-40%
Vehicle Density	0-200 vehicles/km
Maximum Speed	40 miles/h
Transmission Rate	6 Mbps
Packet Size	350 bytes/pkt
Low priority CAV percentage	50%
Middle priority CAV percentage	40%
High priority CAV percentage	10%
MAC protocol	SB-SPS, FDPS
Channel bandwidth	10 MHz
BSM repetition interval	20 msec
maximum number of lanes	4 lanes

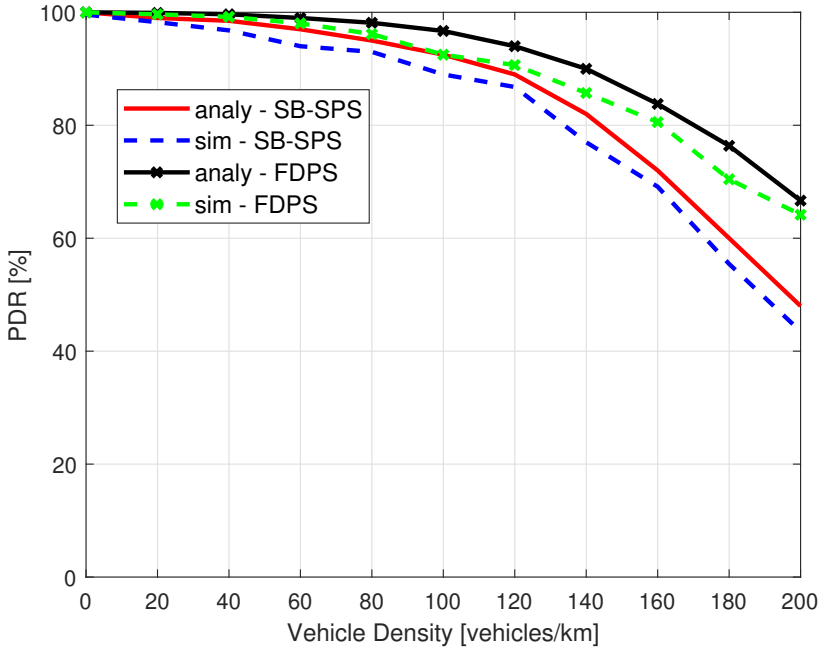

FIGURE 5.11: PDR against vehicle density of the VANET

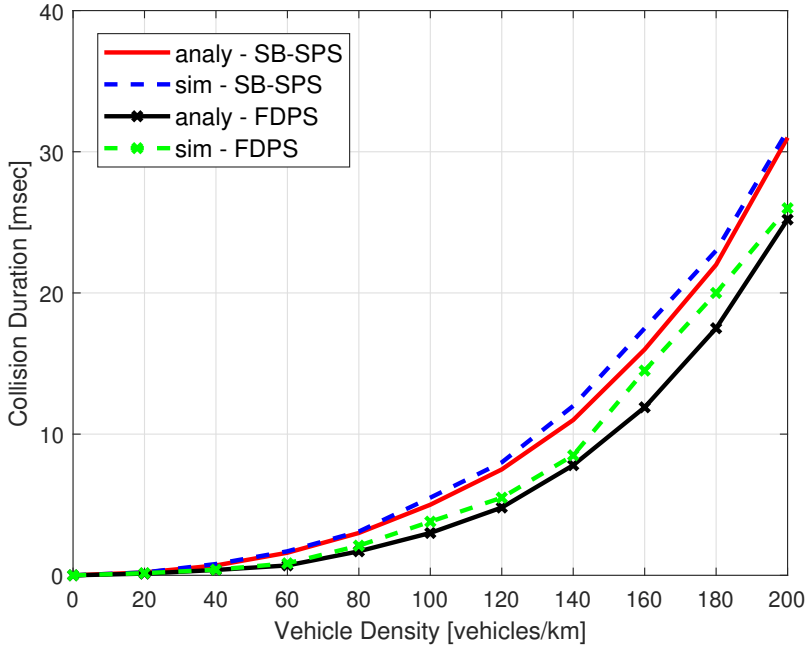

FIGURE 5.12: Collision duration against vehicle density of the VANET

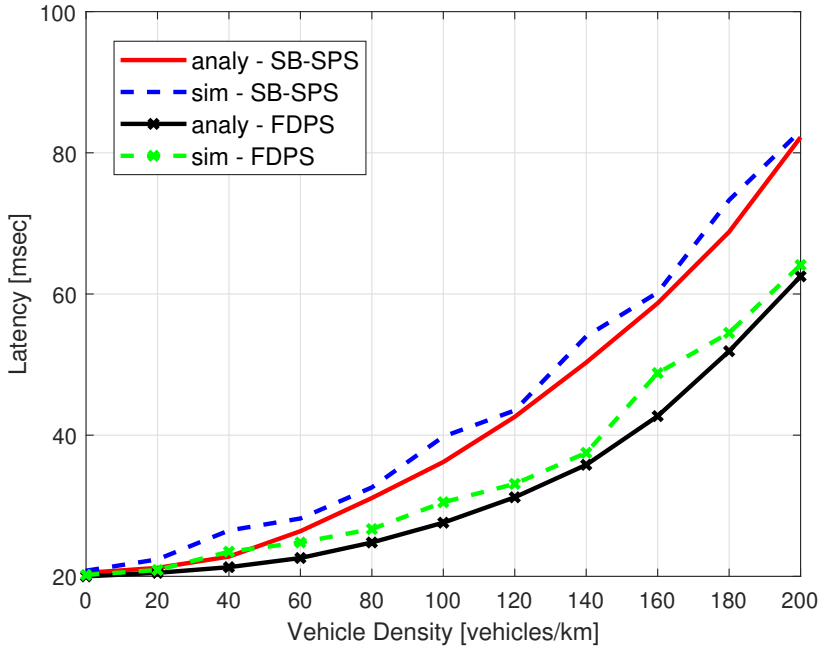

FIGURE 5.13: Latency against vehicle density of the VANET

Fig. 5.11 depicts the PDR performance against the density of the VANET, where the analytical curves are plotted by using Eq. (5.4) and Eq. (5.30). As it is shown,

the analytical and simulation results are close to each other, which means that the analytical PDR and simulation PDR mutually validate each other. In other words, the analytical and simulation results are both correct and accurate, which is also reliable. Otherwise, if any of the result is wrong or not accurate enough, the differences between the analytical and simulation values would be much bigger. In addition, when vehicle density increases, the percentage of successful BSM broadcast drops. The reason is that the available time-frequency resource is limited, and when more CAVs compete for transmission, collisions happen, which reduce the successful packet delivery rate. In addition, I can see that the proposed FDPS protocol outperforms the standardised SB-SPS protocol, because collisions are recognised and collided packets can be re-broadcast, which helps increase the successful delivery rate.

Fig. 5.12 illustrates the average time duration that BSMs are in collision within one resource reservation interval, where the analytical curves are plotted by using Eq. (5.25) and Eq. (5.48). Firstly, I can see that the analytical and simulation results mutually validate each other. In addition, it is shown that the collision duration becomes longer when the density of the VANET increases, because when more CAVs have joined into the VANET, the probability that they select the same resource for broadcast goes up, which leads to longer time in collision. However, the FDPS operates in the FD mode, although sensing is not perfect, partial collisions can be avoided by the FD mode and the added collision resolution mechanism. Thus, FD-enabled CAVs can broadcast with shorter collision duration.

Another key parameter in V2X communications is latency, which is shown in Fig. 5.13, where the analytical curves are plotted by using Eq. (5.29) and Eq. (5.52). First of all, analytical results match simulation results, which shows the validation of the analysis. In addition, no matter which design is deployed, CAVs suffer from the VANET density, since latency increases dramatically when more CAVs are competing for the fixed number of resources. But when FDPS is applied to the CAVs, latency can be significantly reduced due to its collision detection capability and collision resolution capability.

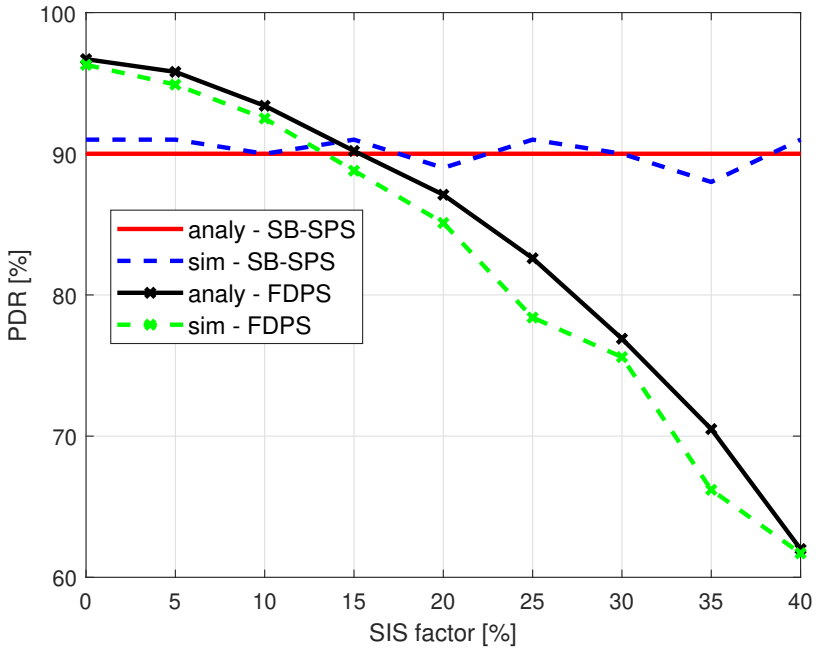

FIGURE 5.14: PDR against SIS factor of the CAVs

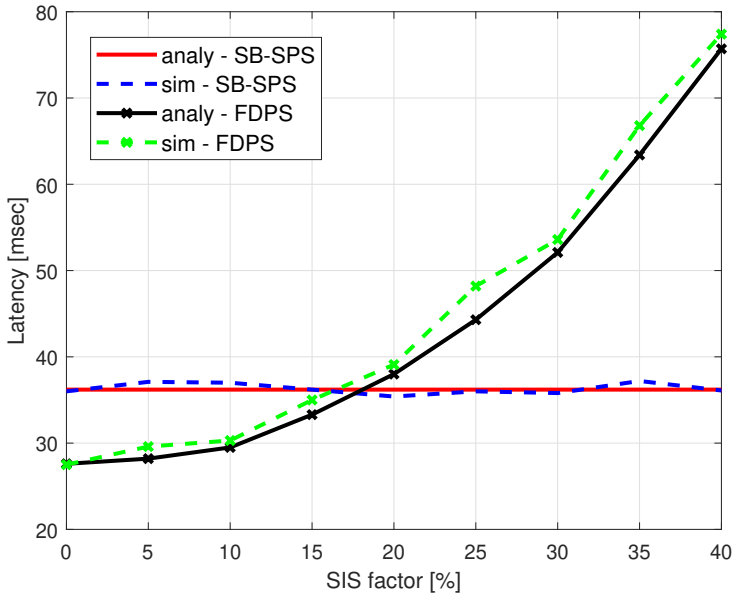

FIGURE 5.16: Latency against SIS factor of the CAVs

However, applying FD technology to CAVs also brings in the RSI signal, which is one of the main challenges in FD communications. Therefore, I evaluate the effect of SIS capability on the PDR, collision duration and latency, which are illustrated

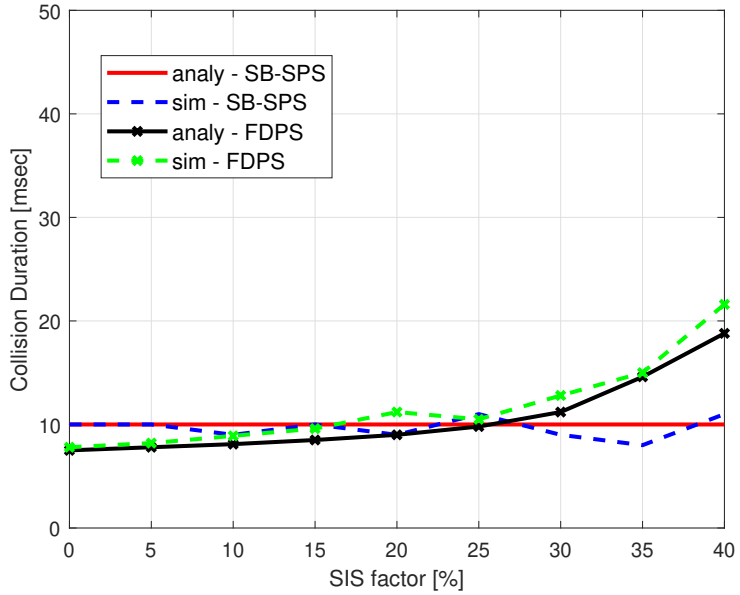

FIGURE 5.15: Collision Duration against SIS factor of the CAVs

in Fig. 5.14 to Fig. 5.16, respectively.

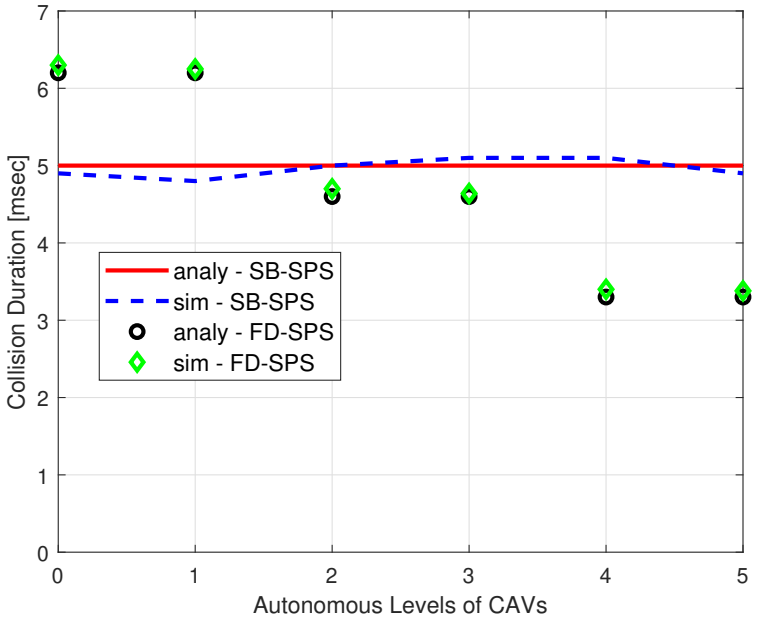

FIGURE 5.18: Collision duration against priority levels of the CAVs

As can be seen, the figures show the correctness of the analysis, as analytical and simulation results match. Next, I can see that when the percentage of RSI signal increases (i.e. SIS factor increases), PDR, collision duration as well as latency all

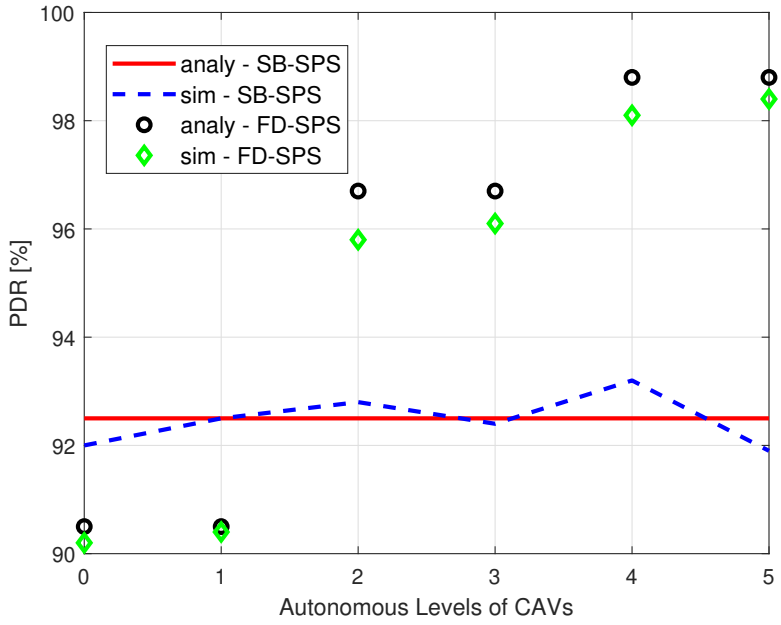

FIGURE 5.17: PDR against priority levels of the CAVs

become worse, because RSI signal will reduce the detection accuracy. However, an intersection points can be found in each figure, which shows the thresholds for deploying the FDPS protocol. In Fig. 5.14, when SIS capability is better than approximately 16%, the FDPS outperforms the SB-SPS protocol in terms of PDR. Similarly, in Fig. 5.15, it is shown that the FDPS can provide shorter collision duration, when SIS factor is smaller than approximately 24%. Besides, as illustrated in Fig. 5.16, when SIS factor goes above roughly 18%, the standardised SB-SPS design has shorter latency performance than my proposed FDPS design. In summary, in order to provide better performance in terms of all metrics (i.e. PDR, collision duration and latency), a minimum of 16% SIS capability is required for the proposed FDPS protocol to be feasible, which is achievable [11].

Finally, it is also important to analyse how each category of priority levels perform in addition to the average performance. PDR, collision duration and latency performance of CAVs operating at each priority level are demonstrated in Fig. 5.17 to Fig. 5.19, respectively. First of all, analytical results and simulation results mutually validate each other. In addition, As can be seen in the figures, compared with the standardised SB-SPS protocol, CAVs operating at middle to high-level priority can obtain much better service from the proposed FDPS protocol, whilst CAVs operating at low-level priority will have slightly worse service. However, I believe a slightly worse average performance will not affect the

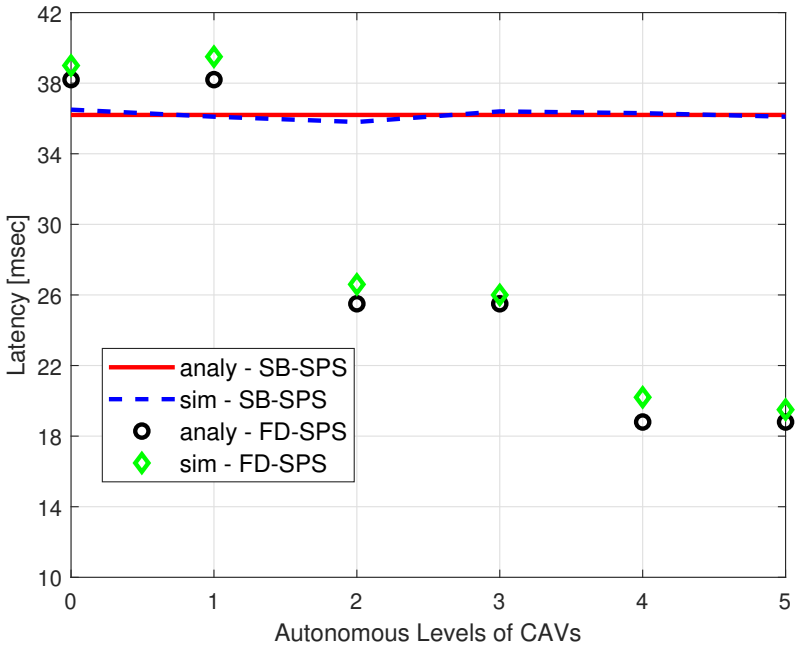

FIGURE 5.19: Latency against priority levels of the CAVs

safety. For example, an approximately 38*ms* average latency can be provided to low-level priority CAVs, which is sufficient for a driver-assistance system such as distance warning. But by deploying the FDPS protocol, middle and high-level priority CAVs can enjoy a much better service. Meanwhile, compared with the SB-SPS protocol, the overall system performance of the VANET is enhanced.

5.6 Future Works

The applicability of the proposed design may be complementary to higher layer technologies, such as the software defined networking in [87], and multipath TCP in [88], since the broadcasting and sensing feature, and the prioritised messaging feature of this work can be applied as the foundation of novel higher layer designs. Besides, this work may also be applicable with suitable federated learning (FL) and block chain technologies to address various other challenges which are described in [89]. For example, in a case where multiple CAVs cooperatively train a surrounding environment model for safety enhancement purpose, spectral efficiency and latency requirements are equally important as the privacy demand. Therefore, the throughput and latency performance can be enhanced by using the FD simultaneous transmission and reception feature in FD device-to-device (D2D) and FD broadcast/multicast/groupcast architecture, whilst the FD simultaneous transmission and sensing feature can be used to prevent malicious attackers, which enhances the privacy protection together with the FL method.

5.7 Summary

In this work, I have proposed a novel prioritisation scheme, which follows the national strategic plans of future ITS development. Besides, I have also proposed a novel MAC layer protocol, named FDPS, to enhance the performance in terms of PDR, collision duration and latency, which is compatible with the current NR eV2X standard, because neither ACK messaging mechanism nor further signalling have been introduced. By deploying my proposal, collision detection is enabled through FD technology, and collision resolution mechanism is also carefully designed. Its performance is evaluated through mathematical and simulation analysis, results have shown that the FDPS proposal have enhanced the performance and feasibility for future NR eV2X VANETs.

6 An Adaptive FD Deep Reinforcement Learning-Based Design

Synopsis of Chapter

This work refers to my paper [90], which exploits full-duplex (FD) technology and deep reinforcement learning (DRL) algorithm jointly and adaptively to enhance the performance of 5G-V2X networks that operate based on the 5G-V2X Mode 4 standard. Specifically, I propose a novel physical- (PHY) and medium access control- (MAC) layer cross-layer design. Besides, the resource reservation scheme, collision resolution mechanism and scheduling policy are also designed. As the proposed adaptive method is fully decentralised, vehicular users adapt to the unknown and fast-changing environment autonomously without any help from gNBs. Simulation results demonstrate the superiority of my proposed design over the standardised sensing-based semi-persistent scheduling (SB-SPS) protocol. Therefore, the proposed cross-layer design can be considered as a solution for future 5G-V2X VANETs.

We introduce the background, motivation and contributions of this work in Section 6.1. Next, I present the considered system model, assumptions and the benchmark SB-SPS solution in Section 6.2. Furthermore, my proposed design is illustrated in Section 6.3. In addition, the simulation setup and the comparison are presented in Section 6.4. Finally, I conclude this work in Section 6.5.

6.1 Introduction

Motivated by increasingly stringent quality-of-service (QoS) requirements in future vehicular networks, 5G-V2X technology is expected to address a wide range of critical challenges, where safety becomes the first and most significant demand [83]. A major challenging scenario is the fully decentralised vehicular network, in which vehicular UEs (VUEs) access spectrum and schedule transmission without any assistance from gNBs. Such a scenario is regarded as the baseline mode, and must be supported in 5G-V2X networks.

However, most existing papers consider the device-to-device communication scenario, which is not fully decentralised, as gNBs are in charge of resource allocation and scheduling, such as [91]-[92]. Only a few papers consider the fully decentralised scenario [82], where VUEs share safety information autonomously without any assistance from gNBs. Furthermore, VUEs are equipped with half-duplex (HD) technology, signal collisions cannot be detected during broadcasting. Hence, the acknowledgement and the collision resolution problems become major challenges [43]-[42]. Recent enhancement in self-interference suppression (SIS) techniques has led to a novel opportunity of applying full-duplex (FD) technology to 5G-V2X networks [11]. With the capability of simultaneous broadcasting and sensing, FD-enabled VUEs can detect collisions during broadcasting and re-schedule the transmission after collisions have been detected. Therefore, FD sensing technique in 5G vehicular ad hoc networks (VANETs) should be analysed and new medium access control (MAC) layer mechanism should be designed [10].

Although the combination of FD technology and MAC protocol can satisfy QoS requirements of partial vehicular applications [45], recent developments in machine learning have also been shown effective in enhancing future V2X communications [93]. For example, high mobility of VUEs lead to rapid environment change, and conventional methods such as the energy detection sensing technique, may be insufficient to provide accurate detection results, especially when the received signal-to-noise-plus-interference ratio (SINR) is relatively low, or when the VUEs are facing the SINR wall effect. On the other hand, machine learning algorithms for coping with the dynamic environment and resource allocation problems have been extensively investigated. Results have presented

the great potential feasibility for next generation vehicular networks [93]. Aforementioned reasons are the motivations of applying machine learning technology to the V2X networks, especially when classical methods are also feasible. In addition, the reason of proposing the combination of classical method (i.e., the FD simultaneous transmission and sensing) and machine learning method is they mutually help each other to address their respective challenges. In particular, although machine learning, especially the deep reinforcement learning, has been shown to be helpful in coping with the dynamic environment and resource allocation problems, especially when the unknown and fast-changing factors have been taken into consideration, such as the effect of the Doppler frequency shift on the PHY layer sensing accuracy, the question of 1) how to learn safely and its exploration problem which is 2) where the data comes from are still not addressed since they are raised in 2017 and 2018, respectively [94].

In this work, I exploit advantages of both FD technology and learning algorithms, and propose an adaptive FD deep reinforcement learning-based (DRL) design. Different from the standardised sensing-based semi-persistent scheduling (SB-SPS) protocol [83], I deploy FD technology for detecting collisions during broadcasting. In addition, I also deploy a deep Q network (DQN) to learn the unknown and fast-changing environment simultaneously. Afterwards, I design an adaptive scheme which operates in either FD mode or DRL mode to reserve resources for broadcasting. Besides, I also design a broadcasting abortion and collision resolution mechanism to address the acknowledgement and the re-scheduling challenges whilst avoiding the broadcast storm problem. Finally, I use the SB-SPS protocol as the benchmark mechanism to demonstrate the enhancement by deploying my proposed design.

6.2 System Model and SB-SPS Solution

6.2.1 System Model

We consider a fully decentralised VANET, in which FD technology is assumed to be equipped onto all VUEs, as shown in Fig. 6.1. Since the VANET is fully decentralised, there is no gNBs that allocate resources and schedule the broadcast for VUEs. I also assume VUEs can accomplish the following tasks. First, VUEs can autonomously sense the channel status in a FD manner through the most widely-applied energy detection method for its simplicity. VUEs can also reserve resource blocks (RBs), aborting concurrent transmission and re-scheduling re-broadcast according to my proposed design.

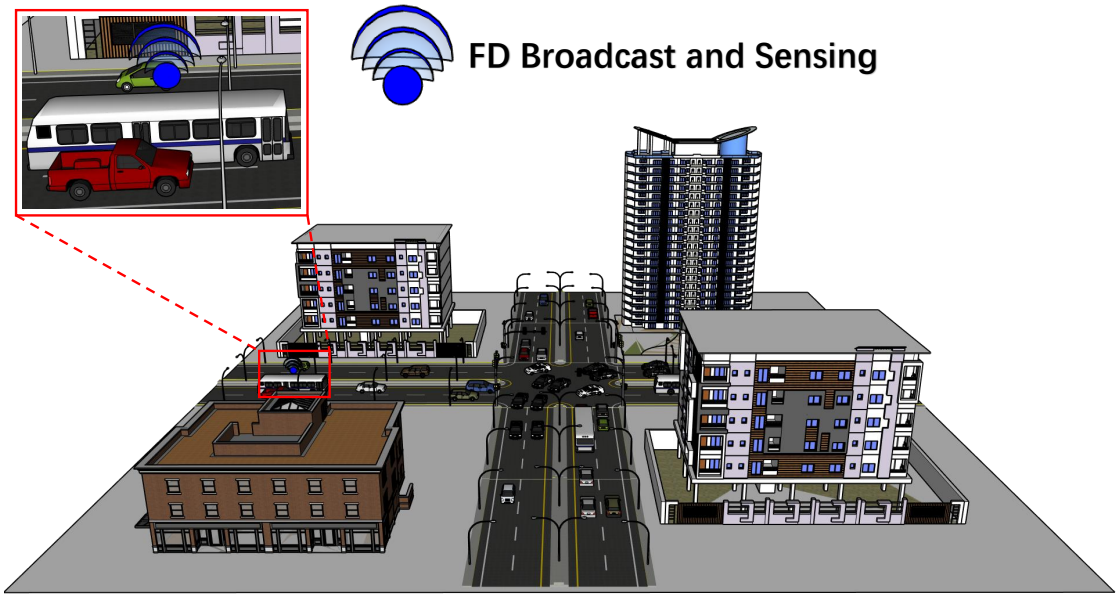

FIGURE 6.1: An illustrative structure of the VANET

In addition, FD sensing is assumed to be imperfect, sensing accuracy will be affected by the environment, such as distance, Doppler effect, interference and threshold setting strategy. I define **detection probability** as the probability that a VUE can successfully detect the occupancy of a RB or a collision. I define **false alarm probability** as the probability that a VUE claims the occupancy of a RB when the RB is not occupied, or the VUE declares a collision when there is no multiple VUEs using the same resource for broadcasting at the same time. I also define the **mis-detection probability** as the probability that a VUE claims

no occupancy of a RB when the RB is occupied, or the VUE declares successful broadcast when a collision has happened.

6.2.2 SB-SPS Protocol

SB-SPS protocol [73] consists of resource reservation phase and broadcast phase. Prior to the broadcast of a basic safety message (BSM), a VUE reserves new resources for a random number of consecutive BSMs. The random number is termed as re-selection counter (RC), whose value depends on the BSM broadcast frequency λ. After each broadcast, the RC decrements by one. When RC value decrements to zero, the VUE reserves a new resource with probability $(1 - P_{res})$, where $P_{res} \in [0, 0.8]$ [83], [73]. The resource reservation phase is executed in 3 steps:

Step 1: Assume a generic VUE, V_{tx}, has to reserve a new resource at sub-frame T_0. Then the time period for V_{tx} to reserve new resources is named as *selection window*, which starts from N_0 and finishes at $(N_0 + \frac{1}{\lambda})$. In addition, V_{tx} identifies and selects available resources according to the sensing results within the sensing window, which starts from $(N_0 - 1000)$ and finishes at N_0.

Step 2: V_{tx} creates a table T_1 which includes all available resources. Then resources that meet either of the following three conditions are excluded from T_1:

1. resources which are indicated to be used by other VUEs within the selection window or next broadcast episode of V_{tx}.
2. sub-frames N_i in the selection window, if V_{tx} used sub-frames N_j in the previous broadcast episode, where $j = i - 100 \cdot k$. For λ = 10 Hz, k is an integer number and its range is $k \in [1, 10]$.
3. resources which have the average reference signal received power (RSRP) higher than a given threshold.

Afterwards, if T_1 has at least 20% of the resources which are identified in the selection window after *Phase 1*, V_{tx} proceeds to the third step [83], [73]. Otherwise, V_{tx} re-executes *Step 2* with a 3 dB higher RSRP threshold.

Step 3: V_{tx} creates another table T_2 whose size is 20% of all identified available resources in *Step 1*. Then V_{tx} selects resources which have the lowest average received signal power indicator (RSSI) from T_1, and store these candidate resources

into T_2. Finally, V_{tx} randomly selects one resource from T_2 for the next transmission episode, and resets RC.

6.3 The Proposed AFD-DRL Design

In this section, I introduce my proposed adaptive FD DRL (AFD-DRL) design.

6.3.1 FD Mode

The FD mode includes the resource reservation phase and broadcast phase, as shown in Fig. 6.2. VUEs sense channel status in both phases in a FD manner. When a BSM is generated at a VUE, the VUE has to reserve resources for the broadcast episode within the selection window according to historical sensing results. The reservation phase is done in the following 3 steps:

Step 1: When a BSM arrives at sub-frame N_0, and the RC value is zero, the VUE initialises the resource reservation process to identify available resources by setting up the RC, sensing window and selection window. The range of the sensing window is between $(N_0 - 1000)$ and N_0, and the range of the selection window is between N_0 and $(N_0 + \frac{1}{\lambda})$.

Step 2: The VUE creates a table T_1 to tabulate all available resources. Then, resources which meet either of the following conditions are excluded from T_1:

1. resources which are indicated to be used by other VUEs within the selection window or next transmission episode of the VUE.
2. resources which were detected to be in collision with any previous transmission from the VUE.
3. resources which have the measured RSRP higher than a given threshold.

Next, if T_1 contains at least 20% of the resources which are identified in the selection window, the VUE proceeds to *Step 3*. Otherwise, the VUE re-executes *Step 2* with a 3 dB higher threshold.

Step 3: the VUE creates another table T_2 to store candidate resources. The size of T_2 is equal to 20% of all identified available resources in *Step 1*. Then it selects resources which have the lowest RSSI values from T_1. Finally, the VUE randomly selects one resource from T_2 for the next transmission episode, and set up the RC.

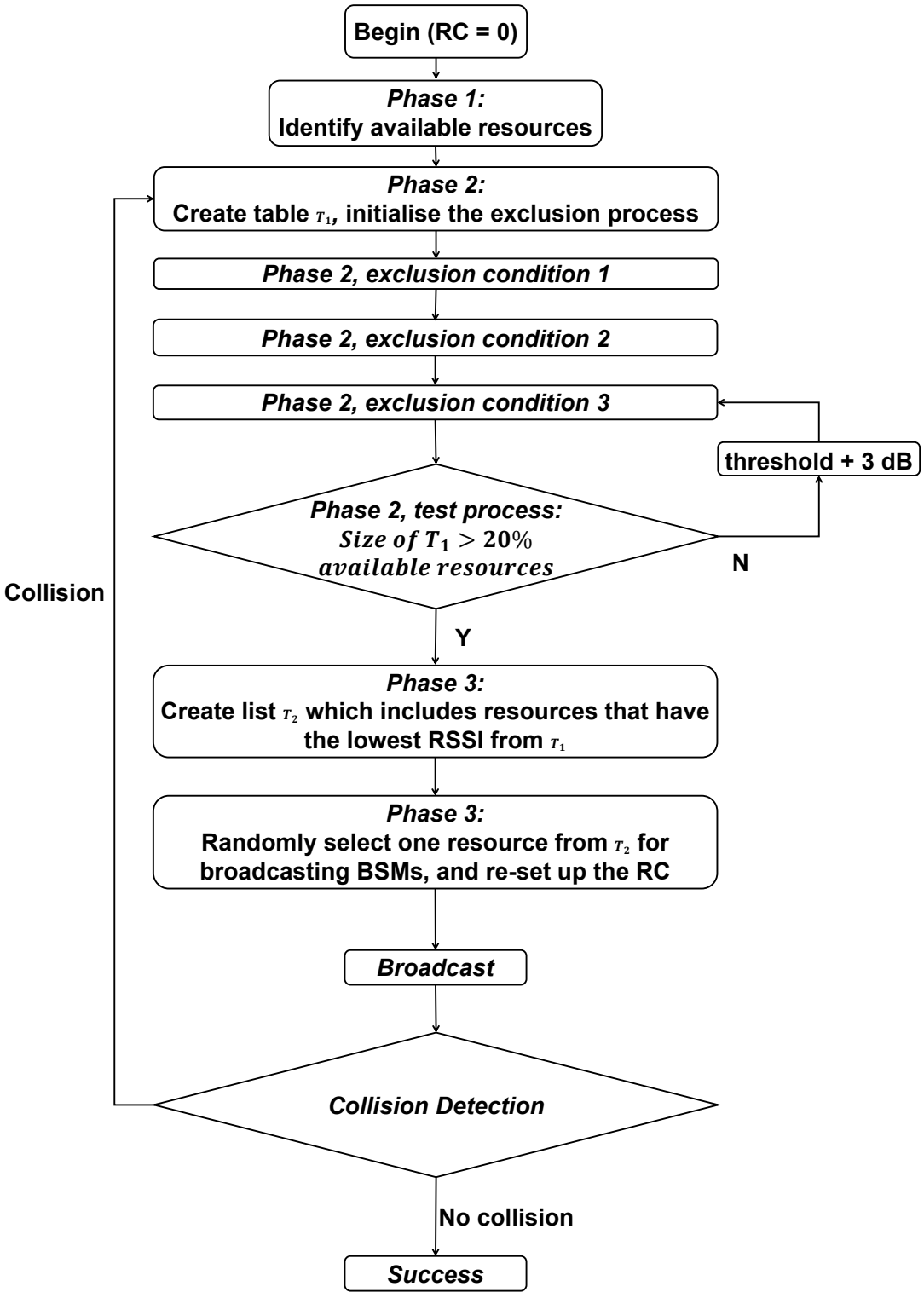

FIGURE 6.2: FD mode work flow

Once the VUE starts to broadcast, it senses for potential collisions simultaneously. If no collision is detected, the corresponding BSM is deemed to be broadcast successfully. Otherwise, the VUE responds to the collision as follows. Firstly, the VUE aborts the broadcast of its current episode of BSMs. Then, it goes back to the resource reservation phase with $P_{res} = 0$ to identify new sub-channels and sub-frames. Meanwhile, the detection results will also be passed to a machine learning framework for training, which is detailed in the next sub-section. Besides, if a new BSM is generated before the successful broadcast of the current BSM, the current BSM will be discarded, and the VUE will start to broadcast the new BSM.

6.3.2 DRL Mode

As shown in Fig. 6.3, the framework of the DRL mode consists of intelligent DQN agents and VANET environment. A deep Q network (DQN) is exploited, which receives sensing results, resource reservation and collision information as input data for training. Each VUE is regarded as an agent, which makes decisions autonomously based on local sensing and interaction results. Thus, the objective is to learn and provide better performance through avoiding collisions.

State Space: I denote the set of VUEs in the VANET by M = {1, 2, ..., M}, RBs that are to be allocated by K = {1, 2, ..., K}, and sub-frames by $\{0, 1, ..., t, ...\}$. Thus, the state observed by each VUE agent, s_t, at sub-frame t consists of three parts: sensing results at the VUE agent, $E_{t-1} = \{E_{1,t-1}, E_{2,t-1}, ..., I_{K,t-1}\}$, the allocated RBs in the previous sub-frame, $N_{t-1} = \{N_{1,t-1}, N_{2,t-1}, ..., N_{K,t-1}\}$, and the collision information during the broadcast of BSMs, C_i, where $C_i \in \{0, 1\}$. If $C_i = 0$, a collision is detected during the broadcast. Otherwise, the BSM is deemed to be broadcast successfully. Therefore, the state can be formulated as

$$s_t = \{E_{t-1}, N_{t-1}, C_i\}. \tag{6.1}$$

The state space, S, can be formulated as $S = \{s^i \mid i = 1, 2, ...\}$, where s^i refers to the potential state i.

Action Space: According to the observed state, s_t, from the state space, S, VUE agents take an action, a_t, from the action space, A, reserving resources based on the policy, π. The action can be expressed as $a_t = \{a, m\}$, in which $a \in K$, referring to resource reservation, and $m \in \{0, 1\}$, referring to mode selection.

If $m = 0$, the VUE agent switches to the FD mode. Otherwise, the VUE agent operates in the DRL mode.

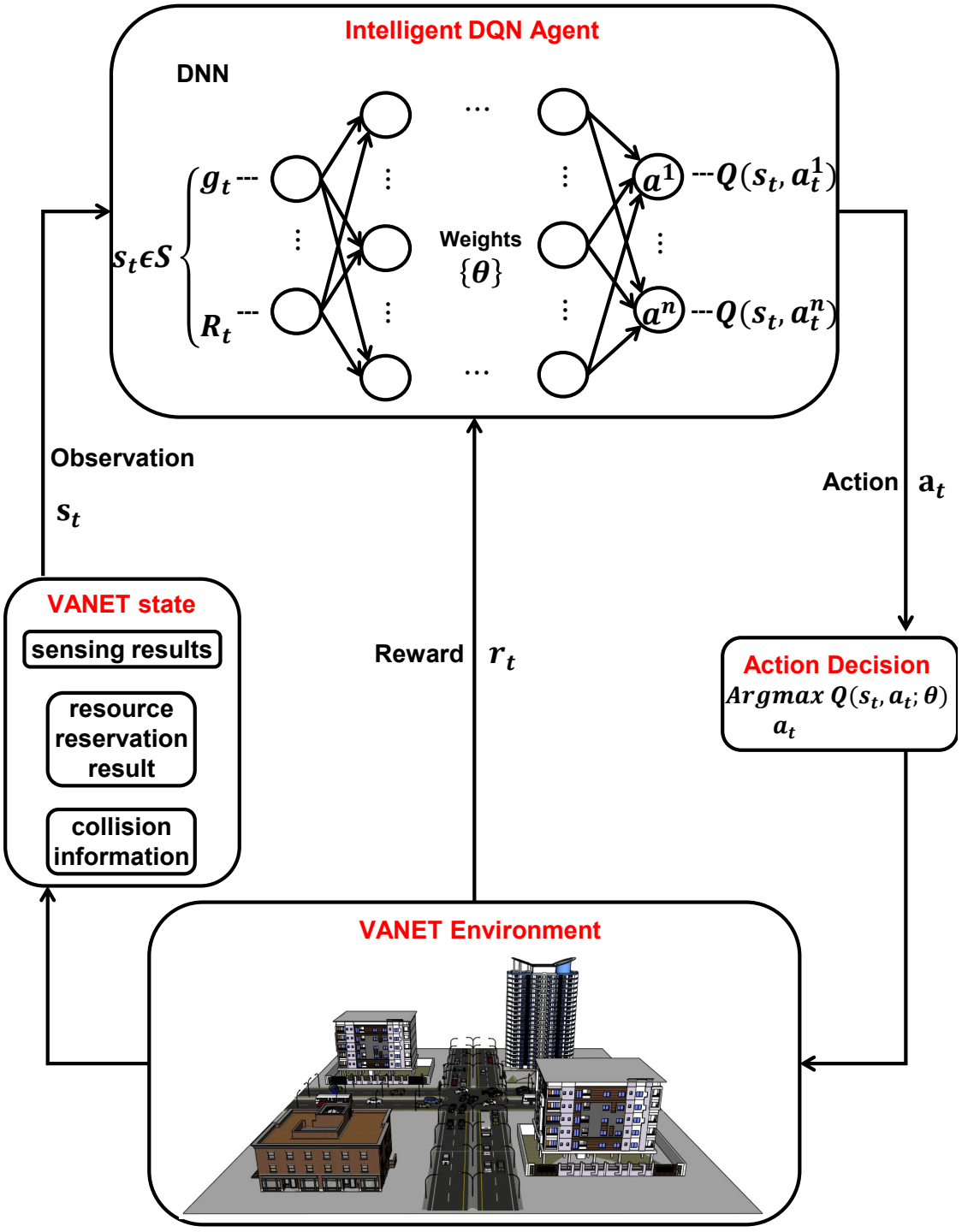

FIGURE 6.3: Framework of the DRL mode

Reward: As the objective of the DRL mode is to find the policy π that maximises

the discounted accumulative reward whilst satisfying the latency requirement through avoiding collisions, the reward function consists of the capacity of the reserved resource and the latency constraint time, which can be expressed as

$$r_t = \lambda_0 \sum_{m \in M} BW \cdot log(1 + \gamma_m) - \lambda_1 (T_{PGI} - T_{RT}), \tag{6.2}$$

where T_{PGI} represents the packet generation interval which is also the maximum latency constraint time, T_{RT} represents the remaining time of the current BSM broadcast to meet the maximum latency constraint time, λ_0 and λ_1 represent the weights of the capacity of the reserved resource and the latency constraint time, respectively, for balancing the revenue and penalty, BW represents the bandwidth of the reserved resource, and γ_m represents the measured SINR. The state transition and reward follow the Markov decision process (MDP) which only depend on the state of the VANET environment and the action taken by the VUE. Thus the expected discounted accumulative reward is defined as

$$G_t = \mathbb{E}[\sum_{j=0}^{\infty} \zeta^j \cdot r_{t+j}], \tag{6.3}$$

where ζ is the discount factor.

Q-learning is deployed to find the policy π. After the observation process, VUEs take action, a_t, based on the Q-value of the state-action pair, $Q(s_t, a_t; \theta)$. Given the Q-values, the updated policy can be obtained by taking the action that maximises the accumulated reward function, which is given by

$$a_t = argmax_{a \in A} Q(s_t, a; \theta). \tag{6.4}$$

After iterative update, it has been proven that the Q-values will ultimately converge to the optimal Q-values, which can be expressed as

$$Q_{new} = Q_{old} + \alpha[r_{t+1} + \zeta max_{s \in S} Q_{old} - Q_{old}]. \tag{6.5}$$

Instead of using a look-up table, I exploit a deep neural network (DNN) to estimate the Q-values with weight $\{\theta\}$. VUEs update the weight by minimising the

following loss function, $L(\theta)$, which is given by

$$L(\theta) = \sum_{(s_t, a_t)} (y - Q(s_t, a_t; \theta))^2, \tag{6.6}$$

where

$$y = r_t + max_{a \in A} Q_{old}. \tag{6.7}$$

Algorithm 1 Training Procedure for the DRL Mode

1: **procedure** TRAINING
2: **Require:**DQN structure, VANET environmental simulator
3: **Ensure:**DQN
4: **start:**
Randomly initialise the policy, π.
Initialise the design and VANET environment.
5: **loop:**
Each VUE reserves a resource for broadcasting based on local policy π.
Simulator returns states and rewards based on the actions taken by the VUE.
Each VUE stores corresponding s_t, s_{t+1}, r_t and a_t into its local memory.
Using the data as input to train the DQN.
Update policy π.
6: **end loop**
7: **return:** DQN
8: **end procedure**

The training procedure of the DRL mode is summarised in Algorithm 1, where the experience replay and ϵ greedy policy are exploited [95].

It should be noted that the ϵ greedy policy refers that each VUE first randomly select an action $a_t \in A$ with probability ϵ (a.k.a. exploring factor), then select the optimal action $a_t = argmax_a Q(s_t, a; \theta)$ with probability $1 - \epsilon$.

6.3.3 Adaptive Mode Selection

Although either the FD mode or the DRL mode can share BSMs in the VANET, each mode has its own limitations. Hence, the proposed design also exploit an adaptive mode selection scheme in order to maximise the advantages of both modes. Prior to the convergence time instant in the DRL mode, VUEs operate in

the FD mode, so that VUEs will not suffer from the instability of the DRL mode before convergence. Afterwards, when the DRL mode can provide a better reservation performance comparing to the traditional FD mode, VUEs operate in the DRL mode, so that VUEs can reserve resources more effectively, and in turn, the latency can be reduced through avoiding collisions. Furthermore, no matter which mode a VUE is operating in, the VUE benefits from the simultaneous collision detection during broadcast capability, and it can abort concurrent broadcast according to the proposed protocol, so that the continuous collision and the acknowledgement mechanism challenges are addressed without introducing neither redundant signalling nor acknowledgement mechanism whilst avoiding the broadcast storm problem.

6.4 Performance Evaluation

6.4.1 Simulation Environment

We developed a NR VANET simulator over the *Veins* framework [84] which integrates the wireless network simulator *OMNeT++* and the traffic simulator *SUMO*. As shown in Fig. 6.4, I chose Strand, London, U.K. as the simulation area, where traffic lights and multiple lanes are both considered, which are generated from *Open Street Map (OSM)* and converted into a *SUMO* network.

FIGURE 6.4: Overview of the simulated area of the VANET

VUEs are generated according to the Poisson Point Process (PPP) model, because the distribution of VUEs has been shown to follow this model [85]. Next, destinations are randomly chosen within the Strand area, VUEs move to corresponding destinations according to the received BSMs in *OMNeT++*. Meanwhile, the developed environment in *SUMO* is also synchronised into *OMNeT++*. In other words, the measured channel status by VUEs depend on their own locations and the surrounding environment. Finally, simulation results are tabulated in *OMNeT++*, and then imported into *MATLAB* to plot figures.

In the DRL mode, the DQN is a fully connected neural network consisting of an input layer, a hidden layer, and an output layer. The number of neurons

used in the hidden layer is 256. The ReLu function and adaptive moment estimation method (Adam) are utilised as the activation function and optimiser, respectively. Detailed parameters and values are listed in Table. 6.1, which are chosen based on 3GPP TR 36.885 [96]. In other words, the chosen parameters and scheme are realistic.

The reason why only the standard has been chosen as the benchmark is elaborated as follows. In [94] and Prof. Andrew Ng's interview with Prof. Geoffrey Hinton and Prof. Pieter Abbeel in 2018, one major challenge in DQN is how to learn safely, and the exploration problem of where the data comes from, in which self-driving systems were used as an example, which were one of the motivations of this work. To the best of my knowledge, this work was the first piece of work that investigates the performance of the combination of a dual-mode system that improves the learning safety whilst improving the performance in terms of the major KPIs in a VANET, in which the conventional FD mode does not only guarantee the safety of learning, but also feed the DQN with better quality data since the beginning. Therefore, I believe the best benchmark for the work is the standard, as if the proposed solution outperforms the standardised technology, this work has value in showing an example of improving the system performance whilst guarantying the safety of applying the DQN to a VANET.

TABLE 6.1: SIMULATION PARAMETERS

Parameters	**Values**
Carrier frequency	6 GHz
Interface	PC5
Learning rate	0.001
Target Detection Probability	90%
Modulation Scheme and Coding Scheme	MCS 9 (QPSK 0.7)
Antenna Height	1.5 m
Transmit Power	20 dBm
Residual Self-Interference	0%-40%
Vehicle Density	0-200 vehicles/km
Maximum Speed	30 miles/hour
Transmission Rate	6 Mbps
Packet Size	350 bytes/pkt
PHY layer	SC-FDMA
MAC protocol	SB-SPS, AFD-DRL
Channel bandwidth	10 MHz
BSM broadcast frequency	50 Hz (i.e. 20 msec/pkt)
maximum number of lanes	2 lanes/direction

6.4.2 Simulation Results

Fig. 6.5 depicts the latency with the increase of residual SI signal. When introducing FD technology into a design, the biggest drawback is the residual SI signal. So I have to find the SIS requirement. It is shown that the latency of the proposed AFD-DRL design increases whilst the residual SI increases, this is because residual SI has affected the detection accuracy, and in turn, has led to re-broadcast, which improves the latency to broadcast a BSM without collisions. However, SB-SPS is shown not to be affected by the SI signal, as it is using the HD technology. Furthermore, it is also shown that the proposed AFD-DRL design can provide a better latency performance compared to the SB-SPS protocol, if the SIS factor is smaller than approximately 16%, which is achievable [11]. Hence, in order to deploy the proposed method, SIS factor has to be contained below 16%.

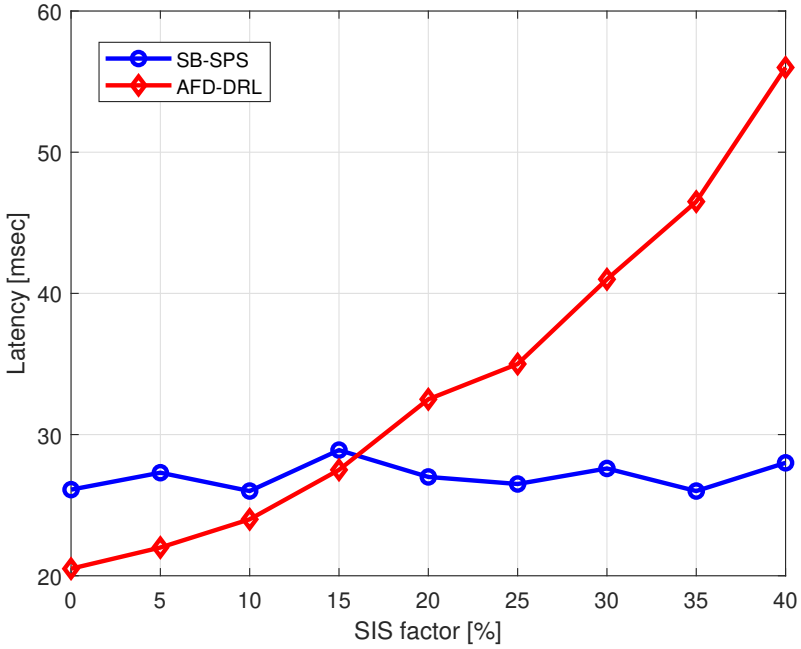

FIGURE 6.5: Latency against SIS factor η

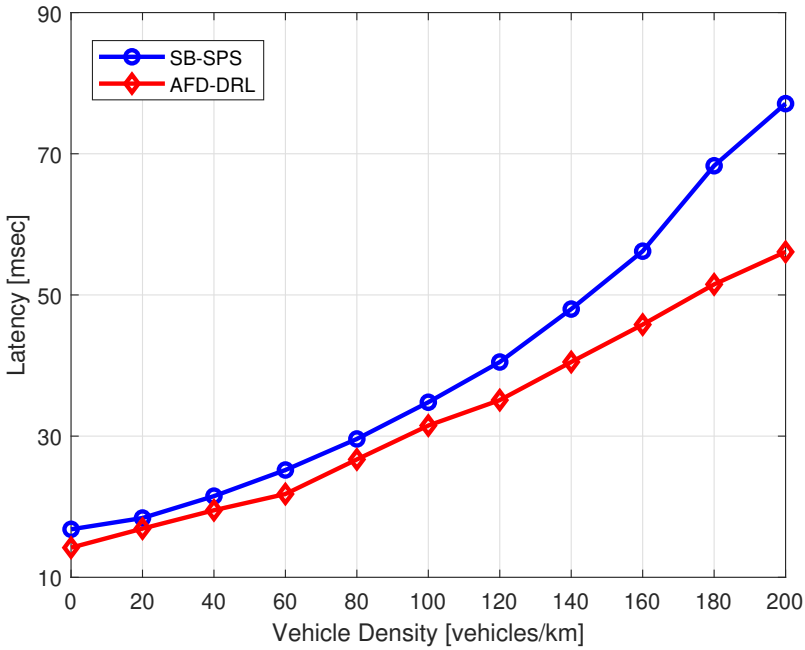

FIGURE 6.6: Latency against Vehicle Density

Fig. 6.6 shows the relationship between the latency and the vehicle density. It can be seen that both SB-SPS and AFD-DRL suffer from dense VANET. When the number of VUEs goes up, both designs will spend much more time to transmit BSMs successfully. However, AFD-DRL performs better in the dense scenario, because collision resolution mechanism is introduced, collided BSMs can be recognised and then re-broadcast. Meanwhile, there is no blind re-broadcast, the spectrum has been used more effectively, and the latency has been reduced through avoiding collisions.

Same conclusion can also be explained by packet delivery ratio (PDR). Fig. 6.7 shows the superiority of AFD-DRL. When the VANET becomes more dense, more collisions would happen, as there are more VUEs competing for the same number of available resources. SB-SPS does not have the collision resolution mechanism, when multiple VUEs have already selected the same resource for the next broadcast episode, all BSMs will be lost. However, the proposed AFD-DRL design has addressed this challenge, thus collided BSMs can be re-broadcast and the PDR is enhanced.

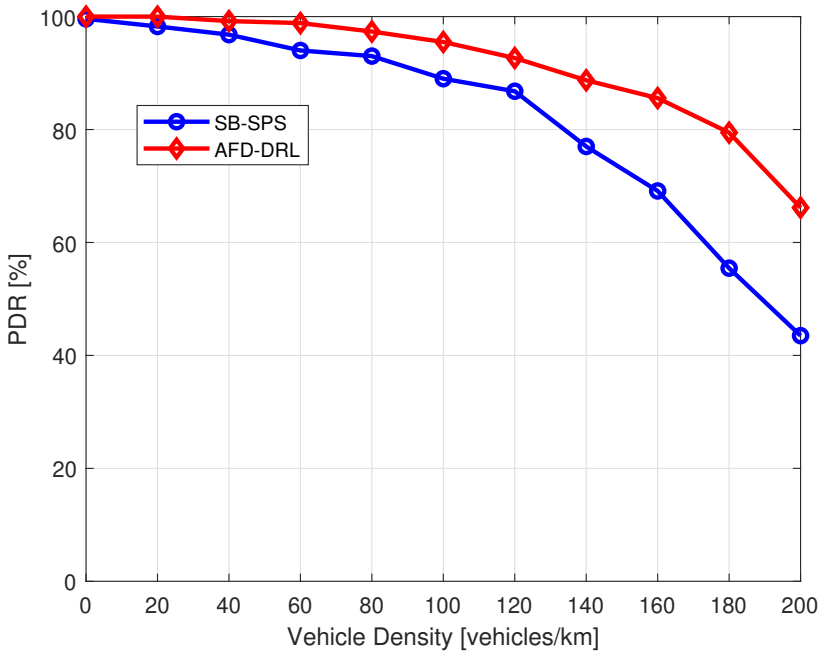

FIGURE 6.7: PDR against Vehicle Density

6.5 Summary

In this Chapter, an adaptive FD DRL-based design has been proposed for 5G VANETs. VUEs exploit advantages of both FD technology and DRL. Compared to the SB-SPS solution, AFD-DRL has addressed the continuous collision and the acknowledgement challenges, VUEs can abort broadcasting and re-select resources immediately. The broadcast storm problem has also been addressed, as there is no blind re-broadcast in FD-DRL. Results have verified the superiority of the proposed AFD-DRL design over the SB-SPS protocol.

7 Next-Generation FD Technology in V2X Communications

Synopsis of Chapter

In this Chapter, I present a diversity of benefits, existing challenges and corresponding example solutions of applying FD technology to next-generation wireless communication systems, including FD 6G vehicular networks, FD unmanned aerial vehicle networks with energy harvesting systems and machine learning aided FD communication systems. This work refers to my paper [97]. Simulation results have demonstrated the superiority of carefully designed FD solutions over the conventional/standardised solutions in each system.

The remainder of this chapter is organised as follows. In Section 7.1, I introduce the background, challenges and contributions of this work. In Section 7.2, I present how 6G-V2X communication architectures can be improved with the help of FD technology. I also introduce the challenges and potential methods of applying FD technology to 6G-V2X networks from physical- (PHY-) to transport- (TRANS-) layer perspectives. In Section 7.3, I present the challenges and corresponding example FD solutions in UAV with energy harvesting networks. Furthermore, in Section 7.4, I discuss the feasibility and potential methods of combining FD and machine learning technologies in various networks. Finally, I conclude this chapter in Section 7.5.

7.1 Introduction

With the worldwide deployment of 5G networks and extensive development of next-generation wireless networks, such as B5G and 6G networks, new technologies are not only required to further improve system performance in terms of key parameters, but they are also expected to provide novel features, such as the modifications on communication architecture, so that next-generation networks can not only provide more efficient communications, but can also support novel applications which are not applicable in existing networks. The in-band full-duplex (FD) technology, which supports simultaneous transmission and reception/sensing over the same frequency band, has emerged as such a promising technology. In this chapter, I present the benefits, existing challenges and corresponding example solutions of applying FD technology to various next-generation wireless networks, including FD 6G vehicular networks, unmanned aerial vehicle (UAV) networks with energy harvesting systems, and machine learning aided FD communication systems.

FD technology can be beneficial for 6G vehicle-to-everything (V2X) networks in many ways, including the enhancements in communication architectures and various advanced driving scenarios. Since the first cellular V2X (C-V2X) specification, 3GPP Rel-14 [2], which operates based on the 4G technologies, numerous research efforts have improved the C-V2X technologies to a brand-new level, 5G NR-V2X [3], which has been shown to be able to support basic V2X applications. Motivated by increasingly stringent quality of service (QoS) requirements, the FD technology has always been a hot technology under discussion in Rel-16 [4] and Rel-17 [5]. With the objective of investigating the potential and feasibility of the FD technology in 6G V2X networks, which has great potential to be incorporated in Rel-18 and future releases, I first present how FD technology can change the communication frameworks in 6G-V2X networks. Then, I provide an insight into novel designs from physical- (PHY) to transport- (TRANS) layer perspectives for supporting advanced driving scenarios.

Unmanned aerial vehicle (UAV) is an emerging technology for future wireless communication systems. Due to the flexible deployment, UAV-enabled wireless communications can provide higher wireless connectivity in areas without infrastructure coverage [98], [99]. Besides, high throughput can always be achieved

in UAV-enabled wireless communications due to the higher probability of line-of-sight (LoS) communication links between devices and UAVs. To fully exploit the design degrees of freedom for UAV-enabled communications, it is crucial to investigate the energy consumption for both flying and wireless communication. Recently, energy harvesting has been an active research area in the circuits and devices side of engineering for a considerable period of time. That side of engineering aims to design and build devices that harvest energy from natural sources and/or transfer energy from one device to another most efficiently. In FD, energy harvesting can be used in the downlink since the devices are always energy-constrained. Combining FD technology with energy harvesting and UAV, the devices can transmit data to the UAV in the uplink, whilst the UAV can also simultaneously broadcast energy to the devices [100].

Apart from the aforementioned networks, machine learning and FD technologies can also mutually aid each other in various scenarios. At the end of the 20^{th} century, machine learning techniques started to flourish in a variety of fields such as industry, education, mathematics and finances, etc. Machine learning has been known as a set of strong methods that are able to automatically solve difficult problems where conventional methods fail to show good performance (e.g., data security, financial trading, and healthcare, etc.). Besides these popular application fields, the application of machine learning into various communication technologies, especially the next-generation wireless communication networks (e.g., cloud radio access networks, and energy harvesting, etc.), has been studied. As one of the most promising enabling technologies in next-generation networks, no doubt that FD machine learning technologies should be considered.

7.2 FD 6G-V2X Networks

7.2.1 Communication Architectures

Based on the latest frozen standard of the communication architectures [101], vehicular information can be shared among vehicular UEs (VUEs), infrastructures and pedestrian UEs in the following three manners, which are depicted in Fig. 7.1.

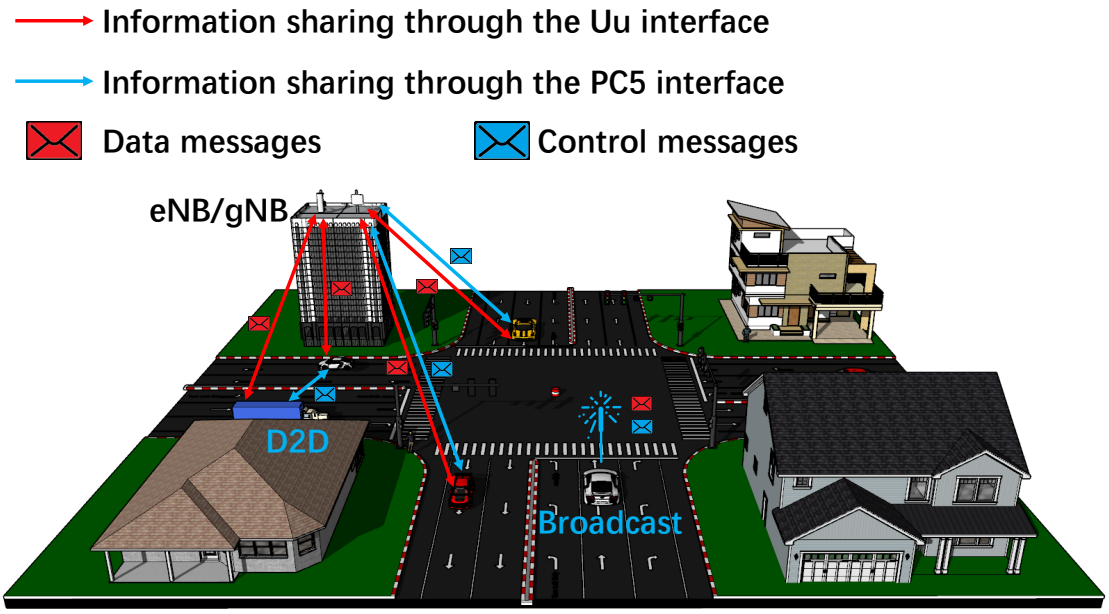

FIGURE 7.1: Communication Architectures of NR-V2X Networks

As can be seen from Fig. 7.1, the first type of information sharing manner is sending and receiving both control and data messages through the Uu interface. This mode is used when VUEs are operating within the coverage area of an eNB or a gNB, and the connection between them is stable. However, because the safety of UEs cannot fully rely on the eNB/gNB coverage, an autonomous broadcast mode has also been designed to support the communication through the PC5 interface when VUEs are operating beyond the eNB/gNB coverage area, or when the connection quality is not sufficient to support the requested V2X service [45]. Besides, a device-to-device (D2D) manner can also be used depending on different V2X applications. In this case, VUEs are controlled by the eNB/gNB through the Uu interface, where data is shared directly between VUEs through the PC5 interface.

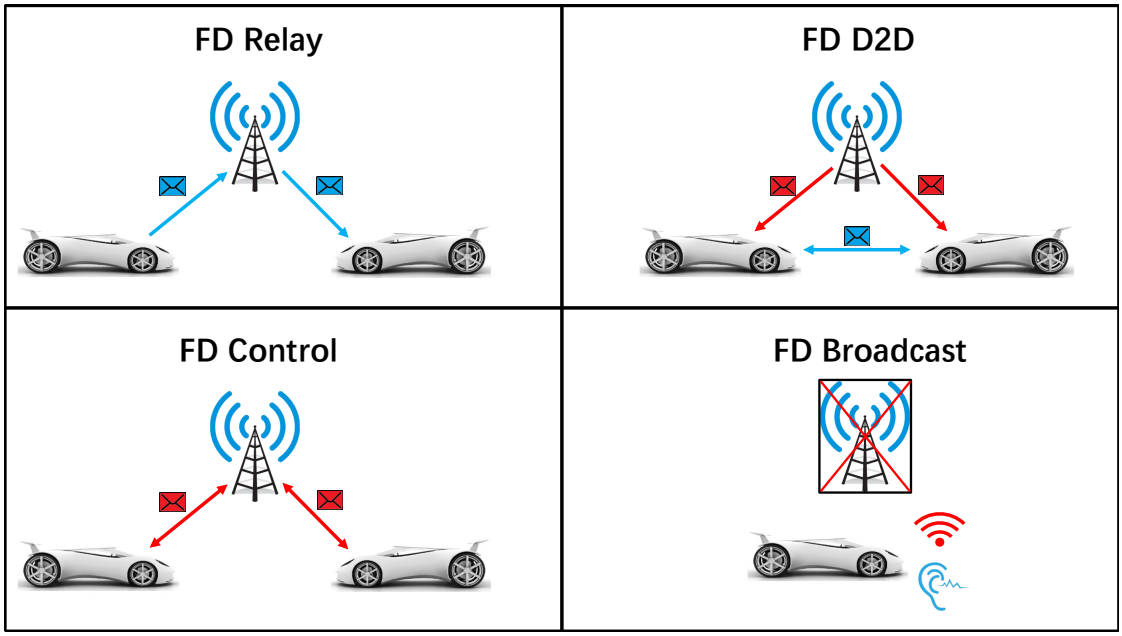

FIGURE 7.2: Communication Architectures of FD 6G-V2X Networks

With the help of FD technology, the introduced communication architectures of NR-V2X networks can be modified in 6G-V2X networks, so that the 6G-V2X system can meet much more stringent QoS requirements, and in turn serve advanced V2X applications. As shown in Fig. 7.2, FD technology can be deployed in four scenarios. First, eNBs/gNBs can be equipped with FD technology and operate as a relay station, where it receives and forwards packets simultaneously, so that the total number of required sub-frames for transmitting the same amount of data will be theoretically halved. In other words, latency will be theoretically halved to transmit the same amount of data. Besides, the theoretical spectral efficiency will be doubled. Second, FD technology can also be beneficial in the D2D communication scenario, in which FD VUEs can now transmit and receive data at the same time. This feature is especially helpful in real-time raw/semi-processed data sharing, which is not supported in 4G/5G-V2X systems. Third, FD technology can be applied to resource control too, so that time-frequency resources are used more efficiently, and in turn dynamic resource allocation and dynamic scheduling solutions can be considered in 6G-V2X networks. In addition to taking advantage of the FD simultaneous transmission and reception feature, FD simultaneous transmission and sensing feature can also be beneficial in the broadcasting scenario. In 4G/5G-V2X networks, VUEs suffer from collisions, because they are not able to detect collision. By deploying FD sensing

technology in 6G-V2X networks, although VUEs still autonomously select resources to broadcast, they can realise collisions and respond to failed broadcast immediately. Last but not least, these four novel FD communication manners do not have compatibility problem, a proper designed system can incorporate all of them at the same time, so that the overall network performance can be boosted significantly.

7.2.2 Challenges & Novel Designs

7.2.2.1 PHY Layer

Whilst embracing the FD simultaneous transmission and reception, and FD simultaneous broadcasting and sensing features in the PHY layer of 6G-V2X networks, I must consider various emerging types of cross-link interference, especially given that vehicular communication has particularly high VUE mobility. These types of interference include base station (BS) to BS, BS to VUE, and VUE to VUE interference. Therefore, knowledge about the self-interference (SI) signal and the propagation channel is the key to design a feasible 6G-V2X solution. As a matter of fact, a BS usually deploys a multiple antenna system for beamforming and radiates high equivalent isotropically radiated power, which leads to large interference to other BSs [102]. Therefore, when VUEs request FD relay or FD D2D types of support, the co-channel interference and SI have to be handled adequately, and the communication architecture has to be designed carefully. In addition, when VUEs operate in broadcast or multi-cast mode, where FD simultaneous transmission and sensing feature is used, different FD spectrum sensing technology has to be investigated, such as FD energy detection and FD cyclostationary feature detection, depending on the considered scenario.

7.2.2.2 MAC Layer

Based on each novel FD V2X scenario, corresponding MAC layer solutions have to be re-designed. Considering a vehicular ad hoc network (VANET) scenario, in which the FD technology is deployed on-board to provide simultaneous broadcast, multicast and collision detection capability in the PHY layer, both of the resource reservation mechanism and the scheduling mechanism can be enhanced. For example, research effort can be invested on the study of dynamic resource reservation mechanisms. Besides, novel designs on excluding collided resources are also needed. Furthermore, with the collision detection capability, various

re-transmission mechanisms have to be evaluated. In addition, current 4G/5G-V2X standards only address internal collisions. But, external collisions can be resolved with the help of FD technology in 6G-V2X networks. For other types of scenarios, novel methods can be considered with the deployment of FD simultaneous transmission and reception feature. For example, considering a vehicle platooning scenario, in which a platoon leader shares real-time information to the member VUEs by using the groupcast communication mode, whilst it receives control messages from a base station simultaneously. This solution can dramatically improve transportation safety, but FD technology and novel FD MAC designs are required.

7.2.2.3 NET Layer

In addition to safety-related communication demand, 6G-V2X should also be able to satisfy infotainment-related communication requirements, which does not only need support from the access network, but also the core network. In particular, the remote driving scenario and the extended sensors data sharing scenario are much more likely to be supported by the service providers in reality. Furthermore, the QoS requirements from vehicular gaming, content sharing that requires huge bandwidth support, and latency-sensitive on-board applications cannot be satisfied only by the access network, but they require much more efficient network (NET) layer support. For example, FD simultaneous transmission and reception has provided a solid background in the PHY layer, but the above services cannot be supported without FD routing protocols. Meanwhile, novel designs should also take the network topology into consideration, because one of the characteristics of 6G-V2X communication is its highly dynamic network topology. Therefore, novel methods such as dynamic FD routing protocols are expected to be proposed.

7.2.2.4 TRANS Layer

In order to benefit from all existing infrastructure as much as possible, 6G-V2X technologies should have great backward compatibility. In other words, the network can use the 4G and 5G resources according to the requested services and novel FD backward compatible designs. For example, a possible TRANS layer design which can be built upon as foundation is the multi-path transmission control protocol (MPTCP). However, since TCP-based protocols are designed to provide reliable transmissions, its latency needs to be shortened for low latency

applications. FD simultaneous transmission and reception can be applied to the connection establishment process, so that novel FD-based TRANS layer protocol has a lower latency. Furthermore, the acknowledgement mechanism in MPTCP is deployed to confirm the successful reception of a packet, or trigger the initialisation of the re-transmission mechanism, this confirmation and trigger can be replaced by proactive detection, so that the confirmation path is shorter, and in turn the latency is reduced. This proactive detection is one of the advantages of the FD simultaneous transmission and sensing feature. However, in order to acknowledge a packet at the transmitting VUE side, advanced and novel FD designs are needed in TRANS layer.

7.3 FD UAV Networks with Energy Harvesting

Energy harvesting has been an active research area in the circuits and devices side of engineering for a considerable period of time. That side of engineering aims to design and build devices that harvest energy from natural sources and/or transfer energy from one device to another most efficiently. The combination of FD and energy harvesting technologies enable the transmitter to broadcast energy to the receiver, whilst the receiver can also simultaneously transmit data to the transmitter. Recently, it has been recognised in the communications, networking and signal processing communities that use of FD with energy harvesting in wireless networks brings in new opportunities and challenges to the communication problem and alters the assumptions under which communication mechanisms have been traditionally designed.

Compared with conventional FD technologies, there are three important application scenarios for FD technology with energy harvesting: 1) Traditional FD theory operates under an average power constraint which assumes the availability of energy for data transmission at all times in arbitrarily large amounts only subject to a long-term average power constraint. Under energy harvesting conditions, the energy available for communication becomes a random and intermittently available quantity. Although an unlimited amount of energy will be collected in an infinite period of time, at any given time, only the energy collected so far can be used. In addition, the size and other characteristics of energy storage devices (e.g. batteries) that can save energy for future use further affect the type of communication. These requirements redesign FD communications and network protocols by considering the energy availability conditions imposed by

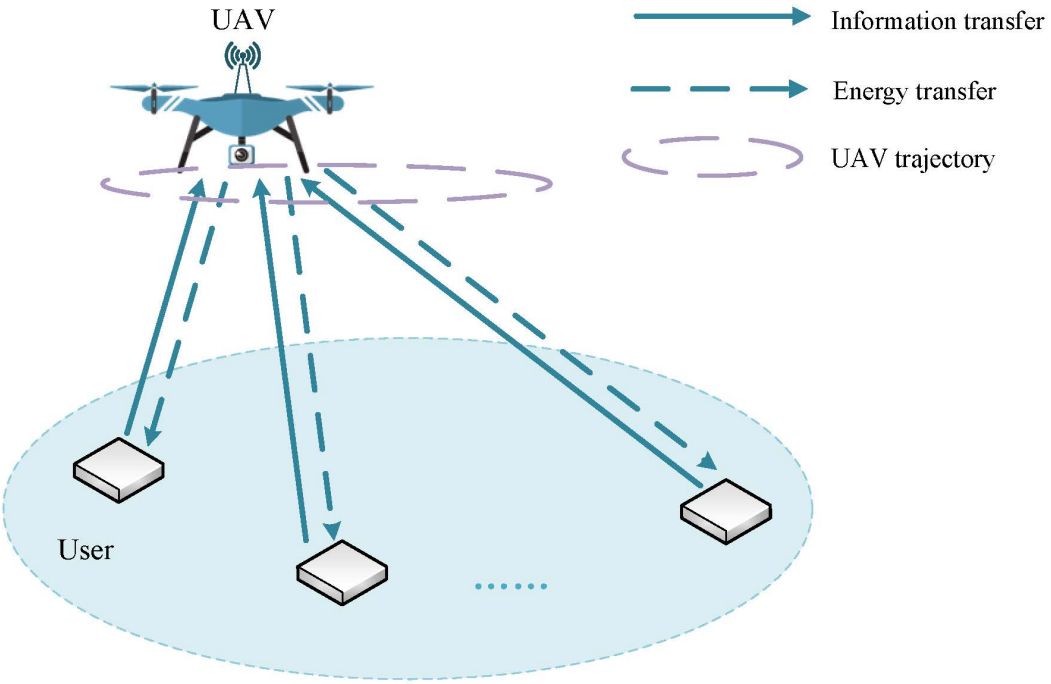

FIGURE 7.3: FD Energy Harvesting System

energy harvesting. 2) FD relay, which operates at the signal level, where wireless nodes utilise the overheard signals to forward each other's messages to improve the overall network performance at FD mode. The ability to transfer energy wirelessly at small distances enables a deeper level of FD relay, where nearby nodes can cooperate not only at the signal level but also at the battery energy level by transferring energy among each other. 3) Transmission of information and distribution of energy have been considered as two distinct and separate problems in FD networks. Since information and energy may be transmitted simultaneously by a single signal from a transmitter, and both information and energy may be extracted from an incoming signal at a receiver, as shown in Fig. 7.3.

Due to the distinctions of simultaneous information and power transfer, FD with energy harvesting can be utilised in UAV communications. In UAV communication networks, due to the mobility of the UAV, it is energy efficient for the UAV to dynamically broadcast data to the wireless devices, whilst the wireless devices use the harvested energy to transmit data to the UAV in a FD manner. Since UAV's flying and data transmitting consume power, it is of importance to consider the joint trajectory and wireless resource allocation. The wireless devices can harvest enough energy from the transmitter only at a short distance. Thus,

the UAV can sequentially fly to a location near to each device for broadcasting energy and receiving data simultaneously.

7.4 FD Machine Learning Solutions

In this section, despite machine learning (ML) technologies can be applied to fields such as financial trading, I focus on discussing the feasibility and potential of combining FD and ML technologies in various wireless communication networks.

ML algorithms are typically categorised into supervised, unsupervised and reinforcement learning. Supervised learning is the task of learning a function that maps an input to an output based on example input-output pairs, whilst unsupervised learning looks for previously undetected patterns in a data set with no pre-existing labels and with a minimum human supervision. Besides, the goal of reinforcement learning is to find the optimal state and action pair that maximises the notion of cumulative reward. Different from supervised learning, reinforcement learning requires no labelled input and output pairs for training. Reinforcement learning works well in the cases that the environment can typically be stated in the form of a Markov decision process (MDP), because many reinforcement learning algorithms for this context utilise dynamic programming techniques.

7.4.1 FD Unsupervised ML

The most common task for unsupervised learning is the clustering, which is the task of grouping a set of objects in a way that objects in the same cluster are more similar to each other than to those in other clusters measured by a defined criterion. Q K-mean algorithm-based clustering method can be proposed to reduce the co-channel interference in an FD cellular network, where the BS is assumed to have the FD capability [103]. Due to the simultaneous uplink and downlink transmission in the FD cellular network, the co-channel interference becomes the many sources of interference that degrade the system performance. Clustering algorithms such as K-means clustering can be used to cluster cellular users into two groups (i.e., one for uplink and one for downlink) that minimise the co-channel interference caused by uplink and downlink transmissions. Simulation

results show that the co-channel interference in the FD cellular network can be retrained effectively by using the proposed algorithm.

In addition, FD sensing methods can also be used to provide data for determining follow-up steps in 6G-V2X networks. Therefore, its sensing accuracy is of great importance in terms of driving safety. Considering the energy detection and power management problem as an example, clustering can be used to enhance the FD energy detection accuracy by using the unprocessed sensing data as the input training data. Then, with adequate and novel algorithms, it can improve the detection probability, and reduce the false alarm and mis-detection probabilities, because conventional FD energy detection is a type of clustering problem, where successful and failed transmissions are determined according to the received signal and the threshold setting strategy. However, the feasibility should be investigated because of the following reasons. First, the complexity of the model will increase significantly with the rise of feature dimensions. Second, FD sensing data incorporates various types of interference such as the SI. So, the learning process will be affected more seriously compared with conventional mobile networks. Third, the features should be considered carefully according to the deployed FD sensing method, because applying ML to most areas require dimension reduction, and some sensing technologies require perfect knowledge about the signal and the channel response, such as the matched filter method, which is more likely to be sensitive to interference.

7.4.2 FD Supervised ML

Two typical tasks for supervised learning are regression and classification. In a regression task, the ML algorithm aims at learning a function that can be used to predict continuous real-value. In a FD system, the most common regression task is for SI suppression (SIS). Different from regression, the classification task requires the algorithm to predict the category or label based on the input features. One application case for classification is to predict the transmission mode in an FD cognitive radio network (CRN), which is proposed in my recent work [104]. The FD operation introduces two new transmission modes in CRNs, namely FD transmission-and-reception (TR) mode and FD transmission-and-sensing (TS) mode, respectively. In FD-TR mode, the secondary user (SU) first senses the primary channel and then transmit and receive data at the same time, whilst it simultaneously transmits and senses the channel in FD-TS mode.

FD-TR mode increase SU's throughput doubling the spectral efficiency but also worsens its collision to the primary user (PU), whilst FD-TS mode reduces the collision between SU and PU at the cost of lower throughput than using FD-TR mode. Therefore, a trade-off between these two modes should be leveraged in FD-CRNs. I propose an NN-based adaptive mode selection (NN-AMS) scheme in [104] to select the better transmission mode based on the channel occupancy status. The DNN model takes the previous channel states as input and then predict the future channel occupancy status. If the channel is predicted to be idle, FD-TR mode is chosen to fully utilise the idle channel; Otherwise, FD-TS mode is a better choice to monitor the channel in case that PU comes back suddenly. Simulation results in Fig. 7.4 have justified that the proposed method can achieve almost the same SU throughput as FD-TR mode. Meanwhile, the results illustrated in Fig. 7.5 demonstrate that the collision probability can be reduced by up to 92% close to that of FD-TS mode.

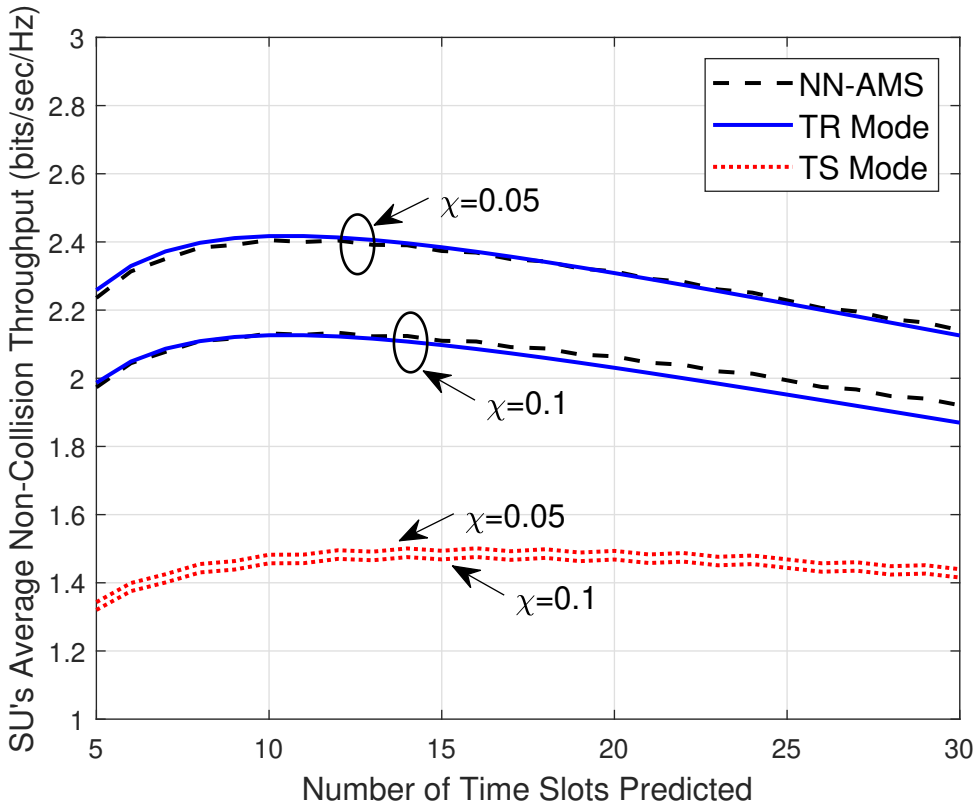

FIGURE 7.4: SU's non-collision average throughput versus the number of time slots M, where χ refers to the SIS coefficient.

Besides the SI and co-channel interference introduced by FD communications,

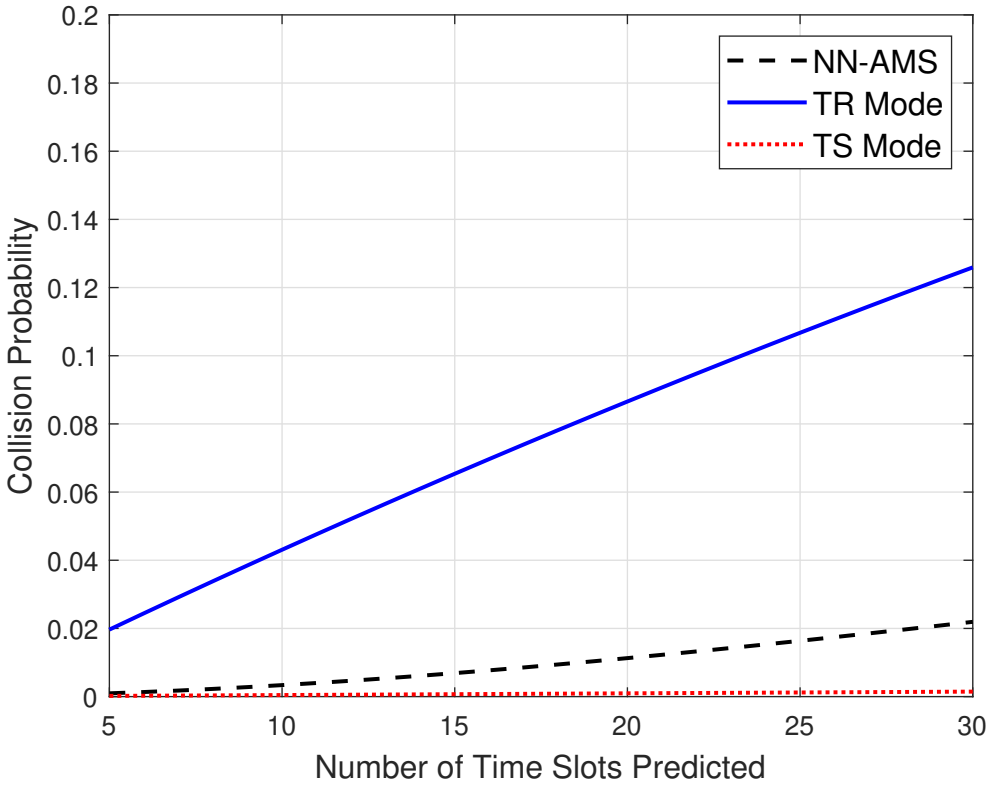

FIGURE 7.5: Collision probability versus the number of time slots M.

the real-world CRNs also suffer from malicious attacks such as Primary User Emulation (PUE) and Spectrum Sensing Data Falsification (SSDF) attacks. In [105], I propose an ensemble learning framework to alleviate the influence of both interference and attack on sensing decision fusion. In such a context, the spectrum waste probability, collision probability and secondary throughput in both FD Listen-Before-Talk (LBT) and Listen-And-Talk (LAT) protocols are analysed. Simulation results show that my proposed EML framework can provide more robust and lower false-alarm probability than the conventional majority vote based fusion strategy for any number of SSDF SUs, only at the cost of slightly higher inference time.

7.4.3 FD Reinforcement Learning

Reinforcement learning (RL) algorithms have become more and more popular in coping with problems with unknown and highly dynamic radio environments,

such as the scenarios in V2X networks. Different from supervised and unsupervised learning, RL takes a further step to not only learn, but also interact with the environment. RL is data-hungry, it also requires time and trials to interact with the environment, in order to maximise the reward. In other words, if a RL solution is applied to V2X networks, it uses the safety of VUEs and human passengers for training. Therefore, the system is not reliable until the long-term objective is achieved, which prevents us from applying RL solutions to safety-related tasks in V2X networks. However, a promising way of applying RL to safety-related applications is to combine with a FD solution, because a FD solution will increase the quality of the training data, and it also provides a backup system for VUEs. Hence, an adaptive mode selection scheme can be designed, and the drawbacks of RL can be avoided. Meanwhile, early-stage actions and rewards from the FD solution are used to feed the algorithm to train, which are also real-time and reliable data. On the contrary, the RL solution provides real-time actions too, which can be designed to have a certain weight in the FD mode. Such an idea has been investigated in [106], where a FD mode and a deep reinforcement mode have been proposed to work cooperatively and adaptively. Results in Fig. 7.6 have shown that the reliability of the proposed adaptive FD deep RL (AFD-DRL) design has been improved compared to the standardised sensing-based semi-persistent scheduling (SB-SPS) method, whilst the latency has been reduced at the same time, as shown in Fig. 7.7.

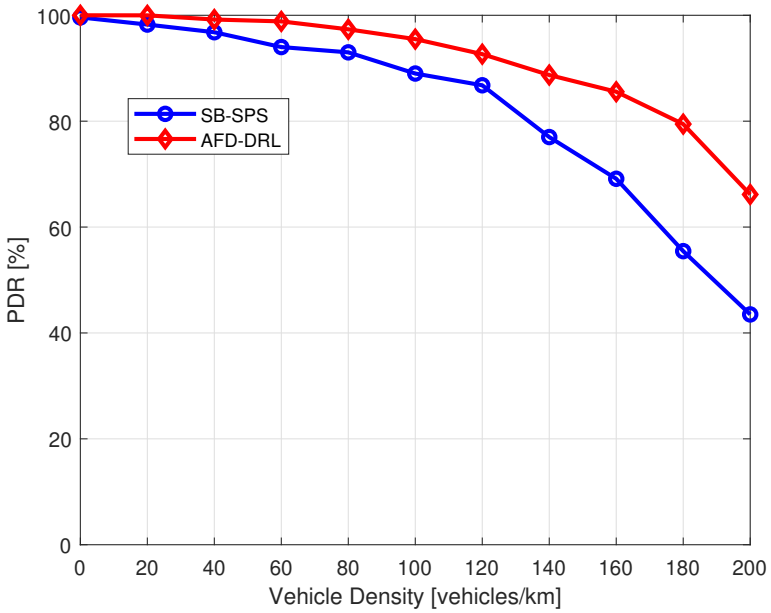

FIGURE 7.6: Packet delivery ratio versus vehicle density.

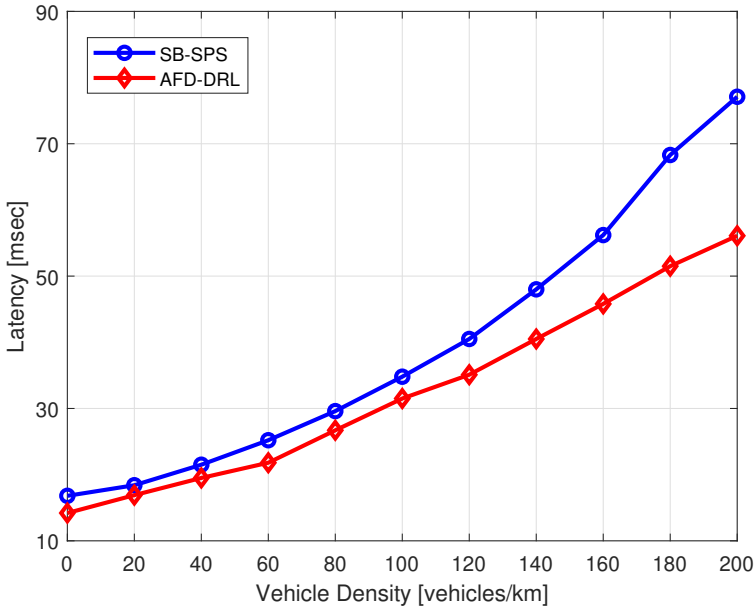

FIGURE 7.7: Latency versus vehicle density.

7.4.4 FD Federated Learning

Federated learning (FL) is usually characterised by its capability of training a global model with privacy protections [107]. Meanwhile, FD and FL technologies can also mutually help each other to provide a better service in terms of efficiency and latency for next-generation wireless networks. Considering an extended sensors data sharing scenario in the research of high-level autonomous driving support, where multiple VUEs cooperatively train a surrounding environment model for safety enhancement purpose. In this case, spectral efficiency and latency requirements are equally important as the privacy demand. Therefore, the throughput and latency performance can be enhanced by using the FD simultaneous transmission and reception feature in FD D2D and FD broadcast/multicast/groupcast architecture, whilst the FD simultaneous transmission and sensing feature can be used to prevent malicious attackers, which enhances the privacy protection together with the FL method. Therefore, novel FD FL technologies are needed to be proposed and analysed for next-generation wireless networks.

7.5 Conclusion

This chapter has reviewed and discussed various applications, research challenges and potential solutions of FD technology in multiple next-generation wireless communication systems. The corresponding solutions are introduced and illustrated by dedicated simulation results, which together with the potential solutions are the key findings and contributions of this work. For example, an FD energy harvesting system has been introduced and various application scenarios have been discussed. For FD MIMO systems, both pure FD/HD MIMO and hybrid FD and HD MIMO systems have been discussed. In 6G-V2X networks, I have studied how FD technologies can be beneficial in designing novel communication architectures as well as PHY- to TRANS- layer challenges and solutions. Furthermore, I have also discussed a diversity of machine learning applications in FD communications in different wireless systems. Simulation results have shown that machine learning techniques and FD technologies can mutually aid each other to further improve the system performance. In a nutshell, FD communications for next-generation wireless systems is an exciting area to be further exploited.

8 Conclusions and Future Work

8.1 Conclusions

FD communications and V2X communications are two promising technologies in developing future ITS. They can reduce accidents, improve efficiency, support a lot of diverse and novel applications, provide more enjoyable transportation experience, and even change the way people travel, and interact with other people and the digital world. FD communications may replace all conventional HD communications in all wireless communication scenarios, especially in the scenario of ITS development. Meanwhile, V2X communications may quickly become a core safety and infotainment system in vehicles due to the advantages, achievements, and the support from many national governments, which are introduced in Chapters 1 - 7.

In Chapter 2, I firstly reviewed the literature of the major modulation, multiple access technologies, and channels. Analytical BER/SER performance of various combinations are provided. In addition, I also regenerated the BER/SER performance through extensive simulations. Results mutually verified the correctness and accuracy of the study. Next, a literature review of the spectrum sensing technologies, FD technologies, and V2X technologies was given, which were the foundations and benchmarks used in Chapters 3 - 7.

In Chapter 3, I considered a VANET in which all vehicles are equipped with FD capability. I applied the FD simultaneous broadcasting and sensing feature to the PHY layer sensing procedure. Mathematical formulations of detection probability, false alarm probability, mis-detection probability, and the two dynamic thresholds are given. The conventional HD spectrum sensing method is used as the benchmark for comparison. Results showed that the proposed FD sensing method does not require further development on the current SIS/SIC technology. They also showed that the proposed method outperforms the benchmark.

In Chapter 4, I proposed a cross-layer design across PHY and MAC layers based on the achievements from Chapter 3. Specifically, in the PHY layer, the Doppler effect is incorporated in the design of the FD sensing method, which implies that the sensing results are also reliable in high mobility scenarios. Besides, in the MAC layer, a complete prioritised FD MAC protocol was designed based on the DSRC standard. It incorporates a resource selection mechanism, a scheduling mechanism, and a prioritised re-transmission mechanism. The performance of this design was evaluated through both mathematical formulations and extensive computer simulations. Results showed that both reliability and latency were improved comparing to the benchmark which is the technology in the DSRC standard.

In Chapter 5, I focused on the other V2X standard, C-V2X standard, and proposed a 5G-based cross-layer design. It includes the PHY layer FD sensing mechanism, and a MAC layer protocol. In particular, this protocol is also a complete protocol. It includes a resource reservation mechanism, a scheduling mechanism, and a prioritised re-transmission mechanism. The performance of this design was analytically evaluated and through extensive simulations in terms of packet delivery rate, collision duration, and latency. Besides, its convergence, complexity, mathematical difference, and assumption and approximation were all analysed. Results showed that the proposed design is a promising FD solution for B5G/6G-V2X communication VANETs.

In Chapter 6, I proposed an adaptive FD DRL-based design. FD technology and a DRL algorithm were exploited jointly and adaptively to enhance the performance of the considered VANET scenario. A resource reservation scheme, a collision resolution mechanism, and a scheduling policy were introduced and design. The 5G-V2X PHY and MAC layer technical specifications were used as the benchmark. Results demonstrated that the proposed method performs better in terms of reliability and latency. Therefore, it can be considered as a solution in future standard.

Last but not least, in Chapter 7, I produced a survey of state-of-the-art and next-generation FD technology in V2X communications. It includes how the communication architecture can be changed in 6G-V2X networks, PHY, MAC, NET, and TRANS layer challenges and corresponding solutions, FD UAV networks with energy harvesting, cognitive radio networks, and various FD ML solutions.

8.2 Future Works

In this thesis, I proposed five novel designs based on the FD technology in V2X communication networking. However, there still lots of topics to be investigated. Both FD technology and V2X technology have huge research potentials and opportunities. Besides of the topics and solutions introduced in Chapter 7, I give a summary of additional research topics in this section.

Firstly, all proposed designs in this thesis focuses on the simultaneous transmission and sensing feature of the FD technology. However, simultaneous transmission and reception feature, and FD relay designs can be studied. Secondly, aperiodic data traffic is not supported in decentralised V2X networks in both V2X standards. Thus, mini-slot and multi-slot transmission in this scenario can be investigated. Thirdly, since V2X communications include many more specific use cases, such as lane merging, overtaking and platooning, a novel FD-based design can be proposed to each use case. Fourthly, since unicast and groupcast modes are introduced besides of the conventional broadcast communication framework, a FD-based design can be proposed to support the simultaneous inter-operation of all three frameworks. Fifthly, although energy detection is the most widely-applied sensing method, there are other types of sensing methods. Feasibility research on FD sensing with other types of methods is another significant opportunity. Especially, the designs that have taken coexistence of safety and infotainment data traffic into consideration.

Bibliography

[1] IEEE, "IEEE Standard for Information Technology - Telecommunications and Information Exchange between Systems - Local and Metropolitan Area Networks - Specific Requirements - Part 11: Wireless LAN Medium Access Control (MAC) and Physical Layer (PHY) Specifications," *IEEE Std 802.11*, 1999.

[2] 3GPP, "Release 14 Description; Summary of Rel-14 Work Items," *3GPP TR 21.914, Rel-14*, 2017.

[3] 3GPP, "Release 15 Description; Summary of Rel-15 Work Items," *3GPP TR 21.915, Rel-15*, 2018.

[4] 3GPP, "Release 16 Description; Summary of Rel-16 Work Items," *3GPP TR 21.916, Rel-16*, 2019.

[5] 3GPP, "Release 17 Description; Summary of Rel-17 Work Items," *3GPP TR 21.917, Rel-17*, 2020.

[6] J. Zheng and Q. Wu, "Performance Modeling and Analysis of the IEEE 802.11p EDCA Mechanism for VANET," *IEEE Transactions on Vehicular Technology*, vol. 65, no. 4, pp. 2673–2687, 2016.

[7] K. A. Hafeez, L. Zhao, B. Ma, and J. W. Mark, "Performance Analysis and Enhancement of the DSRC for VANET's Safety Applications," *IEEE Transactions on Vehicular Technology*, vol. 62, no. 7, pp. 3069–3083, 2013.

[8] M. Chowdhury et al., "Lessons Learned from the Real-World Deployment of a Connected Vehicle Testbed," *Transp. Re. Rec.*, vol. 2672, no. 22, pp. 10–23, 2018.

[9] J. Hu, S. Chen, L. Zhao, Y. Li, J. Fang, B. Li, and Y. Shi, "Link Level Performance Comparison between LTE V2X and DSRC," *Journal of Communications and Information Networks*, vol. 2, no. 2, pp. 101–112, 2017.

[10] G. Naik, B. Choudhury, and J. Park, "IEEE 802.11bd & 5G NR V2X: Evolution of Radio Access Technologies for V2X Communications," *IEEE Access*, vol. 7, pp. 70169–70184, May. 2019.

[11] D. Kim, H. Lee, and D. Hong, "A Survey of In-Band Full-Duplex Transmission: From the Perspective of PHY and MAC Layers," *IEEE Communications Surveys & Tutorials*, vol. 17, no. 4, pp. 2017–2046, 2015.

[12] J.F. O'Hara and G.M. Moore, "A High Performance CW Receiver Using Feedthru Nulling," *Microwave Journal*, vol. 6, no. 9, pp. 63–71, 1963.

[13] C. Campolo, A. Molinaro, A. O. Berthet, and A. Vinel, "Full-duplex radios for vehicular communications," *IEEE Communications Magazine*, vol. 55, no. 6, pp. 182–189, 2017.

[14] F.-L. Luo, *Machine Learning for Future Wireless Communications*. Wiley-IEEE Press, 2020.

[15] M. Simon and M. Alouini, *Digital Communication over Fading Channels: An Unified Approach to Performance Analysis,* 1^{st} *Ed.* John Wiley & Sons, 2000.

[16] Proakis, John G., *Digital Communications,* 4^{th} *Ed.* McGraw Hill, 2001.

[17] S. Shankar N., C. Cordeiro, and K. Challapali, "Spectrum Agile Radios: Utilisation and Sensing Architectures," in *First IEEE International Symposium on New Frontiers in Dynamic Spectrum Access Networks, 2005. DySPAN 2005.*, pp. 160–169, 2005.

[18] A. Saman, T. Chintha, and J. Hai, *Energy Detection for Spectrum Sensing in Cognitive Radio*. Springer, 2014.

[19] D. Cabric, S. Mishra, and R. Brodersen, "Implementation Issues in Spectrum Sensing for Cognitive Radios," in *Conference Record of the Thirty-Eighth Asilomar Conference on Signals, Systems and Computers, 2004.*, vol. 1, pp. 772–776 Vol.1, 2004.

[20] T. Yucek and H. Arslan, "Spectrum Characterisation for Opportunistic Cognitive Radio Systems," in *MILCOM 2006 - 2006 IEEE Military Communications conference*, pp. 1–6, 2006.

[21] K. Eswaran, M. Gastpar, and K. Ramchandran, "Bits through ARQs: Spectrum Sharing with a Primary Packet System," in *2007 IEEE International Symposium on Information Theory*, pp. 2171–2175, 2007.

[22] R. Tandra and A. Sahai, "Fundamental Limits on Detection in Low SNR under Noise Uncertainty," in *2005 International Conference on Wireless Networks, Communications and Mobile Computing*, vol. 1, pp. 464–469 vol.1, 2005.

[23] K. Maeda, A. Benjebbour, T. Asai, T. Furuno, and T. Ohya, "Recognition Among OFDM-Based Systems Utilizing Cyclostationarity-Inducing Transmission," in *2007 2nd IEEE International Symposium on New Frontiers in Dynamic Spectrum Access Networks*, pp. 516–523, 2007.

[24] H. Fan, Q. Meng, Y. Zhang, and W. Feng, "Feature Detection Based on Filter Banks and Higher Order Cumulants," in *2006 IEEE International Conference on Information Acquisition*, pp. 562–566, 2006.

[25] W. Jun and B. Guangguo, "Spectrum Sensing in Cognitive Radios Based on Multiple Cumulants," *IEEE Signal Processing Letters*, vol. 17, no. 8, pp. 723–726, 2010.

[26] H. Wang, E.-H. Yang, Z. Zhao, and W. Zhang, "Spectrum Sensing in Cognitive Radio using Goodness of Fit Testing," *IEEE Transactions on Wireless Communications*, vol. 8, no. 11, pp. 5427–5430, 2009.

[27] N. Nguyen-Thanh, T. Kieu-Xuan, and I. Koo, "Comments and Corrections Comments on "Spectrum Sensing in Cognitive Radio Using Goodness-of-Fit Testing"," *IEEE Transactions on Wireless Communications*, vol. 11, no. 10, pp. 3409–3411, 2012.

[28] F. S. Cattivelli and A. H. Sayed, "Distributed Detection Over Adaptive Networks Using Diffusion Adaptation," *IEEE Transactions on Signal Processing*, vol. 59, no. 5, pp. 1917–1932, 2011.

[29] G. Zhang, X. Wang, Y.-C. Liang, and J. Liu, "Fast and Robust Spectrum Sensing via Kolmogorov-Smirnov Test," *IEEE Transactions on Communications*, vol. 58, no. 12, pp. 3410–3416, 2010.

[30] A. Sabharwal, P. Schniter, D. Guo, D. W. Bliss, S. Rangarajan, and R. Wichman, "In-Band Full-Duplex Wireless: Challenges and Opportunities," *IEEE Journal on Selected Areas in Communications*, vol. 32, no. 9, pp. 1637–1652, 2014.

[31] D. Bharadia, E. McMilin, and S. Katti, "Full Duplex Radios," in *2013 SIGCOMM*, pp. 375–386, 2013.

[32] D. Kim, S. Park, H. Ju, and D. Hong, "Transmission Capacity of Full-Duplex-Based Two-Way Ad Hoc Networks With ARQ Protocol," *IEEE Transactions on Vehicular Technology*, vol. 63, no. 7, pp. 3167–3183, 2014.

[33] G. Zheng, I. Krikidis, J. Li, A. P. Petropulu, and B. Ottersten, "Improving Physical Layer Secrecy Using Full-Duplex Jamming Receivers," *IEEE Transactions on Signal Processing*, vol. 61, no. 20, pp. 4962–4974, 2013.

[34] M. Duarte, A. Sabharwal, V. Aggarwal, R. Jana, K. K. Ramakrishnan, C. W. Rice, and N. K. Shankaranarayanan, "Design and Characterization of a Full-Duplex Multiantenna System for WiFi Networks," *IEEE Transactions on Vehicular Technology*, vol. 63, no. 3, pp. 1160–1177, 2014.

[35] M. Jain et al., "Practical, Real-Time, Full Duplex Wireless," in *17th annual international conference on Mobile computing and networking (Mobicom)*, pp. 301–312, 2011.

[36] IEEE, "Ieee standard for information technology– local and metropolitan area networks– specific requirements– part 11: Wireless lan medium access control (mac) and physical layer (phy) specifications amendment 6: Wireless access in vehicular environments," *IEEE Std 802.11p-2010 (Amendment to IEEE Std 802.11-2007 as amended by IEEE Std 802.11k-2008, IEEE Std 802.11r-2008, IEEE Std 802.11y-2008, IEEE Std 802.11n-2009, and IEEE Std 802.11w-2009)*, pp. 1–51, 2010.

[37] J. Yin et al., "Practical, Real-Time, Full Duplex Wireless," in *1st ACM Int. Workshop Veh. Ad Hoc Net.*, pp. 1–9, 2004.

[38] G. Naik, B. Choudhury, and J.-M. Park, "IEEE 802.11bd & 5G NR V2X: Evolution of Radio Access Technologies for V2X Communications," *IEEE Access*, vol. 7, pp. 70169–70184, 2019.

[39] J. Zang, V. Towhidlou, and M. Shikh-Bahaei, "Collision Avoidance in V2X Communication Networks," in *2019 IEEE Wireless Communications and Networking Conference Workshop (WCNCW)*, pp. 1–6, 2019.

[40] T. V. Nguyen, F. Baccelli, K. Zhu, S. Subramanian, and X. Wu, "A performance analysis of CSMA based broadcast protocol in VANETs," in *2013 Proceedings IEEE INFOCOM*, pp. 2805–2813, 2013.

[41] V. Towhidlou and M. Shikh-Bahaei, "Adaptive Full-Duplex Communications in Cognitive Radio Networks," *IEEE Transactions on Vehicular Technology*, vol. 67, no. 9, pp. 8386–8395, 2018.

[42] A. Bazzi, C. Campolo, B. M. Masini, A. Molinaro, A. Zanella, and A. O. Berthet, "Enhancing Cooperative Driving in IEEE 802.11 Vehicular Networks Through Full-Duplex Radios," *IEEE Transactions on Wireless Communications*, vol. 17, no. 4, pp. 2402–2416, 2018.

[43] C. Campolo, A. Molinaro, and A. O. Berthet, "Improving CAMs Broadcasting in VANETs through Full-Duplex Radios," in *2016 IEEE 27th Annual International Symposium on Personal, Indoor, and Mobile Radio Communications (PIMRC)*, pp. 1–6, 2016.

[44] S. Malluri and V. K. Pamula, "Gaussian Q-function and Its Approximations," in *2013 International Conference on Communication Systems and Network Technologies*, pp. 74–77, 2013.

[45] J. Zang, V. Towhidlou, and M.-R. Shikh-Bahaei, "A Priority-Based Cross-Layer Design for Future VANETs Through Full-Duplex Technology," *IEEE Transactions on Vehicular Technology*, vol. 69, no. 7, pp. 7531–7544, 2020.

[46] IEEE, "IEEE Approved Draft Standard for Wireless Access in Vehicular Environments (WAVE) – Multi-Channel Operation - Corrigendum 1: Miscellaneous corrections," *IEEE P1609.4-2016/Cor1/D3*, pp. 1–12, 2019.

[47] IEEE, "IEEE Guide for Wireless Access in Vehicular Environments (WAVE) Architecture - Redline," *IEEE Std 1609.0-2019 (Revision of IEEE Std 1609.0-2013) - Redline*, pp. 1–219, 2019.

[48] H. P. Luong, M. Panda, H. L. Vu, and B. Q. Vo, "Beacon Rate Optimisation for Vehicular Safety Applications in Highway Scenarios," *IEEE Transactions on Vehicular Technology*, vol. 67, no. 1, pp. 524–536, 2018.

[49] F. Lyu, H. Zhu, H. Zhou, W. Xu, N. Zhang, M. Li, and X. Shen, "SS-MAC: A Novel Time Slot-Sharing MAC for Safety Messages Broadcasting in VANETs," *IEEE Transactions on Vehicular Technology*, vol. 67, no. 4, pp. 3586–3597, 2018.

[50] F. Lyu, H. Zhu, N. Cheng, Y. Zhu, H. Zhou, W. Xu, G. Xue, and M. Li, "ABC: Adaptive Beacon Control for Rear-End Collision Avoidance in VANETs,"

in *2018 15th Annual IEEE International Conference on Sensing, Communication, and Networking (SECON)*, pp. 1–9, 2018.

[51] F. Lyu, H. Zhu, N. Cheng, H. Zhou, W. Xu, M. Li, and X. Shen, "Characterising Urban Vehicle-to-Vehicle Communications for Reliable Safety Applications," *IEEE Transactions on Intelligent Transportation Systems*, pp. 1–17, 2019.

[52] Z. Tong, H. Lu, M. Haenggi, and C. Poellabauer, "A Stochastic Geometry Approach to the Modeling of DSRC for Vehicular Safety Communication," *IEEE Transactions on Intelligent Transportation Systems*, vol. 17, no. 5, pp. 1448–1458, 2016.

[53] S. Sharma, M. Chahal, and S. Harit, "Transmission Rate-based Congestion Control in Vehicular Ad Hoc Networks," in *2019 Amity International Conference on Artificial Intelligence (AICAI)*, pp. 303–307, 2019.

[54] J. Gao, M. Li, L. Zhao, and X. Shen, "Contention Intensity Based Distributed Coordination for V2V Safety Message Broadcast," *IEEE Transactions on Vehicular Technology*, vol. 67, no. 12, pp. 12288–12301, 2018.

[55] A. Dayal, E. Colbert, V. Marojevic, and J. Reed, "Risk Controlled Beacon Transmission in V2V Communications," in *2019 IEEE 89th Vehicular Technology Conference (VTC2019-Spring)*, pp. 1–6, 2019.

[56] V. Towhidlou and M. Shikh-Bahaei, "Adaptive full duplex communications in cognitive radio networks," in *2017 IEEE 28th Annual International Symposium on Personal, Indoor, and Mobile Radio Communications (PIMRC)*, pp. 1–5, 2017.

[57] M. Yang, S. Jeon, and D. K. Kim, "Interference management for in-band full-duplex vehicular access networks," *IEEE Transactions on Vehicular Technology*, vol. 67, no. 2, pp. 1820–1824, 2018.

[58] X. Chen, H. H. Refai, and X. Ma, "A Quantitative Approach to Evaluate DSRC Highway Inter-Vehicle Safety Communication," in *IEEE GLOBECOM 2007 - IEEE Global Telecommunications Conference*, pp. 151–155, 2007.

[59] W. Zhang, Y. Chen, Y. Yang, X. Wang, Y. Zhang, X. Hong, and G. Mao, "Multi-Hop Connectivity Probability in Infrastructure-Based Vehicular Networks," *IEEE Journal on Selected Areas in Communications*, vol. 30, no. 4, pp. 740–747, 2012.

[60] F. Abbas, X. Yuan, M. S. Bute, and P. Fan, "Performance analysis using full duplex discovery mechanism in 5g-v2x communication networks," *IEEE Transactions on Intelligent Transportation Systems*, pp. 1–12, 2021.

[61] J. He, H.-h. Chen, T. M. Chen, and W. Cheng, "Adaptive congestion control for dsrc vehicle networks," *IEEE Communications Letters*, vol. 14, no. 2, pp. 127–129, 2010.

[62] F. Yu and S. Biswas, "A self-organizing mac protocol for dsrc based vehicular ad hoc networks," in *27th International Conference on Distributed Computing Systems Workshops (ICDCSW'07)*, pp. 88–88, 2007.

[63] M. I. Hassan, H. L. Vu, T. Sakurai, and L. L. H. Andrew, "Effect of retransmissions on the performance of the ieee 802.11 mac protocol for dsrc," *IEEE Transactions on Vehicular Technology*, vol. 61, no. 1, pp. 22–34, 2012.

[64] J. Zang and M. Shikh-Bahaei, "Full Duplex-Based Scheduling Protocol for Latency Enhancement in 5G eV2X VANETs," in *2021 IEEE Wireless Communications and Networking Conference (WCNC)*, pp. 1–6, 2021.

[65] J. Zang and M. Shikh-Bahaei, "Full-Duplex Multiple Access Mechanism for Connected Vehicles Operating at Different Autonomous Levels in NR eV2X Networks," *IEEE Transactions on Intelligent Transportation Systems, under review*, 2021.

[66] United States Department of Transportation, "Intelligent Transportation System Strategic Plan 2020-2025," *Strategic Plan of the U.S.A.*, pp. 1–49, 2020.

[67] Department of Transport, The Government of the U.K., "Intelligent Transport Systems in the U.K.," *Department Report*, pp. 1–153, Apr. 2018.

[68] L. Zhao, X. Li, B. Gu, Z. Zhou, S. Mumtaz, V. Frascolla, H. Gacanin, M. I. Ashraf, J. Rodriguez, M. Yang, and S. Al-Rubaye, "Vehicular Communications: Standardisation and Open Issues," *IEEE Communications Standards Magazine*, vol. 2, no. 4, pp. 74–80, 2018.

[69] W. Anwar, N. Franchi, and G. Fettweis, "Physical layer evaluation of v2x communications technologies: 5g nr-v2x, lte-v2x, ieee 802.11bd, and ieee 802.11p," in *2019 IEEE 90th Vehicular Technology Conference (VTC2019-Fall)*, pp. 1–7, Sep. 2019.

[70] F. Abbas, P. Fan, and Z. Khan, "A Novel Low-Latency V2V Resource Allocation Scheme Based on Cellular V2X Communications," *IEEE Transactions on Intelligent Transportation Systems*, vol. 20, pp. 2185–2197, Oct. 2019.

[71] S. Roger, D. Martín-Sacristán, D. Garcia-Roger, J. F. Monserrat, P. Spapis, A. Kousaridas, S. Ayaz, and A. Kaloxylos, "Low-Latency Layer-2-Based Multicast Scheme for Localized V2X Communications," *IEEE Transactions on Intelligent Transportation Systems*, vol. 20, pp. 2962–2975, Oct. 2019.

[72] 3GPP, "Evolved Universal Terrestrial Radio Access (E-UTRA) and Evolved Universal Terrestrial Radio Access Network (E-UTRAN); Overall description; Stage 2," *3GPP TS 36.300, Rel-16, V-16.0.0*, Jan. 2020.

[73] 3GPP, "Evolved Universal Terrestrial Radio Access (E-UTRA); Medium Access Control (MAC) protocol specification," *3GPP TS 36.321, Rel-15, V-15.8.0*, Jan. 2020.

[74] R. Molina-Masegosa and J. Gozalvez, "LTE-V for Sidelink 5G V2X Vehicular Communications: A New 5G Technology for Short-Range Vehicle-to-Everything Communications," *IEEE Vehicular Technology Magazine*, vol. 12, pp. 30–39, Dec. 2017.

[75] A. Mansouri, V. Martinez, and J. Härri, "A First Investigation of Congestion Control for LTE-V2X Mode 4," in *2019 15th Annual Conference on Wireless On-demand Network Systems and Services (WONS)*, pp. 56–63, Jan. 2019.

[76] N. H. Mahmood, I. S. Ansari, P. Popovski, P. Mogensen, and K. A. Qaraqe, "Physical-Layer Security With Full-Duplex Transceivers and Multiuser Receiver at Eve," *IEEE Transactions on Communications*, vol. 65, no. 10, pp. 4392–4405, 2017.

[77] H. Thomsen, D. M. Kim, P. Popovski, N. K. Pratas, and E. de Carvalho, "Full Duplex Emulation via Spatial Separation of Half Duplex Nodes in a Planar Cellular Network," in *2016 IEEE 17th International Workshop on Signal Processing Advances in Wireless Communications (SPAWC)*, pp. 1–5, 2016.

[78] Z. Zhou, H. Liao, B. Gu, S. Mumtaz, and J. Rodriguez, "Resource Sharing and Task Offloading in IoT Fog Computing: A Contract-Learning Approach," *IEEE Transactions on Emerging Topics in Computational Intelligence*, vol. 4, no. 3, pp. 227–240, 2020.

[79] 3GPP, "Study on Enhancement of 3GPP Support for 5G V2X Services," *3GPP TR 22.886, Rel-15, V-16.2.0*, Dec. 2018.

[80] 3GPP, "Evolved Universal Terrestrial Radio Access (E-UTRA); User Equipment (UE) Radio Transmission and Reception," *3GPP TS 36.101, Rel-16, V-16.4.0*, Jan. 2020.

[81] 3GPP, "Evolved Universal Terrestrial Radio Access (E-UTRA); Physical Layer Procedures," *3GPP TS 36.213, Rel-16, V-16.0.0*, Jan. 2020.

[82] M. Gonzalez-Martín, M. Sepulcre, R. Molina-Masegosa, and J. Gozalvez, "Analytical Models of the Performance of C-V2X Mode 4 Vehicular Communications," *IEEE Transactions on Vehicular Technology*, vol. 68, pp. 1155–1166, Feb. 2019.

[83] 3GPP, "Overall Description of Radio Access Network (RAN) Aspects for Vehicle-to-Everything (V2X) based on LTE and NR," *3GPP TR 37.985, Rel-16, V-1.0.0*, Nov. 2019.

[84] C. Sommer, R. German, and F. Dressler, "Bidirectionally Coupled Network and Road Traffic Simulation for Improved IVC Analysis," *IEEE Transactions on Mobile Computing (TMC)*, vol. 10, pp. 3–15, Jan. 2011.

[85] F. J. Martín-Vega, B. Soret, M. C. Aguayo-Torres, I. Z. Kovács, and G. Gómez, "Geolocation-based access for vehicular communications: Analysis and optimization via stochastic geometry," *IEEE Transactions on Vehicular Technology*, vol. 67, pp. 3069–3084, Apr. 2018.

[86] X. Gu, B. Leng, L. Zhang, J. Miao, and L. Zhang, "A stochastic geometry approach to model and analyze future vehicular communication networks," *IEEE Access*, vol. 8, pp. 14500–14512, Jan. 2020.

[87] S. R. Pokhrel, "Software Defined Internet of Vehicles for Automation and Orchestration," *IEEE Transactions on Intelligent Transportation Systems*, vol. 22, no. 6, pp. 3890–3899, 2021.

[88] S. R. Pokhrel and J. Choi, "Low-Delay Scheduling for Internet of Vehicles: Load-Balanced Multipath Communication With FEC," *IEEE Transactions on Communications*, vol. 67, no. 12, pp. 8489–8501, 2019.

[89] S. R. Pokhrel and J. Choi, "Federated Learning With Blockchain for Autonomous Vehicles: Analysis and Design Challenges," *IEEE Transactions on Communications*, vol. 68, no. 8, pp. 4734–4746, 2020.

[90] J. Zang and M. Shikh-Bahaei, "An Adaptive Full-Duplex Deep Reinforcement Learning-Based Design for 5G-V2X Mode 4 VANETs," in *2021 IEEE Wireless Communications and Networking Conference (WCNC)*, pp. 1–6, 2021.

[91] H. Ye, G. Y. Li, and B. F. Juang, "Deep reinforcement learning based resource allocation for v2v communications," *IEEE Transactions on Vehicular Technology*, vol. 68, no. 4, pp. 3163–3173, 2019.

[92] X. Zhang, M. Peng, S. Yan, and Y. Sun, "Deep-reinforcement-learning-based mode selection and resource allocation for cellular v2x communications," *IEEE Internet of Things Journal*, vol. 7, no. 7, pp. 6380–6391, 2020.

[93] L. Liang, H. Ye, G. Yu, and G. Y. Li, "Deep-learning-based wireless resource allocation with application to vehicular networks," *Proceedings of the IEEE*, vol. 108, no. 2, pp. 341–356, 2020.

[94] K. Arulkumaran, M. P. Deisenroth, M. Brundage, and A. A. Bharath, "Deep reinforcement learning: A brief survey," *IEEE Signal Processing Magazine*, vol. 34, no. 6, pp. 26–38, 2017.

[95] V. Mnih *et al.*, "Human-level control through deep reinforcement learning," *Nature*, vol. 518, no. 7540, pp. 529–533, 2015.

[96] 3GPP, "Study on lte-based v2x services," *3GPP TR 36.885, Rel-14, V-14.0.0*, Jul. 2016.

[97] Z. Y. Junwei Zang, Yirun Zhang and M. Shikh-Bahaei, "Next-Generation FD Technology in V2X Communications," *IEEE Vehicular Technology Magazine, under review*, 2021.

[98] Z. Yang, C. Pan, K. Wang, and M. Shikh-Bahaei, "Energy Efficient Resource Allocation in UAV-enabled Mobile Edge Computing Networks," *IEEE Transactions on Wireless Communications*, vol. 18, no. 9, pp. 4576–4589, 2019.

[99] Y. Zeng and R. Zhang, "Energy-efficient uav communication with trajectory optimisation," *IEEE Transactions on Wireless Communications*, vol. 16, no. 6, pp. 3747–3760, 2017.

[100] Z. Yang, C. Pan, J. Hou, and M. Shikh-Bahaei, "Efficient Resource Allocation for Mobile-Edge Computing Networks with NOMA: Completion Time and Energy Minimization," *IEEE Trans. Commun.*, vol. 67, pp. 7771–7784, Nov. 2019.

[101] 3GPP, "Architecture Enhancements for 5G System (5GS) to Support Vehicle-to-Everything (V2X) Services," *3GPP TS 23.287, Rel-16*, 2020.

[102] R. Askar, J. Chung, Z. Guo, H. Ko, W. Keusgen, and T. Haustein, "Interference Handling Challenges toward Full Duplex Evolution in 5G and Beyond Cellular Networks," *IEEE Wireless Communications*, vol. 28, no. 1, pp. 51–59, 2021.

[103] Z. Yang, M. Chen, K.-K. Wong, H. V. Poor, and S. Cui, "Federated Learning for 6G: Applications, Challenges, and Opportunities," *arXiv preprint arXiv:2101.01338*, 2021.

[104] Y. Zhang, J. Hou, V. Towhidlou, and M. R. Shikh-Bahaei, "A Neural Network Prediction-Based Adaptive Mode Selection Scheme in Full-Duplex Cognitive Networks," *IEEE Transactions on Cognitive Communications and Networking*, vol. 5, no. 3, pp. 540–553, 2019.

[105] Y. Zhang, Q. Wu, and M. R. Shikh-Bahaei, "On Ensemble Learning-Based Secure Fusion Strategy for Robust Cooperative Sensing in Full-Duplex Cognitive Radio Networks," *IEEE Transactions on Communications*, vol. 68, no. 10, pp. 6086–6100, 2020.

[106] J. Zang and M. Shikh-Bahaei, "An Adaptive Full-Duplex Deep Reinforcement Learning-Based Design for 5G-V2X Mode 4 VANETs," in *2021 IEEE Wireless Communications and Networking Conference (WCNC)*, pp. 1–6, 2021.

[107] Y. Zhang, Q. Wu, and M. Shikh-Bahaei, "Vertical Federated Learning Based Privacy-Preserving Cooperative Sensing in Cognitive Radio Networks," in *2020 IEEE Globecom Workshops*, pp. 1–6, 2020.

[108] F. Xiong, *Digital Modulation Techniques*. Artech House, 2000.

A PSD of M-PSK Signals

Consider a M-PSK modulated signal in the form of

$$s(t) = x(t)\cos(2\pi f_c t) - y(t)\sin(2\pi f_c t), \tag{A.1}$$

where $x(t)$ and $y(t)$ are the in-phase and quadrature components determined by the data streams x_k and y_k, respectively, which are given by

$$\begin{cases} x(t) = \sum_{k=-\infty}^{+\infty} x_k p(t - kT) \\ y(t) = \sum_{k=-\infty}^{+\infty} y_k q(t - kT), \end{cases} \tag{A.2}$$

where signals $p(t)$ and $q(t)$ are baseband pulse-shaping functions whose Fourier transforms are given by

$$\begin{cases} P(f) = F\{p(t)\} \\ Q(f) = F\{q(t)\}. \end{cases} \tag{A.3}$$

The complex envelope of $s(t)$ is given by

$$\tilde{s}(t) = x(t) + jy(t). \tag{A.4}$$

In order to find the PSD of $\tilde{s}(t)$, we need to find its auto-correlation function, which is given by

$$\begin{aligned} R_{\tilde{s}}(\tau) &= E\{\tilde{s}(t)\tilde{s}^*(t-\tau)\} \\ &= E\{[x(t) + jy(t)][x(t-\tau) - jy(t-\tau)]\} \\ &= R_x(\tau) + R_y(\tau), \end{aligned} \tag{A.5}$$

where

$$\begin{cases} R_x(\tau) = E\{x(t)x(t-\tau)\} \\ R_y(\tau) = E\{y(t)y(t-\tau)\}. \end{cases} \tag{A.6}$$

According to the Wiener-Khintchine theorem, we have

$$\begin{aligned}\Psi_{\tilde{s}}(f) &= F\{R_{\tilde{s}(\tau}\} = F\{R_x(\tau)\} + F\{R_y(\tau)\} \\ &= \Psi_x(f) + \Psi_y(f),\end{aligned} \tag{A.7}$$

where $\Psi_x(f)$ and $\Psi_y(f)$ are the PSD of the in-phase and quadrature components, respectively, and they are given by

$$\begin{cases}\Psi_x(f) = \frac{\sigma_x^2|P(f)|^2}{T} \\ \Psi_y(f) = \frac{\sigma_y^2|Q(f)|^2}{T}.\end{cases} \tag{A.8}$$

Therefore the PSD of M-PSK signals, $\Psi_{\tilde{s}}(f)$, is given by

$$\Psi_{\tilde{s}}(f) = \frac{\sigma_x^2|P(f)|^2}{T} + \frac{\sigma_y^2|Q(f)|^2}{T}, \tag{A.9}$$

which can also be applied to all other quadrature modulated signals, such as the M-QAM signals [108].

B Proof of Virtually Orthonormality

From the $\phi_1^2(t)$ perspective, $\phi_1(t)$ and $\phi_2(t)$ are virtually orthogonal, because

$$\begin{aligned}\int_0^T \phi_1^2(t)dt &= \frac{2}{E_p}\int_0^T p^2(t)\cos^2(2\pi f_c t)dt \\ &= \frac{1}{E_p}\int_0^T p^2(t)[1+\cos(4\pi f_c t)]dt \\ &\approx 1, \quad for \quad f_c >> \frac{1}{T}.\end{aligned} \tag{B.1}$$

Similarly, from the $\phi_2^2(t)$ perspective, they are also virtually orthogonal, since

$$\begin{aligned}\int_0^T \phi_1(t)\phi_2(t)dt &= -\frac{2}{E_p}\int_0^T p^2(t)\cos(2\pi f_c t)\sin(2\pi f_c t)dt \\ &= -\frac{2}{E_p}\int_0^T p^2(t)\sin(4\pi f_c t)dt \\ &\approx 0, \quad for \quad f_c >> \frac{1}{T}.\end{aligned} \tag{B.2}$$